

Role of RBM20 alternative splicing factor for the regulation of neuronal functions

Inauguraldissertation
zur
Erlangung der Würde eines Doktors der Philosophie
vorgelegt der
Philosophisch-Naturwissenschaftlichen Fakultät
der Universität Basel
von

Giulia Di Bartolomei

Basel, 2023

Genehmigt von der Philosophisch-

Naturwissenschaftlichen Fakultät auf Antrag von:

First supervisor: Prof. Dr. Peter Scheiffele

Second supervisor: Prof. Dr. Alexander Schier

External expert: Prof. Dr. Esther Creemers

Basel den, 25. April 2023

Prof. Dr. Marcel Mayor

Dekan der Philosophisch-

Naturwissenschaftlichen Fakultät

«La cultura è ciò che resta quando si è dimenticato tutto»

Burrhus Skinner

Ma anche e soprattutto,

Mario Di Bartolomei

Table of Contents

Summary	7
1. Introduction	10
1.1 General Introduction	11
1.2 Phenotypic diversity: on the road to evolution	12
1.2.1 Proteome vs. transcripts: how can humans and worms look so different?	13
1.2.2 The nervous system leads the way towards complexity.....	14
1.3 Diversity matters: Cell type specification is important for the correct operation of circuits	15
1.3.1 What is a cell type? Characterization of neuronal properties to specify neuronal identity.....	16
1.3.2 Landscape of neuron types and properties.	17
1.3.3 The olfactory bulb: circuitry, molecular diversity and cellular plasticity	19
1.4 How is transcriptomic diversity generated?	26
1.4.1 The power of alternative splicing.....	26
1.4.2 RNA-binding proteins: key post-transcriptional regulators.....	30
1.5 RNA-binding proteins “in sickness and in health”	34
1.5.1 Roles of RBPs in disease state	34
1.5.2 RBM20: “The king of hearts”	37
Rationale of this thesis	41
2. Results	42
Chapter1	43
Mapping RBM20 cell type-specific expression in the brain	43
Chapter 2:	53
Identify RBM20 direct mRNA targets and elucidate the transcriptional modulation induced by RBM20 in the brain	53
Chapter 3:	79
Uncovering the functional impact of RBM20 in neurons	79
3. General Discussion	90
4. Conclusions	102
5. Materials and Methods	105
6. Appendix	125
Book Chapter	126

Index of abbreviations	145
References	149
Acknowledgments.....	169
Curriculum Vitae.....	171

Summary

Neuronal circuits consist of hierarchical assemblies of highly specialized neuronal cell types, each characterized by distinct structural, physiological and molecular features. Formation, maintenance and adaptation of these specific cellular features are instructed by molecular programs that largely depend on alternative splicing to tailor gene expression. Recently, some splicing factors have been discovered to be selectively expressed in subsets of neuronal classes, indicating that they contribute to the diversification of the specific properties of these neurons. However, the molecular programs that these cell type-specific alternative splicing factors regulate as well as their impact on physiological function is largely unknown. In my PhD-thesis, I therefore aimed to investigate whether and how the modulation of alternative splicing programs in neurons contributes to the acquisition of unique structural and functional properties that shape neuronal connectivity.

In a survey of ribosome-associated mRNAs from genetically-defined neuronal populations of the mouse brain, I discovered that the RNA-binding protein 20 (RBM20) seemed to exhibit remarkable neuronal cell class-specific expression. RBM20 had previously been characterized only in the heart and skeletal muscle, where it drives alternative splicing of *Titin* as well as calcium signaling related transcripts such as *Camk1lδ* and *Cacna1c* (Guo *et al.*, 2012; Maatz *et al.*, 2014; van den Hoogenhof *et al.*, 2018). In a series of immunohistochemistry and omics-based experiments in the mouse brain, I then determined that RBM20 protein expression is selective for a population of Parvalbumin positive (PV⁺) GABAergic interneurons in the neocortex and for a glutamatergic (vGlut2⁺) population of mitral and tufted neurons in the olfactory bulb. In a complementary effort to uncover the RBM20-dependent alternative splicing program in these areas, I performed affinity isolation of ribosome-associated mRNAs from genetically-defined neuronal populations, in mice where RBM20 was either expressed or ablated. RBM20 loss led to transcriptomic rearrangements both at the level of gene expression and alternative splicing only in the olfactory bulb but not in PV interneurons of the neocortex. The changes in the olfactory bulb were directed towards genes involved in ion channels, cytoskeleton, cell-adhesion and synapse density. Finally, characterization of mitral cell morphology did not reveal significant differences in structural properties, while behavioral phenotyping of RBM20 mutant mice suggested a potential impact in value-associated odor memory formation.

Collectively, the combination of transcriptomic analysis, morphological studies and behavioral approaches in *Rbm20* conditional knock-out mice, provide a detailed characterization of RBM20's role in the determination of neuronal function and possibly synapse specification. This is partially contrasting its described function in the heart, which was further confirmed by our RBM20-CLIP analysis in this tissue. Together with future efforts

to expand our understanding of how splicing factors determine neuronal properties, this data has the potential to improve therapeutic avenues for neurological diseases.

1. Introduction

1.1 General Introduction

“The brain is a tissue. It is a complicated, intricately woven tissue, like nothing else we know of in the universe, but it is composed of cells, as any tissue is. They are, to be sure, highly specialized cells, but they function according to the laws that govern any other cells. Their electrical and chemical signals can be detected, recorded and interpreted and their chemicals can be identified; the connections that constitute the brain's woven feltwork can be mapped. In short, the brain can be studied, just as the kidney can”. David H. Hubel

Hubel was awarded the Nobel prize in 1960 for his discovery that visual impressions arise from signals generated by light in the eyes, which are then transmitted to and integrated by the brain. Although this may appear to be a simple process that occurs naturally every day as soon as we wake up, it is actually a complex mechanism requiring the interaction of thousands of cells. These cells analyze and interpret contrasts, patterns, directions and movements to create a sophisticated visual experience.

Every feeling, odor, experience, thought, action, memory and movement of the world surrounding us is a function of an intricate ensemble of responses that the brain produces. In fact, neuronal networks, have the ability to discriminate between and adapt to a plethora of external and internal stimuli to support the correct functioning of neuronal circuits and produce an appropriate response. Each neuron can make contacts with thousands or even tens of thousands of others, through very defined structures called “synapses”, a term introduced by Charles Sherrington in 1897 (Foster *et al.*, 1897; Glasgow *et al.*, 2019; Shepherd & Erulkar, 1997). These are highly organized structures that are able to convert incoming electrical signals into outgoing chemical signals, which are released in the form of neurotransmitters. Following new experiences and throughout development, these cells undergo constant remodeling and shaping of circuits as a function of neuronal plasticity, an essential process for circuit establishment and maturation.

The intricacy and spatiotemporal variability of neuronal networks in different brain regions and developmental stages are extremely fascinating, but they also present a challenge in comprehensively dissecting brain function. Specifically, many of the mechanisms that instruct the formation of these functional networks both at the molecular and cellular level, are still poorly characterized and current subject of investigation. The foundation of much of our understanding of the brain comes from the past research of neuroanatomists and neurobiologists. Santiago Ramón y Cajal, considered the father of modern neuroscience, meticulously categorized neurons based on their morphological features and recognized that

their intricate shape is tailored to their specific function in the brain. This pioneering work formed the basis for investigating the highly-structured connectivity patterns of neuronal cells.

In the following sections of this introduction, I will discuss how phenotypic diversity among species is explained from an evolutionary perspective and elaborate on the proposed underlying mechanisms. I will illustrate how post-transcriptional tuning of gene expression shapes neuronal diversity through the acquisition of molecular identity and unique cellular and synaptic properties, to promote the correct assembly and functioning of circuits. I will then focus on alternative splicing, a key process in driving the expansion of the coding power of genes, and describe the role of splicing factors in the context of health and disease.

Finally, I will uncover and discuss the scope of my PhD project, focusing on investigating the role of the RNA-binding protein RBM20 in controlling cell-class specific molecular programs and shaping neuronal functions.

1.2 Phenotypic diversity: on the road to evolution

Comparative studies across different species have highlighted that, following millions of years of evolution, flies (*Drosophila melanogaster*), worms (*Caenorhabditis elegans*), and primates (*Primates Linnaeus*) share some highly conserved protein coding genes. One example is the *homeobox (Hox)* genes, which are involved in the definition of body patterning during development (McGinnis & Krumlauf, 1992; Pearson *et al.*, 2005).

So how can we explain the immense phenotypic differences between these species?

First, there is a solid body of evidence to support the pivotal importance of genome expansion throughout evolution as one of the major drivers of phenotypic diversity. Indeed, while a fly genome is predicted to have a total of ~9'000 protein coding genes, *C. elegans* is estimated to have around 19'000 (McVean, 2000; McVean & Hurst, 2000). In an attempt to explain the emergence of new protein coding genes in the genome, various mechanisms have been described. For example, gene duplication, the integration of retro-genes or post-transcriptional regulation mechanisms provided by noncoding RNAs (ncRNAs), have greatly expanded and diversified gene function during evolution (Kaessmann, 2010). This is illustrated by the Morpheus gene family, which emerged in a primate ancestor and was associated with a strong selective pressure due to the massive amount of segment duplication found in these hominoids. The increase in gene number is considered essential for promoting functional and phenotypic evolution, as gene duplication likely has allowed for the acquisition of new functions

in primates (Ohno, 1970) (Kaessmann, 2010). In addition, de-novo protein coding genes have been found to originate from non-coding stretches of DNA sequence, underscoring the importance of genomic noncoding regions. Finally, while gene expression (GE) is well conserved across species and cannot account for the majority of phenotypic innovation, post-transcriptional mechanisms of gene expression regulation, such as alternative splicing (AS), may represent a significant source of species-specific differences (Barbosa-Morais *et al.*, 2012; Blencowe, 2006; Gallego-Paez *et al.*, 2017; Merkin *et al.*, 2012; Ule *et al.*, 2006).

1.2.1 Proteome vs. transcripts: how can humans and worms look so different?

Technological advances in nucleotide sequencing have enabled the characterization of the full-length DNA sequence of an organism's entire genome (Shendure & Ji, 2008), which allows a more accurate estimation of the number of protein-coding genes in different species. Intriguingly, these technologies revealed that differences in the number of genes between vertebrates and lower-order species are much smaller than previously thought. More specifically, while a mouse genome encodes for 22'437 protein-coding genes, the *C. elegans* genome harbors a similar number of around 20'000 protein coding genes (Mitani, 2017)(WormBase.org). This suggests that the complex tissue organization observed in complex organisms do not exclusively rely on the increase in cell number and organ size, but instead, on an enhanced functional specialization of tissues. In fact, the resulting proteome of these organisms is differing largely, reflecting the increasing complexity between these two species. So, what are the molecular mechanisms that shaped the functional, morphological, physiological and behavioral evolution of these organisms?

Research during the last two decades has massively improved our understanding of the basic principles underlying gene expression regulation. It has thus become clear that mechanisms other than gene duplication must be in place in order to fully explain the immense proteome diversity of organisms with higher tissue complexity (Maniatis and Tasic 2002; Blencowe 2006). One of these mechanisms, and a powerful means by which cells can massively expand the complexity of both their transcriptome and proteome, is alternative splicing.

Alternative splicing is the process through which multiple mRNA isoforms can be generated from one single pre-mRNA molecule. This process is based on the usage of alternative splice sites present in the pre-mRNA that lead to either inclusion or exclusion of a given exon. The differences between the resulting mature mRNA transcripts (isoforms) can fundamentally alter the protein function or subcellular localization.

In humans, around 95% of protein coding genes are estimated to undergo alternative splicing (Wang *et al.*, 2008), while this percentage is drastically decreased in less complex organisms. In particular, there is a strong correlation between the increase of alternatively spliced transcripts and the level of species complexity, indicating that alternative splicing was crucial in driving this evolutionary path (Barbosa-Morais *et al.*, 2012; Blencowe, 2006; Gallego-Paez *et al.*, 2017; Merkin *et al.*, 2012; Ule *et al.*, 2006).

1.2.2 The nervous system leads the way towards complexity

With the advent of RNA-sequencing (RNA-seq) and single-cell sequencing (sc-RNAseq) technologies, our understanding of the complexity and tuning of gene expression regulation has significantly improved. Post-transcriptional mechanisms and the crucial function of alternative splicing in cellular physiology and disease conditions is much better understood. However, very little is known on how the nervous system has developed through evolution to continuously reach higher levels of complexity in modern species, and how neuronal networks in humans differ from those of cognate primates.

As alluded to above, alternative splicing is one of the main mechanisms explaining diversity, besides obvious changes in gene numbers, overall brain size and number of neurons across taxa. A big advancement in the description of alternative exon usage in different species, cells and tissue types or at different stages of development, was achieved by the generation of a genome-wide atlas of vertebrate and alternative splicing transcription database (VastDB), in which 1478 RNA-seq datasets were analyzed (Tapial *et al.*, 2017). One of the main insights revealed by this study was that alternative splicing events that are conserved across tissues and species are mainly involved in the modulation of transcription factors and chromatin regulation, which are directing fundamental steps of organismal development. In contrast, alternative splicing events appear to less frequently drive tissue specific functions. Moreover, and very interestingly, neuronal tissue was identified as the tissue with the highest number of alternative splicing events, followed by muscle and heart tissues (Tapial *et al.*; 2017(Mazin *et al.*, 2021)).

Collectively, this provides further evidence to support the idea that alternative splicing, and the regulation of gene expression in general, correlates with the complexity of tissues (Fig.1).

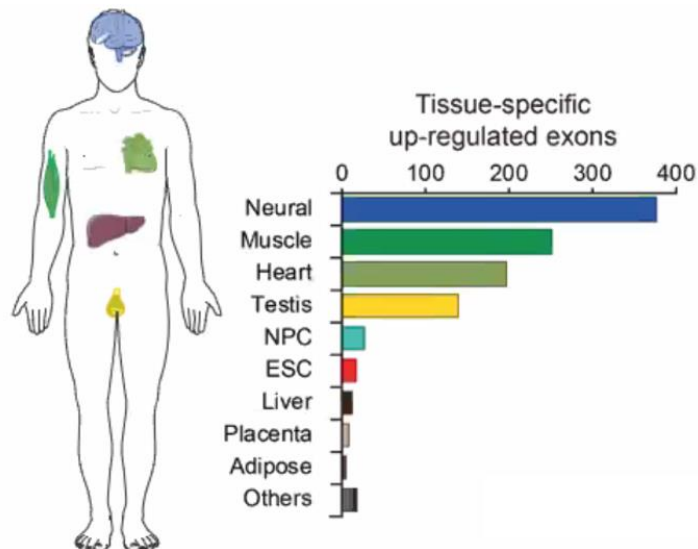


Figure 1: Tissue regulation of exon alternative splicing in different human tissues

The bar plot is showing the number of alternatively spliced exons with increased percent spliced in index (PSI) in different human tissues. Neural, muscle and heart tissue types appear to have the highest alternative splicing regulation. Figure adapted from Tapial et al.; 2017.

1.3 Diversity matters: Cell type specification is important for the correct operation of circuits

Neuronal cells exhibit a remarkable degree of diversification. In any brain region, there are tens to hundreds of specific cell types characterized by unique molecular, morphological, and functional properties. All of these features are crucial for the correct operation of circuits.

In the last decade, sc-RNAseq studies have largely contributed to the fine dissection of transcriptomic programs of individual cell types. They have also provided a better understanding of the molecular signatures that define cell type-identity, and how the molecular profiles match with functional properties of cell types. Importantly, with the help of sc-RNAseq data, subpopulations of neurons can be segregated based on cell-type specific “*marker genes*”. Together with previously established methods, scientists are now able to more acutely classify cells into different groups based on their morphology, neurochemistry, synaptic strength or firing properties (Paul *et al.*, 2017; Tasic *et al.*, 2016; Zeisel *et al.*, 2015). Data emerging from sc-RNAseq studies further indicate that synaptic scaffolding proteins are key to determine neuronal identity and intrinsic properties (Tasic *et al.*; 2016; Tasic *et al.*; 2018). One of the challenges is that, even though belonging to the same subgroup, cells may be integrated

in distinct neuronal pathways. Therefore, it has become increasingly clear that additional parameters might be required to fully distinguish neuronal subpopulations.

However, besides transcriptional differences, some of the morphological and functional diversifications between cell type/classes rely on the specific regulation of post-transcriptional mechanisms. Recent evidence suggests that alternative splicing programs provide a mechanism for protein functional diversification, thus defining neuronal classes.

1.3.1 What is a cell type? Characterization of neuronal properties to specify neuronal identity

Brain function relies on a variety of cell types, including neurons, glia (microglia, astrocytes and oligodendrocytes), and mesenchymal cells. Extensive work from multiple laboratories leveraging the recent technological advances has allowed the characterization of the diversity of brain cell types and transcriptomes. Fast and high-throughput methods enabled the unbiased sampling and categorization of more than 23'822 cells, capturing even rare cell populations (Tasic et al; 2018). However, given the intricacy of this system, a comprehensive understanding of how brain circuits work can only be achieved when taking into account also neuronal morphology and projection patterns and intrinsic features. While many have put their efforts in trying to categorize and profile cells into types and subtypes by looking at which RNAs are expressed in each cell, others tried to tackle the complexity of the brain by combine sequencing data with functional assays and morphological or projection pattern analysis to link neurons to their identity (Tasic et al.; 2018, Zeisel et al.; 2016). In addition, technological advancements have enabled complete brain imaging reconstruction using automated fluorescent and electron microscopy. The combination of Cre-dependent sparse labeling genetic models, (e.g. MOnonucleotide Repeat Frameshift (MORF) transgenic mice (Veldman *et al.*, 2020), and the use of recombinant intrabody fluorescent probes that bind endogenous synaptic components such as PSD-95 or Gephyrin (FingRs, Fibronectin intrabodies generated with mRNA display), provide an efficient approach to selectively target and monitor endogenous proteins as well as neuronal morphological features in both fixed and live tissues using super-resolution imaging platforms (Gross *et al.*, 2013; Rimbault *et al.*, 2019).

Thus, researchers can gain insights into cell morphology and create large datasets of cleared tissues and even entire organs, improving the signal-to-noise ratio and mapping neuron connectomes. Additionally, two-photon microscopy paired with sequencing or spatial transcriptomic approaches can track cellular changes and their molecular signature across development, while calcium imaging data enable scientists to infer neuronal electrical activity (Chen *et al.*, 2015; Cho *et al.*, 2017; Fantuzzo *et al.*, 2020; Wu *et al.*, 2019; Zheng *et al.*, 2018).

Despite the challenges of achieving a more detailed spatio-temporal resolution, the huge amount of available datasets shows the existence of hundreds of individual cell types in the brain and allows us to expand our understanding of the variety among neurons. However, the massive amount of accumulated data brings along the problem of how to store, analyze and integrate different datasets. We therefore need to establish new analysis pipelines, which grant a better insight into the biological questions we are trying to answer.

1.3.2 Landscape of neuron types and properties.

The brain is composed of over 100 billion neurons, organized into complex circuits that enable the processing and transmission of information. Excitatory and inhibitory neurons work together to maintain a balance of activity within the brain. Neurons can be classified into different types, based on their anatomical and functional properties. The two major classes of neurons are the glutamatergic projection neurons (PNs) and the GABAergic interneurons (INs). PNs are the most abundant type of neurons, accounting for 80% of all cortical neurons (Lodato and Arlotta, 2015), while GABAergic INs account for 20% (Meyer et al., 2011). PNs primarily transmit electrical inputs between neurons and across brain areas, while INs have the essential function of sculpting network dynamics through feedback and feedforward inhibition, allowing for precise control of neural activity in circuits (Kepecs and Fishell, 2014).

The classification of neurons based on their anatomical and functional properties is fundamental in understanding their roles in neuronal circuits. While the complete array of PN and IN types is not fully understood, recent studies have shown that there is a great degree of molecular and functional diversity within these neuronal classes (Tasic et al., 2018; Tasic et al.; 2016). This diversity is reflected in the unique patterns of gene expression that define each type of neuron and is critical for their functional specificity. Recent studies support the idea that the orchestration of global and tissue/cell type-specific alternative splicing programs requires a deeper understanding of how splicing factors and cis and trans-acting elements interact and cooperate together (Zhang *et al.*, 2016). Identification of these molecular networks will help to elucidate the function of alternative splicing events and dissect new gene functions at the exon-level resolution in single neuronal classes.

Further, it is important to consider the circuitual organization that a certain neuronal population is forming. In fact, depending on the brain region, interneurons form diverse microcircuit motifs, each contributing to the specific functions of the neural network. For example, in the cerebral cortex, basket cells provide powerful feed-forward inhibition onto the soma of pyramidal

neurons. Another microcircuit motif in the cortex is formed by the dendrite-targeting interneurons, which selectively inhibit dendrites of pyramidal cells and modulate their integration of synaptic inputs (Isaacson & Scanziani, 2011). In contrast, in the olfactory bulb, inhibitory neurons provide lateral inhibition of circuits, meaning that they inhibit neighboring glutamatergic neurons making synapses onto their lateral dendrites, thus promoting competition and enhancing the selectivity of neural responses (Egger *et al.*, 2003).

In my thesis, I examined cellular phenotypes and molecular programs in GABAergic interneurons of the neocortex and glutamatergic neurons of the olfactory bulb microcircuits. For this reason, I will provide the functional and anatomical organization of these cell types and networks in the following sections:

Cortical Interneurons

Cortical interneurons, a type of inhibitory neuron, play a crucial role in regulating the activity of excitatory neurons within the cortex and are divided into several subtypes based on their morphology, electrophysiological properties, and neurochemistry. These neurons produce and release the neurotransmitter Gamma-aminobutyric acid (GABA) at their synaptic terminals, which generates an influx of ions, thus producing a hyperpolarizing effect in the postsynaptic neuron. Unlike PNs, INs mainly form synapses within the brain structure where their soma is located (Fishell & Kepecs, 2020; Kepecs & Fishell, 2014).

The cerebral cortex of mammals contains different subtypes of inhibitory neurons with different morphologies, electrophysiological properties, and connections within the neural circuits. Paul and colleagues (Paul *et al.*, 2017) showed that by using six genetically labeled GABAergic neuronal populations in the murine neocortex, genes involved in the regulation of synaptic properties appeared to be the major drivers of diversification and specification of neuronal identity.

Interneurons in the neocortex exhibit distinct differences in excitability, synapse placement, and morphology depending on their specific subtype, contributing to the overall complexity of cortical processing. Understanding these differences is essential to unravel the precise mechanisms underlying cortical information processing.

Parvalbumin positive (PV⁺) interneurons are a subtype of cortical interneurons that are characterized by the expression of the calcium-binding protein parvalbumin, and are fast-spiking interneurons, regulating the activity of pyramidal neurons within the cortex (Ferguson & Gao, 2018)(Marin, 2012). They have a small cell body and short dendrites, which means

that they have a limited spatial range of inhibition and they form synapses primarily with the soma of pyramidal neurons. On the other hand, Somatostatin (SST) interneurons fire action potentials at a moderate rate. They have long dendrites compared to PV interneurons and they primarily target dendrites of PNs (Riedemann, 2019).

Finally, other groups of INs are identified by the expression of specific markers such as the 5-hydroxytryptamine 3 serotonin receptor (5HT3aR), or the vaso-intestinal peptide (VIP). Despite the great heterogeneity of INs, they all contribute to the fine-tuning of synaptic and neuronal activity within the cortical circuit. The diversity in IN types allows for more precise control over the firing activity of pyramidal neurons, rather than just suppressing excitation. Moreover, VIP interneurons in cortex provide inhibition to Somatostatin positive interneurons, which in turn can disinhibit pyramidal neurons and enhance cortical activity (Apicella & Marchionni, 2022; Pi *et al.*, 2013; Riedemann, 2019).

Given the importance of INs in regulating brain function and maintaining excitatory/inhibitory balance, it is not surprising that defects in IN development and function have been linked to a wide range of neurological and neuropsychiatric disorders, such as epilepsy, schizophrenia, and autism spectrum disorders (ASDs) (Marín, 2012; Yizhar *et al.*, 2011).

1.3.3 The olfactory bulb: circuitry, molecular diversity and cellular plasticity

The sense of vision, hearing, smell, taste, and touch are essential tools we use in our everyday life to perceive and sense our environment. All the information we gather from the external world is integrated in higher areas of the CNS, which involves thousands of neurons that process the incoming signals to generate specific output reactions. In animals, senses are particularly important for survival in the wild. For example, a migratory bird's sense of direction and magneto-reception enables navigation over long distances and prey's sense of hearing or sight allows it to detect the presence of predators. Mice rely heavily on their sense of smell, which they use for essential functions such as looking for food, evading predators and for mating. Their olfactory epithelium has thus evolved to detect odorants with great sensitivity, which is achieved by the expression of a large variety of olfactory receptor (OR) genes (up to 1,000 compared to 350 in humans) (Imai, 2014; Malnic, 2007) and more developed sensorial system compared to humans.

When looking at a drawing of the olfactory murine system from Ramon y Cajal one can appreciate the level of complexity of this circuitry (Fig. 2). Here, many different cell-types with

diverse and sometimes opposite properties interact with each other to detect and correct stimulus processing.

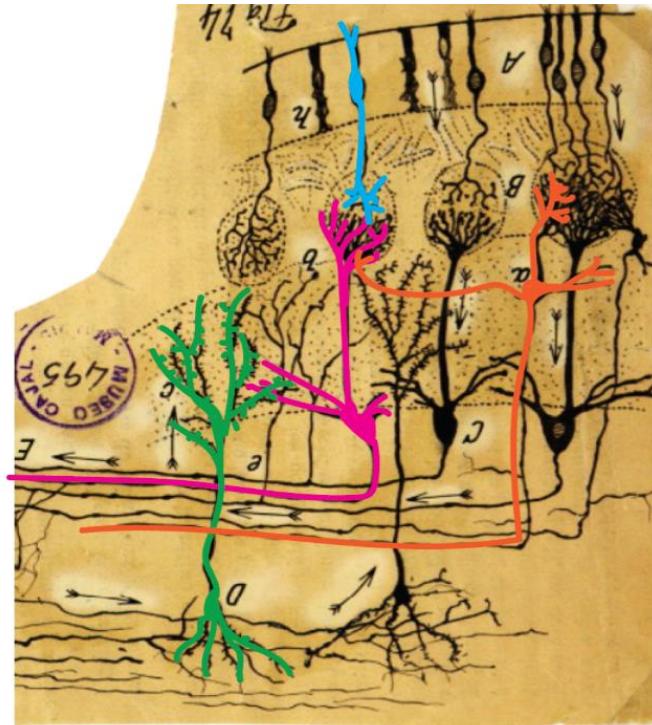


Figure 2: Drawing of neuronal cell types and circuitry of the murine olfactory bulb by Ramón y Cajal

Illustration of the olfactory bulb circuitry with additional modifications. In a simplified view: olfactory sensory neurons (in blue) sense the external environment and transfer information to the glomeruli, the functional units of the olfactory bulb, where they form synapses with mitral and tufted glutamatergic neurons (in magenta and orange, respectively). These neurons are the main output neurons of the olfactory bulb and send their axonal projections to higher olfactory cortical areas as well as to the amygdala and the ventral tegmental area, which are involved in memory formation and reward, which in turn feed-back to inhibitory granule cells of the olfactory bulb (neuron in green). These neurons make dendro-dendritic synapses with mitral and tufted cells to finely tune odor perception and association.

The main olfactory bulb (MOB) is the principal hub for odor processing (Fig.3A,3C), with major glutamatergic neurons transmitting the stimulus to higher cortical olfactory regions for the formation of odor memories and associations. Mitral and tufted cells axons are fasciculated and extend collaterals which project to different areas, amongst which the accessory olfactory nucleus (AON), the olfactory tubercle (OT), the entorhinal cortex and the piriform cortex (Macrides *et al.*, 1985). The piriform cortex is divided into two main regions: anterior (aPCX) and posterior (pPCX) and is a key brain area for odor association. While the axons of tufted neurons selectively innervate the anterior piriform cortex, mitral cells project to both areas; however, a definitive topographic map of the bulbofugal projection pattern to the olfactory

cortex has not been established yet (Macrides *et al.*, 1985; Nagayama *et al.*, 2010; Schoenfeld *et al.*, 1985).

Meanwhile, the MOB receives top-down inputs from central regions of the CNS and cortical areas, mapping out circuits that are pivotal for odor preference and odor memory formation. For example, odor-preferences in mice are in part shaped by connections from the ventral tegmental area (VTA) to the medial olfactory tubercle (mOT) (Zhang *et al.*, 2017). Dopaminergic (DAergic) neurons in these areas are involved in reward and olfaction. Optogenetic activation of VTA-mOT DAergic fibers leads to preference formation for space and neutral odor, while blockade of dopamine receptors in the mOT prevents odor-preference formation. Moreover, specific OT domains represent odor-induced distinct motivated behaviors (Murata *et al.*, 2015) and receive direct axonal inputs from OB tufted cells providing a possible pathway underlying behavioral phenotypes.

Other signals involved in odor responses and social recognition depend on the release of the neuropeptide oxytocin (OXT) (Oettl *et al.*, 2016). Evoked OXT release in the paraventricular nucleus (PVN) enhanced the intensity of olfactory exploration behaviors and improved recognition. Oxytocin activates the AON and its top-down projections to inhibitory granule cells in the MOB, driving inhibition of M/TCs, thus enhancing odor responses and improving social recognition. Finally, great relevance in the context of recognition and social interaction with conspecifics is represented by the vomeronasal system/organ (VNO), which senses pheromones, attractants, and repellents produced by individuals of the same or different species. Vomeronasal sensory neurons (VSNs) project to rostral or caudal regions of the accessory olfactory bulb (AOB) (Berghard & Buck, 1996; Dulac & Axel, 1995), regulating sex-specificity of behavioral responses (Dulac & Kimchi, 2007; Dulac & Wagner, 2006) (Fig.3B). Research conducted over several decades has established significant differences in the functional properties of the vomeronasal and olfactory systems, which are accompanied by distinct neural pathways (Halpern, 1987; Halpern & Martinez-Marcos, 2003). The anterior olfactory bulb (AOB), which is structurally organized similarly to the MOB, also contains mitral cells. However, these neurons project to different regions compared to mitral cells of the MOB, including the limbic system nuclei, the nucleus of the accessory olfactory tract and the medial amygdaloid nucleus. These areas further project to hypothalamic nuclei, which are associated with reproduction, aggression, and parental behavior (Kimoto *et al.*, 2005).

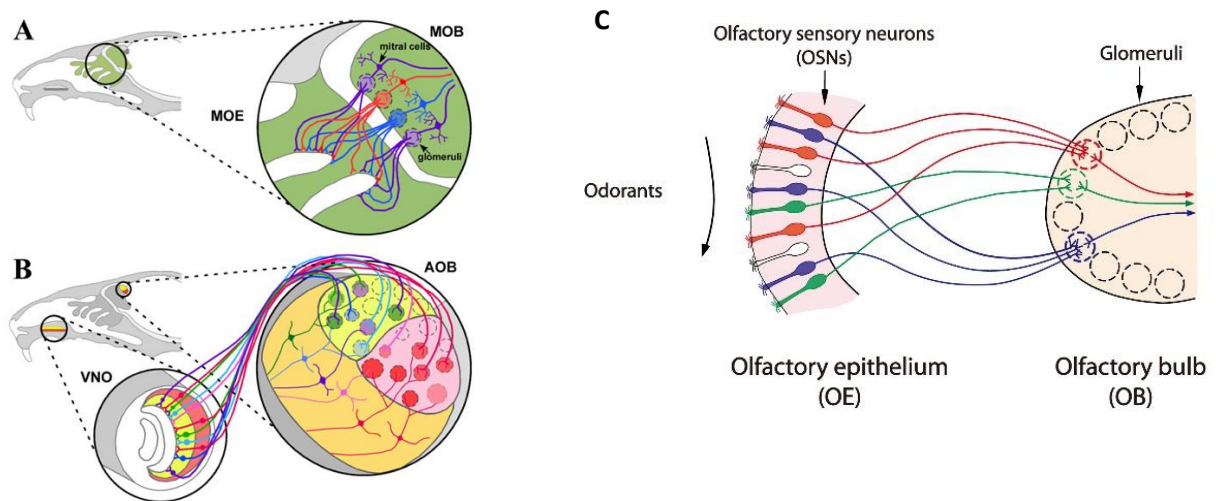


Figure 3: Cellular architecture and odor processing of the main olfactory and vomeronasal systems

A-B) Olfactory sensory neurons in the main olfactory epithelium (MOE) express specific odorant receptors and project to a specific glomerulus in the main olfactory bulb (MOB). Each mitral cell in the MOB receives inputs from only one type of sensory neuron, which results in little integration of signals. In contrast, the vomeronasal system (VNO) has sensory neurons segregated into apical and basal zones based on the position of their cell bodies (yellow and pink zones respectively). Based on their position in the VNO, neurons project to multiple glomeruli in the anterior or posterior half of the accessory olfactory bulb (AOB) (Adapted from Dulac and Wagner, 2006). C) Illustration showing the combinatorial receptor codes for odorants and how these are processed in the MOB. Each OSN expresses only one functional olfactory receptor (OR) gene. OSN axons expressing the same OR converge to a specific glomerulus in the OB, where each glomerulus represents one OR species (Adapted from Sakano et al.; 2010).

Structure and function of the MOB

The main olfactory bulb is composed of several layers (Nagayama *et al.*, 2014; Tufo *et al.*, 2022), the innermost of which is the granule cell layer (GCL), which is where aspiny inhibitory neurons reside and receive centrifugal innervation from the OB afferents. Moving towards the surface, the mitral cell layer (MCL) is home to glutamatergic neurons where the major output neurons of the olfactory system are mitral and tufted cells. The external plexiform layer (EPL) is a zone with few cell bodies (besides some middle-tufted cells and parvalbumin positive interneurons) but it is the region where granule cells make dendro-dendritic synapses onto the lateral dendrites of mitral and tufted neurons, enabling fine tuning of odor perception (Kersen *et al.*, 2022; Naritsuka *et al.*, 2009). Ultimately, mitral and tufted neurons extend their apical

tufts to the glomeruli, where they receive odor information from the external environment by making synapses with olfactory sensory neuron (OSN) axons. This synaptic organization closely resembles the connectivity among bipolar and horizontal receptor cells in the retina described in 1970 by Shepherd, which points towards the possibility of a similar mechanism of sensory processing between olfactory regions.

Specifically, odorant signals are encoded as an odor map of activated glomeruli in the olfactory bulb, with each odorant being recognized by specific combinations of odorant receptors (ORs) (Malnic *et al.*, 1999; Sakano, 2010; Takeuchi & Sakano, 2014). In fact, a single OR recognizes multiple odorants, and conversely, a single odorant is recognized by multiple ORs, therefore, different odorants are recognized by different OR combinations. This leads to the conversion of odorant signals received by olfactory sensory neurons (OSNs) in the olfactory epithelium into a two-dimensional map of activated glomeruli with varying activity levels in the olfactory bulb.

The olfactory bulb is a site of great synaptic plasticity. Throughout adulthood, neurons are generated by stem cells in the subventricular zone (SVZ), from where they migrate through the rostral migratory stream (RMS) and integrate into the olfactory circuitry (Chaker *et al.*, 2016; Fuentealba *et al.*, 2015). Based on their location in the niche, adult neural stem cells (NSCs) produce different subtypes of olfactory bulb interneurons (Merkle *et al.*, 2014). Granule cells are the major class of interneurons in the olfactory bulb. As a very diverse class of neurons, they were grouped into Type I, Type II and Type III based on the position of their soma in the GCL and which class of projection neurons they target for lateral inhibition (Egger *et al.*, 2005; Macrides *et al.*, 1985). In addition, recent research conducted in the laboratory of Prof. Fiona Doetsch has demonstrated that certain life events, such as fasting or pregnancy, can activate various pools of NSCs to promote temporary neurogenesis and gliogenesis (Paul *et al.* 2017, Chaker *et al.* 2021, Biorxiv). In the case of pregnancy, this process results in the sequential maturation of short-lived interneuron subtypes, which integrate in the olfactory bulb circuitry during the perinatal period, offering a new mechanism for spatio-temporal control of brain plasticity under specific physiological needs. During motherhood, mitral cells exhibit a type of cellular plasticity in response to social odors. This plasticity is characterized by an increase in inhibitory tone, which may play a role in the general reduction of responsiveness to odors and the simultaneous enhancement of the representation of specific biologically relevant odors (Vinograd *et al.*, 2017).

Finally, a form of synaptic plasticity associated with mitral cells upon social transmission of food preference (STFP) (Liu *et al.*, 2017; Loureiro *et al.*, 2019). The study shows that mice form long-term memory (up to 14 days) of food odors. This form of long-term potentiation (LTP)

of synaptic strength happens selectively at the GABAergic component of dendro-dendritic synapses of granule and mitral cells in the olfactory bulb. The combination of odor exposure in a social context elicits the secretion of the insulin-growth-factor (IGF1) from mitral cells and the recruitment of additional GABA receptors (GABA-R) in these neurons.

Mitral and Tufted cells of the olfactory bulb

Mitral and Tufted neurons (MC-T; cells respectively depicted in pink and orange in Fig.3), are very heterogeneous classes of glutamatergic neurons of the olfactory bulb (OB) and their responses are shaped by GABAergic inhibition in the glomerular and EPL layer, from short axon cells, granule cells and PV positive neurons. Since these cells receive inhibition mainly onto their secondary dendrites, morphology is critical for their functional properties. Mitral cells (MC) have a relatively simple dendritic tree and a large soma, while in contrast, the dendritic tree of tufted cells (TC) is much more complex. Moreover, while internal tufted neurons and mitral cells have wide and symmetrical dendritic arborization, more superficial TCs have progressively shorter and asymmetrical distribution of dendrites and a smaller receptive field than mitral cells. For example, it has been reported that one single mitral cell in the rabbit olfactory bulb has up to $\sim 15'000 \mu\text{m}$ of secondary dendrites, which is almost four times longer than that of middle tufted cells (Mori *et al.*, 1983).

Previously, these two classes of glutamatergic neurons had been primarily distinguished based on their soma laminar position in the OB, as well as by their morphology, soma shape, and position of lateral dendrites. Mitral cells are located exclusively in the mitral cell layer (MCL) and send their apical dendrites towards the glomeruli – the functional units of the OB – where they connect with olfactory sensory neurons (OSN), each expressing a specific odorant receptor. Furthermore, mitral cells are classified based on the location of their secondary dendrites in either more superficial or deep regions of the EPL (mitral cell type I and type II respectively), (Orona *et al.*, 1984). Tufted cells, in turn, can be found in three possible locations, internal tufted neurons in the MCL, middle tufted neurons in the external plexiform layer (EPL), and external tufted neurons also in the glomeruli layer.

Surprisingly, the belief that mitral cells make synapses in a single glomerulus thus receiving direct input from OSNs expressing a single type of odorant receptor, continues to persist and has to be further investigated (Kato *et al.*, 2012). However, by using two photon imaging, we sporadically observed also cases where one mitral cell had a bifurcation of its apical dendrite, therefore being able to reach out to two distinct but nearby glomeruli. The advent of scRNAseq has enabled a further categorization of these neurons based on their neurochemistry. As such, a recent study categorized these neurons into three different clusters based on the expression of marker genes, one of which being *Eomes* (*Tbr2*). Amongst others, *Pcdh21*, *vGlut2* and

Tbx21 appeared to be enriched in the same neuronal cluster (Tepe *et al.*, 2018). Additionally, differences in neurochemistry between different types of olfactory projection neurons have been observed, with medial and external tufted cells expressing dopamine and those within the glomerular layer being peptidergic (Hayar *et al.*, 2004; Sun *et al.*, 2020). Despite these advancements, there are currently no tools or marker genes available, which allow for the definitive distinction between mitral and tufted cells. Looking at the expression of these marker genes, neuronal tracing studies elucidated the presence of two distinct waves of glutamatergic neurons generated from different niches at different developmental stages (Roybon *et al.*, 2015). More specifically, ND1⁺ progenitors are generated from the sub-ependymal zone (SEZ) at embryonic day 15.5 (E15.5). This first wave of glutamatergic neurons differentiates into mitral cells and tufted cells and around one-third of them express the *Tbr2* marker at P0, and at P5. The same cells are also present in the GL. In the second wave, neurons originating from the dorsal region of the SVZ after birth, integrate into the granule cell layer (GCL) and express *vGlut1* and *vGlut2* markers as well as tufted neuron markers. The first wave of neurons is both *vGlut1*⁺ and *vGlut2*⁺ and during development these neurons transiently also express other markers such as *calbindin* and *calretinin*. However, after postnatal day 5 (P5), GABAergic markers are no longer expressed. Interestingly, a fate mapping study using BrdU incorporation in dividing neurons revealed that *tbr2*⁺, BrdU⁺ neurons in the RMS either lose *Tbr2* expression or fail to reach the olfactory bulb. No BrdU⁺, *Tbr2*⁺, *vglut2*⁺ neurons were observed in the OB, indicating that these neurons are not generated in adulthood but rather during embryonic development (Brill *et al.*, 2009).

Finally, mitral and tufted neurons have distinct intrinsic properties which allow them to play different roles in the processing of olfactory information. Mitral cells have a high degree of odor selectivity, allowing for a high firing rate. In addition, a fast action potential with a large amplitude and a relatively short duration and a high input resistance enables them to respond to small input changes. Tufted cells, on the other hand, have a slower firing rate with a smaller amplitude and a longer duration. While deep mitral cells and internal tufted neurons are less responsive to olfactory sensory neuron stimulation, superficial tufted and mitral cells have a higher probability of response and lower threshold for activation and a tendency for multiple spiking. Furthermore, when presented with different odorant concentrations, tufted cells are activated at lower concentrations, making them more sensitive than mitral cells. Mitral cells that are spatially close to each other respond similarly to odors and are thus called "sister cells", while distal cells, in turn, are regulated by different pools of granule cells and exhibit differences in odor selectivity (Kikuta *et al.*, 2013; Macrides *et al.*, 1985; Schoenfeld *et al.*, 1985).

In conclusion, different projection neurons sharply and heterogeneously tune odor information throughout experience and development.

1.4 How is transcriptomic diversity generated?

Despite the fact that the identity of neurons and their specific connections are, to a large extent, determined by their genetic information, the relationship between cellular diversity in neurons and the high level of specificity in their synaptic connections is not yet fully understood. Transcriptomic diversity is generated through a complex interplay between genetic and environmental factors (Gilbert, 2004). At the genetic level, transcriptomic diversity is driven by the presence of genetic mutations and genetic recombination. For example, genetic mutations can alter the sequence of a gene, leading to differences in the resulting mRNA transcript. Additionally, gene duplication events, which lead to the generation of paralogous proteins, can increase the complexity and diversity of biological systems, as they can provide backup functions or perform different roles in different tissues or under different conditions (Kaessman, 2010; Ohno et al.; 1970). Finally, environmental factors, such as temperature, nutrient availability, and exposure to toxins, can also impact the transcriptome by regulating the expression of genes. This regulation can be achieved through a variety of mechanisms, including epigenetic modifications, changes in chromatin structure, and the activation or repression of transcriptional regulatory elements. The complexity of these interactions means that the transcriptome of an organism can be highly dynamic and responsive to changing environmental conditions thus providing a fitness advantage in certain conditions (Liu *et al.*, 2022; McAllister *et al.*, 2017). Ultimately, the generation of transcriptomic diversity is a critical component of evolution, as it provides the raw material for the evolution of new functions and the adaptation to changing environmental conditions.

1.4.1 The power of alternative splicing

AS was first discovered in the 1970s by a group of scientists led by Philip Sharp and Richard J. Roberts. They found that the same gene could produce multiple different proteins through a process called alternative splicing (Berget *et al.*, 1977; Chow *et al.*, 1977). This discovery was extremely significant at the time, as the prevailing dogma was that one gene equaled one protein. Initially, it was thought that alternative splicing was a rare event, only seen in a few genes. However, subsequent research using high-throughput methods showed that this mechanism plays a much more significant role in gene expression than previously appreciated.

alternative splicing is highly conserved across species as it is fundamental to greatly increase the complexity and diversity of proteins that can be produced from a single gene. The full portfolio of isoforms alternative splicing can produce remains largely underestimated.

Similar to other regions in the brain, alternative splicing is critical for synaptic specification in the central nervous system (CNS). Gene ontology (GO) analysis of transcripts that undergo alternative splicing in different neuronal cell classes in the mouse cortex and hippocampus, indicate that the generation of transcript isoforms is particularly tailored to the production of proteins involved in synapse formation, specification and maintenance (Furlanis *et al.*, 2019; Gomez *et al.*, 2021; Vuong *et al.*, 2018). An example of the significant impact of alternative splicing on neuronal connectivity through remodeling of synapses, is the inclusion of an alternative exon in the segment 5 (AS5) of Neurexin 3 (Nrxn3) mRNA. This alteration results in a change in the NRXN3 protein, promoting the formation of a GPI-anchored protein. Notably, the absence of this isoform in a group of interneurons of the hippocampus, leads to changes in synaptic transmission at GABAergic presynaptic terminals in the dentate gyrus (Hauser *et al.*, 2022).

Another great example to illustrate the importance of alternative splicing is the specific homophilic self-recognition mechanism described in *Drosophila* for the *Dscam*. This process is unique to this organism and not found in vertebrates. The *Dscam* (Down syndrome cell adhesion molecule) gene encodes for a transmembrane receptor, whose extracellular domain composition can be altered by the stochastic selection and splicing of alternative exons (Schmucker *et al.*, 2000). More specifically, this gene can produce over 38'000 different transcripts, resulting in a vast diversity of protein isoforms and unique combination of *Dscam* in each neuron (Hattori *et al.*, 2007). In fact, due to the stochastic nature of the alternative splicing process, the probability of two neurons having the exact same set of *Dscam* isoforms is very low. This leads to a mechanism of self-recognition where neurons with similar *Dscam* isoform combinations are more likely to recognize and adhere to each other, while neurons with dissimilar *Dscam* isoform combinations are less likely to adhere. The high diversity generated through the alternative splicing of the *Dscam* pre-mRNA, allows each neuron to differentiate its own processes from those of other cells, contributing to the establishment of neural connection in the *Drosophila* nervous system.

Finally, mRNA transcription and alternative splicing can be strongly influenced by activity-dependent stimulation resulting in the production of different protein isoforms and leading to changes in neural function and plasticity. Thus, in response to changes in neuronal firing, alternative splicing can modulate the expression of ion channels, neurotransmitters receptors and intracellular signaling molecules, and therefore affect the electrical activity and

synaptic transmission and structural properties (Leslie and Nedivi, 2011; Yap and Greenberg, 2018) (Mauger *et al.*, 2016; Mazille *et al.*, 2022).

A great example for the activity-dependent production of protein isoforms is the regulation of the NMDA receptor1 (NR1) (Ehlers *et al.*, 1995). The NMDAR is a type of glutamate receptor that plays a critical role in synaptic plasticity and learning. Different studies have shown activity-dependent modulation of NMDA receptor1: when neurons are active, there is an increased inclusion of exon 21 in the final mRNA product, resulting in a different protein isoform with higher sensitivity to glutamate, associated with the formation of synaptic plasticity events. Moreover, inclusion of this cassette exon redirects the subcellular distribution of the NR1 receptor to plasma membrane (Ehlers *et al.*, 1995).

Alternative splicing is a process that can control the generation of isoforms with high spatio-temporal precision. Recent studies elucidated the mechanism through which intron-retaining transcripts can be specifically regulated upon various types of external stimuli, including neuronal activity (Braunschweig *et al.*, 2014; Shalgi *et al.*, 2014). Upon sustained neuronal depolarization, introns contained in pre-existing pools of immature transcripts can be excised and translocated to the cytosol, where they can be transported and used for protein synthesis (Mauger *et al.*, 2016; Mazille *et al.*, 2022). The control of gene expression programs in response to cues through intron retention and transcripts nuclear sequestration in neurons, plays a crucial role in the quick generation of protein products that are necessary for synaptic plasticity and learning. Finally, alternative splicing can control gene expression through transcript abundance and mRNA stability by targeting transcripts to nonsense-mediated mRNA decay (NMD) (Black, 2003; Lejeune and Maquat, 2005).

Type of alternative splicing patterns

At the molecular level, the splicing reaction is orchestrated by a macromolecular RNA-protein complex called spliceosome. The spliceosome consists of five small nuclear ribonucleoproteins (snRNPs - U1, U2, U4, U5 and U6) that interact with more than a hundred auxiliary proteins to coordinate splicing (Chen & Manley, 2009). One major aspect in constitutive or alternative pre-mRNA splicing is determining the appropriate combination of donor and acceptor sites to be connected after intron or exon removal. Exon/intron splice sites are characterized by special sequences: while at the 5'end there is a distinctive GU dinucleotides followed by non-conserved intronic sequence, the 3'end is characterized by the presence of a branch point, a polypyrimidine tract and a terminal AG base-pair. Additionally, also more distant sequences take part in the regulation of the splicing process. Indeed, exonic or intronic splicing enhancers (ESE) or silencers (ISE) are fundamental for the recruitment of

trans-acting factors such as RBPs, splicing factors and long non-coding RNAs (lncRNAs), which influence the efficiency of the splicing process (Black & Grabowski, 2003; Grabowski & Black, 2001; Marin & Muller, 2014; Park *et al.*, 2018) (Fig.4B).

Finally, the consecutive coupling of donor and acceptor splice sites results in the generation of mature mRNAs (Black, 2003; Breitbart *et al.*, 1987; Chen and Manley, 2009; Grabowski and Black).

The splicing pattern can be altered in many ways (Fig.4A): although the most common splicing event is the “cassette exon” (one single exon that is either incorporated or skipped in the mRNA isoforms), other times, multiple exons can be mutually exclusive. Moreover, exons can be altered in length at the 5’ end or 3’ end of the exons, resulting in the generation of variant mRNAs. Alternative splicing can occur also at untranslated regions (UTRs), influencing the stability and the localization of mRNAs.

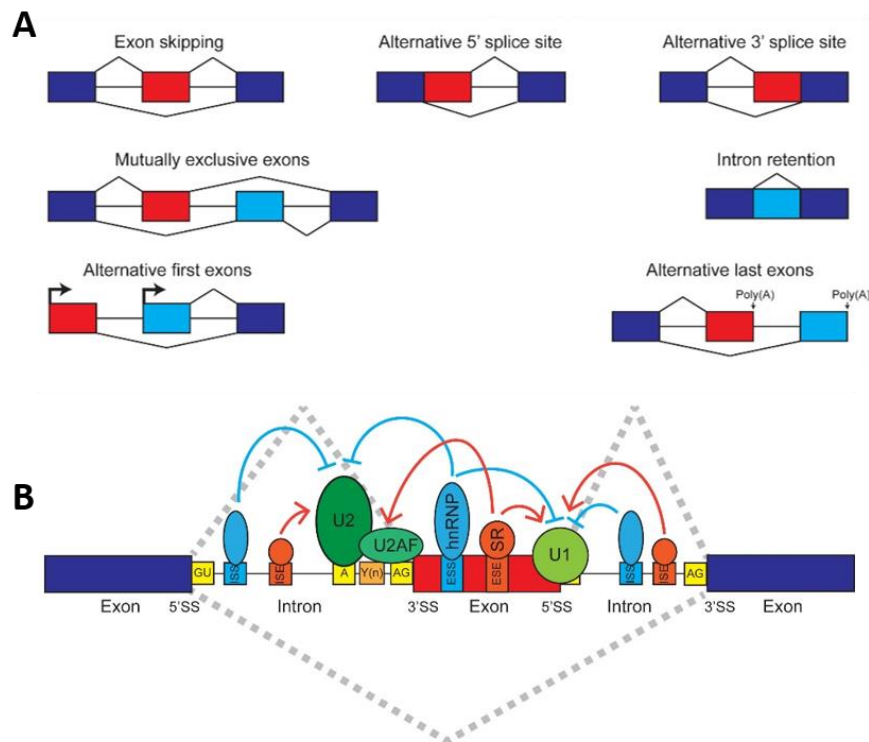


Figure 4: Schematic illustration of isoform diversification by alternative splicing regulation

A) Illustration of the different patterns of constitutive and alternative splicing regulation and resulting transcript isoforms. From the top: exon skipping, mutually exclusive exons, alternative first exon (left of the panel), Alternative 5' donor splice site (middle), Alternative 3' Acceptor splice site, intron retention, Alternative last exon (right). Constitutive exons are marked in blue, alternative exons in red. B) Schematic representation of Alternative regulation by an extensive array of RBPs (SR and hnRNP proteins) and spliceosome complex. The interaction network involves *cis* elements and *trans*-acting factors that bind to these *cis* elements. Within the pre-mRNA the 5'

splice site (5'SS), 3' splice site (3'SS), the branch site (A) and polypyrimidine tract (Y(n)) are in yellow. The U1- U2 snRNP complex and U2AF factors recognize these elements. Other proteins and co-factors in light blue and orange bind to Exonic splicing enhancers (ESEs), exonic splicing silencers (ESSs), intronic splicing enhancers (ISEs) and intronic splicing silencers (ISSs). Figure adapted from (Park et al.; 2018).

Beyond AS, two other events can have a big impact on the generation of transcript isoforms and therefore regulate protein function: alternative first exon usage (diverse transcription start sites usage, TSS) and alternative polyadenylation (APA). As 3'UTR regions harbors functional binding sequences for microRNAs, lncRNAs and RBPs, the different length of the polyadenylated tail of mRNAs can have a big impact on polyadenylation of the transcripts, therefore altering its stability or localization (Bae & Miura, 2020; Mayr, 2019; Mayr & Bartel, 2009). Furthermore, the presence of cis-acting and trans-acting elements in a certain transcript as well as the presence of RNA modification (e.g. RNA methylation N6-methyladenosine m6A) can be another ways through which regulation of RBPs and spliceosome recruitment is achieved (Dominissini *et al.*, 2012; Liu *et al.*, 2015; Ule *et al.*, 2006). Finally, there are evidences for epigenetic modification (e.g. DNA methylation) to be influencing recruitment and binding kinetics of proteins involved in transcription and splicing, therefore impacting the inclusion or exclusion of exons in a mature transcripts (Yearim *et al.*, 2015).

In conclusion, the interplay between alternative splicing and alternative TSS and APA serves as a mechanism for generating transcriptomic diversity and modulating protein function. Moreover, the degree at which an mRNA is alternatively spliced can be influenced by the binding of RBPs to either weak or strong splice sites.

Overall, genome-wide analyses have revealed a high prevalence of alternative splicing in neuronal tissue, suggesting a potential role in specifying neuronal cell identities and synaptic wiring properties. However, the intricate regulation and diversity of alternative splicing programs in neuronal subclasses, as well as the extent to which detected splice isoforms are translated into proteins, requires further investigations.

1.4.2 RNA-binding proteins: key post-transcriptional regulators

Brain function relies on complex assemblies of multiple types of neurons, each characterized by unique molecular, morphological, and functional properties. These cellular features are instructed by molecular mechanisms such as AS, which allow for the cell type-specific generation of transcript isoforms. RNA-binding proteins (RBPs) that are thought to play a role

in the regulation of alternative splicing of transcripts, which can lead to the development of specific neural subtypes. Hobert and colleagues (Hobert, 2016; Hobert & Kratsios, 2019) proposed that these so called “*terminal selectors*” are conserved across species, due to their key role in regulating AS, indicating that these proteins are crucial for the formation and maintenance of distinct neuronal subtypes. However, the molecular mechanisms that maintain the function of terminal selectors across species are not fully understood.

RNA-binding proteins interact with RNA molecules and play key roles in various post-transcriptional regulatory processes. They can bind to specific sequences on stretches of RNAs, modulating the stability, localization, translation, constitutive and alternative splicing of transcripts. Moreover, RBPs can also interact with other proteins and co-factors to form ribonucleoprotein complexes, which can further modulate the post-transcriptional fate of RNA molecules. For instance, the protein hnRNP L (heterogeneous nuclear ribonucleoprotein L) has been shown to bind to APE1 (apurinic/apyrimidinic endonuclease 1), an enzyme that is involved in DNA repair, and binding to Hnrnp L leads to its own down-regulation (Kuninger *et al.*, 2002). Another example of an RBP that participates in multiple cellular processes is RBM25. Although RBM25 has a primary function as a splicing factor, it can also be involved in the control of transcriptional processes by binding to the transcription factor Yin Yang 1 (YY1) (Xiao *et al.*, 2019).

An extensive study from the Yeo laboratory (Van Nostrand, Freese, *et al.*, 2020) characterized the function of more than 356 RBPs employing a combination of high-throughput techniques such as RNA-seq, cross-linking immunoprecipitation (CLIP)-seq, and mass spectrometry. They not only identified the RNA targets of a large number of human RBPs, but in addition, provided evidences of the functional roles of these proteins in regulating gene expression and other cellular processes by using cellular assays or computational methods to gain insights into the functional impact of RBP-RNA interactions. Collectively, this allowed the generation of a comprehensive map of the binding sites and RNA targets of human RBPs as well as a detailed understanding of their functional implications.

In summary, RBPs are involved in a wide range of biological processes, including development, cell differentiation, metabolism, and disease and their dysfunction has been linked to various human diseases, such as cancer, neurodegeneration, and developmental disorders.

RNA-binding protein families and their function in gene expression regulation

SR and hnRNP proteins are the two major classes of RNA-binding proteins (RBPs) that play key roles in the regulation of mature transcripts. The majority of proteins belonging to these two families are broadly expressed across tissues and are critical for the spliceosome

assembly. Serine-arginine (SR) repeat domain proteins are a family of RBPs that contain a SR rich domain, which allows binding to specific sequences on RNA molecules besides their involvement in promoting protein-protein interactions. SR repeat domain proteins primarily act by regulating AS, by binding to exonic and intronic *cis*-acting elements. For example, the protein SF2/ASF is an SR protein that promotes the inclusion of exons in pre-mRNA (Black, 2003; Ibrahim *et al.*, 2005).

Heterogeneous nuclear ribonucleoproteins (hnRNP) proteins, on the other hand, are a family of RBPs that are composed of different subfamilies, each with unique structural and functional characteristics. They are involved in many post-transcriptional regulatory processes such as splicing, transport, stability, and translation of RNA molecules. They have a variety of domains that bind RNA, including RRM (RNA recognition motif) and KH (hnRNP K homology) domains, in a sequence-specific or non-specific manner and they can form different ribonucleoprotein complexes with other proteins (Geuens *et al.*, 2016). For example, hnRNP A1 protein has many different RNA-binding domains (RBD) and it has been described to bind specific exonic splicing enhancer (ESE) sequences and exonic splicing silencer (ESS) sequences in the introns of pre-mRNA either promoting or inhibiting the inclusion of exons during splicing. However, hnRNP A1 can also bind to unstructured single-stranded RNA sequences or associate with poly(A) binding protein (PABP) to recruit polyadenylation factors, thereby promoting the formation of the poly(A) tail, which is necessary for mRNA stability and translation (Burd & Dreyfuss, 1994; Mayeda *et al.*, 1998).

Taken together, SR proteins and hnRNPs often play counteracting roles within the same splicing regulatory segment, as often, these are composed by clusters of several, overlapping binding sequences for these proteins (Caceres *et al.*, 1994; Han *et al.*, 2005).

1.4.3 Pan-neuronal vs. cell-class specific action of RBPs

In recent years, multiple studies suggested that alternative splicing frequency is higher in the CNS compared to other tissues, thus reflecting the complexity of neuronal circuits. In further support of the critical role of alternative splicing in neuronal cells, mutations in RBPs have been shown to drive alternative splicing programs in the brain, which in turn have been implicated in several neurodegenerative diseases (Licatalosi & Darnell, 2006). Therefore, the fine tuning of alternative splicing mechanisms may reflect the demand for molecular diversification as neuronal cells need to acquire unique morphological and physiological synaptic properties to ensure the correct operation of circuits.

While splicing regulators like NOVA Alternative Splicing Regulator 2 (*Nova2*) and RNA-Binding Fox-1 Homolog 1 (*Rbfox1*) are significantly expressed in most neurons of the mouse brain and have hundreds of target mRNAs (Saito *et al.*, 2019; Vuong *et al.*, 2018; Wamsley *et al.*, 2018a),

recent evidence suggests that the selective expression of splicing modulators in certain neuronal classes may contribute to the specification of neuronal and synaptic properties (Norris *et al.*, 2014; Traunmüller *et al.*, 2016; Traunmüller *et al.*, 2023). However, whether and how these cell type-specific splicing factors act to specify molecular programs in neurons is poorly understood.

The working mechanism of the splicing regulators NOVA1/2 or RBFOX1, which are significantly expressed in most neurons of the mouse brain, has been established by joint efforts of multiple laboratories (Saito *et al.*, 2019; Vuong *et al.*, 2018; Wamsley *et al.*, 2018a). Loss-of-function and CLIP-seq mapping studies suggest that each of these proteins has hundreds of target mRNAs in the mouse brain and that alternative splicing choices strongly depend on the motif position relative to the regulated exon. For instance, the binding of NOVA1/2 in intronic sequences upstream of an exon will likely cause the exon to be excluded from the final mature mRNA. However, when NOVA1/2 binds to regions downstream of the exon, it will likely result in the inclusion of it in the resulting transcript (Ule *et al.*, 2006). In general, most regulatory elements are located within ~ 300 bp from the splice sites. Moreover, these elements appear to be conserved across species, compared to more distal intronic regions, indicating their crucial role in alternative splicing choices (Barash *et al.*, 2010; Raj & Blencowe, 2015).

Numerous studies aimed to understand the role of splicing factors across different neuron classes in various brain areas. To this end, NOVA2 alternative splicing function was investigated in excitatory and inhibitory neurons, concluding that this factor has differential effects on alternative splicing in each cell class (Saito *et al.*, 2019). Research conducted in the Fishell lab also supports this notion, as the broadly expressed neuron-enriched splicing factor Rbfox1 regulates transcripts that have important neuronal functions and can control different splicing events in two non-overlapping neuronal populations, promoting broad phenotypes in mice (Wamsley *et al.*, 2018a). These examples demonstrate how the splicing code can be expanded, potentially resulting in opposite effects depending on the biological context. Beyond the action of broadly expressed RNA-binding proteins, recent evidence suggests that the selective expression of splicing modulators in certain neuron classes may contribute to neuronal diversification. The cell type-specific action of RBPs onto specific sets of target mRNAs raises the intriguing hypothesis that alternative splicing can shape neuronal connectivity in a cell type-specific manner (Furlanis *et al.*, 2019).

However, these proteins are broadly expressed across many neuronal cell classes and brain regions and the compelling hypothesis that there may be alternative splicing factors, which are uniquely expressed in certain cell types to fine-tune specific target transcripts AS,

remains to be further addressed. In particular, it was only recently elucidated whether RBPs exert specific actions within cardinal classes of interneurons. Studying the function of the splicing regulator Slm2 in a somatostatin positive (SST⁺) population of neurons in the murine hippocampus it was demonstrated that this protein is crucial for the alternative splicing of a restricted pool of target mRNAs which play a crucial role in the functioning of synapses (Traunmüller *et al.*, 2016)(Traunmüller *et al.*; 2023).

In summary, the studies described above suggest that alternative splicing programs in neurons arise from the complex interplay of multiple *cis* and *trans-acting factors* (RBPs) that are co-expressed and can either have antagonistic or synergistic effects. Although the logic of their regulatory mechanisms has yet to be fully understood, their action is dependent on cellular context and state. Whether and how these cell type-specific splicing factors act to drive such selective programs is, however, largely unknown. The collective evidence prompts us to further investigate the potential role and mechanism of cell-type specific RBPs expression in the acquisition of neuronal properties, ultimately shaping the complex neuronal networks

1.5 RNA-binding proteins “in sickness and in health”

RBPs are important post-transcriptional gene regulators that bind to specific RNA molecules to control their fate. The direct interaction helps regulating processes such as splicing, stability, localization, and translation. It is therefore of no surprise that RBPs are essential for the normal functioning of most cells and that they are involved in fundamental biological processes, including development, differentiation, and cellular stress responses (Glisovic *et al.*, 2008; Kishore *et al.*, 2010). Recent advances in RNA sequencing technologies and computational biology identified numerous RBPs and their specific RNA targets. As outlined in the following sections, understanding the mechanisms by which RBPs exert their functions on target RNAs under both physiological and pathological conditions, is essential for developing novel and effective diagnostic and therapeutic avenues (Brinegar & Cooper, 2016; Pilaz & Silver, 2015).

1.5.1 Roles of RBPs in disease state

So far, around 1500 RBPs have been identified in humans (Gerstberger *et al.*, 2014) and it is estimated that at least 15% of human genetic diseases arise from mutations that have downstream effect on mRNA splicing (Faustino & Cooper, 2003; Pagani & Baralle, 2004).

There are various examples where the balanced regulation of splicing factor abundance is determining tissue specification or disease development (Kalsotra *et al.*, 2008; Kanadia *et al.*, 2006) highlighting the importance of alternative splicing as a key regulatory mechanism in human biology. For example, splicing alterations are linked to cancer, autism spectrum disorder, and neurodegenerative diseases such as amyotrophic lateral sclerosis (ALS) (Cookson, 2017; David & Manley, 2010; Irimia *et al.*, 2014; Kaida *et al.*, 2012; Parikshak *et al.*, 2016; Quesnel-Vallieres *et al.*, 2016). Recent work highlighted a shared pathological mechanism observed for multiple RBPs. Specifically, it has been shown that mutations in the coding sequence of RBPs lead to the cytoplasmic translocation of these proteins and aggregation into phase-separated granules, thus promoting mRNA sequestration and regulation. This is well described for proteins such Fused in Sarcoma (FUS) and MATRIN3 (MATR3) and TAR DNA-binding protein 43 (TDP-43) proteins, which harbor the , 97% of ALS-associated genomic mutations (Ling *et al.*, 2013). Moreover, in addition to this pathological gain of function, the aberrant localization also prevents these proteins from exerting their canonical nuclear functions (e.g. AS), which likely contributes to disease pathology of ALS. For examples, TDP-43, which is part of the hnRNP-binding protein family it has diverse functions ranging from stabilization of mRNA to alternative splicing, where it mainly represses the inclusion of cassette exons or non-conserved cryptic exons (Baughn *et al.*, 2023; Humphrey *et al.*, 2017; Ling *et al.*, 2015; Ma *et al.*, 2022; Tan *et al.*, 2016)

In my thesis I focused on the study of the RNA-binding protein motif 20 (RBM20), a protein that we find selectively expressed in specific neuronal populations and whose function has extensively been described in the heart and skeletal muscle.

Very interestingly, all of the proteins described above share functional and structural homology with RBM20. In particular, MATRIN3, together with ZNF 638m are considered RBM20 paralogue proteins (Coelho *et al.*, 2016; Watanabe *et al.*, 2018). Paralogue proteins are homologous proteins that have originated from a single gene, but have evolved distinct functions due to genetic changes such as mutations, deletions, or insertions (Peterson *et al.*, 2009). Similarities in the genetic sequence lead to structural homology of at least parts of the resulting proteins. In the case of RBM20, there is more than 60% homology to MATRIN3 and ZNF 638 in the two ZNF domains, which are known to be involved in DNA binding (Upadhyay & Mackereth, 2020). However, while MATRIN3 and ZNF638 can bind to DNA and therefore potentially regulate gene expression by interacting with gene promoters, no association of RBM20 with chromatin regions has been described so far. In contrast, all three proteins can bind RNAs and are therefore involved in AS. Reporter deletion studies revealed that the ZNF2 motif at the C-terminus of RBM20 is essential for its splicing function (Upadhyay & Mackereth,

2020), even if no direct evidence exists that this motif directly binds RNA targets. The exact mechanism through which RBM20 C-terminal domain is regulating splicing therefore warrants further investigations.

From a functional perspective, MATR3 is regulating mRNA stability by sequestering mRNAs *via* binding to their 3' UTRs within phase-separated granules (Watanabe *et al.*, 2018). Mutant RBM20 upon translocation to the sarcoplasm of cardiomyocytes, also binds to the 3' UTRs of mRNAs and it has been observed to co-localize with P-bodies (Schneider *et al.*, 2020), similar to what has been described in neurodegenerative diseases such as Alzheimer's disease and ALS.

These insights gained into the role of RBM20 and other RBPs in pathobiology could likely have broader implications that go beyond neurodegenerative disease, as covered in more detail in the following sections.

RBM20- related pathobiology in the heart and skeletal muscle

RBM20 is an RNA-binding protein with two zinc finger (ZnF) domains, one RNA-recognition motif (RRM) RNA-binding domain (RBD) and an arginine/serine (RS)-rich region. The arginine-serine-arginine-serine-proline (RSRSP) stretch, which spans exon 6 to 11, is an important phosphorylation site and crucial for ensuring nuclear localization of RBM20 (Filippello *et al.*, 2013; Murayama *et al.*, 2018; Watanabe *et al.*, 2018). Mutations in the RS region or RRM domain of *Rbm20* have been linked to an aggressive form of dilated cardiomyopathy, which ultimately results in cardiac arrest in affected individuals (Parikh *et al.*, 2019). More than 44 pathogenic variants have been identified, however, the molecular bases linking RBM20 to the development of cardiomyopathy symptoms are still incompletely understood. What is known though, and extensively described in the literature, is that aberrant splicing of cardiac mRNA fundamentally disrupts contractile function of cardiomyocytes. Further, it has been hypothesized that the most severe DCM dysfunction is due to the combination of the loss of function phenotype linked to the alteration of alternative splicing and the gain of function of RBM20 mis-localization in the sarcoplasm (Fenix *et al.*, 2021; Schneider *et al.*, 2020). More detailed mechanistic insights into the role of RBM20 in disease development were provided by studies on the phenotypes arising from either RBM20 knock-out (KO) or a R636S mutation model in induced pluripotent stem cells derived cardiomyocytes (iPSC-CMs) (Fenix *et al.*, 2021). Intriguingly, the R636S mutant caused vast changes in the way the spliceosome interacted with RNA targets. In addition, and in accordance with previous observations on other mutants, the R636S mutants shifted RBM20's localization to the cytosol and induced its granular phase separation. Interestingly, in comparison to the effects of a total loss of RBM20

in KO models, the mutation-induced gain of function of cytosolic RBM20 had an even greater impact on cellular homeostasis.

While the involvement of specific mutations to certain domains in *Rbm20* gene is linked to the cardiac dysfunction, it remains controversial as to which of these conserved features is crucial for the correct regulation of cardiac alternative splicing. In fact, when Titin reporter mini-genes were over-expressed in non-cardiac cells, mutations in the RRM or ZNF domains did not alter exon repression.(Murayama *et al.*, 2018). In contrast, *Rbm20* Δ RRM mice show defects in splicing regulation of some known mRNA targets (*Camk1l1 δ* , *Ldb3*, *Ttn*). However, these mouse models did not present with a DCM-like phenotype, therefore suggesting that mutations in this RBM20 domain are necessary but not sufficient to generate full pathology (Watanabe *et al.*, 2018). It is worth mentioning though that DCM patients mainly have heterozygous mutations of RBM20 in the RSRSP stretch (aa 634-638 in mice), indicating that correct phosphorylation of these residues is fundamental for the correct nuclear localization of the protein. Characterization of a knock-in animal model for the mutated phosphorylation sites S637A and S639A showed alterations in splicing products, resembling the *Rbm20* knock-out phenotype observed in rats (Murayama *et al.*, 2018).

Along the same line, genome-edited pigs as well as reprogrammed cardiomyocytes (iPCS-CM) from patients with DCM carrying the homozygous R636S variant show an accumulation of RBM20 in the sarcoplasm in RNP granules. Electron microscopy analysis in pig cardiomyocytes revealed that these membrane-less granules (~300–500 nm in diameter) associate with actin microfilaments and thereby contribute to the generation of a cytoskeleton-linked liquid condensate mesh. The accumulation of these liquid droplets accounts for changes in cardiac homeostasis, thus contributing to the DCM pathobiology and leading to cardiac stiffness and arrhythmia (Schneider *et al.*, 2020).

1.5.2 RBM20: “The king of hearts”

In the 90’s, Merkin and colleagues (Merkin *et al.*, 2012) conducted an interesting study, in which they assessed the number of exons that were alternatively spliced across tissues and in different species throughout evolution. They first found that samples from the same tissue and those of individual species clustered well together. However, when looking at species with a larger evolutionary distance, a more intricate pattern came apparent. While tissues such as the brain and heart/muscle had splicing patterns that were conserved between mammals and chickens, samples from colon, kidney, liver, lung, and spleen clustered much better within individual species rather than by tissue across species. This suggests that alternative splicing

patterns specific to tissues other than brain and heart/muscle were less pronounced and thus less conserved. Based on these results, exon splicing is mostly affected by cell lineage-specific changes in regulatory elements and/or trans-acting factors rather than gene expression.

It is well-known that alternative splicing plays a pivotal role in development, homeostasis and disease states in the heart. There are many RBPs, which have been shown to be strongly involved in these processes. In particular, the antagonistic expression of CELF and MBNL RBPs has a critical role in balancing the temporal expression of numerous transcript isoforms during heart development (Kalsotra *et al.*, 2008). Another key regulator for cardiogenesis is the protein RBM24, which has been implicated in muscle-specific splicing events (Yang *et al.*, 2014). Moreover, it was recently shown that RBM24 and RBM20 cooperate to include exon 11 in *Ehn* transcripts, which is coding for a protein whose splice variants are expressed differentially during cardiac hypertrophy, thus promoting the expression of isoforms that prevent cardiomyocytes hypertrophic remodeling (Ito *et al.*, 2016). Interestingly, in the diseased heart, there appears to be a re-activation of the expression of selected fetal splice isoforms, such as the N2BA isoform of the TITIN protein. The N2BA isoform has a higher compliance or elasticity compared to the adult form of TITIN (Linke & Granzier, 1998; Linke *et al.*, 1998). A shift towards the expression of the fetal N2BA isoform may alter the mechanical properties of the heart and contribute to the progression of heart failure (Guo *et al.*, 2018). Similarly, sarco/endoplasmic reticulum Ca²⁺-ATPase (SERCA2a), an enzyme that pumps calcium ions into the sarcoplasmic reticulum, is highly expressed in the fetal heart, but its expression decreases after birth. In heart failure, there is often a downregulation of SERCA2a, which can impair calcium handling and contribute to contractile dysfunction (Sikkel *et al.*, 2014).

RBM20 has been crowned “king of the heart” as it is considered a master regulator of alternative splicing in this organ (Linke & Bucker, 2012). So far, RBM20’s function has only been characterized in the heart and skeletal muscle, due to its very high abundance in these tissues. RBM20 is a quite large protein (~150 kDa) and its main role is the tight regulation of the alternative splicing of transcripts important for muscle cytoskeletal structure and function. The most prominent of the transcripts targeted by RBM20 include key regulators of cardiac excitation–contraction coupling as Myomesin1 (*Myom1*), Tropomyosin (*Tpm*) and Titin (*Ttn*), while the latter is considered by far the most important. TTN is a large elastic protein found specifically in striated muscle (skeletal and heart muscle) and plays a significant role in generating diastolic force in cardiac cells. There are two classes of TITIN isoforms that result from AS: one is smaller (N2B) and stiffer, and the other is larger (N2BA) and more elastic. TITIN is the largest protein in the body (3-4 MDa in humans) and in mice it comprises 347

exons. RBM20 directly binds and regulates more than 160 of these exons, and the majority of binding sites are found in Proline, Glutamate, Valine and Lysine-rich (PEVK) regions (Linke *et al.*, 1998; Watanabe *et al.*, 2018). Abnormal changes in the ratio of the two different TITIN isoforms (N2B/N2BA) have been linked to both systolic and diastolic heart failure. Moreover, 80 circRNAs that are generated from the *titin* gene have been identified through circRNA profiling of human hearts (Khan *et al.*, 2016). Some of these were found to be regulated in dilated cardiomyopathy and were absent in RBM20 KO mice. Additionally, myocardial tissue from a patient carrying an RBM20 mutation showed severe alterations in *titin* circRNA production, specifically affecting those originating from the RBM20-regulated I-band region of the *Titin* transcript. Even though these new classes of non-coding molecules have possible functions in modulating DCM pathology, the underlying molecular mechanism requires further investigations (Khan *et al.*, 2016).

Besides *Titin*, other transcripts have been reported to be regulated by the heart's master splicing regulator RBM20 in different models (mice, rats, iPSCs derived cardiomyocytes and pig cardiomyocytes), including transcripts involved in ion transport and calcium signaling such as the Ca²⁺/Calmodulin dependent kinase II δ (*Camk11 δ*) and the pore-forming subunit of the L-type voltage-gated-calcium channel (VGCC), *Cacna1c* (Briganti *et al.*, 2020; Fenix *et al.*, 2021; Guo *et al.*, 2012; Guo *et al.*, 2018; Maatz *et al.*, 2014). Moreover, *Rbm20* mutation in specific domains and even its loss has been associated with ~ 3% of cases of a form of familial arrhythmogenic cardiomyopathy (DCM) induced by altered calcium handling. Although the molecular signaling through which RBM20 induces the disease remains poorly understood, a recent study suggests that beyond the aberrant splicing phenotype, *Rbm20* pathogenic mutation promotes RBM20 sarcoplasmic accumulation in ribonucleoprotein granules, thus inducing cellular pathobiology (Fenix *et al.*, 2021). Interestingly, recent evidence indicates that RBM20 is differentially expressed across skeletal muscles and it mediates splicing in a muscle-type specific manner in response to thyroid and insulin hormone levels. Moreover, the PI3K/Akt/mTOR signaling pathway was found to be involved in the regulation of RBM20 dependent isoform switching of *Ttn*, *Camk11 δ* and *Camk11 γ* (Maimaiti *et al.*, 2021).

From a therapeutic perspective, targeting RBM20 could be a solution for treating diastolic dysfunctions, as shown in disease models by modulating *Ttn* pre-mRNA splicing to enhance titin compliance. This approach led to the successful rescue of phenotypes, highlighting the promising nature of RBM20 as a candidate target (Watanabe *et al.*, 2018).

In summary, various pathogenic variants have been identified in the *Rbm20* genomic sequence in patients with DCM and the function and targets of RBM20 have been extensively investigated in the heart and related pathologies. However, RBM20 expression in other organs

has never been reported and therefore no brain-related phenotype has been described yet in patients carrying *Rbm20* mutations (Parikh *et al.*, 2019).

Considering the importance of ions in neuronal synaptic transmission and the shared excitability properties of both neuronal and cardiac cells, the main hypothesis of my project was that RBM20 in the brain could act as a cell type-specific splicing regulator to shape intrinsic and synaptic properties of neurons.

Rationale of this thesis

Alternative splicing is a key mechanism in regulating neuron-specific gene expression (Raj and Blencowe, 2015; Schreiner et al., 2014; Zheng and Black, 2013; Zheng et al., 2013). As central effectors of alternative splicing-regulated gene expression, RNA-binding proteins (RBPs) are broadly expressed across the brain. Accordingly, a plethora of RBPs has been implicated in controlling developmental and neuron-specific alternative splicing programs, with single proteins regulating hundreds of target transcripts (Li et al., 2014; Quesnel-Vallieres et al., 2015; Ule et al., 2005). Interestingly, however, some RBPs are only selectively expressed in subpopulations of neurons, raising the possibility that they may control cell type specification and neuronal properties (Norris et al., 2014; Traunmuller et al., 2023). The combinatorial action of broadly expressed and cell-type specific alternative splicing factors, may provide a mechanism to establish distinct neuronal populations and to specialize the central nervous system in higher organisms.

Previous research in the Scheiffele laboratory has identified RBPs that are enriched in specific classes of neurons in the mouse cortex and hippocampus (Furlanis et al., 2019). However, whether and how these proteins are involved in modulating the cell type-specific alternative splicing program or gene expression, is largely unknown. One of these RBPs is RNA-binding motif protein 20 (RBM20). RBM20 has previously been characterized in the heart and in skeletal muscle, where it exhibits a highly-specialized role in controlling transcripts involved in core functions of the cells forming these tissues (Nakka *et al.*, 2018). So far, single gene studies have only partially described whether and how RBPs have the power to determine intrinsic and synapse specific neuronal properties. Given its critical function in cell-type specialization in muscle, combined with the selective expression in specific neuronal populations, RBM20 is a strong candidate for having the power to shape fundamental neuronal properties.

In my PhD-thesis, I therefore set out to comprehensively assess RBM20's function in the brain. To this end, the thesis has three aims that are addressed in three chapters:

1. Map RBM20 expression in the mouse brain
2. Identify RBM20 direct mRNA targets in the brain and elucidate the transcriptional modulation induced by RBM20 on transcripts
3. Uncover the functional impact of RBM20 in neurons

2. Results

Chapter1

Mapping RBM20 cell type-specific expression in the brain

Preface

In the first part of my thesis, I systematically assessed RBM20 transcript and protein expression across the mouse brain, as well as determined its subcellular localization. To do so, I used a combination of RNA fluorescent *in situ* hybridization (FISH) to detect and quantify amounts of *Rbm20* transcript in different neuronal classes and immunohistochemistry methods, for which I raised an antibody against the C-terminal domain of the RBM20 protein. In cardiomyocyte nuclei, RBM20's localization appears to be restricted to specific nuclear foci in close proximity to *Titin* transcripts, which serve as a backbone for recruitment and formation of a RBM20-dependent splicing factory (Bertero et al., 2019). As *Titin* is not expressed in the brain, I further surveyed the sub-nuclear localization of RBM20 in neurons and directly compared it to the heart. My work provides a pioneer example of the characterization of one RBP expression and function in two structurally and functionally distinct tissues.

Results

To identify RNA-binding proteins (RBPs) that could be involved in cell type-specific alternative splicing programs, we screened existing RiboTRAP-sequencing data (Furlanis *et al.*, 2019) for RBPs that are highly enriched in genetically-defined neocortical cell populations. In line with previous reports (Hu *et al.*, 2018; Saito *et al.*, 2019; Wamsley *et al.*, 2018a), we observed that most RBPs and splicing factors were broadly expressed in different neuronal populations. However, others exhibited a more specific pattern and were expressed only in defined neuronal classes, suggesting that they may play a role in driving cell type-specific alternative splicing programs (Traunmuller *et al.*, 2016). From these cell population-specific factors, we identified six candidates, which 1) presented a highly significant enrichment in their corresponding cell populations, 2) showed a discrete absolute gene expression and 3) have not been extensively characterized for their function in the brain so far: *Rbm20*, *Srsf5*, *hnRNPI*, *srsf12*, *RbmX* and *Raver2*.

Of these candidates, we then focused on *Rbm20*, because it was predicted to be exclusively expressed in a population of GABAergic Parvalbumin positive (PV⁺) neurons in the neocortex (Furlanis *et al.*; 2019). This is of particular interest as up to date, *Rbm20* expression was never identified in the brain.

Subsequent semi-quantitative PCR of the original RiboTRAP samples used for sequencing confirmed the results obtained with sequencing (Suppl. Fig. 1A). To get deeper insights into the expression pattern of *Rbm20* mRNA in different neuronal cell types, we performed fluorescent *in situ* hybridization (FISH) on brain tissue slices of mice expressing the

tdtomato reporter under cell type-specific promoters. More specifically, we used a Ca²⁺/calmodulin-dependent protein kinase 2 (CamK2-Cre) mouse line to target neocortical pyramidal cells and somatostatin-Cre (SST-Cre), parvalbumin-Cre (PV-Cre) and vasointestinal peptide-Cre (VIP-Cre) mouse lines to target the three major populations of cortical interneurons (Fig. 5B). These experiments revealed that expression of *Rbm20* in layer 5 (L5) of the somatosensory cortex (S1) is mainly selective for PV⁺ neurons and a subpopulation of SST⁺ interneurons (Fig. 5A-C). In addition, *Rbm20* expression was detected in various other brain regions, including the sub-thalamic region, nuclei in the brain stem, and surprisingly, in the Mitral Cell Layer (MCL) and Granule Cell Layer (GL) of the olfactory bulb, where deep and superficial glutamatergic neurons reside (Macrides *et al.*, 1985) (Suppl. Fig. 1B).

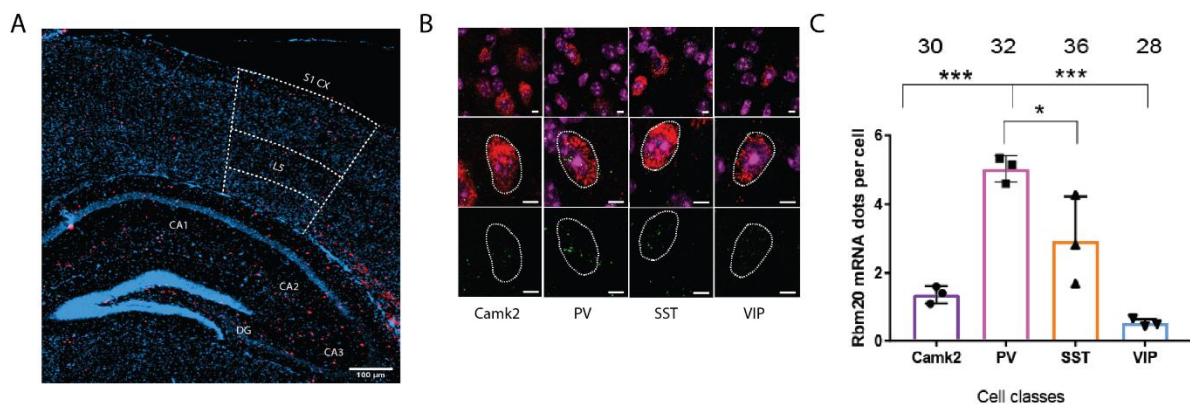


Figure 5: Characterization of Rbm20 mRNA expression in cortical neurons

A) Fluorescent *in situ* hybridization (FISH) of tissue brain slices from mice expressing tdtomato reporter under a cell type specific promoter. The layer 5 (L5) of the somatosensory cortex, is highlighted in the picture, Red: tdtomato, Blue: DAPI. Scale bar 100 μ m; B) Example of tdtomato⁺ cells in the four cell classes expressing different levels of *rbm20* transcript. Scale bar 10 μ m. C) Quantification of *Rbm20* mRNA expression in different cell types of the somatosensory cortex (CamkII, PV, SST, VIP), as absolute number of fluorescent dots per cell. $p < 0.01$ one way anova, N=3.

To obtain a more detailed characterization of these populations of neurons in the olfactory bulb, we performed FISH for a set of molecular markers. We found that the Glutamate decarboxylase 1 (*Gad1*), one of the key markers of inhibitory neurons, expression did not co-localize with *Rbm20* mRNA in these neurons, thus confirming the glutamatergic nature of these cells (Suppl. Fig. 1D).

Next, to further validate and quantitatively evaluate the expression of *Rbm20* in these regions, we conducted FISH on tissue slices of the olfactory bulb for *Rbm20* as well as for *Tbr2* and

vGlut2, two well-established excitatory markers for both the MCL and GL. This revealed that 47%, 31%, and 34% of neurons in the MCL were positive for *Rbm20*, *vGlut2*, and *Tbr2*, respectively (Suppl. Fig. 1C). Interestingly, when only looking at the expression of *Rbm20*, positive cells presented as two distinct populations, which either showed high (High *Rbm20*) or much lower (Low *Rbm20*) *Rbm20* expression. For the quantification of *Rbm20* co-localization with the excitatory markers, we therefore separately analyzed High and Low *Rbm20* neurons. While 91% of cells in the MCL and 79% in the GL were expressing high levels of *Rbm20* co-localized with *vGlut2*⁺ and *Tbr2*⁺ neurons, in cells expressing low levels of *Rbm20* mRNA, this number was reduced to 26% in the MCL and 48% in the GL (Fig. 6B).

Collectively, our findings suggest that the majority of cells expressing high levels of *Rbm20* also co-localize with glutamatergic markers (Fig. 6A and B). In contrast, few neurons in the MCL express low levels of *Rbm20* and do not appear to co-localize with glutamatergic markers (Fig. 6B). These neurons have a smaller nuclear size when compared to mitral and tufted cells, and despite their soma being physically located in the MCL, they likely express the inhibitory marker *Gad1* (Suppl. Fig. 1D).

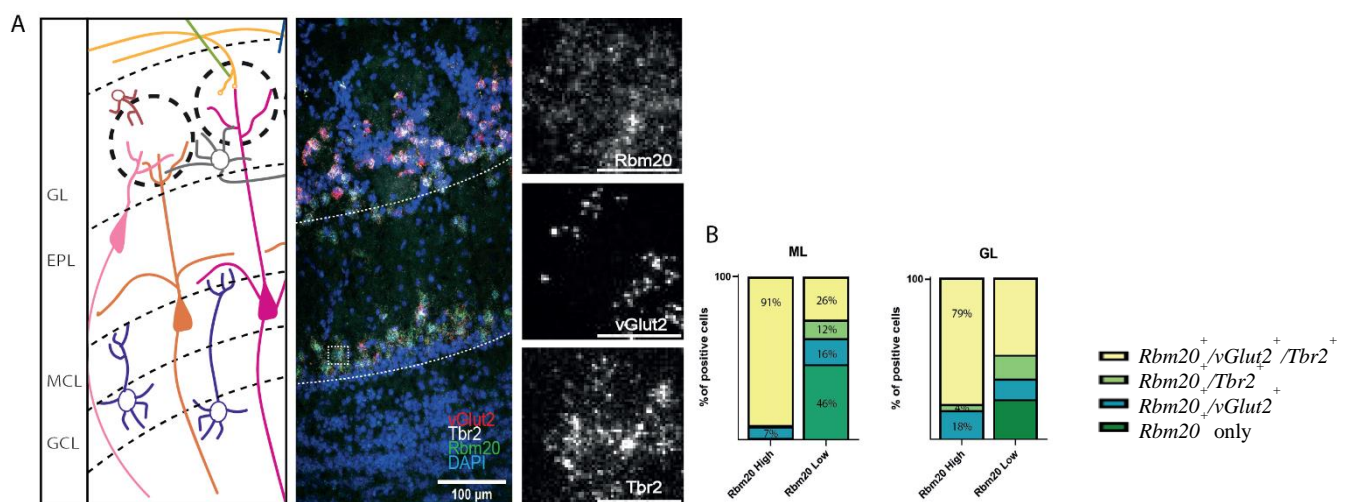


Figure 6: Panel illustrating *Rbm20* expression in the olfactory bulb

A) Schematic illustration of the olfactory bulb circuitry and cell types. GL: glomerular layer, EPL: external plexiform layer, MCL: mitral cell layer, GCL: granule cell layer, (left). Fluorescent *in situ* hybridization (FISH) on brain slices of *Rbm20* (green), *Tbr2* (gray), *vGlut2* (red) mRNA (middle). The insets show an example of a cell expressing all three markers (right). Scale bar 100 μ m; scale bar insets: 10 μ m. B) Quantification of the percentage of neurons of the mitral cell layer (ML) and glomerular layer (GL) expressing high or low *Rbm20* mRNA levels, co-localizing with *Tbr2* and *vGlut2* markers.

To corroborate the expression and subcellular distribution of RBM20 on the protein level in the brain, we raised an antibody against the C-terminal region of endogenous RBM20, as shown

in (Suppl. Fig. 1E). With this antibody, we confirmed the presence of RBM20 in various brain regions, included cortical areas outside S1, such as the motor cortex (M1) and the visual cortex (V1), where lower levels of RBM20 appeared expressed also in principal neurons labelled by the vGlut2Cre::Rpl22HA mouse line (Suppl. Fig. 1F). Moreover, RBM20 in the MCL of the olfactory bulb was found to be expressed already at P0 in neurons labelled by the td-tomato reporter, selectively expressed in *Tbx21*⁺ cells expressing Cre recombinase (Tbx21Cre mice) (Fig. 7A). However, at this developmental stage, only few neurons were found expressing RBM20 in the glomeruli layer and the td-tomato reporter was also not visible in this region. This hints towards the idea that the glutamatergic neurons expressing RBM20 in the GL may either not have reached their final location (they may still be migrating) or they may not have turned on RBM20 expression yet.

Additionally, in a pilot experiment I observed that RBM20-expressing neurons in the olfactory bulb did not express the inhibitory granule cell markers Calretinin (encoded by the *Calb2* gene) (Brill *et al.*, 2009). Furthermore, *Rbm20*-expressing mitral and tufted neurons were lacking the microtubule associated protein Doublecortin (DCX), which labels immature neurons (Merz & Lie, 2013), and the Neuronal nuclei (NeuN) protein (Suppl. Fig. 1G), feature typically observed only in mitral cells in the olfactory bulb and Purkinje neurons in the cerebellum (Kumar & Buckmaster, 2007). Finally, RBM20's co-localization with glutamatergic markers (labelled with the vGlut2Cre :: Rpl22HA mouse line) and absence in PV⁺ neurons in the olfactory bulb (as shown in Fig. 7B), further supported the notion that RBM20 expression is not associated with the type of neurotransmitter the latter type of cells release. Indeed, while RBM20 is expressed in GABAergic neurons PV⁺ in the neocortex, the cells in the olfactory bulb release Glutamate. This notion hints towards the possibility that RBM20 may thus contribute to the functional divergence of neuronal classes (e.g., by instructing specific aspects of neuronal properties and synapse specification).

In an effort to verify the identity of mitral cells and reveal the structure of mitral and tufted neurons, we used viral retrograde labeling of these cells by injecting a retroAAV2-syn-Cre virus into the posterior piriform cortex (pPirCX) of Ai9-tdtomato floxed mice (Fig. 7C and D). The piriform cortex is an olfactory cortical region where both mitral and tufted output neurons project their axons (Schoenfeld *et al.*, 1985). However, while mitral cells project to both anterior and posterior pirCX, tufted neurons only project to the anterior region. It is well established that diverse sub-populations of mitral cells exist and that they can be classified based on the shape of their soma and their dendritic position in the olfactory bulb (Macrides *et. al.*; 1985). Thus,

based on the assessed parameters, our experiments confirmed the expression of RBM20 in a heterogeneous population of back-labeled mitral cells (Fig. 7C).

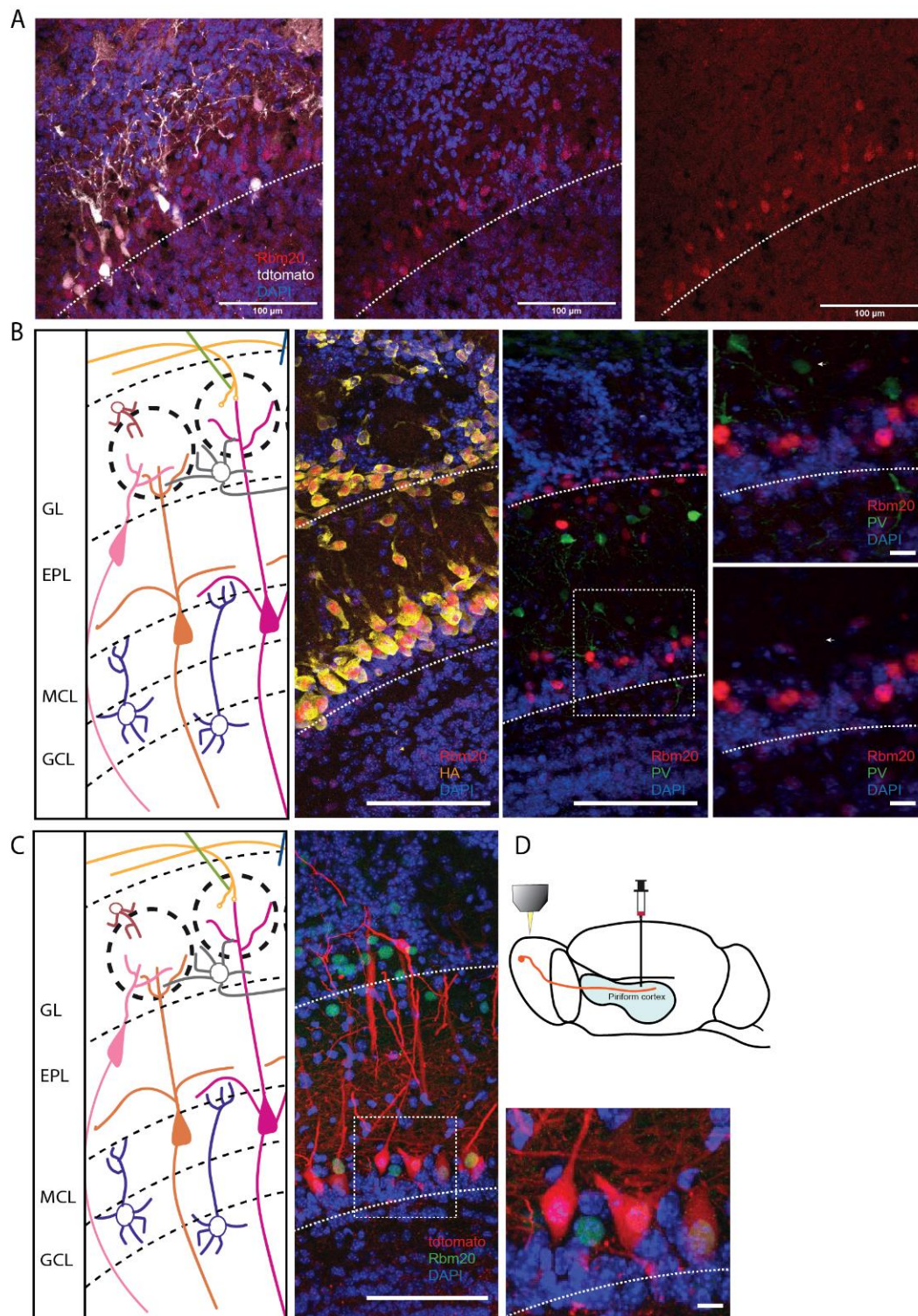


Figure 7: Characterization of RBM20 expression in olfactory bulb neurons

A) Immunofluorescence of RBM20 (red) expression in the mitral cell layer (MCL) of P0 Tbx21Cre mice. MCL neurons are labelled with tdtomato reporter (gray). Scale bar 100 μ m. B) Schematic illustration of the olfactory bulb

circuitry and cell types (left), RBM20 expression (red) is specific to the mitral cell layer and glomeruli layer of the olfactory bulb identified in the vGlut2Cre :: Rpl22HA mouse line (HA staining in orange) (middle). Scale bar 100 μm . The insets show that RBM20 is lacking in parvalbumin positive interneurons (green) (right). Scale bar 10 μm . C) RBM20-positive (green) mitral cells back-labeled through injection of retroAAV2-syn-Cre virus (red) in Piriform Cortex of a CAG-tdtomato floxed mouse at P35. Scale bar 100 μm . Inset scale bar 10 μm .

Characterization of *Rbm20* sub nuclear localization in neurons

Leveraging the specificity of the RBM20 antibody, we further investigated the sub-nuclear localization of the RBM20 protein in neurons. Previous research has shown that, in cardiomyocytes, RBM20 specifically localizes to two foci, which appear as two distinct and intense dots in immunofluorescence staining (Fenix *et al.*, 2021; Schneider *et al.*, 2020). This is likely due to the tethering of RBM20 by *Titin* pre-mRNA, which is its primary target in the heart. The *Titin*-induced proximity promotes the formation of an RBM20 "splicing factory" by allowing other RBM20 target genes to come closer to these foci through chromatin reorganization (Bertero *et al.*, 2019) (Fig. 8A). While we were able to reproduce this localization pattern in heart tissue slices from wild-type (WT) animals, the RBM20 immunofluorescence signal in neurons of the olfactory bulb was found to be much more dispersed throughout the nucleoplasm (Fig. 8B). This suggests that in the absence of *Titin* pre-mRNA, which is not expressed in the brain, RBM20 does not nucleate into foci as there is no other splicing target in neurons to guide RBM20 to a specific chromosomal locus. Based on the observed differences in protein sub-nuclear localization between cardiomyocytes and neurons, one may speculate that RBM20 has distinct roles in neurons, which have yet to be explored.

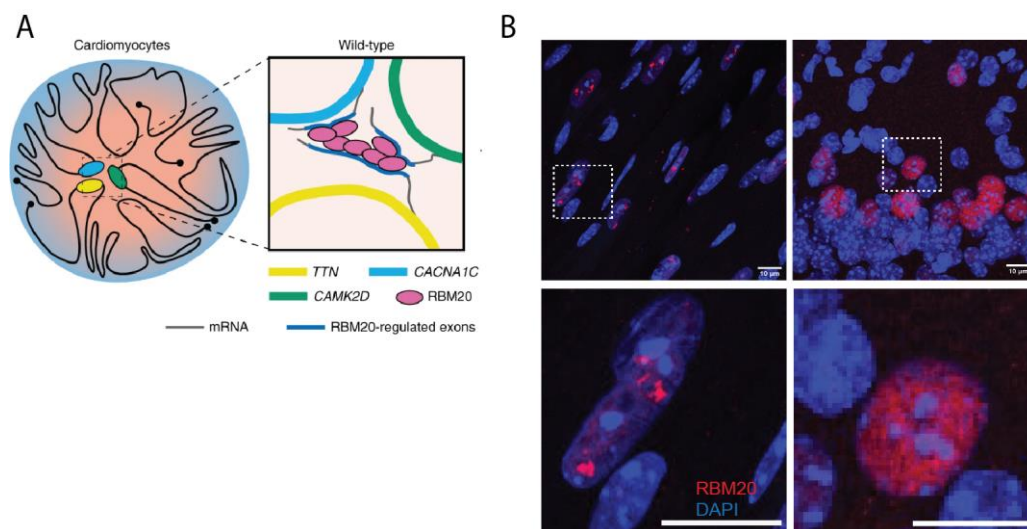
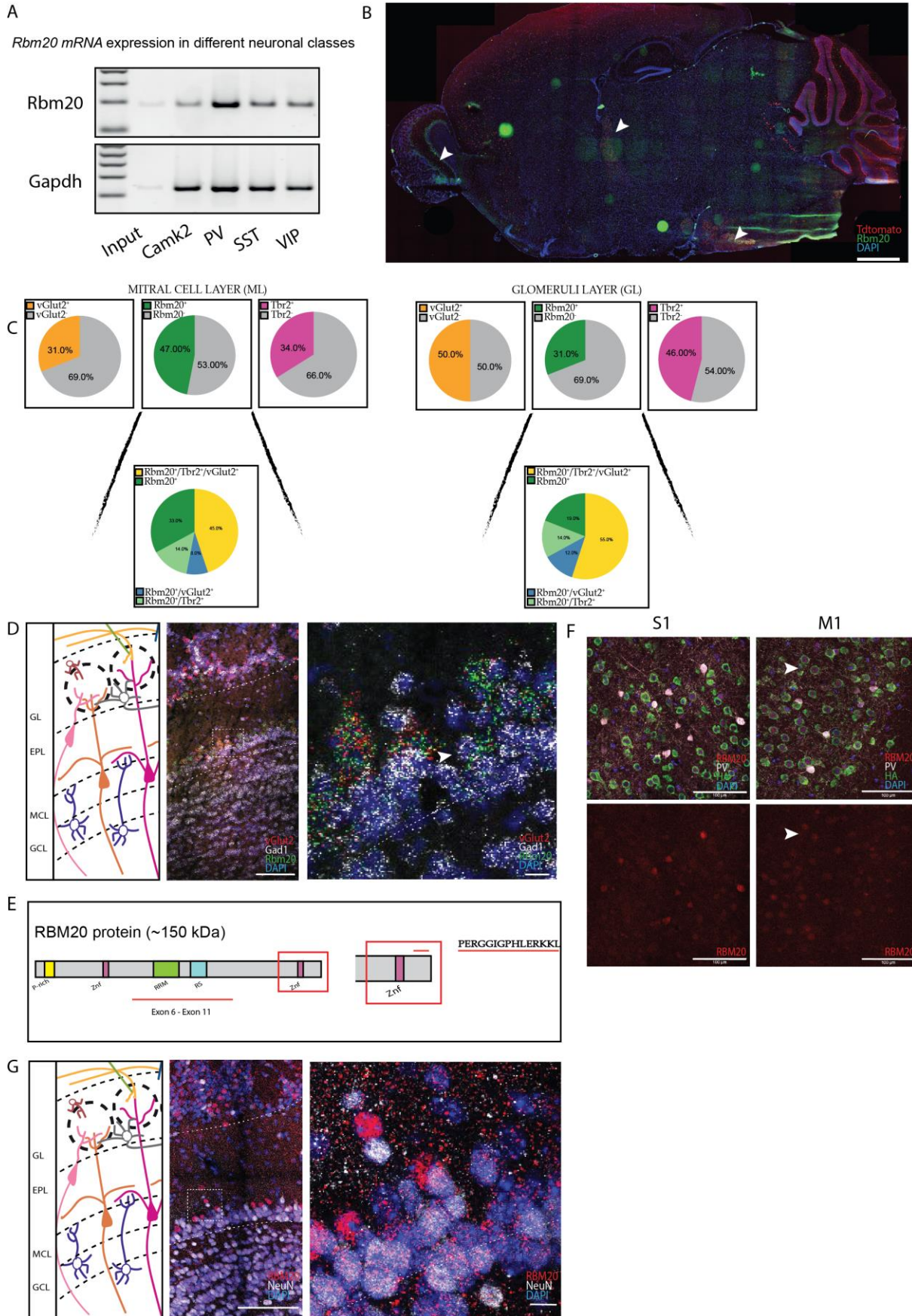


Figure 8: Sub-nuclear localization of RBM20

A) Representation of RBM20 "splicing factory". *Cacna1c* and *Camk1lδ* target genes come closer to *Titin* foci through chromatin reorganization. Adapted from (Bertero *et al.*, 2019). B) RBM20 (red) in heart cardiomyocytes (left) and mitral cells of the olfactory bulb (right) of WT mice at P35. Scale bar 10 μ m.



Supplementary Figure 1: Characterization of Rbm20 expression in the brain

A) Semi-quantitative PCR of the original RiboTRAP samples from different genetically-defined neocortical cell populations. B) Sagittal section of murine brain used for FISH of *Rbm20* (green) and *tdtomato* reporter (red) transcripts (*tdtomato* is identifying PV⁺ neurons). The arrows indicate brain regions where *Rbm20* mRNA was identified. Scale bar 1 mm. C) Pie charts indicating the quantification of the percentage of cells of the MCL and GL expressing *vGlut2*, *Rbm20* and *Tbr2* transcripts. Amongst the *Rbm20*⁺ cells, the percentage of neurons presenting co-localization with glutamatergic markers was calculated. D). Fluorescent *in situ* hybridization (FISH) on brain slices of *Rbm20* (green), *Gad1* (gray), *vGlut2* (red) mRNAs. Scale bar 100 μ m. The arrow in the inset on the right of the panel shows an example of a cell expressing low *Rbm20* levels and co-localizing with *Gad1* marker but not with *vGlut2* marker. Inset scale bar: 10 μ m. E) Predicted Rbm20 domain structure. The inset indicates the C-terminal region and the sequence and of the epitope used to raise RBM20 specific antibody. F) RBM20 expression in the somatosensory (S1) and motor (M1) cortex. While in the somatosensory cortex RBM20 (red) is mainly expressed in PV⁺ neurons (gray), in the motor cortex RBM20 expression is visible also in *vGlut2*Cre :: Rpl22HA neurons (HA stained in green), (example indicated with white arrow). Scale bar 100 μ m. G) representation of RBM20 protein expression in the MCL and GL in neurons which are not expressing NeuN. Scale bar 100 μ m. Inset scale bar 10 μ m.

Chapter 2:

Identify RBM20 direct mRNA targets and elucidate the transcriptional modulation induced by RBM20 in the brain

Preface

Single gene studies for selected RBPs such as NOVA2, RBFOX1 or PTBs have demonstrated the importance of RBPs for neuronal function (Saito et al., 2019; Wamsley et al., 2018; Zhang et al., 2019). However, these proteins are broadly expressed in neuronal tissue. In chapter 1, I have identified multiple splicing factors that exhibit highly selective expression patterns within glutamatergic neurons in the olfactory bulb or in individual inhibitory cell populations of GABAergic cortical neurons expressing Parvalbumin. Alternative splicing programs are used to modulate intrinsic neuronal properties and the synaptic repertoire of individual neuron classes (Furlanis *et al.*, 2019; Traunmüller *et al.*, 2016; Traunmüller *et al.*, 2023). In cardiomyocytes, RBM20 has been shown to exhibit highly-specialized functions in controlling calcium handling through the regulation of alternative splicing of transcripts such as *Camk1 δ* and *Cacna1c*. I therefore hypothesized that in the brain, cell-type specific expression of RBM20 regulates alternative splicing programs that are fundamental for the specification of neuronal properties such as synapse specification, cell adhesion and intrinsic properties.

To study this hypothesis in the second part of my thesis, I therefore identified the direct mRNA targets of RBM20 in the olfactory bulb, found to be enriched in this protein in chapter 1, and characterized the influence of RBM20 on the overall transcriptome of the cells in this area and in parvalbumin positive neurons of the neocortex cells. To achieve this, I generated a mouse line that globally expresses a tagged version of the RBM20 protein to facilitate the identification of RBM20 direct mRNA targets *via* cross-linking and immunoprecipitation followed by sequencing (CLIP-seq) in the olfactory bulb and heart tissues. More in detail, the work covered in this part of my PhD thesis was carried out in collaboration with Dietmar Schreiner and Raul Ortiz, two experienced members of the lab, who established the eCLIP protocol and the bioinformatic peak calling pipeline, respectively.

Further, I performed RiboTRAP-seq to unravel the alternative splicing programs and gene expression regulation driven by RBM20 in neuronal cell types. To determine the RBM20-dependent transcriptome, I generated cell class-specific mutants lacking RBM20 in the specific cell populations in which it is naturally enriched *i.e.*, in a glutamatergic population (MC-T neurons) of the olfactory bulb and in PV⁺ neocortical interneurons. To determine whether in both excitatory and inhibitory neurons, RBM20 function is tailored to modulate the fine-tuning of functional neuronal circuits, the RBM20-dependent splicing program and transcriptome was then compared between the two distinct neuronal populations. The gene expression and alternative splicing analysis of the deep sequencing data was performed by Ariane Jolly, from Genosplice. Finally, in order to provide the first characterization of the function of a RBP in two distinct organs, a comparison between the brain areas and the heart was performed.

Results

Generation of tools for the identification of Rbm20 direct mRNA targets in the olfactory bulb and heart tissues

To understand the role RBM20 plays in the OB, it is necessary to identify the specific transcripts that are directly bound and regulated by RBM20 in this area of the brain. Cross-linking and Immunoprecipitation and sequencing (CLIP-seq) analysis is one of the most widely used methods to determine the RNAs that specifically bind to a protein of interest (Hafner *et al.*, 2021). As a protein-centric method, CLIP requires antibodies with high binding specificity. Unfortunately, the RBM20 antibody that we have raised was not suitable for immunoprecipitation experiments. Therefore, in an attempt to improve both protein and cell-type specificity of our CLIP analysis, we generated Cre-loxP-system based mouse lines to conditionally express a tagged version of the RBM20 protein in selected cell populations (in our case, PV⁺ neurons of the neocortex and vGlut2⁺ neurons of the olfactory bulb). Thus, these mice should enable the study of RBM20-RNA interactions at cell-specific resolution *in vivo* (c-Tag-CLIP) (Hwang *et al.*, 2016; Hwang *et al.*, 2017). For the insertion of the tag sequence, we exploited the COnditional by INversion allele (COIN allele) module design (Economides *et al.*, 2013), which employs the CRISPR/cas9 system and single strand DNA megamers (ssDNA), which leads to the insertion of a tag sequence fused to the last coding exon of a selected gene (Suppl. Fig. 2A). The presence of a strong 3' splice acceptor site inside the COIN module, and the specific cell type expression upon Cre recombination, result in the splice-inclusion of the COIN cassette into the transcript and the expression of the last coding exon fused to a tag. In our case, we fused a Histidine-Biotin acceptor-Histidine-tag for tandem affinity purification (UV-CLAP) (Maticzka *et al.*, 2018), and three consecutive HA-tags for protein visualization to the last coding exon of *Rbm20* (Fig. 9A). The Biotin acceptor domain is in place to be endogenously biotinylated, thus allowing for RBM20 pulldown with streptavidin which forms with biotin a very strong non-covalent bond. Additionally, before streptavidin pulldown, a high affinity and purification is achieved by using histidine pulldown. However, the amount of endogenously biotinylated proteins in tissues is very high and we always observed a certain degree of nonspecific proteins being pulldown with this strategy. For this reason, we ended up using the anti-HA antibody for our eCLIP analysis.

In a series of validation experiments, we never observed an efficient Rbm20-COIN allele recombination in both PVCre :: Rbm20 COIN allele knock-in mice and CMVCre :: Rbm20 COIN allele knock-in mice (Suppl. Fig. 2B). There are different possible reasons that could explain

these results: First, we suspect that, even if we observed the successful insertion of the megamer into the *Rbm20* locus, Cre recombination in PV neurons is not very effective, possibly also due to the fact that the PVCre mouse line is turned on 14 days after birth (P14). Second, as a consequence, to enhance the levels of genomic recombination, we tried to trigger germline recombination by expressing high amounts of CRE recombinase in all cells by using a strong, ubiquitous promoter (human cytomegalovirus immediate–early enhancer promoter, CMV). However, despite some Cre-dependent recombination being detectable, RBM20 tagged protein was never detected. It is possible that the synthetic splice acceptor site may compete with the endogenous splice site, which results in decreased expression of the tagged isoform. This likely resulted in decreased levels of tagged RBM20, which were not detectable with immunohistochemistry or western blot analysis.

To overcome this issue, we electroporated CRE recombinase in *Rbm20*-COIN allele embryos. This was sufficient to induce germline recombination and resulted in the production of RBM20 tagged protein in all tissues. In these mice, we could successfully validate the expression of the tagged RBM20 protein by immunostaining and western blot, both in cortical and in OB neurons (Fig.9B-9C). However, when staining the sections with the previously raised antibody against the C-terminus of endogenous RBM20, staining intensity appeared to be lower in tagged compared to WT tissues. To be sure that this is because of a reduced binding affinity of the antibody to tagged RBM20 and not resulting from lowered protein levels, we performed targeted proteomic analysis. Even though our primary interest was to check for the amounts of RBM20 expression in the brain, with the generation of the constitutive *Rbm20*-COIN tagged mice we ensure that also RBM20 in the heart would be tagged. In this way, we could quantitatively assess RBM20 levels in this tissue, where RBM20 has been proven to be highly abundant (Guo et al.; 2012; Maatz et al.; 2014) and therefore easier to detect with proteomic, and use this information to estimate possible protein levels changes in WT and RBM20-COIN-tagged mice. For all three RBM20 specific peptides tested, there was no difference in abundance between homo- and heterozygous knock-in mice and WT littermate controls (4 mice per genotype) (Fig. 9D). We therefore concluded that RBM20 levels are unchanged in RBM20-tagged knock-in animals. The reduced staining intensity in immunohistochemistry (Fig.9B) thus most likely arises from a lower binding affinity of the RBM20 antibody to the modified C-terminal domain in tagged mice (Fig. 9A).

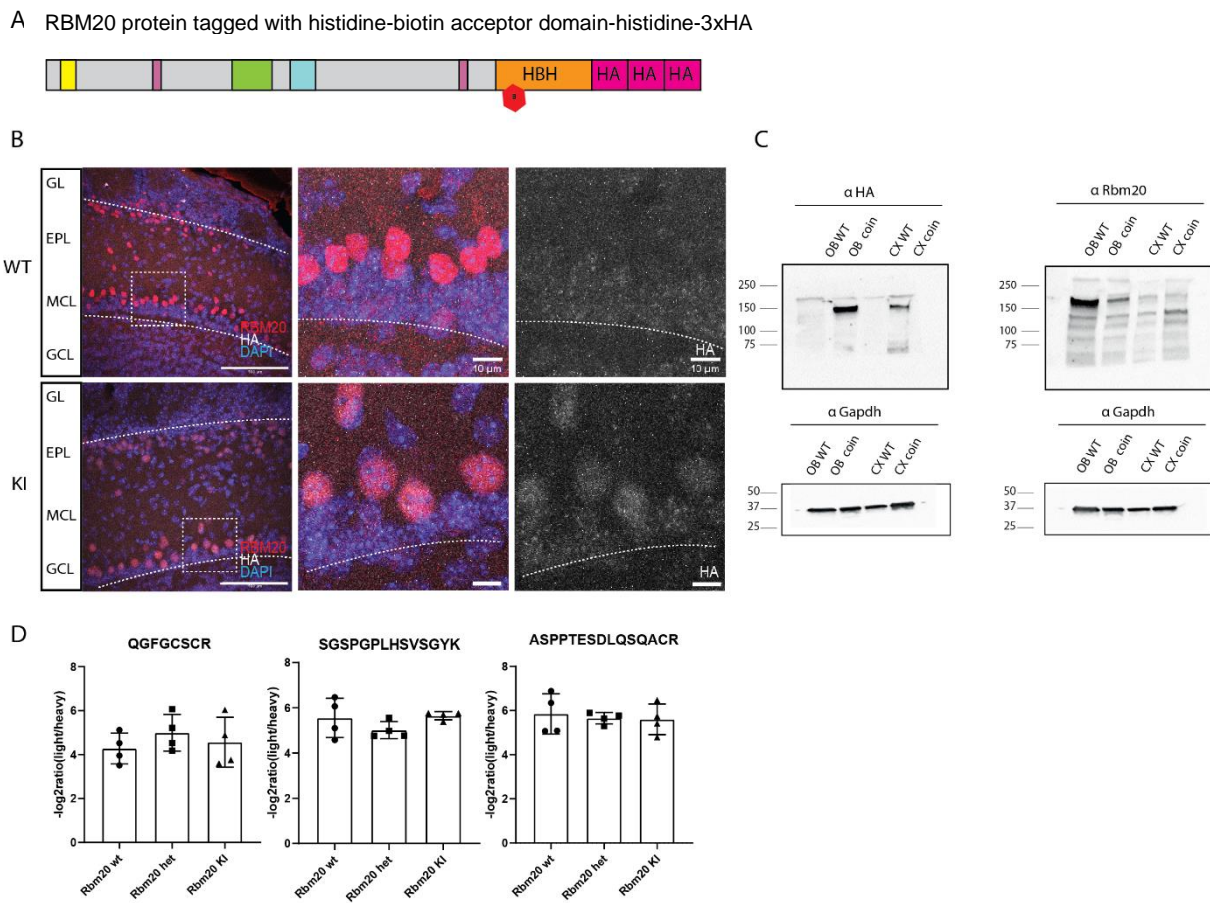


Figure 9: Characterization of RBM20-HBH-3HA tagged mice

A) Schematic representation of RBM20 protein where the last exon of the protein is fused to a histidine-biotin-histidine-3xHA tag. B) Immunofluorescence confirming RBM20 expression in the OB of WT (up) and RBM20-COIN allele knock-in mice (KI, down). RBM20 (red), HA (gray). Scale bar 100 μ m. The inset on the right is showing the selective HA expression in homozygous KI but not in WT mice. Scale bar insets: 10 μ m. C) Western blot showing the validation of RBM20 expression in OB and cortex (CX) tissues of WT and KI mice. GAPDH is used as a loading control. D) Targeted proteomic analysis on heart samples to confirm equal levels of RBM20 in WT, HET and KI mice. 3 peptides were probed and 4 biological replicates per genotype were tested. The $-\log_2$ ratio (light/heavy) peptides was calculated and displayed.

Characterization of RBM20 direct targets in heart and olfactory bulb tissues

After successful generation and validation of the tagged mouse line, we performed RBM20 CLIP-sequencing (seCLIP, 50 Mio reads/sample) (Van Nostrand, Pratt, *et al.*, 2020), with OB as well as heart tissue samples from constitutive COIN-allele mice. By adding the heart samples to our experimental conditions, we not only intended to make a comparison between mRNA targets in the two different tissues, but also to include a control for the quality of our experiments, as several RBM20 mRNA targets have previously been described in this tissue.

Because RBM20 expression in PV⁺ interneurons is substantially lower compared to neurons in the OB, we decided to not include the neocortical samples for this experiment.

To map RBM20-RNA interactions at single nucleotide resolution, we analyzed the eCLIP dataset with a pipeline that allows the identification of the truncations occurring at cross-linking sites (cross-link-induced truncation sites (CITS)), and calls the peaks based on the peak height, which is used as a proxy for coverage (Shah *et al.*, 2017). Importantly, this pipeline circumvents the requirement for normalization of the immunoprecipitated samples to the size-matched input samples (SMI). The input normalization step is currently the subject of extensive and controversial discussion in the field. In fact, even though methods and sophisticated pipelines of analysis are being implemented to remove background signal and enhance the ratio of functionally relevant binding sites, they may also introduce substantial biases (Hafner *et al.*, 2021). In eCLIP, the SMI sample is frequently enriched by RNAs that are cross-linked to a broad set of RBPs, which may be interacting with the RBP of interest. Moreover, the RBP of interest itself may be over-represented in the SMI, causing the peak signal to be mistakenly attributed to the background, hindering the detection of significant binding sites.

We found that RBM20 directly binds to 3333 and 3853 unique genes in the heart and OB, respectively (18832 identified peaks in the heart and 27728 peaks in the OB), with 1053 genes commonly targeted in the two tissues (5107 peaks identified on these genes) ($-\log_{10}$ p-value > 3) (Suppl. Fig. 4B). As expected, the majority of the peaks identified on mRNA targets occur in introns (71% in the heart and 77% in the OB), reflecting the predicted role of RBM20 to drive alternative splicing in the nucleus. A big portion of peaks was also identified in 3'UTR stretches (26% in the heart and 14% in the OB) and coding sequence (CDS) regions (around 4% of peaks in both tissues), (Fig.10A and B). Previous HITS-CLIP studies performed in rat heart tissues described that RBM20 binding sites were overrepresented within a range of ± 400 bp upstream and downstream of the 5' and 3' splice sites of exons that undergo alternative splicing regulation (Maatz *et al.*, 2014). In particular, RBM20 position peaked 50 nucleotides upstream and 100 nucleotides downstream of repressed exons, suggesting that binding at these specific positions is crucial for exon repression. In our CLIP dataset, however, we did not observe a high enrichment of RBM20 binding sites in proximal intronic regions flanking the exons RBM20 may regulate. In fact, the majority of peaks in both HR and OB tissues fall in distal positions of the intronic sequences, with only 7% and 3% of peaks falling in proximal regions in the heart and OB, respectively (distal positions considered as ± 500 bp upstream and downstream of the exon-intron or intron-exon junctions) (Fig. 10C). This suggests that RBM20 may also drive functions that do not involve the control of alternative splicing.

Upon analyzing the CLIP-seq results from heart samples, we were able to find many target mRNAs which had been previously identified in cardiomyocytes (Guo *et al.*, 2012; Maatz *et al.*, 2014; van den Hoogenhof *et al.*, 2018), thus validating the quality of our dataset.

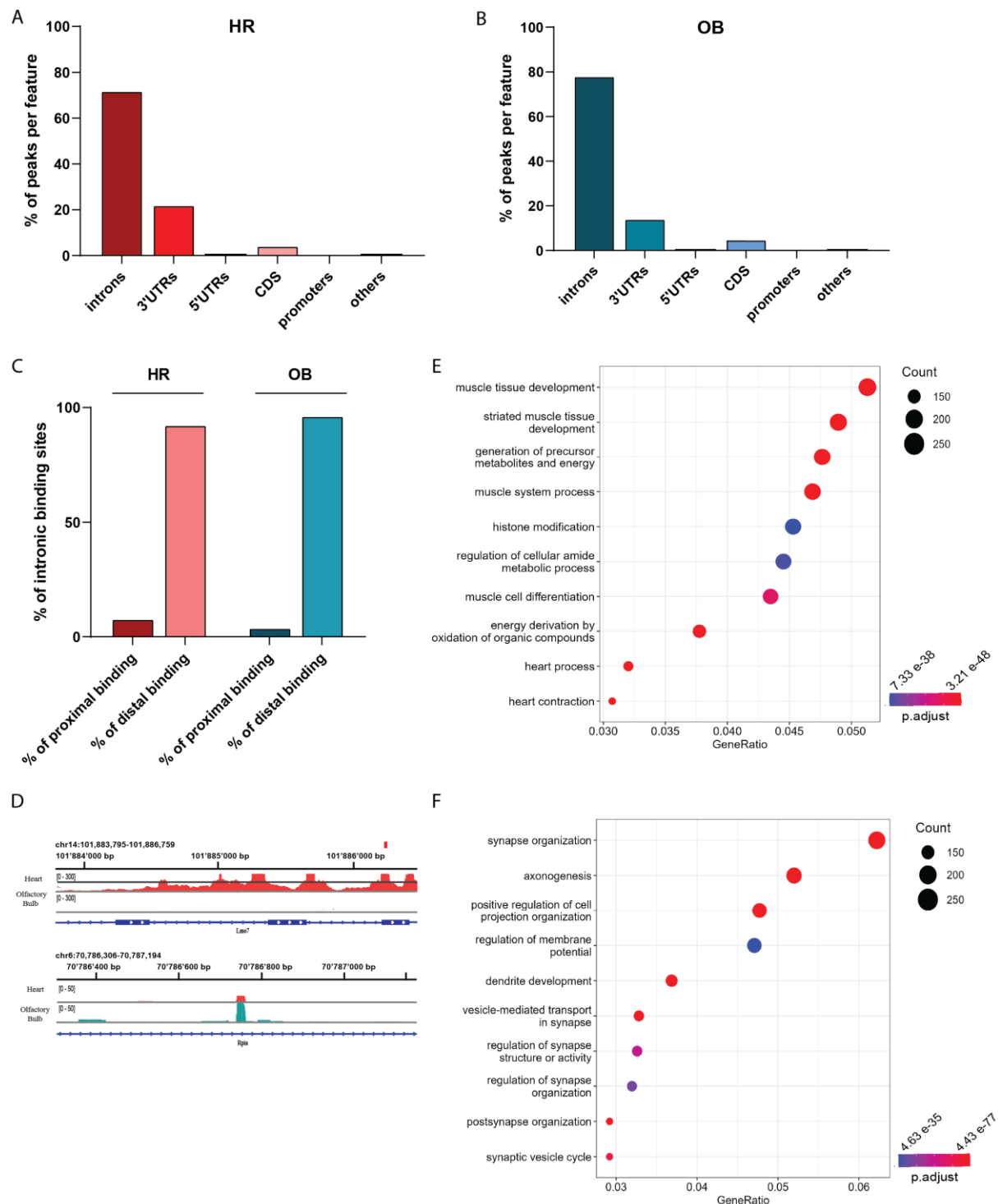


Figure 10: Characterization of RBM20 direct mRNA targets in the heart and olfactory bulb

A) Quantification of the percentage of peaks identified in the heart tissue in each genomic feature: introns, 3'UTR, 5'UTR, CDS, promoters, others (intergenic region, non-coding region). B) Quantification of the percentage of peaks identified in the olfactory bulb tissue in each genomic feature: introns, 3'UTR, 5'UTR, CDS, promoters, others

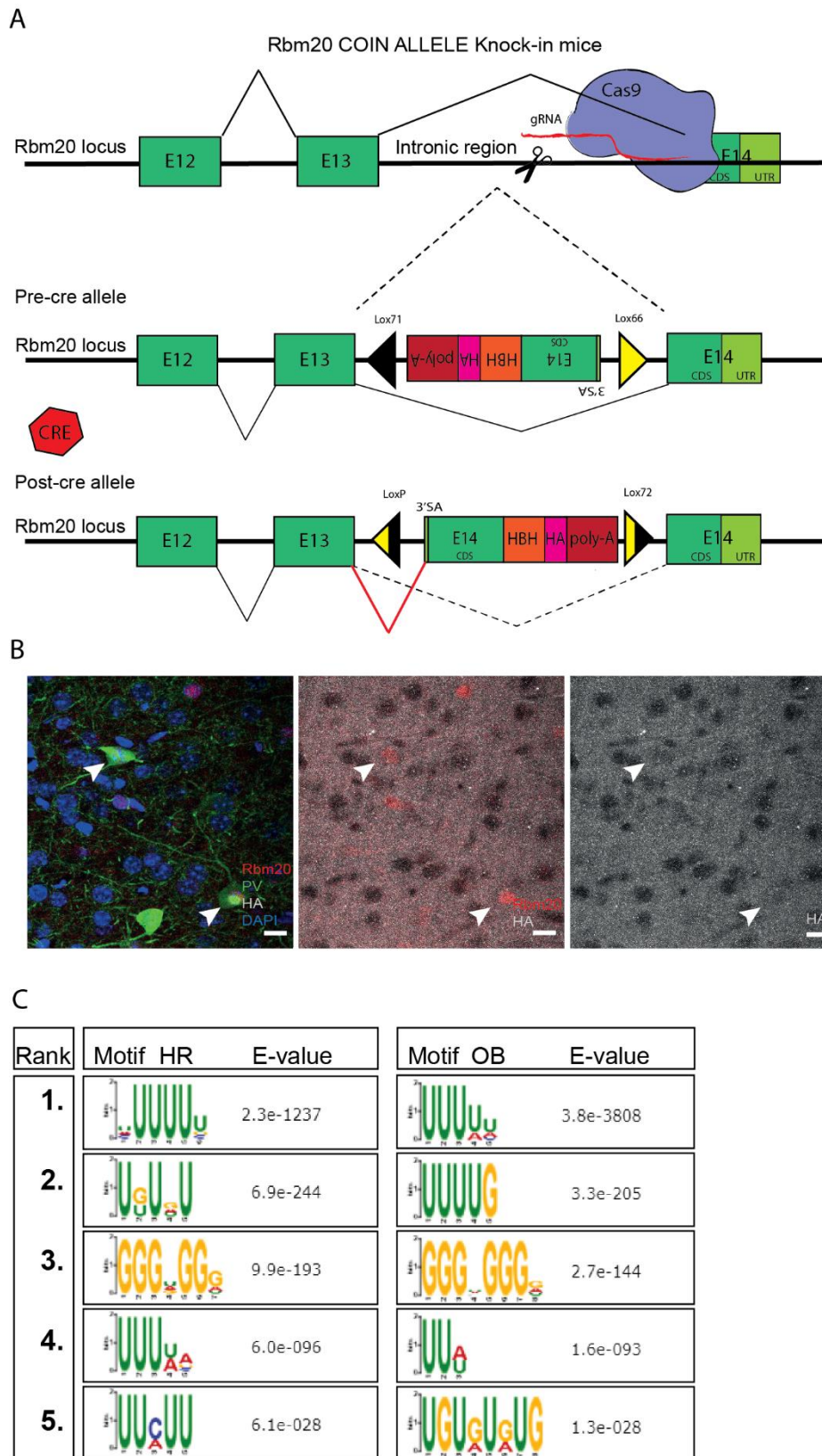
(intergenic region, non-coding region). C) Bar plot showing the percentage of peaks identified in distal or proximal intronic regions in the heart (red) and olfactory bulb (blue). D) Read density observed in eCLIP for *Lmo7* and *Rpia* genes, direct RBM20 mRNA targets in the heart tissue (red traces) and the olfactory bulb (green traces) respectively. E) Illustration of the GO categories of RBM20 targets in the heart. Gene ratio is defined as the number of target genes identified in each category divided by the total number of genes belonging to the category. P-value adjusted is indicated in the scale on the right. F) Illustration of the GO categories of RBM20 targets in the olfactory bulb. Gene ratio is defined as the number of target genes identified in each category divided by the total number of genes belonging to the category. P-value adjusted is indicated in the scale on the right.

In fact, the GO analysis of the genes with peak enrichment for RBM20 binding in the heart showed statistically significant terms for “muscle contraction”, “muscle development” and “metabolism” categories (Fig. 10E). Conversely, and intriguingly, GO analysis of target genes in the OB showed an enrichment for terms such as “presynaptic and postsynaptic structures and activity”, “vesicles mediated transport in synapses” and “regulation of membrane potential” (Fig. 10F). RBM20 may therefore play an important role for synapse specification and regulation of neuronal intrinsic properties, revealed by comparing the CLIP results between the heart and the brain, RBM20 has a different set of targets in either tissue. We therefore, for the first time, provide evidence that RBPs can have distinct roles in two different organs.

CLIP reveals the exact sites of protein-RNA cross-linking with nucleotide precision. The binding motifs that RBPs use to interact with their mRNA targets can thus be accurately identified. RBM20 in cardiomyocytes has been shown to bind to a UCUU consensus motif in adjacent introns (Fenix *et al.*, 2021; Guo *et al.*, 2012; Maatz *et al.*, 2014). Other RBPs, in contrast, have been described to bind to multiple different consensus motifs on mRNAs. HuR RBP, for example, has been found to bind to targets with both AU-rich elements (AREs) as well as U-rich sequences (Scheiba *et al.*, 2014), while hnRNP A1 has been described to be a sequence specific RBP, which is able to bind a broad range of sequences with different affinity (Burd & Dreyfuss, 1994). Given the diverse array of mRNA targets that RBM20 binds in the brain compared to the heart, we reasoned that it is possible that RBM20's preferred binding motif may also change in these two tissues. Consistent with the literature, our CLIP dataset from the heart revealed that RBM20 binds primarily its established consensus motif UUCUU (Suppl. Fig. 2C). However, this was not the only motif that reached statistical significance in our analysis, but also UGUGU and UUUUA which could be explained by the degenerate nature of the binding motif sequences (*i.e.*, all these motifs are rich in pyrimidine *e.g.*, UUCUU and CUCUCU). It is worth mentioning though, that U-rich sequences are more likely to be found in motif searches due to facilitated cross-linking of uridine, which is the most photoactivatable nucleotide. In addition, GGWGG elements have also been suggested to be artifacts specific

to the eCLIP analysis pipeline (Feng *et al.*, 2019; Traunmuller *et al.*, 2023) and therefore were excluded from our final results. We observed that even if the UCUU motif is not appearing in the list of ranked statistically significant RBM20-associated motifs in the OB tissue, the overall motif sequences in the OB are similar to those found in the heart. This was confirmed also by quantifying the UUCUU motif enrichment at the cross-linking sites in both heart and brain samples (Suppl. Fig. 2D).

Collectively, our data suggest that the RBM20 binding motif is conserved across heart and brain tissues. However, we cannot exclude that other motif sequences (statistically significant in our analysis), may be bound by RBM20 with different binding affinities. This hypothesis is supported by recent work that elucidated the complete structure of the RBM20 RRM domain by spectroscopy (Upadhyay & Mackereth, 2020). To achieve high-affinity binding with RNAs, the folding of a C-terminal helix (encoded by exon 8) seems to be required and the RNA molecule needs to harbor the final uracil in the motif sequence.



Supplementary Figure 2:

A) Schematic illustration of the strategy used for the generation of the COIN-allele RBM20 tagged mouse line. The COIN allele module is inserted in the *Rbm20* locus with the CRISPR-CAS9 system. Upon Cre recombination of the

flox sites, the COIN module is inverted and the presence of a strong synthetic 3' splicing acceptor site (3'SA) allows for the transcription of the tagged *Rbm20* isoform over the endogenous isoform. B) Validation of RBM20-tagged protein expression in PVCre neurons of the neocortex of P35 heterozygous knock-in mice. The HA-tag is not visible by immunohistochemistry. RBM20 (red), HA (gray), DAPI (blue). The arrows indicate two examples of cells which are positive for the expression of the endogenous RBM20 but negative for the expression of the RBM20-HA tagged protein. Scale bar 10 μ m. C) Motif finding analysis performed with DREME on heart and olfactory bulb eCLIP datasets. Only the first 5 motifs are reported in this image, ranked based on the enrichment p-value (E-value) (indicated on the right of each panel). E-value is defined as the p-value times the number of candidate motifs tested. The enrichment p-value is calculated using Fisher's Exact Test for enrichment of the motif in the positive sequences, calculated after erasing sites that match previously found motifs.

RBM20 tunes molecular programs in PV⁺ cortical interneurons and vGlut2⁺ neurons of the olfactory bulb

A primary goal of this project was to uncover whether and how RBM20 modifies transcriptomes in different cell types and to look at common and divergent targets in vGlut2⁺ cells of the OB and GABAergic PV⁺ interneurons of the neocortex. As a general approach, we performed RBM20 loss-of-function experiments using both constitutive knock-out (global KO) and conditional knock-out (cKO) mouse lines, in the latter of which RBM20 was selectively lost in a subset of neurons (either PV⁺ neocortical neurons or vGlut2⁺ glutamatergic neurons of the olfactory bulb) upon Cre-recombinase cell type specific expression. The cKO lines were a kind gift of Prof. Esther Creemers in the Netherlands.

The specificity of the KO was confirmed by western blot analysis of WT and cKO protein lysates, and RBM20 was observed at increasing levels in cortical, PB and heart samples (Suppl. Fig. 3A). Interestingly, even though RBM20 has a predicted size of 150 kDa based on its amino acid sequence, in our hands, it appeared to run at around 170-180 kDa on western blot gels. This altered electrophoretic mobility could be due to post-translational modifications, as RBM20 is heavily phosphorylated on its RS domain (Filippello *et al.*, 2013; Zhang *et al.*, 2022). Moreover, even though no RBM20 isoforms have been reported so far, we observed an additional band at ~75 kDa in WT heart samples, which was absent in KO littermates (Suppl. Fig. 3A). However, additional experiments are necessary to determine whether this band indeed represents an isoform or, alternatively, is a degradation product of full-length RBM20.

Pilot experiments using the *Rbm20* cKO mice, suggested that RBM20 protein turnover is slow and 25 days after birth (P25) the protein is still expressed in the cortex and OB. Therefore, we decided to perform the subsequent experiments at P35, when the protein was not detected anymore in both cortical PV⁺ neurons and the OB (Suppl. Fig. 3B). In order to understand the transcriptomic rearrangements induced by the loss of RBM20, we optimized an affinity-isolation protocol from small tissues (RiboTRAP) (Di Bartolomei & Scheiffele, 2022). RiboTRAP sequencing is used to identify and isolate mRNA transcripts associated with ribosomes, thus providing a snapshot of the genes that are actively being translated by ribosomes (Sanz *et al.*, 2019; Sanz *et al.*, 2009). While bulk RNA sequencing is used to analyze the transcriptome of an entire population of cells or tissues, ribosomal tagging allows for the conditional tagging of ribosome subunits in specific cell types (Mahadevan *et al.*, 2020). RiboTRAP is particularly useful to circumvent the drawbacks associated with FACS sorting techniques, which prove to be restrictive for neuronal cells owing to their intricate morphology

and the resulting loss of dendrites during the sorting process. Finally, this technique facilitates the discrimination between pre-mRNAs and mature transcripts as only the latter undergo translation. This further enables a better characterization of the mRNA isoforms that are the final products of alternative splicing process.

To isolate ribosome-associated mRNAs from neuronal population of interest, we used genetically-defined neuronal populations PVCre :: Rpl22HA and vGlut2Cre :: Rpl22HA, where the ribosomal protein RPL22 was conditionally HA-tagged (Sanz *et al.*, 2019), in mice where RBM20 was either expressed or ablated (Fig. 11A). First, we found that in the neuronal population targeted by the vGlut2Cre :: Rpl22HA mouse line, around 50% of cells in the mitral cell (MC) layer and 80% of glutamatergic neurons in the glomeruli layer were expressing RBM20 (Fig. 11B). This suggests that the vGlut2Cre mouse line is a valid tool to target the majority of the neurons expressing RBM20. Next, we performed qPCR as a quality control measure to check for the enrichment of markers specific for either PV⁺ or vGlut2⁺ neurons (Fig. 11C). For subsequent deep RNA-sequencing, we selected only samples showing enrichment for the correct markers and a high RNA quality score (RIN>7). In total, 12 samples (6 WT and 6 cKO) from the OB and 8 samples (4 WT and 4 KO) from PV⁺ interneurons were sequenced. Quality control analysis revealed that the samples did not exhibit a 3' bias, they had around 60% of uniquely mapped reads, and more than 85% of reads in all samples were mapped to mRNAs (Suppl. Fig. 2C-E).

Principal component analysis (PCA) including all sequenced samples showed that parvalbumin interneuron (PV) samples clustered well together, indicating homogeneity among biological replicates. In contrast, the OB samples showed much higher variability and thus scattered along the PC2-axis (Fig. 11D), indicating that they did not cluster well based on genotype (Fig. 11E). For this reason, we calculated an activity score to evaluate the level of enrichment of glutamatergic marker genes in each sample, based on a list of genes known to be enriched in three clusters of glutamatergic neurons (Tepe *et al.*, 2018) (Fig. 11F). As expected, while PV⁺ neurons did not show enrichment of glutamatergic markers (given their GABAergic nature), OB samples displayed a broader range of enrichment scores. Some samples exhibited a strong enrichment for glutamatergic markers (red arrows in Fig. 11F), others appeared to have the opposite trend (blue arrows in Fig. 11F). These two samples, that seemed to drive most of the variability because strongly de-enriched in excitatory markers and enriched for genes expressed in inhibitory neurons, were not considered for further analysis. Additional efforts were taken to determine the source of variability e.g., to rule out possible contaminations or spurious Cre recombination. However, no differences in the enrichment for

olfactory sensory neurons markers, which could potentially arise from inaccurate dissection of the OB, were found between samples (Fig. 11F). Even though the exact cause remains unknown, it seems conceivable that variability at least in part arises from intrinsic differences within the circuits of the OB, as sensory neurons are directly affected by environmental inputs.

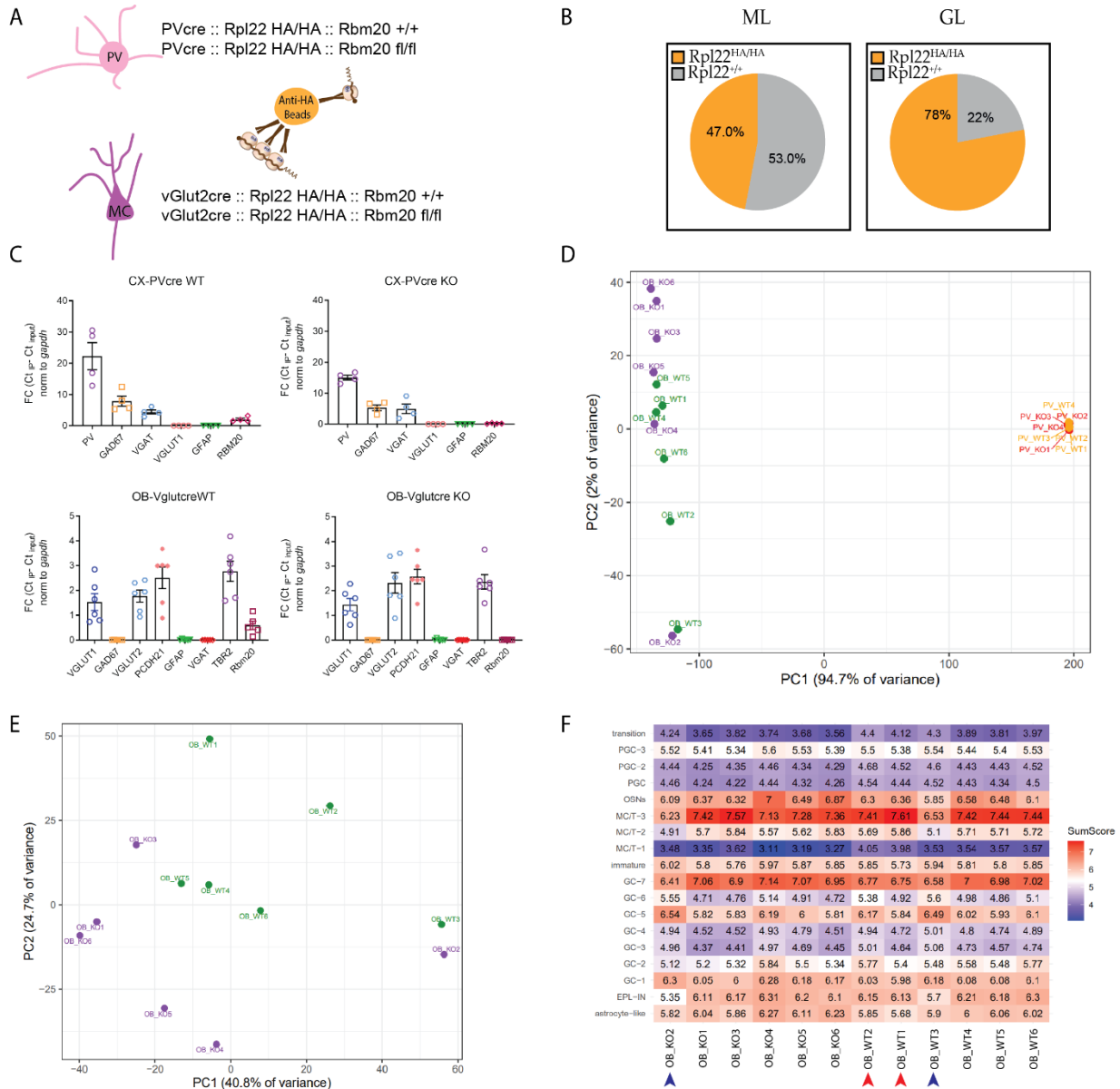


Figure 11: Quality control analysis of Ribo-TRAP samples

A) Pie charts representing the percentage of neurons of the MCL and GL positive for the HA marker in vGlut2Cre :: Rpl22HA mice. B) Schematic representation of cell type-specific conditional Rpl22-tagging in mitral cells of the olfactory bulb and cortical PV⁺ interneurons. Pulldowns of polysome-associated transcripts give access to transcripts actively translated into proteins in *Rbm20* WT and conditional KO mice. Upon tissue lysis, ribosome-associated mRNAs are immuno-precipitated using magnetic anti-HA beads. mRNAs are then purified and used for RNA-sequencing analysis. C) Fold-enrichment (FC) of markers specific to inhibitory cortical neurons or glutamatergic neurons for WT and cKO samples. For PV samples, the following markers were tested: PV,

Glutamate decarboxylase (GAD67), vesicular GABA transporter (VGAT), VGLUT1, Glial fibrillary acidic protein (GFAP), RBM20, (up). For glutamatergic: VGLUT1, VGLUT2, GAD67, Protocadherin21 (PCDH21), GFAP, VGAT, TBR2 and RBM20, (down). D) Principal component analysis (PCA) of genes expressed in each olfactory bulb and cortical PV interneurons samples (biologically independent samples per genotype, n=6 for the OB and n=4 for cortex). Variance explained by the principal components 1 and 2 (PC1 and PC2) is indicated. Gene expression values were normalized by Variance Stabilizing Transformation (VST) E) PCA of genes expressed in each olfactory bulb sample (n=6 biologically independent samples per genotype). Variance explained by the principal components 1 and 2 (PC1 and PC2) is indicated. Gene expression values were normalized by Variance Stabilizing Transformation (VST). F) Heatmap showing the “activity score” enrichment of a set of glutamatergic marker genes, calculated for 18 classes of neuronal types identified from scRNA-seq data (Tepe et. al.; 2017), in each of the OB samples. Cluster of neuron types for which the enrichment was calculated: from the top: transition neurons, progenitor cells (PGC), olfactory sensory neurons (OSN), mitral and tufted cells (MC-T), immature neurons, granule cells (GC), EPL interneurons (EPL-IN) and astrocyte like cells.

To determine the number of splice variants regulated by RBM20, we subjected the sequencing data to a PATTERN analysis (see methods for details). This splicing analysis revealed a small set of regulated target exons both in PV⁺ neurons of the neocortex (126 regulated splicing events falling on 94 uniquely regulated genes) (Fig. 12A), and in glutamatergic vGlut2⁺ neurons of the OB (373 regulated splicing events belonging to 244 uniquely regulated genes) (Fig. 12B) [\log_2 fold-change (\log_2 FC) in splicing index (SI) ≥ 1.5 or ≤ -1.5 , p-value ≤ 0.01]. The regulated events were mainly attributed to alternative transcription start sites and alternative polyadenylation categories and only a handful of them were classified as exon skipping (Fig. 12C and D). Interestingly, RBM20 mRNA targets in PV⁺ and vGlut2⁺ neurons were different (only 2 shared splicing target mRNAs), indicating that RBM20 is driving different splicing programs in distinct neuronal populations (Suppl. Fig. 4A). GO analysis did not reveal any enriched category of genes for both neuronal populations (FDR<0.05), however, it suggested that the regulated exons belonged to genes that are mainly involved in protein complex, cell signaling, cell metabolism and cytoskeleton architecture. Moreover, of a hand-curated list of 61 known RBM20 target transcripts in the heart (Fenix *et al.*, 2021; Guo *et al.*, 2012; Guo *et al.*, 2018; Maatz *et al.*, 2014; Schneider *et al.*, 2020), only 4 alternative splicing target genes overlapped with the regulated mRNAs found in the OB. However, this has to be interpreted in light of the very low expression levels of these transcripts in the brain. No common targets were found between these 61 genes and the PV⁺ neuronal dataset. Taken together, results from the splicing analysis suggest that RBM20 is shifting the splicing pattern of different mRNA targets in the heart and in the brain.

We next tried to validate the splicing changes on mRNAs with the highest predicted FC from both datasets. However, while some of the splicing changes predicted to occur in OB neurons

could successfully be validated (Suppl. Fig. 3G), we failed to do so for those in PV⁺ interneurons (data not shown).

One of our main goals was to understand the function of RBM20 on the transcripts that it directly binds and that are also undergoing differential exon usage in vGlut2⁺ neurons. When intersecting the list of genes undergoing in the OB with the CLIP datasets generated from the same glutamatergic neurons, we noticed that only a subset of genes (96 genes) appeared to be directly targeted by RBM20 (Suppl. Fig. 4C). This suggests that all the remaining alternative splicing events that are predicted to be modulated by RBM20 in glutamatergic neurons may be the result of indirect changes in the transcriptome of MC-T neurons induced by the loss of RBM20.

Although we initially focused on the alternative splicing programs driven by RBM20 in neurons, not many splicing changes appeared to be a consequence of a direct binding of RBM20 to mRNAs. On the other hand, the differential gene expression (DGE) analysis showed that, while in PV⁺ neurons only few genes are regulated in absence of RBM20 (7 genes, data not shown), in vGlut2⁺ neurons, the lack of RBM20 influenced the expression of around 410 genes [\log_2 fold-change (\log_2FC) in splicing index (SI) ≥ 1.5 or ≤ -1.5 , adj.p-value ≤ 0.01] (Fig. 12D). In particular, 366 of these genes decreased their expression in RBM20 cKOs compared to WT animals, pointing towards a role for RBM20 to serve as a stabilizer and preventer of degradation for these transcripts.

Of the DR genes, 149 appeared to be also directly bound by RBM20 (with more than 2500 peaks identified in CLIP analysis on these genes) (Suppl. Fig. 4D), and 39/149 genes were involved in synapse specification (SynGO analysis (Koopmans *et al.*, 2019)) (Suppl. Fig. 4E). However, none of these genes has RBM20 binding sites close to the promoter region. It is known though, that binding of certain splicing factors influences gene expression levels even in distal regions from the promoter of the genes e.g., binding to enhancer sequences further away from the TSS (Kubo *et al.*, 2021). Another possible explanation for the differential expression of genes in *Rbm20* cKO mice may arise from RBM20 splicing regulation of mRNA targets. Indeed, if RBM20 acts on these transcripts inducing Nonsense-mediated-mRNA-decay (NMD), the total levels of these genes would decrease, therefore appearing downregulated in the differential gene expression analysis. To test this hypothesis, qPCR analysis of the pre-mRNAs levels of these target genes is required.

GO analysis on the regulated transcripts in OB neurons showed that the DE genes are significantly enriched in “voltage-gated calcium channel”, “presynaptic and postsynaptic active

zones” and “actin cytoskeleton” categories (Fig. 12E). Interestingly, 8 of the OB genes downregulated under RBM20 KO conditions, are well described RBM20 targets alternatively spliced in heart tissue (Fenix *et al.*, 2021). Two of these genes are the voltage-gated calcium channel subunits CACNA1c and CACNA1d (Fig. 12F). VGCCs are important for regulating the flow of calcium ions into neurons. They are heteromultimeric complexes consisting of a central pore-forming Cav α 1 subunit and several auxiliary (β and $\alpha_2\delta$) subunits. The choice of the subunit can affect the firing of the neurons and the release of neurotransmitters and may play a role in synaptic plasticity (Langwieser *et al.*, 2010; Simms & Zamponi, 2014). There are ten different Cav α 1 subunits, classified into high-voltage activated (HVA) and low-voltage activated (LVA) channels, with HVA channels requiring stronger depolarization to reach activation threshold and showing prolonged channel opening. Importantly, localization of these channels varies among different brain areas. In the olfactory bulb, contrasting data exists regarding the expression of VGCCs. While some laboratories suggested that the L-type calcium channel mRNAs are present in MC (Davila *et al.*, 2003; Tanaka *et al.*, 1995), other studies in neonatal rats and mice showed that only the α 1A (Cav2.1, P/Q-type) and α 1B (Cav2.2, N-type) calcium channel subunits are expressed by MC in dendrites and that the α 1C (Cav1.2, L-type) or α 1D (Cav1.3, L-type) subunits are lacking (Yuan *et al.*, 2004).

Additionally, mutations in the family of the CACNA genes, may lead to alterations in the function of the channels and have been associated with a variety of psychiatric disorders, including bipolar disorder, schizophrenia, and major depressive disorder (Bhat *et al.*, 2012). Given the fundamental role in calcium signaling in neurons, it is not surprising that the composition of these channels undergo a fine regulation from many RBPs (Allen *et al.*, 2017; Morinaga *et al.*, 2019).

All together, these reasons prompted us to pursue a more in-depth analysis on RBM20 modulation of CACNAs subunits. We performed qPCR analysis to confirm the differential expression of these and other CACNAs subunits (*i.e.*, CACNA subunits 1a,1b,1c,1d,1h,1g) in the cKOs. Even though most of the tested subunits showed a trend towards reduced expression in the cKO, none of them reached statistical significance (Fig. 12G). This again may reflect the large variability which we have previously observed in the Ribo-TRAP samples from the OB.

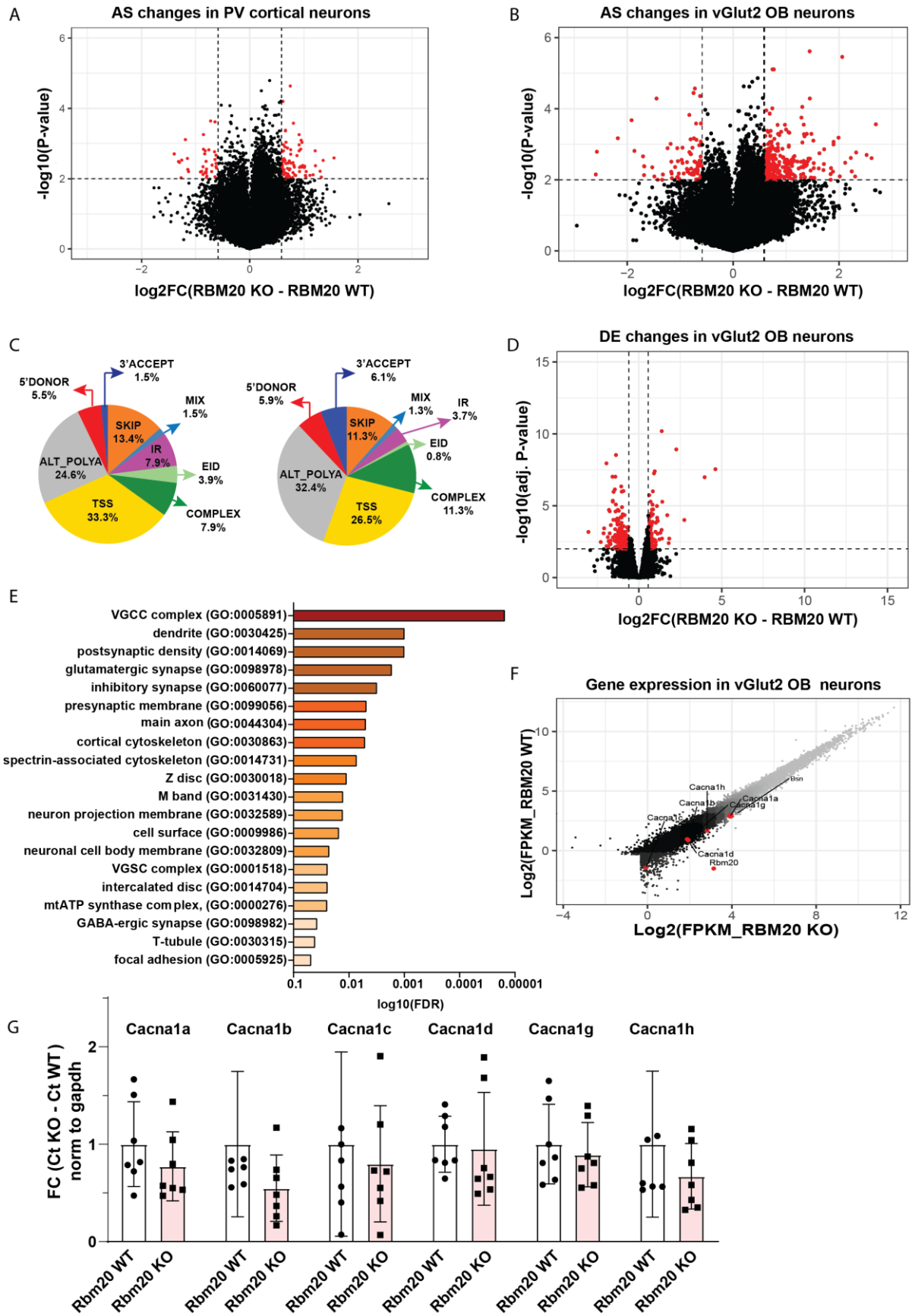
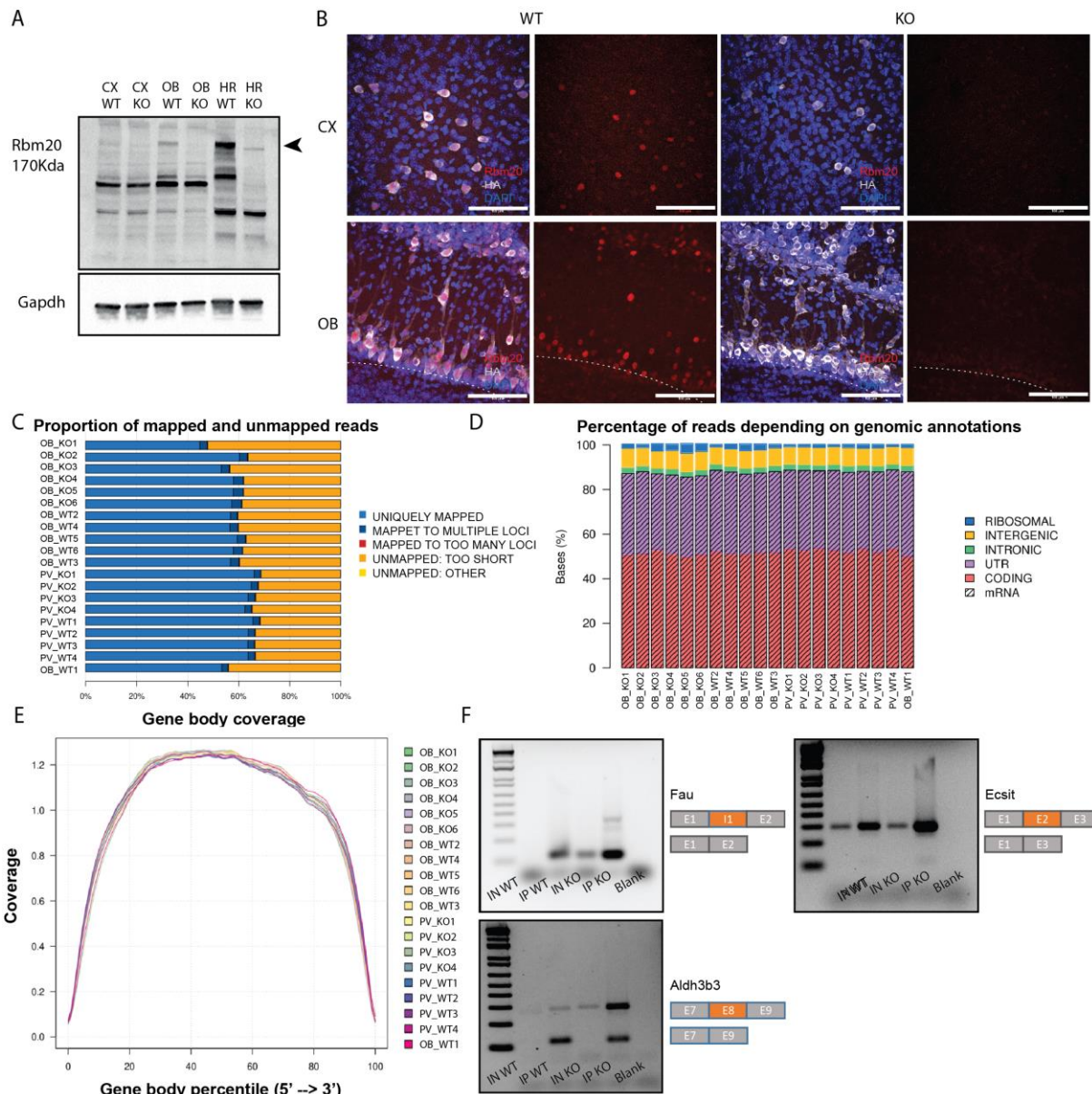


Figure 12: Transcriptomic rearrangements induced by RBM20 in PV⁺ and vGlut2⁺ neurons

A) Volcano plots representing the splicing changes (left) and the differentially expressed genes (right) induced upon Rbm20 KO in PV⁺ interneurons of the neocortex (FC>1.5, p-value<0.01). B) Volcano plots representing the splicing changes (left) and the differentially expressed genes (right) induced upon Rbm20 KO vGlut2⁺ neurons of the olfactory bulb. Regulated exons are shown in red (total of 284 regulated splicing events from 178 uniquely regulated genes; FC>1.5, p-value<0.01). C) Pie charts representing the percentage of alternative splicing types induced upon Rbm20 ablation (cortical interneurons on the left, olfactory bulb neurons on the right). D) Volcano plot of the differential gene expression in RBM20 WT vs. KO condition. Each dot represents a gene. Regulated genes are shown in red (total of 221 upregulated and 144 downregulated genes; FC>1.5, adj. p-value<0.01). E) Illustration of the GO category of genes which result to be differentially expressed in glutamatergic neurons of the olfactory bulb in absence of RBM20. F) Scatterplot of the mean gene expression in RBM20 WT vs. cKO conditions. Highlighted in red are the genes of the voltage gated calcium channels (VGCC) subunits which appear to be differentially expressed in the two conditions. G) qPCR validation of all the CACNAs subunits predicted to be differentially expressed by RNA-sequencing in OB neurons. Two-way ANOVA, Sidak's multiple comparison test. All the comparisons resulted to be non-statistically significant.

Collectively, our data support the idea that RBM20 is regulating both mRNA splicing and gene expression in the OB. In particular, it seems that the majority of down-regulated mRNAs targeted by RBM20 at the DGE level in MC-T neurons, have functions associated with the specification of intrinsic properties of these cells. It is conceivable that in absence of RBM20, the electrophysiological properties of these neurons are changed, thus modulating fundamental properties of the OB circuitry. However, further experiments are required to address the specific role RBM20 plays in these neurons.

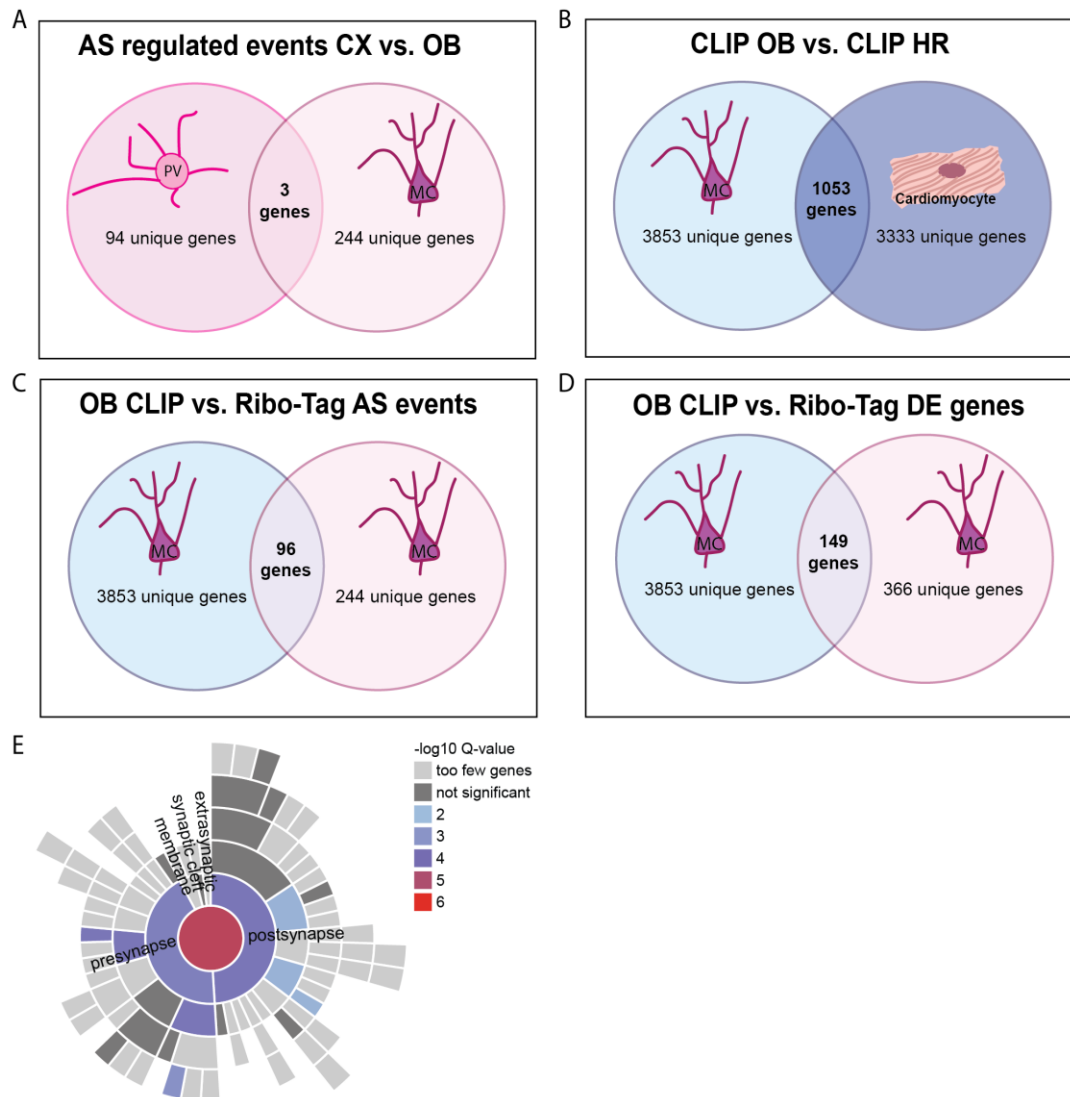
Finally, it is important to note that only a percentage of all the mRNA targets directly bound by RBM20 identified in the CLIP dataset appear to be changed at the transcriptome level. It is possible that RBM20 may be acting on these transcripts in different ways than what has previously been described. For example, RBM20 binding may induce the formation of secondary structures, therefore masking the binding sites for other broadly expressed master regulators. Competition for binding sites on mRNA targets has been extensively characterized for many splicing factors and even RBM20 in the heart has been observed competing for the binding of transcripts targeted by PTBP1 RBP (Lorenzi *et al.*, 2019). It cannot be excluded that a similar mechanism may exist also in the brain, especially given the complex and fundamental spatio-temporal control that neurons must achieve to enable the correct operation circuits.



Supplementary Figure 3:

A) Western blot showing RBM20 levels in cortex (CX), olfactory bulb (OB) and heart (HR) samples of WT and constitutive KO mice. RBM20 band at 150-170 kDa is indicated with an arrow. GAPDH is used as loading control. B) Immunostaining of RBM20 (red), HA (gray) and DAPI (blue) in the cortex (upper row) and olfactory bulb (lower row) of *Rbm20^{wt/wt}::PVCre::Rpl22^{HA/HA}* and *Rbm20^{wt/wt}::vGlut2Cre::Rpl22^{HA/HA}* mice at P35 (left of the panel) compared to conditional KO littermates (right of the panel). C) Bar plot of each biological replicate where for each sample the following parameters are indicated: the proportion of number of reads uniquely mapped, mapped to multiple loci, mapped to too many loci or unmapped reads for all the samples. All samples show highly similar values across biological replicates, as well as across brain region and genotype, suggesting a high consistency and homogeneity of the RNA-seq data. D) Bar plot representing the relative percentage of reads falling on genomic features for all the biological samples. E) Coverage plot indicating the percentage of read bases at a given position of the transcript. No sample appeared to display a 3' or 5' coverage bias across the transcript length. F) Analysis of alternative splicing events in total olfactory bulb WT and KO (inputs) and immuno-isolated RNAs samples. Flanking

primers were used to amplify exons involved in the events found to be differentially regulated in olfactory bulb samples by RT-PCR. The names of genes and schematic representation of the exons amplified are indicated on the right. Representative images are shown out of 2 technical replicates. For the 7 predicted differentially regulated events tested, 3 were experimentally validated.



Supplementary Figure 4:

A) Venn's diagram showing the number of genes overlapping between the alternatively spliced genes in PV⁺ interneurons and alternatively spliced genes in vGlut2⁺ neurons. Only 3 genes appear to be commonly targeted for alternative splicing in the two neuronal populations. B) Venn's diagram showing the number of genes overlapping between heart and olfactory bulb mRNA targets bound by RBM20 (predicted by eCLIP). 1053 unique genes are in common between the two tissues. C) Venn's diagram showing the number of genes overlapping between the alternatively spliced genes in vGlut2⁺ neurons and the olfactory bulb mRNA targets bound by RBM20 (predicted by CLIP). D) Venn's diagram showing the number of genes overlapping between the DEG in vGlut2⁺ neurons in WT vs. cKO conditions and the genes directly bound by RBM20 in the same neurons (predicted via eCLIP). 149 unique

genes appear to be both bound and regulated by RBM20. E) GO analysis on the 149 genes differentially regulated in vGlut2⁺ neurons in RBM20 WT vs. KO conditions and directly bound by RBM20. 39 of these genes belong to the GO categories involved in synapse specification. The gene set analysis intersects the gene list with SynGO annotated genes and compares this to a background list of genes set using a Fisher exact test. As background, the set of genes considered expressed in the olfactory bulb glutamatergic neurons from Ribo-TRAP analysis was used. (threshold for a gene to be considered expressed: DESEQ>200).

Is one single splicing factor able to shift the transcriptome of a specific neuronal population?

To study the function of RBM20 in the modulation of splicing programs, we performed a gain-of-function experiment where RBM20 was over-expressed upon lentivirus infection in cortical primary neuronal cultures from embryonic day 16 (E16.5) embryos of WT mice (Fig. 13A). At day *in vitro* 1 (DIV1), we infected neocortical neuronal cultures with a lentivirus expressing either *Rbm20* or the red fluorescent protein (RFP) reporter gene as a control (hereby referred to as Rbm20-LV and RFP-LV, respectively). Both viruses also expressed the green fluorescent protein (GFP) reporter, to facilitate the control for equal levels of infection rate in treated vs. untreated cells. After 8 days (DIV8), cells were harvested and subjected to RNA and protein extraction (Fig. 13A).

As lentiviruses are RNA viruses, it is challenging to quantify the concentrations of their viral particles. Therefore, we performed serial dilutions to evaluate the infection rate of different virus amounts (20 μ l, 100 μ l and 500 μ l). Quantification of the number of RBM20⁺ cells over the total number of neurons in the two experimental conditions is shown in (Fig.11B). In the *Rbm20* over-expression group, no significant differences in infection rate were observed when the virus volume was increased to 100 μ l or 500 μ l. For subsequent experiments, we therefore took the cells transfected with 100 μ l as this was the minimum volume that achieved an infection rate of around 70% (Fig. 13B).

As expected, we did not observe any RBM20⁺ neurons in the control conditions (both RFP-LV and non-infected cells) (Fig. 13B), as excitatory neurons in the neocortex do not express the RBM20 protein under WT conditions. This was further validated by western blot analysis, where RBM20 and RFP were only detected in neurons where they have been over-expressed but not in non-infected cells (Fig. 13C). In addition, equal infection efficiency in the two experimental conditions was confirmed by quantifying the number of GFP⁺ neurons (Fig. 13B).

Finally, to ensure that the lentivirus infection has not induced toxicity in the neuronal cultures that were selected for subsequent deep RNA-sequencing analysis, we performed qPCR for two known marker genes involved in cell death (*Chop*) and the unfolded protein response (UPR) cascade (*Atf4*). Both of these stress marker genes responded similarly to both Rbm20-LV and RFP-LV infection and showed an even lower expression relative to non-infected cells (Fig. 13D).

The majority of neocortical neurons in culture are glutamatergic neurons (only ~10% of neurons are inhibitory). We therefore hypothesized that over-expression of *Rbm20* in these neurons would result in a transcript isoform repertoire similar to that observed in WT glutamatergic olfactory neurons, which canonically express *Rbm20*. Further, we aimed to determine the degree to which the mis-expression of a single splicing factor could shift the splicing program of that specific cell type. To assess this, we performed deep RNA-sequencing and analyzed the transcriptome changes in the different conditions.

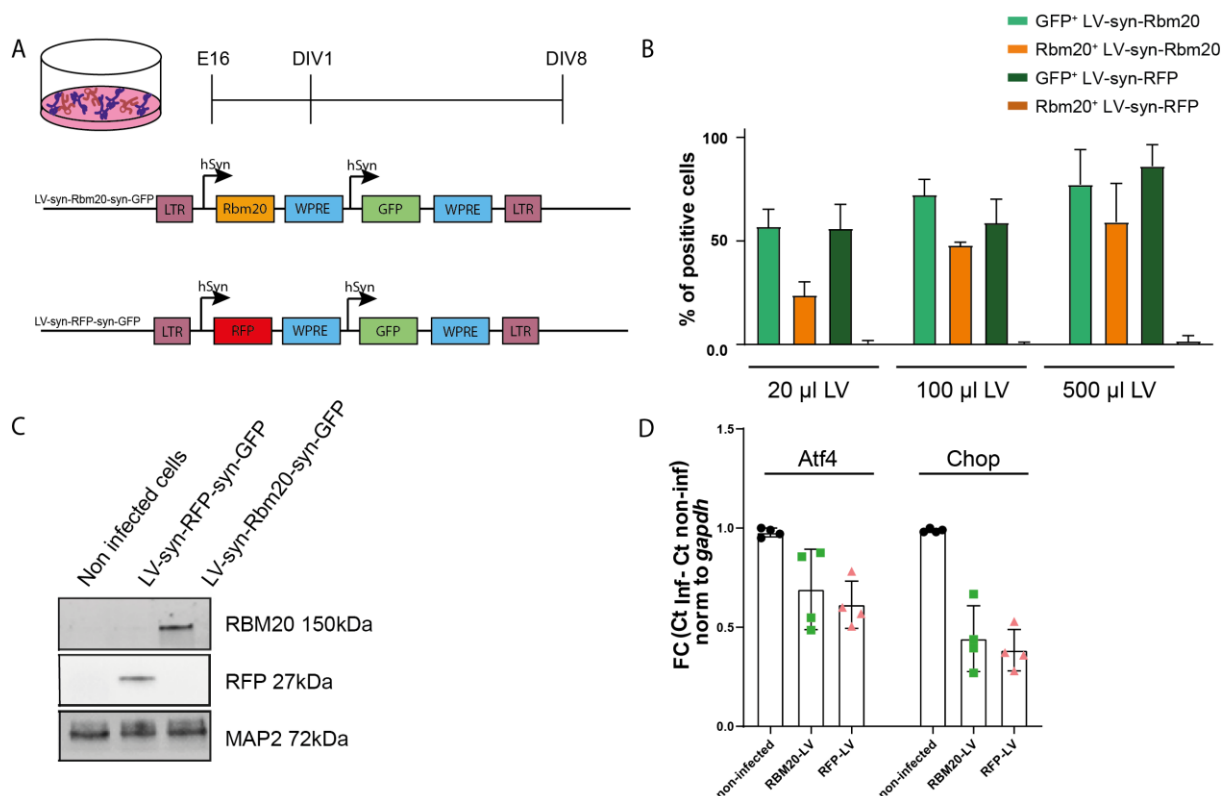


Figure13: Mis-expression of *Rbm20* in neuronal neocortical cultures

A) Schematic representation of set up and timeline for Rbm20 mis-expression in neuronal cultures. The schematic structure of the two viruses is on the left. B) Bar plot representing the number of RBM20⁺ and GFP⁺ cells in the two conditions, upon serial dilution of virus used. C) Western blot showing the selective expression of RBM20 in cultures

infected with the Rbm20 expressing lentivirus compared to non-infected cultures and cultures infected with the RFP expressing lentivirus. D) qPCR of *Atf4* and *Chop* mRNAs levels normalized over *Gapdh*, in cultures infected with Rbm20-LV and RFP-LV. Normalization was performed over non-infected cultures.

The quality of the sequencing results was evaluated by examining the sample coverage (Fig. 14A). We identified a notable 3' bias in one of the samples, and hence decided to remove this particular sample from our analysis. Additionally, PCA analysis revealed the presence of a “batch effect” among the samples, potentially influenced by the variance between biological replicates (Fig. 14B).

Differential gene expression (DGE) analysis showed that there is no change at the transcriptional level between the two conditions (Fig. 14C).

To characterize RBM20 induced alternative splicing programs we then used the WHIPPET pipeline, which enables the local detection and quantification of alternative splicing events based on an “event-level” approach (Sterne-Weiler *et al.*, 2018). WHIPPET detects exon-exon junctions and calls alternative splicing events, such as exon skipping, intron retention, and alternative 5' and 3' splice sites, based on the junctions identified. Finally, this pipeline allows for the quantification of the PSI value for each splicing event and assigns a *Probability* value, which estimates the likelihood of that particular alternative splicing event to be true. The splicing analysis revealed a total of 246 regulated events arising from 172 different genes (Fig. 14D).

Interestingly, these genes did not show enrichment for any specific functional Gene Ontology (GO) category, suggesting that RBM20 is involved in regulating small sets of transcripts of different biological processes. Among the observed splicing events, 60% were categorized as tandem alternative polyadenylation, followed by tandem transcription start site at 34% (Fig. 14E).

However, we failed to validate the regulated events *via* semi-quantitative PCR, indicating that RBM20 in cultured neocortical neurons was unable to strongly shift the splicing program. This is in accordance with previous studies, which showed that the co-expression of several RBPs in Neuroblastoma 2A (N2A) cells was not always sufficient to shift the splicing patterns in *in vitro* reporter assays (Furlanis *et al.*, 2019). Conversely, the overexpression of PTBP1 RBP in HEK 293T cells significantly reduced the inclusion of exon 4 of SRSF3, while of overexpression of SRSF3 autoregulated its own expression by increasing inclusion of the same exon, hence providing an example of context-dependent regulation of this target mRNA (Guo *et al.*, 2015). These findings demonstrate that the co-expression of different RBPs can shift the alternative

splicing of transcripts in a context-dependent manner, and highlight the complex regulation of alternative splicing in gene expression. Thus, it is possible that a context-dependent component may be required for a RBM20 to drive cell type-specific splicing programs, especially considering that some transcripts that are RBM20 targets may not be expressed in neocortical excitatory neurons.

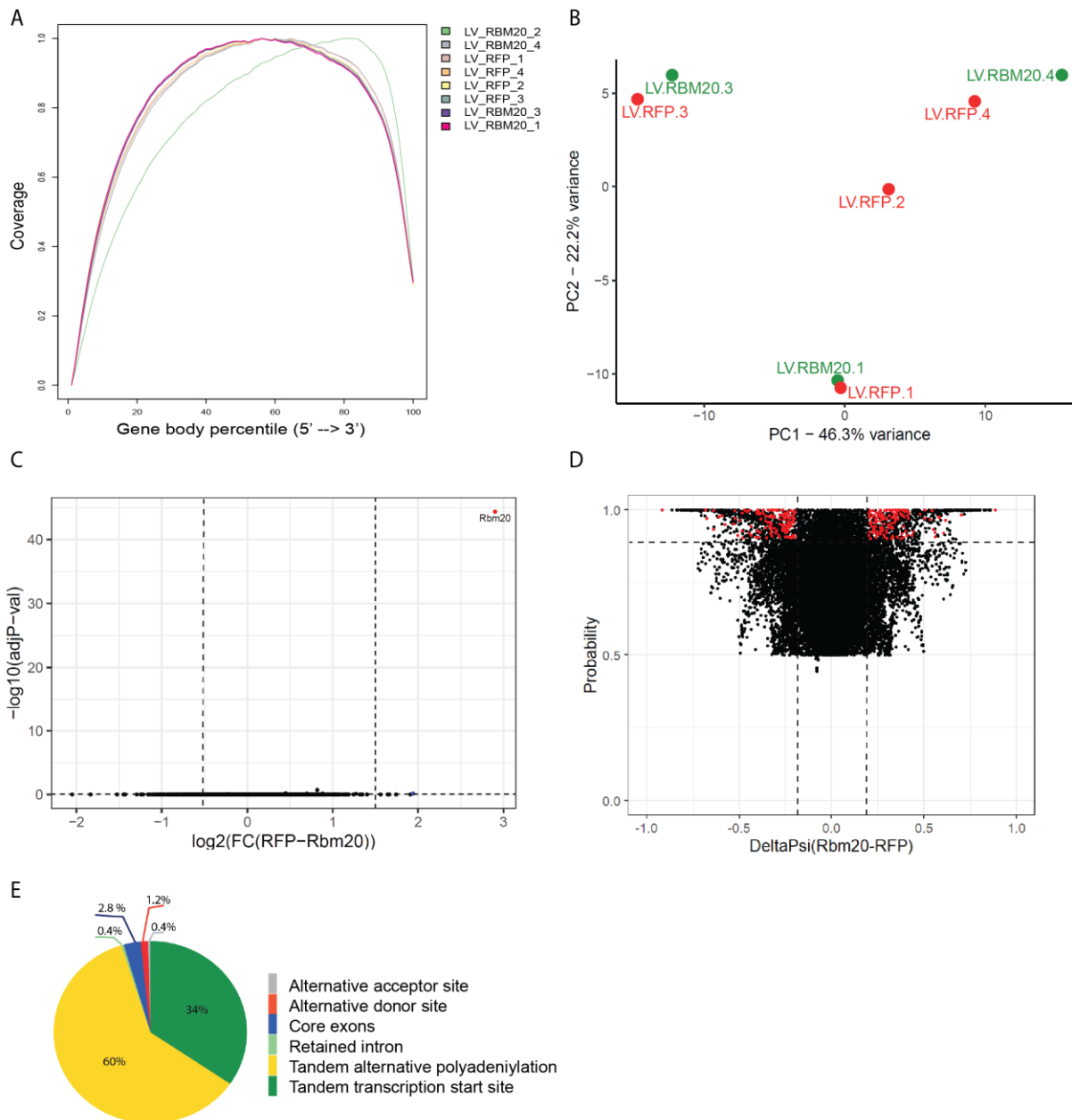


Figure14: Mis-expression of *Rbm20* in neuronal neocortical cultures

A) Plot showing the percentage of gene body coverage across the transcript length for all biological samples. The sample RBM20_LV_2 (green) is displaying a 3' bias. B) Principal component analysis of genes expressed in each neocortical neuronal culture sample (biologically independent samples are $n=3$ for LV-Rbm20 and $n=4$ for LV-RFP). Variance explained by the principal components 1 and 2 (PC1 and PC2) is indicated. Gene expression values were

normalized by Variance Stabilizing Transformation (VST). LV-Rbm20 samples are in green, RFP samples in red. The samples display a batch effect. C) Volcano plot of genes differentially expressed in RFP vs. Rbm20 infected neuronal cultures ($-1.5 > \text{Log}_2\text{FC} > 1.5$; $\log_{10}(\text{adj.p-value}) > 0.05$). In red is *Rbm20*, the only upregulated gene. D) Volcano plot of genes differentially expressed in RFP vs. *Rbm20* infected neuronal cultures ($-1.5 > \log_2\text{FC} > 1.5$; $\log_{10}(\text{adj.p-value}) > 0.05$). *Rbm20* is the only upregulated gene and is marked in red. H) Volcano plot of the ΔPSI of regulated exons and the probability value associated with it. Probability > 0.9 , $-20\% > \Delta\text{PSI} > 20\%$. In red are all the alternatively spliced events, which appear to be statistically significant. E) Pie charts indicating the relative percentage of alternative splicing regulated events (Probability > 0.9 , $-20\% > \Delta\text{PSI} > 20\%$).

Chapter 3:

Uncovering the functional impact of RBM20 in neurons

Preface

Previous work on the global removal of RBM20 in the heart and skeletal muscle tissue revealed a highly dedicated alternative splicing program tailored to genes involved in cytoskeleton maintenance such as *Titin* and *Tropomyosin* transcripts (Guo et al.; 2012, Maatz et al.; 2014). Moreover, it is well described how pathological *Rbm20* mutations induce the translocation of the protein to the sarcoplasm, leading to the formation of stress granules that fuse and impact actin filaments of the cytoskeleton in cardiomyocytes (Fenix et al.; 2021, Schneider et al.; 2020). Our analysis of RBM20 direct targets in olfactory bulb neurons revealed that RBM20 binds to a set of genes involved in microtubule and actin cytoskeleton maintenance and cell adhesion molecules (e.g., Cytoplasmic Linker Associated Protein 1 (Clasp1), dystonin (Dst) and Kinesin Family Member 21B (Kif21b)). In addition, a few genes involved in cytoskeleton structure appeared to be also regulated at the level of differential gene expression and/or alternative splicing. Based on these results, we hypothesized that the absence of RBM20 could change the morphology of mitral cells (MCs) in the olfactory bulb.

To test this hypothesis, we analyzed the morphology of MCs by using adeno associated viral vectors expressing the GFP reporter upon viral infection in the posterior piriform cortex, a brain region where MCs axons project. The 2-photon microscopy acquisition of olfactory bulb samples was performed by Susanne Falkner, a senior postdoc in the lab. The high resolution provided by 2-photon imaging was crucial to: first, observe the structural features of these neurons; second, analyze diverse morphological features (e.g. dendritic length, dendritic number) of these MCs in RBM20 WT and cKO mouse models.

Finally, we aimed at understanding the role of RBM20 in the regulation of intrinsic properties in MC-T neurons of the olfactory bulb. Specifically, by adapting a social transmitted food preference paradigm, we assessed the physiological relevance of RBM20 in the olfactory bulb, *i.e.*, we tested whether the lack of RBM20 leads to deficits in odor discrimination, odor memory formation or association of social stimuli with odor cues.

Results

Morphological characterization of mitral cells of the olfactory bulb in *Rbm20* mutant mice

Mitral cells are the major output neurons of the olfactory bulb and their dendrites receive lateral inhibition from granule cells. As for many neuronal cell types, morphology is fundamental for the functional properties of mitral cells. Consequently, morphological changes could lead to neuronal circuit remodeling. To investigate the possible role for RBM20 in the modulation of mitral cell properties, we therefore investigated how ablation of *Rbm20* in conditional knock-out (cKO) mice affects mitral cell morphology.

We injected an AAV2-flexGFP retrovirus in the posterior Piriform Cortex (pPCX) of vGlut2Cre mice and after 14 days, we performed 2-photon imaging of the back-labelled GFP⁺ neurons in the olfactory bulb. More specifically, in order to increase the S/N ratio and allow for a better reconstruction of mitral cell morphology, we applied the CUBIC/L clearing protocol (Tainaka *et al.*, 2018) and imaged up to 700 μm of olfactory bulb tissue (Fig.15A and B). In order to account for cell-to-cell heterogeneity, we decided to restrict our analysis to mitral cells, therefore excluding superficial, middle and internal tufted neurons, which were also targeted with our viral delivery strategy. We then reconstructed the morphology of neurons, whose soma was localized in the mitral cell layer (5 cells per genotype) and analyzed the absolute number of branches, the mean length and the tortuosity of their glomerular tufts. As we did not find any differences between *Rbm20* WT and cKO mice (Fig.15C-E) we conclude that the loss of RBM20 is not inducing morphological rearrangements in neurons. However, we cannot fully exclude that the high diversification of mitral cells subtypes (previously classified in type I and type II (Macrides *et al.*, 1985; Orona *et al.*, 1984)) or their topographical organization in the antero-posterior axis may influence or mask possible differences amongst neurons. Moreover, possible morphological differences of tufted neurons remain to be further investigated.

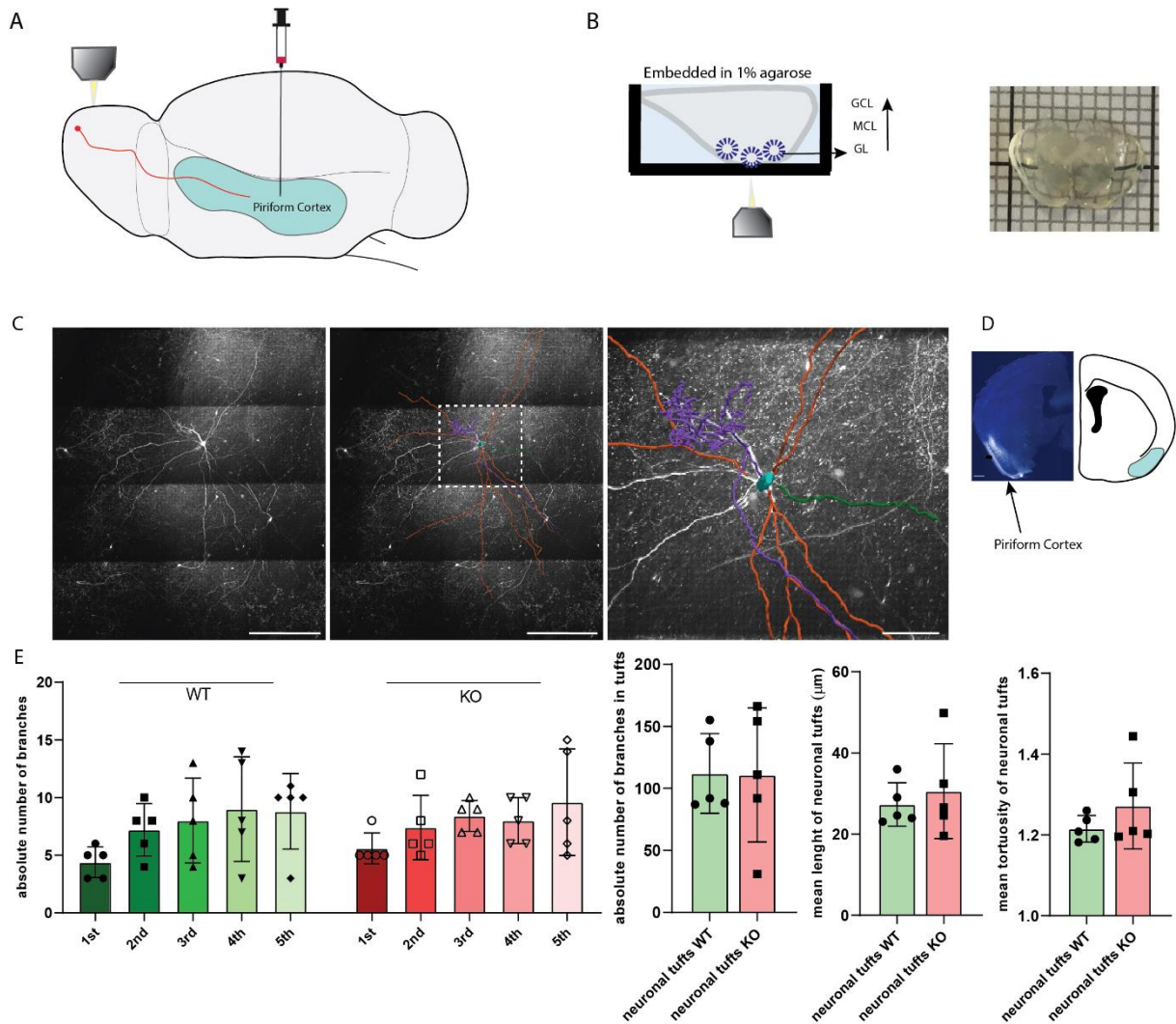


Figure 15: Morphological characterization of mitral cells of the olfactory bulb

A) Schematic illustration of retroAAV2-syn-flex-GFP viral delivery in the Piriform cortex of vGlut2Cre mice for back labelling of olfactory bulb mitral cells. B) Left: Illustration of the 2-photon imaging approach: Olfactory bulb is sliced in half and positioned in a chamber embedded in 1% agarose. The most anterior tip of the olfactory bulb containing the glomerular structures is positioned close to the objective. Right: A picture of the olfactory bulb upon clearing with CUBIC-L procedure (see methods for details). C) GFP⁺ mitral cell (gray) back-labeled through injection of retroAAV2-syn-flex-GFP virus in the Piriform cortex and tracing (right and inset) of the neuronal arborization. Scale bar 500 μm. D) Representative image of the site of viral injection in the Piriform cortex. Scale bar 500 μm. E) Quantification of the absolute number of dendrites and branches in the neuronal tufts as well as their mean length and tortuosity index in reconstructed cells of *Rbm20* WT and conditional KO (cKO) mice.

The role of RBM20 in odor discrimination and odor memory formation

The olfactory bulb plays a central role in the processing of olfactory information. Through continuous neurogenesis and replenishment of granule cell neurons, the bulb preserves its ability to adapt to external and internal changes even after maturation. This high level of

plasticity makes the olfactory bulb one of the most interesting brain regions to study (Wilson *et al.*, 2004) (Fuentelba *et al.*, 2015). A centerpiece of plasticity in the olfactory bulb is the mitral cell population, the major resident output neurons and initial processing station of sensory information. Recently, these neurons have been implicated in a form of olfactory learning, which links synaptic plasticity to memory formation, a process driven by the association of social contexts with sensory cues (Liu *et al.*, 2017; Loureiro *et al.*, 2019). Since RBM20 appears to directly bind and regulate the transcription levels of calcium channel transcripts in olfactory bulb glutamatergic neurons, we hypothesized that its loss may result in olfactory defects or alterations in olfactory memory formation. To test this hypothesis, we used different Cre mouse lines (*i.e.*, the vGlutCre, Pcdh21Cre and Tbx21Cre mouse lines), to ablate *Rbm20* specifically in mitral cells of the olfactory bulb and performed behavioral studies to test how this would affect olfactory bulb function.

First, we confirmed the specificity of Cre recombination to mitral and tufted neurons of the olfactory bulb of Tbx21Cre mice by immunostaining (Fig. 16A). Second, to ensure that possible behavioral phenotypes would be mitral cell specific, we verified that no other brain region undergoes Cre recombination and that also cardiomyocytes in the heart tissue do not express this protein during development (Haddad *et al.*, 2013; Nguyen & Imamura, 2019) (Fig. 16B). Third, we crossed these mice with the *Rbm20*^{fl^{ox}} mouse line and implemented a behavioral test from the Social Transmitted Food Preference paradigm (STFP) (Liu *et al.*, 2017; Loureiro *et al.*, 2019), to elucidate whether RBM20 indirectly regulates the formation and/or maintenance of olfactory memory. In short, we took advantage of the inherent preference mice have for flavors *i.e.*, high preference for thyme and low preference for cumin flavored food. The experiment was then designed to evaluate whether social interaction with demonstrator mice that have been exposed to cumin, could increase preference of observer mice for this type of flavor. As such, we fed demonstrator mice cumin flavored food and let them socially interact with naïve observer WT and *Rbm20* KO mice for 30 min (Loureiro *et al.*, 2019) (Fig. 16C and D). Directly after (day 0), one day (day 1) and 14 days (day 14) later, we presented cumin and thyme flavored food to observer mice and measured their preference as the ratio of the amount of food eaten of either flavor over the total amount of food eaten. As a control for the effect of the social interaction component, we included demonstrator mice that have not been exposed to any flavor and thus should not change the innate preference for thyme of WT and KO observers.

All observer mice (males and females) spent a similar amount of time smelling and interacting with the demonstrator mouse (Suppl. Fig. 5A and B). Independent of sex or genotype, all mice

ate similar amounts of food when presented a choice at day 0, day 1 and day 14 (Suppl. Fig. 5C). When pooling data of male and female WT mice, exposure to cumin fed demonstrators did not significantly reduce the innate preference for thyme flavored food and thus observer mice showed a similar behavior as the control group (Fig. 16F, top row). However, when looking deeper into the data at day 0, there seems to be a slight trend for cumin preference (although not statistically significant), which was mainly driven by WT female mice (Fig. 16E graph on the top, Fig. 16F top row). This suggests that WT males and females may respond differently to social interaction.

In KO observers, social interaction with the cumin-exposed demonstrators seems to increase cumin preference in both males and females, however, statistically significant only in female mice (Fig. 16E top graph and Fig. 16F, lower row). At day0, while males show no significant differences for genotype or food exposure, females post-hoc analysis for food exposure for KO mice presented a p -value $<0.01^*$; and the main effect for genotype was close to statistical significance ($p=0.054$). At day 1, mice's food preference is unchanged and no statistical significance is reached by the different groups (Fig. 16E middle graph and Suppl. Fig. 5E). After a period of 14 days, the effects of the social interaction on food preferences in WT mice seem to disappear. In particular, WT male mice have regained their natural preference for thyme, and WT female mice also exhibit a lack of preference between the two food options. KO male mice, however, keep displaying a preference towards cumin-flavored food, supported by the post hoc analysis for food exposure p -value $<0.04^*$, (Fig. 16E bottom graph and Suppl. Fig. 5F).

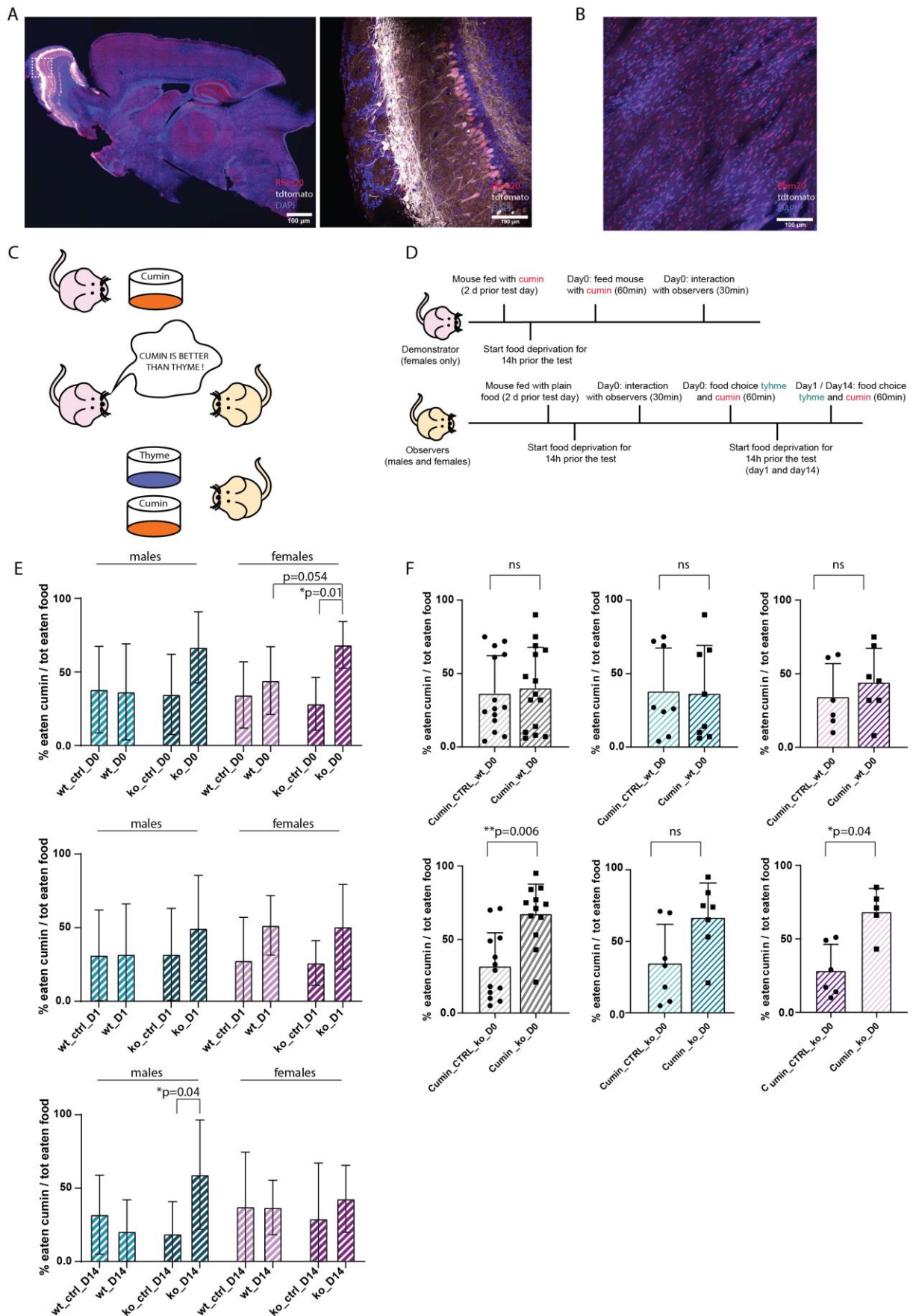


Figure 16: Characterization of RBM20 function in odor discrimination

A) Characterization of the specificity of the Tbx21Cre mouse line for selective targeting of mitral and tufted neurons of the olfactory bulb. The image is a sagittal section isolated from a TbxCre :: tdtomatoFlox P35 mouse, showing selective tdtomato recombination (gray) in the olfactory bulb. Axons from mitral and tufted neurons are visible in the Piriform cortex, a region to which these neurons project. Scale bar 100 μ m. In the inset is a zoomed image of the olfactory bulb, where tdtomato positive mitral and tufted neurons (gray) express RBM20 (red). Scale bar inset 100 μ m. B) Image of the right ventricle of a TbxCre :: tdtomatoFlox P35 mouse heart section showing no tdtomato recombination. RBM20 (red) localization is in foci as expected in cardiomyocytes. Scale bar 100 μ m. C) Schematic representation of the social transmitted food preference (STFP) paradigm. Demonstrator mice are in pink and observer mice in yellow. D) Schematic representation of the timeline of the STFP paradigm for both demonstrator and observer mice during the 14 days of the test. E) Graphs representing the percentage of cumin flavored food eaten over the total amount of food eaten in males (blue) and females (pink) mice at day 0 (left), day 1 (right) and day 14 (lower row). Data are shown as mean \pm SD. In the graphs, only post-hoc analysis which were statistically significant for either the food exposure or the genotype factors are reported. Two-way ANOVA followed by Tukey's multiple comparisons. Mice n= 14 WT observers; n= 14 WT controls; n= 12 KO observers; n= 13 KO controls. F) Graphs representing the percentage of cumin flavored food eaten over the total amount of food eaten in pooled animals (males and females, gray), males (blue) and females (pink) in WT (upper row) and cKO (lower row) mice at day0 compared to control mice. Data are shown as mean \pm SD including individual values. Unpaired T-test; non parametric, Kolmogorov-Smirnov correction. In the graphs, only post-hoc analysis which were statistically significant for either the food exposure or the genotype factors are reported

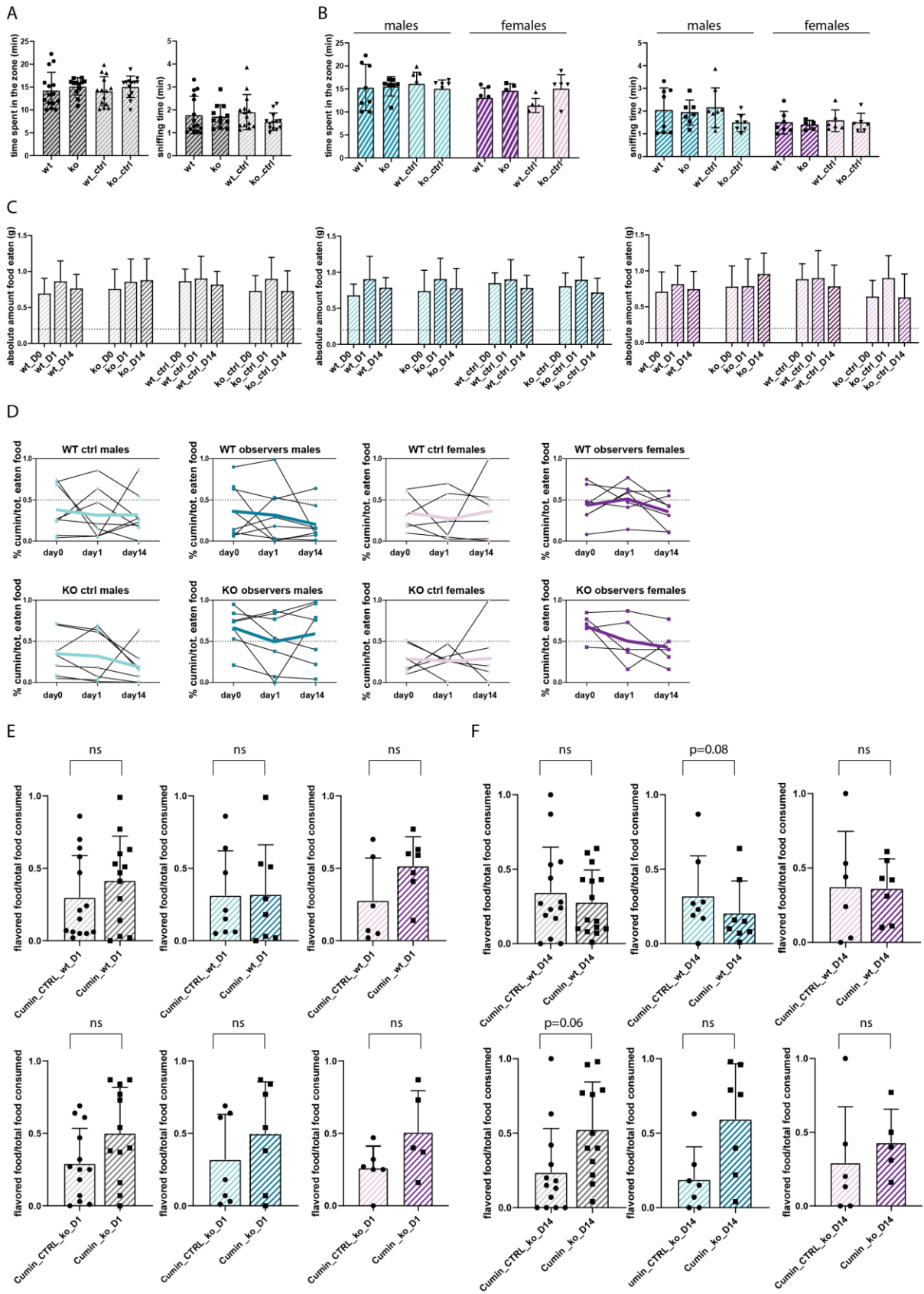
It is important to note that the interpretation of the results obtained from this behavior experiment is challenging and the mechanisms underlying the formation of olfactory memory are likely non-trivial. For example, as a control for the effect of flavored food alone, we performed pilot experiments where we exposed observer mice to flavored food in absence of any social interaction. Surprisingly, this was already sufficient to influence subsequent food choice of observer mice. We therefore decided to not include this second type of control in our experiment, even though others have described that flavored food exposure alone did not lead to electrophysiological and plasticity changes in the mitral cells of the OB (Liu *et al.*;2017). Unfortunately, actual consumption of the flavored food was not reported in this paper, which makes it difficult to conclude whether our observations were indeed different from theirs. However, that flavor preference is influenced even in the absence of social interaction, indicates that the behavioral phenotype revealed by our experiments is not exclusively driven by social cuing.

In contrast to WT animals, KO mice showed clear trends towards increased receptiveness to social cues in both males and females. The ablation of RBM20 could thus lead to molecular changes that affect the intrinsic properties of neurons. As the observed behavioral effect cannot solely be attributed to social interactions (as outlined above), the combination of social

interaction and exposure to flavored food seems to generate a reinforcing property of the message conveyed by the demonstrator mice, potentially due to circuit rearrangements present in KO mice. This phenotype appeared to be more pronounced in female mice, although the reasons for this sex difference remain elusive. Since we did not measure the physiological properties of the *Rbm20* lacking neurons, the comparisons to other studies that exploited the STFP paradigm to infer differences in MC plasticity, is difficult (Liu *et al.*, 2017).

Overall, we hypothesized that selective loss of RBM20 in MC-T cells (which are targeted by the *Tbx21*Cre mouse line), alters their proteome, possibly resulting in changes in the intrinsic properties of these neurons and leading to circuitry rearrangements. We previously showed that RBM20 binds and regulates the expression of ion channels, including the subunits of the voltage-gated calcium channel (CACNAs). The modulation of these transcripts may affect the firing rate of MC-T neurons. MC-T project to the medial olfactory tract (mOT) areas, which are targeted by dopaminergic fibers of the ventral tegmental area (VTA), suggesting that the reward system may play a role in the reinforcing value that KO mice display in the social transmission of food preference (STFP) paradigm.

It is important to define the role that the individual preferences of mice may have on this test. In fact, mouse behavior in selecting the flavored food to eat was recorded, and it was noted that mice typically smell and investigate both flavored foods before making a definitive choice, suggesting that their decision is not random. Individual food preferences at day 0, day 1 and day 14 are presented in the (Suppl. Fig. 5D). Interestingly, the field acknowledges that the investigation of inter-individual differences is crucial for in-depth understanding of mouse behavior (Pittaras *et al.*, 2016; Pittaras *et al.*, 2022). Many clinically relevant behaviors are not well understood and one of the challenges is that existing data are often statistically underpowered due to small sample sizes. To explore whether RBM20 regulates intrinsic properties of MC-T neurons, it is necessary to determine whether the electrophysiological properties of these cells are changed in KO animals. Patch clamp experiments have been conducted extensively in the OB (Jones *et al.*, 2020; Liu *et al.*, 2017; Wachowiak *et al.*, 2013), but multielectrode array recordings could provide a more time efficient readout to probe differences in the conductance level of the OB circuit between RBM20 KO and WT mice (Doucette & Restrepo, 2008). Another essential experiment to support our hypothesis, is validating the changed levels of CACNAs subunits in cKO mice. Given the high degree of heterogeneity in the RNA pull-down samples, fluorescent *in situ* hybridization may provide a more consistent and robust approach to investigate this further.



Supplementary Figure 5: Social transmitted food preference paradigm in Rbm20 WT and cKO mice

A) Graphs illustrating the amount of time that WT and cKO observer mice (all: gray; males: blue and females: pink) spent interacting with the demonstrator mouse (time spent in the zone) and B) the time spent directly sniffing the demonstrator mouse on the day of interaction (day 0). C) Absolute amount of food eaten by observer mice (all, gray; males, blue and females, pink) at day0 (left), day1 (middle), day14 (right). D) Graphs showing the percentage of eaten food (thyme or cumin) of individual data points and means (bold lines) for WT (upper row) and cKO (lower row) observers and controls, (males (blue) and females (pink)) mice at day 0, day 1 and day 14. E-F) Graphs representing the percentage of flavored food over the total food eaten in pooled animals (gray), males (blue) and females (pink) in WT (upper row) and cKO (lower row) mice at day 1 and day 14 compared to control mice. Unpaired T-test; non parametric, Kolmogorov-Smirnov correction.

3. *General Discussion*

Discussion

Synapse specification is fundamental for the proper functioning of neuronal circuits. Alternative splicing and its central regulators RBPs, are crucial components in regulating neuron-specific gene expression (Raj and Blencowe, 2015; Schreiner et al., 2014; Zheng and Black, 2013; Zheng et al., 2013). In thi thesis I focused on one of such specific regulators, RBM20, a splicing factor first described in heart muscle, is enriched in specific classes of neurons in the mouse brain (Furlanis et al., 2019). In fact, even though a link between aberrant RBM20 function and dilated cardiomyopathy has long been established, the mechanism driving pathology was not yet completely elucidated. Our attention towards RBM20 was also drawn by its characterized target mRNAs in cardiomyocytes, where RBM20 is involved in the modulation of alternative splicing of ion channels and calcium handling transcripts such as *Camk1lδ* and the voltage-gated calcium channel (VGCC) subunit *Cacna1c* (Morinaga *et al.*, 2019). Besides cardiomyocytes, neurons are the only other excitable cells in our body and in the brain, calcium is an important intracellular second messenger. Various cellular processes are calcium-dependent, including neurotransmitter release, cell growth and many processes underlying synaptic plasticity. Calcium influx into cells is achieved through calcium release from internal stores or entry via the cell membrane: voltage-gated calcium channels are one of the main routes (Bauer *et al.*, 2002; Simms & Zamponi, 2014).

In my PhD thesis, I therefore aimed to determine the role of RBM20 in different neuronal cell types and to elucidate whether and how this splicing factor regulates neuronal intrinsic properties. Moreover, by also studying the heart, I wanted to directly compare RBM20's role between two structurally and functionally distinct tissues in a comprehensive manner.

First, I mapped RBM20 gene expression and protein levels in the brain and identified the olfactory bulb as the main brain region where this protein is expressed. I further uncovered that RBM20 in both neuronal cell types is dispersed throughout the nucleoplasm instead of being restricted to specific foci as previously described in cardiomyocytes (Bertero et al., 2019). This suggests that RBM20 in neurons is not primarily binding to a single “master mRNA” as it is the case for *Titin* mRNA in cardiomyocytes. Moreover, the absence of a highly abundant mRNA-binding partner prevents RBM20 from forming a “splicing factory” (complex of small nuclear ribonucleoproteins and splicing factors recruited on pre-mRNA) in close proximity to this transcript. RBM20 in the brain may thus also have additional functions other than regulating alternative splicing. Second, the characterization of RBM20's direct target mRNAs in the olfactory bulb and comparison to those in the heart, revealed that only a fraction of transcripts is commonly regulated in these two different tissues. Intriguingly, in glutamatergic neurons of the olfactory bulb and in parvalbumin positive neurons of the neocortex, I identified

transcripts that undergo either changes in alternative splicing or gene expression. Therefore, the diversification of these cell classes does not only rely on genetically encoded gene expression, but also on co-transcriptional mechanisms of gene expression regulation. Third, although additional experiments are required to fully understand the functional role of RBM20, I established a link between the molecular changes induced by the lack of RBM20 in cKO mouse models and the functional deficits in olfactory bulb neurons.

Data emerging from this thesis support the idea that cell type-specific alternative splicing programs are fundamental for the correct neuronal wiring and specification of intrinsic neuronal properties. In depth understanding of the RBM20-mediated regulatory mechanisms has the potential to improve the design and generation of new therapeutic avenues for a broad array of diseases related to aberrant alternative splicing.

Alternative splicing: A mechanism to provide functional specialization in neurons

A diverse set of intricate alternative splicing programs govern a range of biological processes, such as chromatin and RNA regulation, ion homeostasis, and mitochondrial function. While these splicing-mediated functions are diverse and universal, many cell types have highly-specialized splicing programs. In neuronal cells, these specialized splicing programs are key for regulating synaptic and intrinsic neuronal properties. Central to the specificity of splicing programs are RBPs such as SLM2, which regulate different aspects of synapse structural and functional properties (Traunmüller et al., 2023). In general, the regulation of alternative splicing choices in genetically defined neuronal populations primarily involves synaptic-related genes (Furlanis et. al.; 2019). This could be due to the phenotypic complexity of the nervous system, which requires the assembly and communication between thousands of cell types through large synaptic networks. Moreover, compared to other cell types such as those in cardiac muscle, single neurons have a more complex morphology that requires highly specialized compartments and precise spatio-temporal control to make afferent and efferent synapses with other cells. Accordingly, RBM20 in the brain binds and regulates target mRNAs mainly involved in the regulation of synaptic properties and cytoskeleton, while in the heart and skeletal tissues, it is mainly required for the splicing of *Titin*, and other key components of the contractile apparatus. Thus, RBPs' modulation of transcript abundance, alternative splicing and other post-transcriptional mechanisms (e.g. transcript stabilization) plays a crucial role in achieving the required level of specialization and isoform diversification in a cell class-specific manner. Furthermore, some RBPs are activated upon specific stimuli to produce pools of transcripts on demand, such as activity-dependent splicing factors that remodel synaptic structures in response to neuronal activity. Finally, although synaptic genes are expressed in all neuronal

cell types, the capacity of RNA-binding proteins to contribute to the specification of neuronal properties in a cell type dependent manner, is crucial for proper brain functioning.

In this work, we describe RBM20 as a cell-type specific alternative splicing factor that is expressed in two neuronal cell types with very different functional and structural properties. Intriguingly, the transcripts regulated by RBM20 at the alternative splicing level are different in the two neuronal classes, but overall the regulated genes do not belong to specific gene ontology categories. However, these transcripts are mainly targets involved in protein complex, cell metabolism and cytoskeleton. This is in accordance with the targets found in the heart, which are involved in cytoskeleton components. However, the changes observed in transcript abundance, intersected with the direct mRNA targets identified by eCLIP in the olfactory bulb of RBM20 WT vs. cKO mice, point towards a possible role of this alternative splicing factor involved in the specification synaptic structural and functional properties. Further experiments are required to uncover whether RBM20 is able to contribute to the specification of intrinsic properties of MC-T neurons. In this sense, RBM20 could provide a mechanism of cellular specialization for the fine tuning of odor discrimination and/or perception.

How do RBPs achieve binding specificity on target mRNAs?

Research from multiple laboratories has recently shown that RBPs can regulate unique subsets of targets and differentially determine splicing choices depending on the cell type (Saito *et al.*, 2019; Traunmuller *et al.*, 2023; Wamsley *et al.*, 2018a). Similarly, results from this thesis suggest that RBM20 regulates distinct alternative splicing programs in PV⁺ and vGlut2⁺ neuronal populations and heart tissue. So what are the potential mechanisms that lead to the achievement of cell type-specific differences in alternative splicing? In general, the interaction between RBPs and RNAs are based on well-defined RNA-binding domains on the proteins that interact with RNA molecules in a sequence- and/or structure-specific manner. Common RNA-binding domains include the RNA recognition motif (RRM), the heterogeneous ribonucleoprotein (hnRNP), K-homology domain (KH), and the C3H1 zinc-finger (ZF) domain (Gerstberger *et al.*, 2014). The combination of different domains as well as the density and specific sequence of RNA-binding motifs on transcripts are crucial in determining interaction affinity between RBPs and RNA targets. In addition, the availability and recruitment of RBPs to specific binding sites are influenced by the competition between RBPs for the same binding motif. Further, RBPs achieve cell type-specific splicing control by differentially binding to enhancer or silencer sites and thus recruiting co-factors and regulating how efficiently the spliceosome assembles nearby the acceptor sites. Additionally, the prediction of the position of the RNA-binding sites, relative to the splice-sites, appears to be a major element controlling the mode of action of these proteins. Finally, structural studies have revealed diverse

modalities of binding for RBPs, such as non-canonical binding achieved through the formation of secondary structures in the RNA, making it difficult to predict RNA target preferences based solely on the amino acid sequence of the protein (Dominguez *et al.*, 2018).

Even though CLIP studies and sequencing approaches have helped to better understand RBP-RNA interactions, the precise mechanisms by which RBPs achieve high binding specificity for certain RNAs remain to be fully elucidated. An *in vitro* binding assay characterized over 70 human RBPs, which revealed that these proteins tend to bind to a defined subset of primary RNA sequence, rich in low-complexity motifs. However, the contextual features of RNAs, such as secondary structure and base composition, also contribute to binding specificity and different classes of RBP domains exhibit different binding tendencies. For example, ZF-containing proteins prefer binding to structured motifs, while proteins with KH domains (such as SLM2) tend to favor large hairpin loops and bipartite motifs (Dominguez *et al.*, 2018).

The comparison of RBM20 binding motifs between the olfactory bulb and the heart did not reveal differences in motif preference in these two tissues. We speculate that for RBM20, the binding specificity may be driven primarily by the presence of the specific UCUU motif on target mRNAs, thus highlighting the central role of binding motifs in RBP-RNA interactions. However, we cannot exclude the possibility that additional binding motifs have been overlooked or not detected by our analysis pipeline. To this end, we plan to re-analyze our data with a more specific pipeline, developed by the laboratory of Prof. Chaoling Zhang (Feng *et al.*; 2022), which takes in account the enrichment of RNA-binding motifs at the cross-linking sites.

Further, we have to consider that the binding affinity of RBM20 to RNAs in the different tissues, may be influenced also by proteins that can bind to other domains on RBM20. For example, RBM20 harbors a RS domain, through which it could interact with RS domains of other proteins. Many protein binding partners have been identified for RBM20 through stable isotope labeling by amino acids in cell culture (SILAC) proteomic experiments (Paul *et al.*, 2011) in both HEK293T cells and in cardiomyocytes (Maatz *et al.*; 2014). In this system, it was described that RBM20 interacts with both U1 and U2 small nuclear ribonucleic particles (snRNPs) and the spliceosome component U2AF35, in addition to other well characterized splicing factors such as MATR3, HnRNPU and RBMX. Due to the low expression levels of RBM20 in the brain compared to heart tissue, we were not able to detect possible binding partners *via* immunoprecipitation. However, it is possible that RBM20 drives splicing regulation in relation to the binding with other RBPs and core components of the spliceosome machinery *in vivo*. Furthermore, complex formation with other splicing factors could also depend on the presence of RNA or DNA strands, which are often found in multiprotein assemblies (Cid-Samper *et al.*, 2018; de Groot *et al.*, 2019). Such interactions may also be favored by domains

different from the RBD (e.g. Znf domains). Finally, it is important to note that some mRNA transcripts are selectively expressed in one but not the other tissue (e.g. *Titin* is only expressed in cardiomyocytes but not in neurons) and therefore RBM20's target mRNAs are also depending on the cell-type and/or physiological context analyzed. In addition, the levels of expression of a particular RBP in a specific tissue or cell type can impact the incorporation or exclusion of exons following a "graded" regulation rather than a binary on/off activation (Feng *et al.*, 2021).

Future directions in the functional characterization of RBM20's role in neurons

The core of my results suggests that RBM20 in glutamatergic neurons of the olfactory bulb regulates transcripts abundance and exon incorporation through alternative splicing. However, due to the lack of a strong and obvious functional phenotype of KO animals, a direct functional role of RBM20 in the olfactory bulb is not trivial to identify. TRAP-seq analysis revealed the differential regulation of many genes involved in cytoskeleton organization. However, morphological analysis on OB neurons in WT and cKO mice, did not reveal significant changes on the structure of these cells, indicating that the loss of RBM20 is not as dramatically impacting the cytoskeleton as the case in cardiomyocytes. One possible explanation for this could be that RBM20 loss does not directly impact neuronal arborization but is regulating other processes fundamental for neuronal functioning that rely on cytoskeletal proteins. For example, one of the terms that we found to be enriched in GO analysis of transcripts that are directly bound by RBM20 in the eCLIP dataset of OB neurons, is "vesicles mediated synaptic transport and membrane fusion". Axonal transport is mediated by a broad set of proteins including kinesin, dynein and Soluble NSF attachment protein receptor proteins (SNAREs). It is therefore possible that protein levels of fundamental components of anterograde and retrograde pathways of axonal transport are regulated by RBM20. RBM20 loss could thus produce a more downstream functional effect in the regulation of neuronal properties. Unfortunately, our morphological analysis on RBM20⁺ WT and cKO neurons was not set up in a way to detect these differences and further approaches such as transmission electron microscopy would have to be implemented to be able to detect these potentially subtle differences in vesicle transport.

Nevertheless, to quantitatively assess changes in the number of synapses of MC-T neurons in RBM20 WT and cKO mice, is the expression of genetically encoded intrabodies (Fibronectin intrabodies generated by mRNA display, FingRs) directed against PSD-95 synaptic protein (Gross *et al.*, 2013). FingR probes could be selectively expressed in MC of the olfactory bulb through delivery of a Cre-dependent retro-AAV in the pPirCX of Tbx21Cre mice. Synaptic

density, focusing either on the dendro-dendritic synapses formed between MC-GC or on the MC-OSN synapses formed in the glomeruli, could then be mapped.

In parallel, observations made in the behavioral STFP paradigm, suggest that RBM20 cKO mice may indeed display differences in olfactory functions. This is supported by the changes in CACNAs subunits at the DGE level in these neurons, even if a final validation of these predictions was not possible to achieve by qPCR on RiboTRAP samples due to high levels of inter sample variability. We were not able to identify the exact source of this variability but one possibility to overcome the possible technical errors introduced by sample processing and RNA extraction could be the quantification of the level of these genes through fluorescent *in situ* hybridization approaches.

Further, to characterize possible differences in intrinsic properties of MC-T neurons and draw conclusions as to the functional role of RBM20 in these neurons, electrophysiological studies are required. Patch clamp recording has been performed in glutamatergic neurons of the olfactory bulb by many laboratories and it is an approach that grants a comprehensive insight into neuronal functional properties. This would for example enable the measurement of individual ion channels properties (e.g. testing the impact of VGCC composition in WT and cKO conditions). If one considers the high level of heterogeneity within MC-T neuronal populations, it is still possible that we would not be able to pick up significant differences in WT and cKO mice. Instead, we are now designing an experiment that allows for the detection of differences in neuronal activity using multielectrode arrays (MEAs). This type of electrophysiological technique is commonly used for recording from multiple neurons simultaneously, providing a large amount of data in a short period of time and giving indications on physiologically relevant context for the study of the activity of neuronal circuits. MEAs do not provide access to intracellular activity, so it is not possible to measure the activity of individual ion channels or to manipulate the intracellular environment to measure subcellular processes. For example, we will not be able to directly infer on the role of CACNAs in regulation of RBM20 cKO intrinsic properties. We will nevertheless record possible activity changes and consider them as representative of the overall population.

Finally, RBM20 has two ZNF motifs, which could contribute to the binding of nucleic acids, thus bringing RBM20 in close proximity with other transcription factors or RBPs, which in turn could influence RBM20's function (Upadhyay & Mackereth, 2020). However, interactions of RBM20 with DNA strands have never been reported. To probe RBM20's ability to interact with DNA via direct and/or indirect binding, we tried to set up chromatin immunoprecipitation (ChIP) in heart and olfactory bulb tissues. However, we did not manage to precipitate sufficient amounts of protein as a result of the inherent challenges with this experimental procedure applied to

tissue samples (e.g., low abundant nature of target proteins or weak, indirect or transient binding to DNA). Further experimental optimization and/or implementation of a more effective and high-throughput pipeline such as the alternative to CHIP, recently developed methods such as CUT&RUN and CUT&TAG which have been shown to be a non-invasive and suitable for low amount of material could be further tested and optimized for RNA-binding proteins such as RBM20 (Meers *et al.*, 2019; Miura & Chen, 2020; Skene *et al.*, 2018; Skene & Henikoff, 2017; Zhu *et al.*, 2019).

Challenges and perspectives in predicting the cell proteome

The major aim of my thesis was to understand whether RBM20 in neurons acts as a cell type specific splicing factor, regulating transcripts encoding for proteins that are involved in entrance, transport or usage of calcium and/or other ions, thus influencing neuronal function. To address this question, we first needed to find means to capture changes in isoform expression and the rate of gene expression in specific types of neuronal populations. Our needs could in part be addressed with bulk RNA-sequencing, but to extract mRNAs from individual classes of neurons, we would have required a FACS sorting approach to isolate target neuronal populations from the others. FACS sorting in neurons results in the loss of dendrites and axons, thereby impacting cell viability and thus the quality of the RNAs that are sequenced. Moreover, bulk RNA-seq cannot provide information on cellular heterogeneity or rare cell types within a given population. As an alternative approach, single-cell RNA-sequencing (scRNA-seq) and single-nucleus RNA-sequencing (snRNA-seq) have the advantage of providing unbiased clustering of cells based on their gene expression, thus offering the potential of capturing cell type heterogeneity in a given tissue. In our case, the high degree of diversity amongst mitral and tufted neurons of the olfactory bulb could have been addressed with this approach. In fact, it is possible that by analyzing mitral and tufted neurons together as one glutamatergic neuronal population of the olfactory bulb (e.g., by using a genetically modified mouse line expressing Cre recombinase under the vGlut2 promoter), some inter-class differences may be masked or diluted and therefore not trivial to identify. Moreover, scRNA-seq is able to capture homeostatic changes within a tissue by profiling the transcriptomes of individual cells at a given point in time, thus reflecting alterations in cellular states or functions and providing insights into cellular dynamics or developmental trajectories. In the olfactory bulb, this could be changes in cellular processes or activation of specific signaling pathways at the circuit level that may contribute to shifts in homeostasis in *Rbm20* cKO compared to WT animals. Despite these advantages, scRNA-sequencing data are noisier due to technical variability and low sequence coverage. Additional challenges include uneven

capturing of the transcript coverage, low molecular capture rate, low cDNA conversion efficiency, limited amount of starting material, and variability in cell size (amount of RNA molecules inside a cell) that inevitably result in lower coverage and higher technical noise (Chen *et al.*, 2019; Jaitin *et al.*, 2014; Trapnell & Salzberg, 2009).

Finally, another recent emerging technology is spatial transcriptomics, one of the most recently emerging approaches to provide single-cell resolution. Spatial transcriptomics allows for the possibility to analyze gene expression patterns *in situ* *i.e.*, the mapping of localized gene expression across tissue sections, thereby keeping the spatial context otherwise destroyed by cell or nuclei isolation. This provides single-cell resolution of gene expression and reveals the spatial organization of cell types as well as their interactions within tissue sections. However, the currently available resolution is much lower compared to scRNA-seq. While scRNA-seq provides a comprehensive coverage of the transcriptome of individual cells, spatial transcriptomics can thus far only provide information about a subset of genes (approximately 500-1000 genes), limiting the ability to identify novel cell types and to quantitatively analyze gene expression levels. Ultimately, the requirement of high quality tissue sections may be limiting for generating high quality and reproducible results.

Considering the above, we decided to apply a RiboTRAP approach (Sanz *et al.*, 2009), which combines some of the advantages of both scRNA-seq and bulk sequencing and allows for the selective profiling of specific cell types or subcellular compartments. In fact, it grants the power of high-throughput sequencing of a large number of cells *i.e.*, greater coverage and statistical power compared to scRNA-seq. It also reduces the technical noise associated with scRNA-seq by amplifying transcripts from each cell in bulk, which reduces the impact of amplification bias and sequencing noise. Conversely, technical variability and efficiency of the tagging approach can impact sensitivity and specificity of the method. Moreover, one of the biggest challenges is that the output of RiboTRAP sequencing is a series of exons predicted to be regulated, but the full-length sequence of the isoforms in which these exons are expressed is missing. It is therefore unknown to which specific transcript isoform these exons belong and even harder to predict the protein product that derives from it.

To address the issue of the missing full-length sequence of target RNAs, PacBio long-read sequencing would offer a much better resolution. PacBio has the ability to capture full-length transcripts, enables the detection of complex genomic structures (e.g. epigenetic modifications such as DNA methylation or histone modifications), and the accurate annotation of alternative splicing and isoform diversity (Eid *et al.*, 2009; Korlach *et al.*, 2010). These techniques use single molecule, real-time (SMRT) sequencing technology to generate long reads of up to 100 kilobases (kb) in length. The technology relies on the use of a polymerase that incorporates

nucleotides into a growing DNA strand in real-time, while a light sensor detects the fluorescent signal from each base. However, the technology is still relatively expensive, it requires a very high sample quality and the throughput is lower, meaning that fewer reads can be generated in a single run. Further, at the time of our method evaluation, the output data of long-read sequencing was still very challenging to analyze and needed specialized computational resources, also because of the higher error rate of this type of sequencing. As the cost of long read sequencing continues to decrease and the technology improves, it is likely that this method will become increasingly important for many different applications as it allows for a better prediction of cell proteomes.

Modulating alternative splicing for the development of novel therapeutic avenues

In my thesis, I focused on the physiological relevance of alternative splicing by using RBM20 as a study example. Alternative splicing is the major mechanism increasing the protein coding power of genes, allowing for the synthesis of structurally and distinct protein variants from a single pre-mRNA, with similar, broader, more specific, or even opposing functions. Because of its importance in normal physiology, alternative splicing can contribute to the development of various diseases including cancer, neurodegeneration, and genetic disorders. In cancer, for instance, aberrant splicing can lead to the expression of oncogenic isoforms or the loss of tumor suppressor variants (El Marabti & Younis, 2018; Kitamura & Nimura, 2021; Surget *et al.*, 2013). In neurodegenerative diseases such as Alzheimer's and Parkinson's, the mis-regulation of splicing can result in the accumulation of toxic protein aggregates and neuronal dysfunction (Li *et al.*, 2021). Finally, in genetic disorders, mutations affecting splicing sites or regulatory elements can disrupt normal splicing patterns and cause disease. From these examples, it becomes clear that understanding the molecular mechanisms underlying aberrant splicing in different pathological conditions is crucial for developing effective therapies. Harnessing alternative splicing modulation as a therapeutic strategy has already been done successfully: One example is the use of Antisense oligonucleotides (ASOs), which are short synthetic single-stranded RNA or DNA molecules (~20 nucleotides) that can bind to specific pre-mRNA sequences either induce the mRNA degradation by endogenous RNase H or block the mRNA translation (Liang *et al.*, 2017). This ultimately decreases the expression of certain proteins. ASOs retain the properties of creating RNA-RNA and DNA-RNA duplexes that knock-down or correct genetic expression. For instance, ASOs can act as splicing enhancers or inhibitors, depending on their design and target site, thus promoting either exon inclusion, or exclusion. These small molecules promise a therapeutic approach for various genetic disorders caused by aberrant splicing, as they can be designed for gene therapy to specifically target disease-

causing splicing events, such as mutations or aberrant splice sites, while leaving normal splicing patterns intact. In spinal muscular atrophy (SMA), a neuromuscular disorder caused by mutations in the survival motor neuron 1 (SMN1) gene, ASOs targeting the splicing silencer element in SMN2 pre-mRNA can promote exon 7 inclusion and restore functional SMN protein expression. This approach has been approved by the FDA as the first-ever RNA-targeted therapy for a genetic disease. Similarly, a second-generation ASO that targets the abnormal splicing of the superoxide dismutase (SOD1) in amyotrophic lateral sclerosis (ALS), have been shown to prolong survival and improve motor function in mouse models (Fang *et al.*, 2022; Miller *et al.*, 2020; Smith *et al.*, 2006). Additionally, precise regulation of TDP-43 and FUS expression and subcellular localization is critical in ALS. Therefore, gene therapy aimed at controlling these properties may offer a promising therapeutic strategy for individuals with TARDBP and FUS-associated diseases. Recently, a clinical trial has been launched to evaluate the efficacy of ASOs targeting the FUS gene (Korobeynikov *et al.*, 2022). These results suggest that ASOs could be a potential therapeutic strategy for treating neurodegenerative diseases and/or restore alternative splicing changes. In this sense, in DCM patients some of RBM20's target mRNAs (*Titin*, *Camk1lδ* and *Cacna1c*), fundamental for the heart's correct contractile function, could be targeted by ASOs and physiological isoforms could be restored, increasing the life span of these patients. However, big advancements are still needed to solve challenges arising from the delivery of ASOs to specific target cells or tissues and to mitigate this risk of off-targets, thus ensuring specificity and safety. In fact, the efficacy of ASOs also depends on their stability, biodistribution, and pharmacokinetics, which can vary depending on their design and target site. Further, the potential for off-target effects is one of the biggest limitations as ASOs can bind to unintended targets, leading to unintended splicing changes or other undesirable effects, which could harm the patients' health conditions.

Another powerful therapeutic approach that can be used to correct mutations or aberrant splice sites that cause disease is CRISPR/Cas9 genome editing. The system works by using a guide RNA to direct the Cas9 enzyme to the specific DNA sequence that needs to be edited. Once there, the Cas9 enzyme cuts the DNA, and the cell's repair machinery can then introduce the desired edits. CRISPR/Cas9 has shown promising results in the treatment of brain-related diseases caused by genetic mutations, such as Huntington's disease and amyotrophic lateral sclerosis (ALS). In ALS, CRISPR/Cas9 has been used to correct mutations in the SOD1 gene, which is associated with familial ALS (Duan *et al.*, 2020; Fang *et al.*, 2022; Gaj *et al.*, 2017; Lim *et al.*, 2020). In the same way, DCM patients harboring a mutation in the *Rbm20* sequence, could employ gene therapy to correct the mutation and restore the correct function of the RBM20 protein.

Finally, one of the major challenges in developing therapies for neurodegenerative diseases is delivering drugs or therapeutic agents to the brain. The blood-brain barrier (BBB) is a selectively permeable barrier that prevents most drugs from entering the brain parenchyma. Compared to small molecules (low molecular weight compounds), ASOs cannot bypass the BBB because of their size and thus it is difficult to deliver therapeutic agents directly to the target cells. However, a great effort has been made to grant some brain access to these molecules. For example, ASOs conjugated with brain-targeting peptides or antibodies hold a great potential as therapeutic as they can accumulate in specific brain regions, thus resulting in a very powerful tool for treating brain tumors. In fact, the Cancer Genome Atlas (TCGA) database reported that mutations in 119 genes responsible for splicing may function as cancer-causing factors. Additionally, it has been uncovered that over 70% of splicing factors and 84% of RBPs exhibit abnormal expression levels at the mRNA stage in cancer (Murphy *et al.*, 2022; Seiler *et al.*, 2018; Stanley & Abdel-Wahab, 2022). Thus, the dysregulation of the splicing machinery and regulatory factors in disease states highlights the necessity to promote the development of small molecule inhibitors that target the spliceosome or its auxiliary proteins as new therapeutic approaches (Yoon *et al.*, 2006). Further, clinical trials for novel non-invasive drug delivery systems such as focus ultrasound (FUS) or extracellular vesicle (EVs) delivery hold the potential for major advancement for the treatment of neurological diseases (Morse *et al.*, 2019; Ye & Chen, 2022; Yuan *et al.*, 2022).

Collectively, alternative splicing modulation holds great promise as a therapeutic strategy for treating brain-related diseases. ASOs, small molecules, and CRISPR/Cas9 genome editing are three of the most promising approaches for employing alternative splicing modulation to cure brain-related diseases. Further research is needed to fully explore the potential of these approaches and to develop safe and effective therapies for patients.

4. Conclusions

Conclusions

In the last decade, the term “terminal selector” emerged, to describe the battery of genes that confers unique identities to neurons (Hobert, 2016; Hobert & Kratsios, 2019). As an extension of this concept, we postulate that RBM20 and other RBPs, and in particular splicing factors, are also part of this “terminal gene battery”, which 1) are expressed early in development (I observed RBM20 expression in the olfactory bulb already at embryonic day 16 (E16)) to specify the intrinsic and synaptic properties of individual neurons, and 2) can modify splicing in a cell type-specific manner, thereby promoting neuronal diversification.

In my PhD thesis, I investigated the role of RBM20 in two different neuronal cell types, GABAergic neurons in the neocortex and glutamatergic neurons of the olfactory bulb. In the latter neuronal population, RBM20 is targeting and modulating transcripts involved in synaptic structural and functional properties and in forming the cytoskeleton. Further, I provided the characterization of the function of a splicing factor in two structurally and functionally different tissues, the heart and the olfactory bulb. I conclude that the majority of the direct mRNA targets in these two tissues are different and therefore propose that the role of RBM20 could be context-dependent.

In summary, my work contributes to the notion that the combination of broadly and selectively expressed RBPs in neurons create codes that generate distinct properties, resulting in unique neuronal functions. The Ribo-TRAP-seq results offer valuable insights into the specific transcript isoforms that are linked with ribosomes and have the capability to undergo translation, which facilitates the assessment of alternative isoforms that are ultimately translated into proteins. However, it is difficult to predict the proteome solely based on transcriptome studies. Moreover, to obtain a more comprehensive understanding, investigation on the spatio-temporal control and the localization of transcripts in neuronal sub-compartments (*i.e.*, axons, dendrites or synapses) at a given point in time and/or in presence of specific stimuli is required. In addition, information of exon and intron regulation will have to be intersected with studies on protein features (e.g., motifs, binding domains), to infer potential functional impact of specific or new isoforms. Single gene studies on a selected splicing factor using knock-in and knock-out mice combined with targeted proteomic approaches will be fundamental for the functional characterization of specific individual transcript isoforms. Overall, our analysis on the role of RBM20 in neocortical and olfactory bulb samples of genetically-defined cell classes provides a starting point to further investigate a possible molecular code for neuronal function and wiring specificity. Altogether, this work provides insights into how alternative splicing mechanisms contribute to the specification of neuronal properties in a cell type-specific manner. The fine tuning of genes coding for synaptic

components underlines the involvement of alternative splicing in synaptic and cellular plasticity.

5. Materials and Methods

Mice

All procedures involving animals were approved by and performed in accordance with the guidelines of the Kantonales Veterinärat Basel-Stadt. Male and female mice were used in this study. Primary neuron culture *in vitro* studies were done using JAX Swiss outbred mice obtained from Janvier Labs (Le Genest-Saint-Isle, France). *Rpl22-HA* (RiboTag) mice, *Pvalb-cre* mice (Hippenmeyer *et al.*, 2005), *Ai9* mice (Madisen *et al.*, 2010), and *vGlut2-cre* mice (Vong *et al.*, 2011) were obtained from Jackson Laboratories (Jax stock no: 011029, 017320, and 007909, 028863 respectively). *Rbm20^{flox}* conditional knock-out mice (cKO) and *Rbm20* constitutive KO mice were obtained from Prof. E. E. Creemers' Laboratory, Amsterdam. These mice were backcrossed and maintained on a C57BL/6J background. *Tbx21-cre* mice (Haddad *et al.*, 2013), were obtained from Prof. R. Datta's Laboratory, Harvard Medical School, Boston, USA. The specificity of the Cre-lines for the recombination of the *Rpl22*-allele was confirmed by immunohistochemistry and matched previous reports in the literature (Furlanis *et al.*, 2019; Nguyen *et al.*, 2016; Traunmuller *et al.*, 2016). The *Rbm20*-COIN allele knock-in mouse line was generated at the Center for Transgenic Mouse (CTM) lines in Basel. The line was generated using the Crispr-Cas9 system. gRNAs targeting the last intron of *Rbm20* and template "*coin allele*" construct were injected together with RNA encoding for Crispr-Cas9 nuclease into C57BL/6J zygotes. The surviving embryos were transferred into recipient females. The *coin* module fused to a histidine-biotin-histidine-3HA tag. The *coin allele* is inserted in an orientation opposite to the gene's direction of transcription. The gRNA used were: 5' TTGAGTCGGGGTCCCACTG 3'. The 1311 bp megamer containing the upstream homology sequence, *coin module* and downstream homology sequence used:

```
5'ggcgaggctgctgctggagagccctgattcttctctgtttgactcgcaattctgaggggataagcgccctgcatatgtatgcatt
cttctttgggagcctgcagccacctcatgccagtaaggctatgcttactgtgccagatcaccctgtaggctcacatagagccat
gaccagcaacagcatagcgggattccagaggctcactgaggcagctatgacctgcttgcctcccagggcatCCCCAGT
ACCGTTCGTATAatgtatgcTATACGAAGTTATGGGCCCTCTGCTAACCATGTTTCATGCCTT
CTTCTTTTTCTACAGAAGTACCTGTCTCAGCTGGCAGAGGAGGgactcAAGGAGACGGA
GGGACAGACAGCCCAAGCCCCGAGCGTGGTGGGATTGGTCCACACTTGGAAAGGAA
GAAGCTAGCtGGcCAcCATCACCAcCATGGTGCcGCTGGAAAGGCCGGTGAAGGTG
AAATCCCTGCCCCTCTTGCTGGTACaGTTTCTAAGATACTcGTAAAAGAAGGTGACACTG
TTAAAGCTGGTCAAACAGTTCTGGTGGTGGAGGCCATGAAAATGGAGACAGAAATTAAC
GCTCCTACTGACGGAAAAGTTGAAAAGGTGTTAGTTAAGGAAAGAGATGCTGTTCAAGG
TGGTCAAGGTCTAATCAAGATCGGCGTTGCAGGTCATCAcCACCAcCATCAcGGcGCcgcc
gggTATCCCTACGATGTGCCTGACTATGCTgctggcTATCCTTACGACGTGCCCGATTATGC
AgccggcTATCCATACGATGTCCCAGATTACGCTgcccTAGGATCTTTTTCCCTCTGCCAAAA
ATTATGGGGACATCATGAAGCCCCTTGAGCATCTGACTTCTGGCTAATAAAGGAAATTTA
```

TTTTTCATTGCAATAGTGTGTTGGAATTTTTTGTGTCTCTCACTCGGAAGGACATATGGGA
 GGGCAAATCATTAAAACATCAGAATGAGTATACCGTTCGTATAgcatacatTATACGAAGTT
 ATGGGACCCCGACTCAA^{Aggtctctgatgaatgctaactttctaagttgcctgactgagtcagctggcacctgccct}
^{gtgggtcagacttctcactttcacacttggtggttgagtaaagtgaggagaggctgtagagactgaggcattcattctgccaaggc}
^{ccctgacagaaacgctacctgagatggctgtggcagaggctcctggctccctgataaaaggtgtaccagggaaacgtgagctg}
^{aggtgggaggagtgagg}. The entire insert sequence is highlighted in capital letters. Activation by
 Cre-recombinase inverts the *coin* module, resulting in alternative splicing of the tagged exon.
 All lines were maintained on a C57Bl6/J background. Both males and females were used for
 all the experiments unless stated otherwise in the respective method sections.

Generation of anti-RBM20 antibody

For the generation of the anti-RBM20 antibody, the peptide used as antigen was adapted to
 the mouse amino acid sequence based on previous description (Guo *et al.*, 2012): C+
 PERGGIGPHLERKKL (single amino acid code, N to C-terminus, C+ indicates a cysteine
 added to the N-terminus of one of the peptides for thiol-mediated coupling). The synthetic
 peptides were conjugated to keyhole limpet hemocyanin for immunization of two rabbits and
 two guinea pigs (Eurogentec, Belgium). Initial immunization was followed by two additional
 boosts (2–4 week intervals), after which animals were exsanguinated. All sera recognized the
 RBM20 protein in HEK293T cells transfected with *Rbm20* expressing plasmids (Origene,
 CAT#: MR218951). Rabbit anti-Rbm20 antibodies were affinity purified on the peptide antigens
 coupled to sepharose beads, and eluted with glycine-HCL, pH2.5. Affinity-purified rabbit
 antibodies were used for western-blot and immunohistochemistry analyses, as they performed
 better than the antibodies produced in guinea pigs.

Immunochemistry, imaging and statistical analysis

Animals (males and females) from postnatal day 25 to 40 were anesthetized with
 ketamine/xylazine (100/10 mg/kg *i.p.*) and transcardially perfused with fixative (4%
 paraformaldehyde). The brains and hearts were post-fixed overnight in the same fixative at
 4°C and washed 3 times with 100 mM phosphate buffer (PB). Coronal brain slices were cut at
 40 µm with a vibratome (Leica Microsystems VT1000).

For immunohistochemistry, brain sections were kept in 1X PBS before incubation for 1.5 h with
 a blocking solution containing 0.1% Triton X-100 and 5% normal donkey serum (NDS). Slices
 were incubated with primary antibodies in blocking solution at 4°C overnight and washed three
 times (10 min each), in 1X PBS containing 0.1% Triton X-100. Secondary antibody was diluted
 in 1X PBS + 0.05% Triton-X100 for 2 h at RT. Hoechst dye or DAPI dye was co-applied with

secondary antibodies at a final concentration of 0.5 µg/ml or 1.0 µg/ml respectively. Sections were washed three times in 1X PBS before mounting on Menzel-Gläser microscope slides SUPERFROST® PLUS (Thermo Scientific, J1800AMNZ) with Fluoromount-G (Southern Biotech, 0100-01).

The following primary antibodies were used in this study: rat anti-HA (Roche, 11867431001, 1:1000); goat anti-Parvalbumin antibody (Swant, PVG213), rabbit anti-Rbm20 antibody (made in house), rabbit-anti-NeuN (Novus Biologicals cat. n. NBP1-77686SS), rabbit-anti- Doublecortin (Cell Signaling cat. n. 4604S), rabbit-anti-Calretinin (Swant, cat. n. 7697).

Secondary antibodies included donkey anti-rat IgG-Cy3 and Cy5 (Jackson ImmunoResearch, 712-165-153, 706-175-148, 1:1000); donkey anti-goat IgG-Cy3 and donkey anti-chicken IgG-Cy3 (Jackson ImmunoResearch, 705-165-147, 703-165-155). Stacks of 30 µm width (0.44 to 1 µm z-step) were acquired at room temperature on an upright microscope (Zeiss) using 40x Aplanachromat objectives (numerical aperture 1.30) controlled by the Zen 2010 software. Following acquisition, images were processed and assembled by performing maximum projection or sum intensity projections using Fiji (Schindelin *et al.*, 2012), OMERO and Adobe Illustrator software.

For quantifications of RBM20 positive neurons in the olfactory bulb, tile-scan images from 30 µm slices from the olfactory bulb of P35 mice were acquired. Mean intensity analyses for RBM20 signal were performed in Fiji (Schindelin *et al.*, 2012) using a custom-made Python script, as previously described (DOI-https://github.com/imcf-shareables/3D_spots_count/blob/main/README.md). In brief, neuronal cells were identified based on the nuclear DAPI signal. The mean intensity of RBM20 protein in each nucleus was then measured and the background signal was subtracted.

For the characterization of RBM20 sub-nuclear localization, brain and heart samples from *Rbm20* WT and *Rbm20* cKO mice (P35-P40) were anesthetized with ketamine/xylazine (100/10 mg/kg *i.p.*) and transcardially perfused with fixative (4% paraformaldehyde). The brains and hearts were post-fixed overnight in the same fixative at 4°C and washed 3 times with 100 mM phosphate buffer (PB). Coronal brain slices were cut at 40 µm with a vibratome (Leica Microsystems VT1000). Brain samples were immersed in 15% and subsequently 30% sucrose in 1X PBS for 48 h, cryoprotected with Tissue-Tek optimum cutting temperature (OCT) and frozen at -80° until use. Tissue was sectioned at 40 µm on a cryostat (Microm HM560, Thermo Scientific) and collected in 1X PBS. Immunohistochemistry and imaging were performed as described above.

Fluorescent *in situ* hybridization

Fluorescent *in situ* hybridization was performed as described in the RNAScope Fluorescent Multiplex Kit user manual (Advanced Cell Diagnostics, Catalog Number 320851). P25 mouse brains from *CamK2Cre*, *SSTCre*, *PVCre* and *VIPCre* mouse lines crossed with the *tdtomato* reporter (C57BL/6j background) were snap frozen in liquid nitrogen and 15 μm coronal sections were cut on a cryostat (Microm HM560, Thermo Scientific). Sections were fixed at 4°C overnight with 4% paraformaldehyde in 100 mM phosphate buffered saline, pH 7.4.

Images were acquired at room temperature with an upright LSM700 confocal microscope (Zeiss) using 40X Apochromat objectives. Stacks of 10-15 μm width (0.44 μm interval between stacks) were acquired from layer 5 (L5) of the primary somatosensory area (S1). Cell types were identified based on the presence of the *tdtomato* marker. The following commercial probes (ACD) were used to detect *Rbm20* and *tdtomato* transcripts. *Rbm20* (549251), *tdtomato* (317041). A region of interest (ROI) was drawn to define the area of the cell and dots in the ROI were manually counted throughout the z-stacks. The number of dots in the ROI were then normalized to the cell area (measured in μm^2). Images were assembled using Fiji and Adobe Illustrator Software. Three mice per *Cre*-line were used and images from both brain hemispheres were analyzed.

For quantification of *vGlut2*, *Tbr2* and *Rbm20* transcripts expression in mitral and tufted neurons of the olfactory bulb, P25 animals were euthanized and the brains were harvested and processed as described above. Stacks of 10-15 μm width (0.44 μm interval between stacks) were acquired from olfactory bulb slices at room temperature with an upright LSM700 confocal microscope (Zeiss) using 40X Apochromat objectives. A ROI was drawn to define the area of each cell residing either in the mitral cell layer or glomeruli layer of the olfactory bulb. Dots in the ROIs were detected automatically throughout the z-stacks for each channel, using a custom-made Python script, as described in (DOI-https://github.com/imcf-shareables/3D_spots_count/blob/main/README.md). The following commercial probes were used: *Rbm20* (549251), *slc17a6* (319171), *Tbr2* (Eomes): (429641). Images from 3 mice were used for the quantification (2 images per slice). *Gad2* (415071) *in situ* hybridization was performed on 15 μm olfactory bulb slices of P25 mice.

Western Blot

Lysis of mouse neocortices, olfactory bulb and heart samples were performed with lysis buffer (50 mM Tris HCl pH 8.0, 150 mM NaCl, 0.1% SDS, 5mM EDTA, 1% Igepal, protease inhibitor, Roche complete™ mini). The lysate was sonicated (100 Hz Amplitude 0.5 cycles x 10 pulses) and centrifuged for 20 min at 13'000 g at 4°C, followed by supernatant collection. To 80 μl of lysate, 20 μl Lämmli buffer was added. The mixture was denatured at 95°C for 5 min. Proteins

were separated by gel electrophoresis on 4%–20% gradient PAGE gel (BioRad, 4561093) in 1% SDS-PAGE running buffer and transferred onto nitrocellulose membrane (BioRad 1704158). The following antibodies were used: rabbit-anti-RBM20 (made inhouse), rat-anti-HA (Roche, cat. n 11867431001) and rabbit-anti-GAPDH (Cell Signaling, 5174), rabbit-anti-MAP2 (Synaptic Systems, cat n. 188002), rabbit-anti-RFP (Rockland cat. n. 600-401-379), chicken-anti-GFP (Aves Labs Inc. cat. n. GFP-1020). Secondary antibodies coupled to horseradish peroxidase (HRP) were from Jackson ImmunoResearch (goat anti-rabbit HRP #111-035-003; goat anti-rat HRP #112-035-143)

Sample preparation for LC-MS

Murine nuclear extracts of heart tissue were lysed in a buffer containing 100 mM TEAB pH 8.5 / 5% SDS / 10 mM TCEP using 20 cycles of sonication (30 s on / 30 s off per cycle) on a Bioruptor system (Dianode) followed by heating to 95° C for 10 min. Protein extracts were alkylated using 15 mM iodoacetamide at 25°C in the dark for 30 min. For each sample, 50 µg of protein lysate was captured, digested, and desalted using STRAP cartridges (Protifi, NY, US) following the manufacturer's instructions. Samples were dried under vacuum and stored at –80°C until further use.

Targeted LC-MS analysis

For targeted LC-MS analysis, parallel reaction-monitoring (PRM) assays (Peterson *et al.*, 2012) were generated for 12 proteotypic peptides of RBM20 previously identified by LC-MS. Therefore, a mixture containing 100 fmol of each heavy reference peptide (JPT, Berlin, Germany) including iRT peptides (Biognosys, Schlieren, Switzerland) were LC-MS analyzed. The setup of the µRPLC-MS system was as described previously (Pubmed-ID: 27345528). Chromatographic separation of peptides was carried out using an EASY nano-LC 1000 system (Thermo Fisher Scientific), equipped with a heated RP-HPLC column (75 µm x 30 cm) packed in-house with 1.9 µm C18 resin (Reprosil-AQ Pur, Dr. Maisch). Peptides were analyzed per LC-MS/MS run using a linear gradient ranging from 95% solvent A (0.15% formic acid, 2% acetonitrile) and 5% solvent B (98% acetonitrile, 2% water, 0.15% formic acid) to 45% solvent B over 60 min at a flow rate of 200 nl/min. Mass spectrometry analysis was performed on a Q-Exactive HF mass spectrometer equipped with a nanoelectrospray ion source (both Thermo Fisher Scientific). Each MS1 scan was followed by high-collision-dissociation (HCD) of the 10 most abundant precursor ions with dynamic exclusion for 20 s. Total cycle time was approximately 1 s. For MS1, 3e6 ions were accumulated in the Orbitrap cell over a maximum time of 100 ms and scanned at a resolution of 120'000 FWHM (at 200 m/z). MS2 scans were acquired at a target setting of 1e5 ions, accumulation time of 50 ms and a resolution of 30'000

FWHM (at 200 m/z). Singly charged ions and ions with unassigned charge state were excluded from triggering MS2 events. The normalized collision energy was set to 30%, the mass isolation window was set to 1.4 m/z and one microscan was acquired for each spectrum.

The acquired raw-files were database searched against a *mus musculus* database (Uniprot, download date: 2020/03/21, total of 44'786 entries) by the MaxQuant software (Version 1.0.13.13). The search criteria were set as following: full tryptic specificity was required (cleavage after lysine or arginine residues); 3 missed cleavages were allowed; carbamidomethylation (C) was set as fixed modification; Arg10 (R), Lys8 (K) and oxidation (M) as variable modification. The mass tolerance was set to 10 ppm for precursor ions and 0.02 Da for fragment ions. The best 6 transitions for each peptide were selected automatically using an in-house software tool and imported to SpectroDive (v10.5, Biognosys, Schlieren, Switzerland). A mass isolation lists containing all selected peptide ion masses were exported and imported into the QE-HF operating software for PRM analysis using the same LC and MS setting as above with the following modifications: The resolution of the orbitrap was set to 240'000 FWHM (at 200 m/z) and the fill time was set to 500 ms to reach a target value of 3e6 ions. Ion isolation window was set to 0.4 Th and the scan range was set to 100-1500 Th. Normalized collision energy was set to 27%. A MS1 scan using the same conditions for DDA was included in each MS cycle. All raw-files were imported into SpectroDive for protein / peptide quantification. For final quantification of RBM20, a single targeted LC-MS analysis including only PRM assays of the 3 most intense peptide ions (ASPPTESDLQSQACR, QGFGCSCR and SGSPGPLHSVSGYK) was performed. To control for variation in sample amounts, the total ion chromatogram (only comprising peptide ions with two or more charges) of each sample was determined by Progenesis QI (version 2.0, Waters) and used for normalization. All calculations were carried out in Excel and PRISM (v9, GraphPad).

Surgeries and stereotactic injections

vGlut2Cre::Rpl22HA::Rbm20^{flxed} and Rbm20^{WT} littermate mice (postnatal day 24 to 27) were placed on a heating pad in a stereotaxic frame (Kopf Instrument) under isoflurane anesthesia (Baxter AG, Isoflurane 3-4% oxygen 800 CC). A small incision (0.5–1 cm) in the skin overlying the area of interest was made, and bilateral injections of retro-pAAV2-pCAG-flex-GFP or retro-pAAV2-syn-Cre virus (2.0*10¹² C/ml viral titer) were performed in the posterior Piriform Cortex using a Picospritzer III pressure injection system (Parker) with borosilicate glass capillaries (length 100 mm, OD 1 mm, ID 0.25 mm, wall thickness 0.375 mm, provided by Hilgenberg). Coordinates: ML = + 2,2 mm, AP = + 2,35 mm, DV = - 3,95 mm from Bregma. A volume of 100 nl of virus was delivered to each side, through repeated bursts over several minutes. After 10 days of incubation, mice were anesthetized and transcardially perfused with PBS 1X followed by 4% PFA in PBS 1X (Electron Microscopy Sciences, 15700). Dissected brains were then

incubated in PFA 4% for 2 h at 4°C followed by 3 washes in 1X PBS. The Olfactory bulb and part of the anterior prefrontal cortex was cut and further processed for clearing as described below. The remaining brain tissue was stored at 4°C in 1X PBS and coronal brain slices were cut at 50 µm with a vibratome (Leica Microsystems VT1000) to control for correct injection sites. Prior to mounting on glass microscopy slides with Fluoromount G (Thermo Fisher, 00-4958-02), the sections were stained with DAPI 1:10000 for 3 min and then washed with 1X PBS. Images of coronal brain sections to assess the correct injection site, were acquired at room temperature on a Slide scanner AxioScan.Z1 (Zeiss) using a 20X objective.

Tissue clearing, two photon imaging and analysis

The Cubic L protocol used for tissue clearing is based on work from Tainaka and colleagues (Tainaka et al., 2018). In brief, the olfactory bulb of *Rbm20* WT and conditional KO mice, injected bilaterally with retro-pAAV-flex-EGFP virus, was placed in a 5 ml Eppendorf tube filled with pre-warmed CUBIC L solution (10% N-butyl-di-ethanolamine and 10% Triton X-100 dissolved in MilliQ water). The tissue was incubated on a shaking plate at 37°C for 48 h to ensure complete delipidation. The cleared bulbs were then washed in 50 mM PBS 3 times for 10 min and then cut in two coronal halves under a Binocular Stereo Microscope (Olympus #MVX10). The two halves of each bulb (anterior or posterior) were then embedded in 1% agarose in 1X TBE solution in an imaging chamber (Ibidi, Cat.No:80426), with the glomeruli layer of the olfactory bulb facing the bottom of the slide chamber, closer to the objective of the two-photon microscope. Z-stacks of GFP⁺ neurons with the soma residing in the mitral cell layer of the olfactory bulb were acquired on a two-photon microscope (Olympus, FMPE-RS) fitted with a MaiTai eHP laser (Spectra-Physics) and a 25X objective with 1.05NA (Olympus). A total volume of 1.5 x 1.5 mm (xy) x 500-700 µm in depth was acquired in tiles of 3x3, with x = 0.995 µm, y = 0.995 µm and z = 3 µm pixel size. Laser power was linearly adjusted with imaging depth and typically ranged between 0.5 to 20 mW.

The high-resolution two-photon z-stack images of GFP⁺ mitral cells of the olfactory bulb were used to trace neurons using the NeuroLucida 360® software. A total of 10 neurons (5 neurons per genotype from at least 3 biological replicates) were analyzed. Both apical and lateral dendrites of mitral cells were traced semi-automatically by using the user-guided 3D image detection algorithm. Tracings were checked and corrected manually when needed. Subcellular components, such as spines and other small protrusions were not traced. The lateral dendrites of mitral cells were often prematurely cut or longer than the z-stack and could not be traced entirely. Furthermore, axons were not always recognizable and therefore not traced. The thickness of all dendrites and glomeruli tufts was set to 0.5 µm for image presentation. To

describe the neuronal morphology, commonly used parameters were derived using the software NeuroLucida Explorer®. The following parameters were extracted for traced neurons: the number of dendrites from different centrifugal orders (*i.e.* primary dendrites, secondary dendrites etc.), the number of segments (*i.e.* branches between nodes), the total dendritic length, the length of individual dendrites and individual segments. The tortuosity parameter (described as the ratio of the actual length of the segment divided by the distance between the endpoints of the segment), was calculated for the glomeruli tufts and used as a proxy for glomeruli complexity. Average values were calculated for each neuron analyzed. Graphs and statistical analyses (t-tests) were made using GraphPad Prism.

RNA isolation and purification by RiboTrap pulldowns

Ribotag purification was performed following the procedure of Heiman and colleagues for affinity-purification of polysomes associated mRNAs (Heiman *et al.*, 2008). For small brain areas such as the olfactory bulb, the protocol was modified to ensure a higher RNA recovery (Di Bartolomei & Scheiffele, 2022). In brief, neocortices and olfactory bulbs from *PV-cre* and *vGlut2-cre* mice between postnatal day 35 and 40 (males and females) were dissected in ice-cold PBS. Control samples from animals negative for either Rpl22 or cre-recombinase were used to ensure specificity of the pulldown. For each biological replicate, 2 cortical hemispheres and 2 olfactory bulbs were used (1 animal per condition). Tissue was homogenized in respectively 500 μ L or 7 mL (1:20 weight per volume) of homogenization buffer containing 100 mM KCl, 50 mM Tris-HCl pH 7.4, 12 mM MgCl₂, 100 μ g/mL cycloheximide (Sigma-Aldrich), 1 mg/mL heparin (Sigma-Aldrich), 1X complete mini, EDTA-free protease inhibitor cocktail (Roche), 200 units/ml RNasin® plus inhibitor (Promega) and 1 mM DTT (Sigma-Aldrich). The samples were then centrifuged at 2'000 x g for 10 min and the supernatant was lysed with Igepal-CA630 (Sigma-Aldrich), at a final concentration of 1%. Upon 5 min incubation on ice, the lysate was centrifuged at 12'000 x g for 10 min. Before incubation with beads, 1% of the supernatant was taken (Input) and re-suspended in 350 μ l of RLT plus buffer from RNeasy Plus Micro Kit (Qiagen, 74034) supplemented with 2-Mercaptoethanol (Sigma-Aldrich), following the manufacturer's instructions. Anti-HA coupled magnetic beads (Pierce, 88837) were added to the supernatant: 140 μ l of beads for all neocortical samples, 20 μ l for *vGlut2-cre* olfactory bulb samples. Incubation was performed under gentle rotation at 4°C for 4 h. After incubation, beads were washed 3-4 times in washing buffer containing 300 mM KCl, 1% Igepal-CA630 (Sigma-Aldrich), 50 mM Tris-HCl, pH7,4, 12 mM MgCl₂, 100 μ g/mL Cycloheximide (Sigma-Aldrich) and 1 mM DTT (Sigma-Aldrich). Beads were then eluted in 350 μ l of RLT plus buffer from RNeasy Plus Micro Kit (Qiagen) supplemented with 2-Mercaptoethanol (Sigma-Aldrich). RNA samples were stored at -80°C until use.

RNA quality control, quantification and qPCR analysis

For all the RNA-seq experiments, the quality of RNA integrity was analyzed using an RNA 6000 Pico Chip (Agilent, 5067-1513) on a Bioanalyzer instrument (Agilent Technologies) and only RNA with an integrity number higher than 7 was used for further analysis. RNA concentration was determined by Fluorometry using the QuantiFluor RNA System (Promega #E3310) and 50 ng of RNA was reverse transcribed for analysis of marker enrichment by quantitative PCR. The following neuronal markers were tested: for the olfactory bulb pull-down samples: *Rbm20*, *vGlut2*, *vGlut1*, *Tbr2*, *Pcdh21*, *Igf1*, *vGAT*, *GFAP*, *GAD1* (*GAD67*). For pulldowns from cortex of PVCre mice: *Rbm20*, *PV*, *vGAT*, *GAD67*, *vGlut1*, *GFAP*. In both cases, *Gapdh* mRNA was used as a housekeeping gene for normalization. The fold enrichment and de-enrichment values of each marker were calculated for each cell population in immunoprecipitated RNA, comparing it to input purifications. Only samples that showed correct enrichment or de-enrichment for excitatory or inhibitory neuronal markers and a de-enrichment for glia markers were further used for sequencing. DNA oligonucleotides were used with FastStart Universal SYBR Green Master (Roche, 4913914001) and comparative C_T method. For each assay, three technical replicates were performed and the mean was calculated. RT-qPCR assays were analyzed with the StepOne software. DNA Oligonucleotides used (name and sequence 5'-3' are indicated):

List of primer sequences:

Primer Name	Sequence
<i>Rbm20</i>	Forward (Sense) TGCATGCCCGAGAAATGCCTGCT Reverse (AntiSense) AAAGGCCCTCGTTGGAATGGCT
<i>Tbr2</i>	Forward (Sense) ATAAACGGACTCAACCCACC Reverse (AntiSense) CCCTGCATGTTATTGTCCGC
<i>Pcdh21</i>	Forward (Sense) ATCACTGTCAACGACTCAGACC Reverse (AntiSense) GTCAATGGCAGCTGAGTTTTCC

<i>Igf1</i>	Forward (Sense) GTCGTCTTCACACCTCTTCTAC Reverse (AntiSense) CTCATCCACAATGCCTGTCT
<i>vGlut2</i>	Forward (Sense) GCATGGTCTGGTACATGTTCTG Reverse (AntiSense) GACGGGCATGGATGTGAAAAAC
<i>Gad67</i>	Forward (Sense) GTA CT TCCCAGAAGTGAAAC Reverse (AntiSense) GAATAGTGACTGTGTTCTAGG
<i>Gfap</i>	Forward (Sense) CTCGTGTGGATTTGGAGAG Reverse (AntiSense) AGTTCTCGAACTTCCTCCT
<i>vGlut1</i>	Forward (Sense) ACCCTGTTACGAAGTTTAACAC" Reverse (AntiSense) CAGGTAGAAGGTCCAGCTG
<i>vGAT</i>	Forward (Sense) CGTGACAAATGCCATTCAG Reverse (AntiSense) AAGATGATGAGGAACAACCC
<i>PV</i>	Forward (Sense) CATTGAGGAGGATGAGCTG Reverse (AntiSense) AGTGGAGAATTCTTCAACCC

Library preparation and illumina sequencing

Four and six biological replicates per PV⁺ and vGlut2⁺ neuronal populations in WT and cKO mice were analyzed. Library preparation was performed with 50 ng of RNA using the TruSeq PolyA⁺ Stranded mRNA Library Prep Kit High Throughput (Illumina, RS-122-2103). Libraries were quality-checked on a Fragment Analyzer (Advanced Analytical) using the Standard Sensitivity NGS Fragment Analysis Kit (Advanced Analytical, DNF-473), revealing high quality

of libraries (average concentration for PV sample libraries was 77 ± 1 nmol/l and average library size was 319 ± 1 base pairs; average concentration for OB sample libraries was 61 ± 1 nmol/l and average library size was 305 ± 1 base pairs). All samples were pooled to equal molarity and the pool was quantified by PicoGreen Fluorometric measurement. The pool was adjusted to 10 pM for clustering on C-Bot (Illumina) and then sequenced Paired-End 151 bases using the HiSeq SBS Kit v4 (Illumina, FC-401-4003) on a Nova-seq 600 system. Primary data analysis was performed with the Illumina RTA version 1.18.66.3 and bcl2fastq-v2.20.0.422.

Ribo-TRAP data analysis

The gene expression and splicing analysis of the RNA-Sequencing data were performed by GenoSplice technology (www.genosplice.com) and as described in detail in (Furlanis *et al.*, 2019). In brief, sequencing, data quality, reads repartition (e.g., for potential ribosomal contamination), and insert size estimation were performed using FastQC, Picard-Tools, Samtools and RSeQC tool packages. Reads were mapped using STAR (v2.4.0) (Dobin *et al.*, 2013) on the mm10 Mouse genome assembly. The input read count matrix was the same as used for the splicing analysis. Two samples from the olfactory bulb were excluded from the analysis after the quality control of the data (see markers enrichment analysis). The remaining olfactory bulb and cortical samples were normalized separately.

Gene expression regulation study was performed as already described (Furlanis *et al.*, 2019; Noli *et al.*, 2015). Read counts were summarized using featureCounts (Liao *et al.*, 2014). For each gene present in the FASTDB v2021_4 annotations, reads aligning on constitutive regions (that are not prone to alternative splicing) were counted. Based on these read counts, normalization and differential gene expression were performed using DESeq2 (values were normalized to the total number of mapped reads of all samples) (Love *et al.*, 2014) on R (v.3.5.3). Genes were considered as expressed if their FPKM value is greater than 96% the background FPKM value based on intergenic regions. A gene is considered as expressed in the comparison if it is expressed in at least 50% of samples in at least one of the 2 groups compared. Results were considered statistically significant for adjusted p-values ≤ 0.01 (Benjamini Hochberg for p-value adjustment as implemented in DESeq2) and $\log_2(\text{FC}) \geq 1.5$ or ≤ -1.5 . For the principal component analysis, counts were normalized using the variance stabilizing transform (VST) as implemented in DESeq2. The internal normalization factors of DESeq2 were used to normalize the counts for generation of heatmaps. The alternative splicing analysis was performed with two types of analysis methods: The EXON and the PATTERN analysis, as described in (Furlanis *et al.*, 2019). The \log_2 fold change (FC) and p-value (unpaired Student's t-test) for both the EXON and PATTERN analysis was calculated by

pairwise comparisons of the respective Splicing Index (SI) values. The SI is defined as the ratio between the read density on the exon of interest and the read density on constitutive exons of the gene. The following types of alternative splicing events can be analyzed: Alternative transcription start site (TSS), alternative last exons (ALE), cassette exon (CE), mutually exclusive exons, alternative 5' donor splice site (5'AD), alternative 3' acceptor splice site (3'AA), intron retention (IR), internal exon deletion (IED) and complex events (corresponding to mix of several alternative event categories, MX). Results were considered significantly different for p -values ≤ 0.01 and $\log_2(\text{FC}) \geq 1$ or ≤ -1 .

Enrichment of olfactory neuron markers

An “activity score” was computed for each of the 12 Ribo-Tag samples and each of the 18 marker lists related to olfactory neurons (cell classes are based on the clusters identified by scRNA-seq from the olfactory bulb; Tepe et al.; 2017). The activity score is the sum of the FPKM expression values of the marker genes weighted by their average $\log_2\text{FC}$, divided by the sum of the gene’s weights. A Heatmap of the weighted activity scores was plotted using R base functions.

Heatmaps and volcano plots

In order to conduct clustering analysis of gene expression, Normalized Feature Counts values were used, and the data were standardized based on the rows. For clustering analysis of Splicing Index (SI) values obtained from PATTERN analysis, both rows and columns were standardized. Exons with *NA* or *Inf* values were removed to prevent bias caused by genes or exons with very low expression. In all instances, the Pearson correlation method was employed to calculate the distance, and the Ward.D2 method was used to cluster the resulting distance matrix. Heatmaps were created in R with the *ggplot2* package.

Virus and plasmid constructs

Retro-pAAV2-pCAG-flex-EGFP-WPRE virus was acquired from Addgene (51502).

Viruses were generated in HEK293T cells using standard protocols with AAV2 capsids. Viral preparations were concentrated in 100K Millipore Amicon columns at 4°C. Samples were then suspended in PBS, aliquoted and stored at –80°C. Viral titers were determined by qPCR and were $>10^{12}$ particles/ml.

The following plasmids were used to generate lentivirus for *Rbm20* mis-expression in neuronal cultures: *Rbm20* (Myc-DDK-tagged) plasmid (Origene, CAT#: MR218951), Syn-DsRed-Syn-GFP plasmid (Gascon et al., 2008). The DsRed sequence was replaced by the *Rbm20*

sequence to obtain the following plasmids which were then used for lentivirus production: Syn-Rbm20-Syn-GFP and Syn-DsRed-Syn-GFP. Viruses were generated in HEK293T cells (Petri dish growth surface area is 150 cm²), incubated in 25 ml of media (5% FCS + 50mM Hepes), at 37°C. DNA was introduced into host cell by transfection with 400 µl polyethylenimine (PEI, in 5 ml Media w/o FCS), (Boussif *et al.*, 1995) and 20 µg of target gene containing plasmids, 13 µg of MV delta R 8.9 and 6.5 µl cmv-VSV-G were added to each plate for 15 min at RT. Cells were incubated in fresh media for 2 days at 37°C. Viral particles were harvested and the media was filtered and frozen at –80°C.

Cell cultures and lentivirus infection.

Primary cortical neuron cultures were prepared from E16.5 mouse embryos of RjOrl:SWISS mice (Janvier Laboratories). Neocortices were dissociated with papain (Worthington Biochemical, LK003176) for 30 min at 37°C. 250'000 cells/wells were plated in 12-well plates and they were maintained in Neurobasal Medium (Gibco, 21103-049) containing 2% B27 supplement (Gibco, 17504-044), 1% GlutaMAX supplement (Gibco, 35050-038), and 1% penicillin/streptomycin (Sigma, P4333). At DIV1, cortical cultures were infected with lentivirus. 10 days after infection, cells were harvested for RNA extraction and purification.

RNA isolation and reverse transcription

10 days after infection with plv-Syn-Rbm20-Syn-GFP or plv-Syn-DsRed-Syn-GFP lentiviruses in primary cortical cultures, neurons were washed 1 time with PBS and lysed using Trizol reagent (Sigma, T9424). The RNA was treated with DNase for 15 min at room temperature. Purification of RNA was performed following the manufacturer's instructions (RNeasy Micro kit, Qiagen, 74004). RNA quality control and RNA quantification were performed as described above. 100 ng of total RNA was reverse transcribed with ImPromII Reverse Transcriptase (Promega, #M314A), RNasin™ Plus RNase Inhibitor (Promega, #N261B), ImPromII 5X Reaction Buffer (Promega, #M289A), dNTPs (Sigma, D7295) and oligo(dT)₁₅ primer (Promega, C1101) and 50 ng cDNA was used for library preparation as previously described. Real-time quantitative PCRs were performed with FastStart Universal SYBR GreenMaster (Roche, 04-913-850-001) was used for qPCR on a StepOnePlus qPCR system (Applied Biosystems) and were analyzed with the StepOne software. The mRNA levels of ER-stress, unfolded protein response (UPR) cascade and apoptotic markers were calculated and normalized to housekeeping β -actin or *Gapdh* mRNAs. Two technical replicates were performed and the mean was calculated. Primers used for SybrGreen were custom designed and obtained from IDT DNA Technologies.

List of primer sequences:

Primer Name	Sequence
<i>Atf4</i>	Forward (Sense) CTGAACAGCGAAGTGTTGGC Reverse (AntiSense) TCTGTCCCGGAAAAGGCATC
<i>Chop</i>	Forward (Sense) GTCCCTGCCTTTACCTTGG Reverse (AntiSense) CTTTGGGATGTGCGTGTGAC

Library preparation, sequencing and analysis of alternative splicing events with Whippet

For the *Rbm20* mis-expression experiment in neocortical cultures four biological replicates per condition were analyzed. The quality of RNA integrity was analyzed as described above (see *Ribo-seq data analysis* section). RNA samples with RIN > 9 were further processed for sequencing. Library preparation and sequencing were performed by MacroGen Europe. Library preparation was performed with 100 ng of RNA using the TruSeq Stranded mRNA LT Sample Prep Kit (Illumina). Size Check to verify the size of PCR enriched fragments was performed on an Agilent Technologies 2100 Bioanalyzer using a DNA 1000 chip, revealing high quality of libraries (average concentration was 36 ± 14 ng/ μ l and average library size was 380 ± 2 base pairs). All samples were pooled to equal molarity and then sequenced Paired-End 151 bases using the NOVAseq6000 platform at a sequencing depth > 80 million reads/sample. For the analysis of alternative splicing events the Whippet pipeline was used (Sterne-Weiler *et al.*, 2018). Briefly, reads were aligned to the mm10 Mouse genome assembly using STAR (Dobin *et al.*, 2013). Whippet detects exon-exon junctions and calls alternative splicing events, such as exon skipping, intron retention, and alternative 5' and 3' splice sites, based on the junctions identified. Finally, Whippet quantifies the PSI value for each splicing event and assigns a *Probability* value, which estimates the likelihood of that particular alternative splicing event to be real. The *Probability* of observing a real AS event must be > 0.9. For a gene to be considered expressed the number of raw read counts must be > 10 counts in 75% of the samples in one of the two conditions. Threshold for Δ PSI value for each splicing event was set at 20%. We also calculated a confidence interval (CI) width around the Δ PSI which we set at $-20\% > CI < +20\%$. Finally, for an exon to be considered regulated, the size must be > 10 bp.

seCLIP and library preparation

The CLIP experiments were performed according to the eCLIP protocol from Nostrand et al. (Van Nostrand *et al.*, 2016) with some minor modifications, as previously described in (Traunmüller *et al.*; 2023). More in detail, olfactory bulbs (7 olfactory bulbs were pooled for each biological replicate) and heart (1 heart per biological replicate) samples were ground on dry ice first in a metal grinder and a porcelain mortar. The frozen powder was transferred into a plastic Petri dish (10 or 6 cm diameter) and distributed in a thin layer. The samples were UV-crosslinked 3 times at 400 mJ/cm² on dry ice with a UV-crosslinker (Clever Scientific). The powder was mixed and redistributed on the Petri dish each UV exposure. The crosslinked powder was re-suspended 3.5ml / 7 OB or 5.5 ml/ heart in the lysis buffer (50 mM Tris-HCl pH 7.5, 100 mM NaCl, 1% NP-40, 0.1% SDS, 0.5% sodium deoxycholate). 1 tablet of the protease inhibitors (Roche) and 4 U per ml buffer Turbo-DNase (Thermofisher), were used per 10 ml of buffer.

The lysate was transferred into a glass homogenizer and homogenized by 30 strokes on ice. 1 ml aliquots of homogenized tissue were transferred to 2 ml tubes, 10 µl of RNaseI (Thermofisher) diluted in PBS (1:5 -1:40) were added to each tube. Samples were incubated at 37°C with shaking for 5 min at 1200 x rpm and then put on ice. 10 µl RNasin RNase-inhibitor (40 U/µl, Promega) were added to each tube. Sample were mixed and centrifuged at 16.000 x g for 15min at 4°C. The supernatants were transferred to a new tube and 60 µl from each sample were taken and further processed for sized matched INPUT (SMIn). 10 µl HA-magnetic beads (Pierce) was added to each sample and incubated at 4°C for 4h in a rotating shaker. Following incubation, the beads were washed 2x with a high salt wash buffer (50mM Tris-HCl pH7.5, 1 M NaCl, 1 mM EDTA, 1% NP-40, 0.1% SDS, 0.5% sodium deoxycholate), 2x with the lysis buffer, 2x with low salt wash buffer (20 mM Tris-HCl pH7.5, 10mM MgCl₂, 0.2% Tween-20) and 1x with PNK buffer (70 mM Tris-HCl pH6.5, 10 mM MgCl₂). Beads were re-suspended in 100 µl PNK-mix (70 mM Tris-HCl pH6.5, 10 mM MgCl₂, 1 mM DTT, 100 U RNasin, 1 U TurboDNase, 25 U Polynucleotide-Kinase (NEB)) and incubated at 37°C for for 20 min on a shaking termomixer (1200 x rpm). Upon RNA dephosphorylation, the beads were washed (2x high salt, 2x lysis and 2x low salt buffers as before) and additionally with 1x Ligase buffer (50 mM Tris-HCl pH7.5, 10 mM MgCl₂). Beads were then re-suspended in 50 µl ligase mix (50 mM Tris-HCl pH7.5, 10 mM MgCl₂, 1 mM ATP, 3% DMSO, 15% PEG8000, 30 U RNasin, 75 U T4 RNA-ligase (NEB)). 10 µl of the beads / ligase mix were transferred to a new tube and 1 µl of pCp-Biotin (Jena Bioscience) were added to validate IP of the RNA-protein-complexes by western blot. 4 µl of the RNA-adaptor mix containing 40 µM of each InvRi L19 & InvRand3Tr3 (IDT) were added to the remaining of the samples (40 µl). Samples were placed at RT for 2 h for adaptor ligation. Samples were washed 2x with high salt, 2x with lysis

and 1x with low salt buffers. Finally, beads were re-suspended in 1x LDS sample buffer (ThermoFisher) supplemented with 10 μ M DTT and incubated for 10 min at 65°C, shaking on a thermomixer at 1200 x rpm. Eluates or inputs were loaded on 4-12% Bis-Tris, 1.5 mm gel (ThermoFisher) and separated at 130 V for ~ 1.5 h. Proteins were transferred overnight at 30 V to a nitrocellulose membrane (Amersham). The membranes were placed in a 15 cm Petri dish on ice and an area between 55 and 145 kDa was cut out small pieces and transferred in a 2 ml tube.

RNA extraction, reverse transcription using InvAR17 primer, cDNA clean-up using silane beads (ThermoFisher), second adaptor ligation (InvRand3Tr3) and cDNA purification steps were performed as previously described (Van Nostrand *et al.*, 2016). The sequencing libraries were amplified using Q5-DNA polymerase (NEB) and i50X/i70X Illumina indexing primers (IDT). Final libraries were amplified with 14 cycles Libraries were purified and concentrated with ProNEX size selective purification system (Promega) using sample/beads ratio of 1/2.4. Samples were loaded on a 2% agarose gel and the area corresponding to the size between 175 bp and 350 bp was cut out. The amplified and purified libraries were then extracted from the gel using gel extraction kit (Machery&Nagel) and eluted with 16 μ l.

The concentrations and the size distributions of the libraries were determined on the Fragment analyzer system (Agilent). 75 bp single-end sequencing was performed on the NextSeq500 platform using Mid Output Kit v2.5 (75 cycles).

Adaptor and primer sequences used in this study:

Name	Sequence
InvRi L19	/5Phos/rArGrArUrCrGrGrArArGrArGrCrArCrA rCrGrUrC/3SpC3/
InvRand 3Tr3	/5Phos/NNNNNNNNNAGATCGGAAGA GCGTCGTGT/3SpC3/
InvA R17	CAGACGTGTGCTCTTCCGA
i501	AATGATACGGCGACCACCGAGATCTACACTATAGCCTACACTCTTTCCCTA CACGACGCTCTTCCGATC*T
i502	AATGATACGGCGACCACCGAGATCTACACATAGAGGCACACTCTTTCCCT ACACGACGCTCTTCCGATC*T
i503	AATGATACGGCGACCACCGAGATCTACACCCTATCCTACACTCTTTCCCTA CACGACGCTCTTCCGATC*T
i504	AATGATACGGCGACCACCGAGATCTACACGGCTCTGAACACTCTTTCCCT ACACGACGCTCTTCCGATC*T

i701	CAAGCAGAAGACGGCATAACGAGATCGAGTAATGTGACTGGAGTTCAGAC GTGTGCTCTTCCGATC*T
i702	CAAGCAGAAGACGGCATAACGAGATTCTCCGGAGTGACTGGAGTTCAGAC GTGTGCTCTTCCGATC*T
i703	CAAGCAGAAGACGGCATAACGAGATAATGAGCGGTGACTGGAGTTCAGAC GTGTGCTCTTCCGATC*T
i704	CAAGCAGAAGACGGCATAACGAGATGGAATCTCGTGACTGGAGTTCAGAC GTGTGCTCTTCCGATC*T

X* = Phosphorothioated base

eCLIP data processing

eCLIP processing was performed as described in (Traunmuller *et al.*, 2023). In brief, the raw reads were processed as described previously (Feng *et al.*, 2019) to obtain unique CLIP tags mapped to mm10 using CTK (Shah *et al.*, 2017). Unique tags from replicates were combined for all analyses. Significant CLIP tag clusters were called by requiring p-value<0.01 after Bonferroni multiple-test correction. Crosslinking-induced truncation sites (CITS) were called by requiring FDR<0.001. Peaks with length < 30bp were removed using StoatyDive (Heyl & Backofen, 2021).

For motif finding, sequences from -10bp to +10bp from significant CITS (FDR<0.001) were used as input sequences for DREME software (Bailey *et al.*, 2009; Bailey *et al.*, 2015; Nystrom & McKay, 2021). As a control, sequences of the same length coming from 500 bp upstream of the (-510 to -490 bases) from the CITS site were used. Enrichment of the known UCUU motif at the CITS sites was calculated.

Gene Ontology analysis

Gene ontology analysis was performed by using a statistical overrepresentation test and the cellular component function PANTHER (<http://pantherdb.org/>). All genes being detected as expressed in RNA-sequencing data were used as reference. GO cellular component annotation data set was used and Fisher's Exact test with Benjamini-Hochberg false discovery rate correction for multiple testing was applied. GO terms with at least 10 genes, at least 1.5-fold enrichment with less than 0.05 false discovery rate (FDR) were considered as significantly enriched. Significant GO terms were plotted in Prism 9. The input list for the background was the list of all genes detected in olfactory bulb samples analyzed by Ribo-TRAP RNA-sequencing. For heart samples, the whole mouse transcriptome was used as a background.

For eCLIP any gene that had significant peak expression in the CLIP dataset either for olfactory bulb or heart samples were used. GO analysis was performed with the R package “clusterProfiler” (Bioconductor version: Release (3.16)) (Wu *et al.*, 2021; Yu *et al.*, 2012). The top ten significant (Benjamini Hochberg for p-value correction), and non-redundant, terms were displayed in Fig.10E and F.

Statistical methods and data availability

Sample sizes were determined based on the 3R principle, past experience with the experiments and literature surveys. Pre-established exclusion criteria were defined to ensure success and reliability of the experiments: for stereotaxic injection, all mice with mis-targeted injections were excluded from analysis (e.g. if no eGFP signal was detected in the mitral cell layer of the OB). Investigators performing image analysis and quantification were blinded to the genotype and/or experimental group. For Ribo-TRAP pull-down experiments, all the samples presenting enrichment of the wrong marker genes were excluded. For the quantification of RBM20 expression in the olfactory bulb statistical analysis was performed with Prism 9 (GraphPad software) using unpaired t-test. Data presented are mean \pm SD. Images were assembled using Fiji, Omero (Swedlow *et al.*, 2003) and Adobe Illustrator software.

A detailed description of the exclusion criteria for different experiments is included in the respective method sections. Statistical analyses were conducted with GraphPad Prism 9. The applied statistical tests were chosen based on sample size, normality of data distribution and number of groups compared. Details on *n*-numbers, p-values and specific tests are found in the figure legends. All raw data files, excel analysis tables and additional data supporting the findings of this study could not be included in the manuscript due to space constraints but are available from the corresponding author upon reasonable request.

Behavioral Analysis

Observer and demonstrator mice were single housed for 1 week prior to the test and habituated to eating powdered food (triturated chow) during this time. For two days prior to the test, demonstrator mice were fed with powdered food supplemented with cumin (50 mg of cumin in 20 g of chow food). The night before the test, both demonstrator and observer mice were deprived of food for 12 h. For the test, demonstrator mice were allowed to eat cumin flavored food for 1 h, and then were put into a new cage with the observer mice for social interaction (30 min). Demonstrators and observers were separated by a plexiglas transparent wall with holes to allow the mice to smell each other and poke their noses through. Immediately (day 0), 1 day (day 1) and 14 days (day 14) after social interaction, the observer mice were placed into

their home cage and tested for 1 h for food preference between cumin-flavored (50 mg in 20 g) and thyme-flavored (100 mg in 20 g) food. The positioning of the beakers containing thyme-flavored and cumin-flavored food was random to avoid position preference of the observer mice. The amount of thyme-flavored or cumin-flavored food eaten by the observer mouse was then measured in grams and expressed as the ratio to the total amount of food consumed (Liu *et al.*, 2017; Loureiro *et al.*, 2019). As a control, mice of each genotype were exposed for 30 min to demonstrator mice that have eaten unflavored food (powdered but no flavor added). To be considered a true interaction, the following criteria had to be met. First, both demonstrator and observer mice had to eat at least 0.2 g of flavored food on the day of the interaction. Second, observer mice were considered for the analysis only if they spent at least 10 min in the interaction area (defined as 2 cm apart from the separator) and if they spent at least 1 min poking their nose into the holes of the Plexiglas separating the demonstrator (sniffing time). When mice were positioned in the interaction area but they were either grooming or showing freezing behavior, the time was not scored. The total interaction time and sniffing time were manually quantified using ChronoMouser v1.0.

Mice used for behavioral experiments were males and females between 6-8 weeks of age, maintained on a C57BL/6J background and housed under standard laboratory conditions on a 12 h light/dark cycle. For the social transmitted food preference paradigm (STFP), demonstrator mice were only females, to avoid fighting between males. All tests were carried out during the light cycle, with standard ceiling light (< 300 lux) and in at least 6 independent trials. All statistical data are mean \pm SD and significance was assessed by Two-way ANOVA followed by Tuckey's multiple comparisons correction or unpaired t-test with Kolmogorov-Smirnov multiple testing correction, for pairwise comparisons.

6. Appendix

Book Chapter

An optimized protocol for the mapping of cell type-specific ribosome-associated transcript isoforms from small mouse brain regions.

Giulia Di Bartolomei and Peter Scheiffele

Biozentrum of the University of Basel, Klingelberstrasse 50-70, CH-4056 Basel, Switzerland

Correspondence:

peter.scheiffele@unibas.ch

giulia.dibartolomei@unibas.ch

Running head: Isolation of ribosome-associated transcripts

Abstract

Over the past years, technological advances in transcriptomics provided deep insights into gene expression programs and their role in tissue organization and cellular functions. The isolation of ribosome-associated transcripts is a powerful approach for deep profiling of cell type-specific transcripts, and particularly well-suited for quantitative analysis of transcript isoforms. This method employs conditional ribosome epitope-tagging in genetically-defined cell types, followed by affinity-isolation of ribosome-associated mRNAs. Advantages of this approach are twofold: first, the method enables rapid retrieval of mRNAs without tissue dissociation and cell sorting steps. Second, capturing of ribosome-associated mRNAs, enriches for transcripts recruited for active translation, therefore providing an approximation to the cellular translome. Here we describe one application of this method for the identification of the transcriptome of excitatory neuronal cells (mitral and tufted cells) of the mouse olfactory bulb, through RiboTag isolation from the vGlut2-IRES-cre mouse line as genetic driver of endogenously tagged ribosome expression.

Key Words: Ribosome-affinity purification, TRAP, RiboTag, Transcriptomics, Cell-type specificity, Alternative Splicing, mRNA isolation

1 Introduction

The past decade has seen breathtaking advances in transcriptomics which contributed to a detailed molecular dissection and classification of cell types and cell states. Next-generation sequencing approaches eliminated challenges posed by microarray technologies, including high variability especially for lowly expressed genes, dynamic range of detection, and caveats arising from incomplete genome annotations. Single cell sequencing proved particularly powerful for a detailed cell type classification based on gene expression profiles (Zeisel *et al.*, 2018; Zeng & Sanes, 2017). Advanced transcriptomic studies also uncovered a major role for alternative splicing and alternative transcription start sites in controlling cellular functions in development and disease states (Furlanis & Scheiffele, 2018; Gonatopoulos-Pournatzis *et al.*, 2020; Nguyen *et al.*, 2016; Parikshak *et al.*, 2016; Wamsley *et al.*, 2018b). However, accurate mapping of alternative transcripts across cell types remains a significant challenge, as the limited and stochastic transcript coverage from single cell sequencing results in low sampling of exon spanning junctions. Moreover, there is some debate whether transcript isoforms detected by transcriptomics are indeed recruited for translation to produce protein isoforms that are functionally relevant in vivo (Liu *et al.*, 2016; Vogel & Marcotte, 2012; Weatheritt *et al.*, 2016).

A key step for uncovering cell type-specific splicing programs is the access to deep, high quality transcriptomic data from the cell type of interest. The most commonly applied methods include enzymatic tissue dissociation followed by immune-isolation or fluorescence activated cell sorting (FACS), (Crouch & Doetsch, 2018; Tischfield & Anderson, 2017). However, artifacts and variability introduced during the dissociation and sorting process pose a notable challenge (van den Brink *et al.*, 2017). Moreover, in morphologically complex cells – such as neurons or vascular cells - RNA isoforms are lost from cellular processes that are severed during the generation of single cell suspensions. A complementary approach overcoming some of these limitations is the isolation of ribosome-associated mRNAs from genetically-defined cell populations. Based on cell type-specific epitope-tagging with genetic

tools, two closely related methods were developed, named TRAP (Translating Ribosome Affinity Purification) (Heiman *et al.*, 2008) and RiboTag (Sanz *et al.*, 2009). In both methods, an epitope-tagged core ribosomal protein is expressed in the cell population of interest. This tag then enables the selective affinity purification and analysis of ribosome-associated mRNAs. Whereas TRAP is based on bacterial artificial chromosome (BAC) transgenic mice that overexpress EGFP-tagged ribosomal protein L10 (RPL10A), RiboTag employs cre-recombinase-dependent HA epitope tagging of the endogenous ribosomal protein RPL22. Crossing with cell-type specific cre lines or viral delivery of cre-recombinase then enables selecting the desired population of cells for tagging and mRNA isolation. Selective capture of cell type-specific mRNAs overcomes many challenges posed by dissociation-based gene expression profiling approaches. Moreover, RNA-sequencing of TRAP / RiboTag samples enables the enrichment of transcripts that are engaged by the ribosomes, a closer approximation to the transcript isoforms recruited for mRNA translation. In the past years, the TRAP / RiboTag approach has proven versatile and effective in characterizing cell type-specific transcriptomes in a broad range of experimental systems, ranging from *Drosophila* and mouse models to cultured human-induced pluripotent stem cells (Gregory *et al.*, 2020; Mardinly *et al.*, 2016; Thomas *et al.*, 2012). More recent studies have capitalized on the high yield of cell type-specific mRNAs to assess cell type-specific alternative splicing and translational regulation (Furlanis *et al.*, 2019; Gonzalez *et al.*, 2014; Lee *et al.*, 2020; Thomson *et al.*, 2017).

This chapter describes an optimized protocol for RiboTag-isolation of intact mRNA from sparse cell populations in small regions of the mouse brain. This protocol has been used successfully to obtain high quality preparations from a single cortical layer of the neonatal mouse visual cortex (area V1) or a subset of hippocampal interneurons. The example protocol is described for mRNA isolation from VGLUT2-positive tufted and mitral cells of the mouse olfactory bulb, but can be readily transferred to other preparations with limiting and highly complex starting materials.

2 Materials

2.1 Preparation of work environment

1. RNase AWAY® for molecular biology
2. Sterile, nuclease-free pipette filter tips.
3. Glass homogenizers (or motor driven Teflon glass homogenizer)
4. Nuclease-free 1.5 mL LowBind “microcentrifuge tubes”.
5. Diethylpyrocarbonate (DEPC) water (0.1% DEPC in ultrapure 18.2MΩxcm water, autoclaved).

2.2 Preparation for immunoprecipitation of tagged ribosome and associated RNAs

1. Ice-cold sterile, nuclease-free phosphate buffered saline (PBS).
2. Homogenization buffer: 50mM Tris-HCl, pH7.4, 100mM KCl, 12mM MgCl₂ in DEPC water. Good for 2 months when stored at 4 °C.
3. Supplements to homogenization buffer: 1mg/mL Heparin from porcine intestinal mucosa, 200 units/mL RNasin RNase inhibitor, 100µg/mL cyclohexamide, 1mM DTT, 1x protease inhibitor (e.g. Roche “complete” EDTA free). The “supplemented homogenization buffer” has to be made fresh on the day of the experiment and always kept on ice.
4. 10% IGPAL stock (molecular biology grade) in DEPC water (store at 4°C).
5. High salt washing buffer: 300mM KCl, 1 % IGEPAL, 50mM Tris-HCl, pH7.4, 12mM MgCl₂, 1mM DTT, 100µg/mL cyclohexamide, in DEPC water. The high-salt washing buffer has to be made fresh on the day of the experiment and always kept on ice.
6. Anti-HA Magnetic Beads, Monoclonal IgG1 antibody, clone 2-2.2.14, (Thermo Scientific). Store at 4 °C.
7. Magnetic rack
8. Rotating wheel

2.3 Reagents and equipment for RNA purification and clean-up

1. RNeasy Micro plus kit (Qiagen) containing RLT buffer, wash buffers, gDNA eliminator columns, and RNeasy MinElute Spin Columns
2. Beta-mercaptoethanol
3. 70% and 80% ethanol (molecular biology grade, nuclease-free, diluted with RNase free water)
4. DEPC water

2.4 RNA quantification and library preparation

1. RNA 6000 Pico kit (Agilent)
2. Reverse Transcription System, containing 25mM MgCl₂, Reverse Transcription 10X Buffer, 10mM dNTP Mixture, Recombinant RNasin Ribonuclease Inhibitor, 15 units AMV Reverse Transcriptase, Oligo(dT)15 Primer, Random Primers, 1.2kb Kanamycin Positive Control RNA, 1µg poly(A)⁺ mRNA, Nuclease-Free Water
3. Agilent Bioanalyzer
4. NanoDrop Spectrophotometer
5. QuantiFluor RNA System (Promega)
6. TruSeq RNA Library Prep Kit v2 (Illumina) or Smart-Seq library Prep v4 Plus Kit (TakaraBio)

2.5 Transgenic mouse lines

The conditional RiboTag allele in C57BL/6J background is available from the Jackson laboratory (B6J.129(Cg)-*Rpl22*^{tm1.1^{Psam}}/SjJ; JAX Stock No: 029977). The vGlut2-cre mouse line in C57BL/6J background used to direct cell class-specific Rpl22-HA expression is B6J.129S6(FVB)-*Slc17a6*^{tm2(cre)^{Low}}/MwarJ JAX Stock No: 028863). TRAP BAC transgenic mouse lines driving RPL10A-GFP in various cell classes are available from JAX.

2.6 Time Considerations

The preparation of the RNase free environment, set-up of equipment prior the start of the experiment takes about 1h. One complete round of pull-down takes around 7 hours. The subsequent RNA purification and Reverse Transcription and Polymerase Chain Reaction (RT-PCR) require ~3-4 hours. One day is required for quality checks of RNA concentration quantification by fluorometry, RNA integrity number (RIN) calculation, and quantitative-Polymerase Chain Reaction (qPCR) enrichment analysis for cell type-specific markers.

3 Methods

3.1 Preparation of reagents and sterile equipment

1. Wipe work surfaces and pipettes with RNase AWAY® for molecular biology or similar.
2. Autoclave glass homogenizers, flush with RNase AWAY just before use, and wash 3 times with 50 mL of DEPC water (see **Note1**).
3. Prepare the “supplemented homogenization buffer” and the “high salt buffer” using DEPC water.
4. Use sterile, pipette filter tips throughout the entire procedure.
5. Clean dissection tools with water and 70% Ethanol and let them air dry?.
6. Prepare a petri-dish for tissue dissection with PBS on ice.

3.2 Preparation of tissue homogenate

1. Euthanize mice (in this example protocol postnatal day 35, *Rpl22^{HA/HA}::vGlut2^{RES-cre}*) according to institutional guidelines, e.g. by decapitation under isoflurane anesthesia and rapidly collect the brain in ice-cold PBS. See **Note 2** for number of animals and RNA yields from different brain regions.

2. Take a toe biopsy for potential re-confirmation of genotype (see **Note 3**)
3. Rapidly dissect the region of interest and transfer the tissue into a new dish with fresh ice cold PBS to remove blood (see **Note 4-5**).
4. Immediately transfer tissue into a glass homogenizer containing ice-cold supplemented homogenization buffer. For the olfactory bulbs (~ 30 mg tissue from 1 animal), we advise to use 0.5 mL of supplemented homogenization buffer (1:20 weight per volume of homogenization buffer). Disrupt the tissue with 40 strokes-fitting homogenizers (see **Note 6**).
5. Transfer the homogenate to an ice-cold 1.5 mL microcentrifuge tube (see **Note 7** for larger volume samples).
6. Centrifuge at 2'000 x g for 15 min at 4°C to pellet nuclei and debris.
7. During the centrifugation step, prepare anti-HA magnetic beads: for RiboTag pulldown from the olfactory bulbs from 1 mouse, use 5µL of packed beads (equivalent to ~20 µL of beads from the commercial vial). Wash beads 3 times with 1 mL of supplemented homogenization buffer (vortex at medium speed 5 sec. – put tube on magnetic rack – remove liquid without disturbing the beads– add buffer). Resuspend beads in 20 µL of ice-cold supplemented homogenized buffer (see **Note 8**). Scale up the amount of beads according to the number of samples.
8. Transfer supernatant from step 5 to a new ice-cold 1.5 mL microcentrifuge tube (see **Note 9**).
9. Add 55µL of 10% IGEPAL (to a final concentration of 1%) to solubilize cellular membranes. Invert 3-4 times until the lysate becomes clear.
10. Incubate on ice for 5 min (see **Note 10**).
11. Keep the sample in the same ice-cold 1.5 mL microcentrifuge tube and centrifuge at 13'000 x g for 10 min at 4°C, to separate insoluble material from lysate.

3.3 Immunoprecipitation of epitope-tagged ribosomes

1. After the centrifugation, transfer the supernatant to a new ice-cold 1.5 mL microcentrifuge tube.
2. Take an aliquot (4.5 μ L, corresponding to 1 % of total) of the lysate supernatant to be analyzed as “input” material and immediately mix this aliquot with 350 μ L of RLT plus buffer (Add 10 μ L of β -mercaptoethanol per 1 mL Buffer RLT plus). Vortex few seconds and store at - 80°C until RNA purification step.
3. Add 20 μ L of washed and resuspended anti-HA-coupled magnetic beads (equivalent of 5 μ L of packed beads) to the lysate sample (for bead volumes refer to **Note 8**).
4. Incubate 3-4 hours at 4°C on rotating wheel (see **Note 11**), at low speed.
5. Place the microcentrifuge tube on the magnetic rack on ice (see **Note 7** for higher volume samples).
6. Wait ~1 minute for the beads to be collected at the bottom of the tube.
7. Carefully aspirate the supernatant with the vacuum pump without disturbing the beads, then wash 3 times with 1 mL of ice-cold high salt washing buffer: Aspirate supernatant – add high salt washing buffer – vortex gently until the beads are dispersed in the washing buffer – collect beads again on the magnetic rack (see **Note 12**).
8. After the last wash, remove supernatant and resuspend the beads directly in 350 μ L of RLT plus buffer supplemented with 3.5 μ L of β -mercaptoethanol.

3.4 RNA extraction and purification

1. Vortex gently for 5 seconds at room temperature. Place the tubes back on the magnetic rack and wait for ~1 minute.
2. Pipette the supernatant containing the purified nucleic acids in a new ice-cold 1.5 mL microcentrifuge tube. Discard the beads.
3. Proceed with the purification of input (IN) and ribosome-associated RNA (IP) according to the RNeasy Micro plus kit. In brief, the samples are first loaded onto the gDNA columns to ensure elimination of genomic DNA contaminants from the sample (see **Note**

13). The flow-through is then loaded on the RNeasy columns for purification (binding capacity of a single column is up to 100 µg RNA). Upon washes of the columns with the buffers provided in the RNeasy Micro plus kit, the RNA is finally eluted in 15µL of nuclease-free water and stored at - 80°C until further processing. The RNA purification procedure is to be performed on ice.

3.5 Testing RNA concentration and quality

1. Determine RNA concentration in input and IP samples with NanoDrop Spectrophotometer (the typical yield of RNA retrieved from vGlut2-cre positive neurons of the olfactory bulbs from one P35 mouse, two hemispheres, is ~500 ng).
2. Use a few ng of IN and IP RNA for Reverse Transcription with random hexamers according to instructions of the transcriptase manufacturer (see **Note 14** for cases with low RNA recovery).
3. Perform qPCR on IN and IP cDNA with primers amplifying transcripts known to be enriched or de-enriched in the cell type of interest (see **Note 15-16**). Additionally, two or three “housekeeping genes” should be assessed. For example, in pull-downs from the *Vglut2^{Ribo}* mouse line we use *Vglut1* (*Slc17a7*), *Vglut2* (*Slc17a6*) and *Tbr2* (*Eomes*) genes to probe for marker enrichment and parvalbumin (*Pvalb*), *Gfap*, and *Vgat* (*Slc32a1*) to test for de-enrichment of contaminants. Enrichment values are calculated based on the ratio of target mRNA over housekeeping genes in the IP relative to IN samples. As housekeeping genes, we use *Gapdh*, and *Actb* (see **Note 17**).
4. For accurate calculation of RNA concentration perform fluorocytometry analysis, using the QuantiFluor RNA System.
5. Evaluate the quality of isolated RNA by calculating the RNA Integrity Number (RIN) using a pico-chip (Agilent RNA 6000 Pico kit). We used for RNA-sequencing only samples with RIN > 7.5. Moreover, we selected for RNA-sequencing samples displaying

RIN values in the same range, thus excluding outlier samples with either too high or too low RIN.

6. Proceed with RNA-sequencing library preparation. At least 50 ng of immune-isolated RNA should be used for PolyA-enrichment Truseq library preparation for RNA-sequencing (see **Note 18**), see Figure 1

Insert figure 1 here

4 Notes

1. It is critical to establish an RNase-free environment and minimize the risk of RNase contamination throughout the procedure.
2. Typical total RNA yields from RiboTrap purifications from a single mouse (two brain hemispheres), obtained with this protocol are as follows: P35 olfactory bulbs *Vglut2^{Ribo}* ~500ng, P25 neocortex *CamK2^{Ribo}* ~1.5µg, P25 hippocampi *CamK2^{Ribo}* ~450ng, P35 neocortex *Pvalb^{Ribo}* ~250ng, P4 visual cortices *Rorb^{Ribo}* 20ng.
3. Depending on the cre mouse-line used, extra attention needs to be taken to ensure that no aberrant germline recombination of the Rpl22HA-allele has occurred (see (Luo *et al.*, 2020) for discussion of this issue). Thus, it is strongly encouraged to use genotyping primers that detect germline recombination (e.g., the primer combination used to detect the floxed ribotag allele shows a band of ~320 bp size when abnormal germline recombination has occurred (RiboTag Forward primer: 5'-GGGAGGCTTGCTGGATATG-3'; RiboTag Reverse primer : 5'-TTTCCAGACACAGGCTAAGTACAC-3'). In developmental studies, the onset of cre-recombinase expression needs to be carefully evaluated to assess the efficiency of Rpl22 HA-tagging at early developmental timepoints.
4. During tissue dissection, it is critical to minimize carrying over blood as much as possible, given its content of RNase activity. Perform the dissection step on ice in pre-

chilled PBS as quickly as possible. Upon dissection, tissue needs to be placed immediately into the ice-cold homogenization buffer containing RNase inhibitors.

5. Alternatively, tissue can be immediately flash-frozen in liquid nitrogen upon dissection and stored at -80°C until ready to use. Upon thawing, homogenize the tissue immediately, when it is still frozen. Note that quality and total mRNA yield retrieved from frozen tissue is reduced as compared to tissue processed immediately after dissection.

6. Wherever possible, we recommend using tissue from single animals as replicates. Typical tissue weights for P30-P40 mouse brain regions from a single animal (2 hemispheres) are: visual cortices (~ 10 mg), olfactory bulbs (~ 30 mg), hippocampi (~ 70 mg), whole neocortex (~300 mg). Adjust the volume of homogenization buffer to 1:20 weight per volume (e.g., 20 mL of buffer per 1 g of tissue) for optimal tissue homogenization. However, when using very small amounts of tissue, work with a minimal volume of 500 μL of homogenization buffer to improve the handling of the sample.

For replicates, always use the same number of strokes to homogenize the tissue. Upon homogenization, the sample should appear dense and viscous, without any remaining tissue chunks visible. Efficiency of homogenization can be evaluated for an aliquot of the homogenate under a bright field microscope.

7. When working with larger amounts of starting material and the corresponding higher volumes of homogenization buffer, transfer the homogenate to a 15 mL plastic tube for low-speed centrifugation ($2'000 \times g$ for 10 min at 4°C to pellet nuclei). Then transfer the supernatant to a new 15 mL plastic tube for tissue lysis with IGEPAL (adapt the amount of IGEPAL to add, depending on the resulting volume of supernatant). For high-speed centrifugation, distribute the lysate into pre-chilled 2 mL microcentrifuge tubes and spin for 10min at 4°C at $13'000 \times g$. Transfer supernatant to new pre-chilled 2 mL microcentrifuge tubes and incubate with the HA-magnetic beads (5 μL packed beads per tube) for 3-4 hours. Use 1.5 mL high salt buffer per tube for washes and collect beads

- sequentially in a total of 350 μ L of RLT buffer supplemented with 3.5 μ L of β -mercaptoethanol.
8. Carefully choose the amount of magnetic beads used for immuno-isolation when applying the protocol to a new tissue and/or cell type. Bead concentration should be optimized for maximum ribosome recovery with low unspecific mRNA recovery. When trying to perform pulldown from a new type of sample, we recommend to test the correct amount of beads to use in a pilot experiment (background increases when an excess of beads is employed).
 9. Ensure that no nuclear pellet is carried over during the transfer of the clarified supernatant to a clean microcentrifuge tube. It is preferable to leave and discard few microliters of homogenized tissue, instead of risking carry over of nuclear contaminants
 10. Incubation time with IGEPAL is necessary in this step to achieve optimal membrane solubilization (assessed by lysate clearing). Instead of IGEPAL, 1% NP-40 can also be used.
 11. We observed that 3 hours incubation of beads with the lysate are sufficient for ribosome binding and yield a good amount of retrieved RNA. We observed no differences between 3 hours and 5 hours incubation step. We do not recommend overnight incubation prolonged incubation frequently results in increased RNA degradation and unspecific binding.
 12. Three washes with 1 mL of high salt buffer and gentle vortexing for 5 seconds is sufficiently stringent to minimize unspecific binding. Longer washing times (15-25 minutes on a rotating wheel) significantly decrease the quality and integrity of the isolated RNA. The washing step needs to be performed on ice.
 13. DNA removal on a gDNA column (RNeasy Micro plus Qiagen kit) is usually sufficient to eliminate DNA contamination. However, in some cases, additional DNA digestion by DNase improves RNA recovery. This is recommended in particular when performing

- pull-down from small neuronal structures/small brain regions, where low yield of total RNA recovery is expected.
14. When working with very small brain regions or sparse cell populations, perform fluorometric RNA quantification, which is more reliable at low concentrations. When RNA yield is too low to quantify, take a fixed percentage (e.g., 10%) of the eluted RNA to perform the reverse transcription. For experimental questions where higher RNA recovery is expected (e.g. an abundant cell population of neocortex), elute RNA in 25 μ l of DEPC water and use ~25 ng RNA for reverse transcription.
 15. Input aliquots are necessary in order to assess the quality of the pull-down through enrichment of cell type-specific markers by qPCR. For our experiments, input RNA aliquots were not analysed for RIN and were not used for RNA sequencing. We recommend diluting resulting cDNA samples at least 1:5 before proceeding for qPCR. Use 3 μ l of diluted cDNA in a total volume of 20 μ l qPCR reaction. Markers of interest used to assess by qPCR the enrichment of mitral and tufted neurons in the olfactory bulb using the *vGlut2*-cre mouse line are: *vGlut2*, *Pcdh21*, *Tbr2*. (*vGlut2* Forward primer: GCATGGTCTGGTACATGTTCTG; *vGlut2* Reverse primer: GACGGGCATGGATGTGAAAAC; *Tbr2* Forward primer: ATAAACGGACTCAACCCACC; *Tbr2* Reverse primer: CCCTGCATGTTATTGTCCGC; *Pcdh21* Forward primer: ATCACTGTCAACGACTCAGACC; *Pcdh21* Reverse primer: GTCAATGGCAGCTGAGTTTTCC).
 16. Note, that RiboTag isolation of mRNAs from abundant cell types will result in only modest marker enrichment (e.g. for broad classes of abundant glutamatergic cells such as CamK2-cre defined neurons in neocortex). By contrast, pulldowns for sparse cell classes (such as VIP interneurons) results in a very high enrichment of markers.
 17. Many genes that are widely considered “housekeeping genes” are differentially expressed across neuronal cell types and cell states. Thus, multiple such “housekeeping genes” should be assessed to allow for accurate enrichment analysis of target mRNAs.

18. In experiments aimed at quantifying transcript isoforms, we recommend to use paired-end sequencing with read length of 100-150 bases and a sequencing depth of 50 to 100 million reads per sample (depending on what type and complexity of splice variants will be examined). For low input RNA samples <15ng RNA, we recommend using the SMART-seq v4 library preparation kit.

List of figures:

Fig. 1 Illustration of cell type –specific ribosome-associated mRNAs pull-down approach in the olfactory bulb.

a. Schematic representation of the olfactory bulb circuitry, where genetically defined vGlut2⁺ neurons of the olfactory bulb conditionally express HA-tagged ribosomes. Highlight of the different cellular populations defined by the Slc17a6-cre::Rpl22-HA mouse line, namely mitral and tufted neurons of the olfactory bulb. These cells express HA-tagged ribosomes. **b.** Upon tissue lysis (IN), ribosome-associated mRNAs are immuno-precipitated using magnetic anti-HA beads (IP). **c.** mRNAs are then purified and used for RNA-sequencing analysis. Expected qPCR fold-enrichment / de-enrichment values for cell type-specific markers upon mRNAs pull-down from vGlut2⁺ neuronal population are displayed on the right panel.

References

1. Zeisel A, Hochgerner H, Lonnerberg P, Johnsson A, Memic F, van der Zwan J, Haring M, Braun E, Borm LE, La Manno G, Codeluppi S, Furlan A, Lee K, Skene N, Harris KD, Hjerling-Leffler J, Arenas E, Ernfors P, Marklund U, Linnarsson S (2018) Molecular Architecture of the Mouse Nervous System. *Cell* 174 (4):999-1014 e1022.
2. Zeng H, Sanes JR (2017) Neuronal cell-type classification: challenges, opportunities and the path forward. *Nat Rev Neurosci* 18 (9):530-546.

3. Nguyen TM, Schreiner D, Xiao L, Traunmuller L, Bornmann C, Scheiffele P (2016) An alternative splicing switch shapes neurexin repertoires in principal neurons versus interneurons in the mouse hippocampus. *eLife* 5.
4. Wamsley B, Jaglin XH, Favuzzi E, Quattrocchio G, Nigro MJ, Yusuf N, Khodadadi-Jamayran A, Rudy B, Fishell G (2018) Rbfox1 Mediates Cell-type-Specific Splicing in Cortical Interneurons. *Neuron*.
5. Gonatopoulos-Pournatzis T, Niibori R, Salter EW, Weatheritt RJ, Tsang B, Farhangmehr S, Liang X, Braunschweig U, Roth J, Zhang S, Henderson T, Sharma E, Quesnel-Vallieres M, Permanyer J, Maier S, Georgiou J, Irimia M, Sonenberg N, Forman-Kay JD, Gingras AC, Collingridge GL, Woodin MA, Cordes SP, Blencowe BJ (2020) Autism-Misregulated eIF4G Microexons Control Synaptic Translation and Higher Order Cognitive Functions. *Mol Cell* 77 (6):1176-1192 e1116.
6. Parikshak NN, Swarup V, Belgard TG, Irimia M, Ramaswami G, Gandal MJ, Hartl C, Leppa V, Ubieta LT, Huang J, Lowe JK, Blencowe BJ, Horvath S, Geschwind DH (2016) Genome-wide changes in lncRNA, splicing, and regional gene expression patterns in autism. *Nature* 540 (7633):423-427.
7. Furlanis E, Scheiffele P (2018) Regulation of neuronal differentiation, function, and plasticity by alternative splicing. *Annual Review of Cell and Developmental Biology* 34:451-469.
8. Vogel C, Marcotte EM (2012) Insights into the regulation of protein abundance from proteomic and transcriptomic analyses. *Nature reviews Genetics* 13 (4):227-232.
9. Liu Y, Beyer A, Aebersold R (2016) On the Dependency of Cellular Protein Levels on mRNA Abundance. *Cell* 165 (3):535-550.
10. Weatheritt RJ, Sterne-Weiler T, Blencowe BJ (2016) The ribosome-engaged landscape of alternative splicing. *Nat Struct Mol Biol* 23 (12):1117-1123.
11. Crouch EE, Doetsch F (2018) FACS isolation of endothelial cells and pericytes from mouse brain microregions. *Nature protocols* 13 (4):738-751.
12. Tischfield DJ, Anderson SA (2017) Differentiation of Mouse Embryonic Stem Cells into Cortical Interneuron Precursors. *J Vis Exp* (130).
13. van den Brink SC, Sage F, Vertesy A, Spanjaard B, Peterson-Maduro J, Baron CS, Robin C, van Oudenaarden A (2017) Single-cell sequencing reveals dissociation-induced gene expression in tissue subpopulations. *Nat Methods* 14 (10):935-936.
14. Heiman M, Schaefer A, Gong S, Peterson JD, Day M, Ramsey KE, Suarez-Farinas M, Schwarz C, Stephan DA, Surmeier DJ, Greengard P, Heintz N (2008) A translational profiling approach for the molecular characterization of CNS cell types. *Cell* 135 (4):738-748.

15. Sanz E, Yang L, Su T, Morris DR, McKnight GS, Amieux PS (2009) Cell-type-specific isolation of ribosome-associated mRNA from complex tissues. *Proc Natl Acad Sci U S A* 106 (33):13939-13944.
16. Thomas A, Lee PJ, Dalton JE, Nomie KJ, Stoica L, Costa-Mattioli M, Chang P, Nuzhdin S, Arbeitman MN, Dierick HA (2012) A versatile method for cell-specific profiling of translated mRNAs in *Drosophila*. *PLoS One* 7 (7):e40276.
17. Gregory JA, Hoelzli E, Abdelaal R, Braine C, Cuevas M, Halpern M, Barretto N, Schrode N, Akbalik G, Kang K, Cheng E, Bowles K, Lotz S, Goderie S, Karch CM, Temple S, Goate A, Brennand KJ, Phatnani H (2020) Cell Type-Specific In Vitro Gene Expression Profiling of Stem Cell-Derived Neural Models. *Cells* 9 (6).
18. Mardinly AR, Spiegel I, Patrizi A, Centofante E, Bazinet JE, Tzeng CP, Mandel-Brehm C, Harmin DA, Adesnik H, Fagiolini M, Greenberg ME (2016) Sensory experience regulates cortical inhibition by inducing IGF1 in VIP neurons. *Nature* 531 (7594):371-375.
19. Thomson SR, Seo SS, Barnes SA, Louros SR, Muscas M, Dando O, Kirby C, Wyllie DJA, Hardingham GE, Kind PC, Osterweil EK (2017) Cell-Type-Specific Translation Profiling Reveals a Novel Strategy for Treating Fragile X Syndrome. *Neuron* 95 (3):550-563 e555.
20. Gonzalez C, Sims JS, Hornstein N, Mela A, Garcia F, Lei L, Gass DA, Amendolara B, Bruce JN, Canoll P, Sims PA (2014) Ribosome profiling reveals a cell-type-specific translational landscape in brain tumors. *J Neurosci* 34 (33):10924-10936.
21. Furlanis E, Traunmuller L, Fucile G, Scheiffele P (2019) Landscape of ribosome-engaged transcript isoforms reveals extensive neuronal-cell-class-specific alternative splicing programs. *Nature neuroscience* 22 (10):1709-1717.
22. Lee H, Fenster RJ, Pineda SS, Gibbs WS, Mohammadi S, Davila-Velderrain J, Garcia FJ, Therrien M, Novis HS, Gao F, Wilkinson H, Vogt T, Kellis M, LaVoie MJ, Heiman M (2020) Cell Type-Specific Transcriptomics Reveals that Mutant Huntingtin Leads to Mitochondrial RNA Release and Neuronal Innate Immune Activation. *Neuron* 107 (5):891-908 e898.
23. Luo L, Ambrozkiwicz MC, Benseler F, Chen C, Dumontier E, Falkner S, Furlanis E, Gomez AM, Hoshina N, Huang WH, Hutchison MA, Itoh-Maruo Y, Lavery LA, Li W, Maruo T, Motohashi J, Pai EL, Pelkey KA, Pereira A, Philips T, Sinclair JL, Stogsdill JA, Traunmuller L, Wang J, Wortel J, You W, Abumaria N, Beier KT, Brose N, Burgess HA, Cepko CL, Cloutier JF, Eroglu C, Goebbels S, Kaeser PS, Kay JN, Lu W, Luo L, Mandai K, McBain CJ, Nave KA, Prado MAM, Prado VF, Rothstein J, Rubenstein JLR, Saher G, Sakimura K, Sanes JR, Scheiffele P, Takai Y, Umemori H, Verhage M,

Yuzaki M, Zoghbi HY, Kawabe H, Craig AM (2020) Optimizing Nervous System-Specific Gene Targeting with Cre Driver Lines: Prevalence of Germline Recombination and Influencing Factors. *Neuron* 106 (1):37-65 e35.

Acknowledgements:

We are thankful to O. Mauger and E. Furlanis for constructive comments on the chapter manuscript and to T.M. Nguyen, L. Traunmüller, E. Furlanis and S. Falkner for discussions and help in setting up the protocol for RiboTRAP purifications. Work in the laboratory was supported by funds to P.S. from the Swiss National Science Foundation, a European Research Council Advanced Grant (SPLICECODE), EU-AIMS and AIMS- 2-TRIALS which are supported by the Innovative Medicines Initiatives from the European Commission. The results leading to this publication has received funding from the Innovative Medicines Initiative 2 Joint Undertaking under grant agreement no. 777394. This Joint Undertaking receives support from the European Union's Horizon 2020 research and innovation programme and EFPIA and AUTISM SPEAKS, Autistica, SFARI. The Scheiffele Laboratory is an associate member of the Swiss National Science Foundation's National Competence Centre for Research (NCCR) RNA and Disease.

Index of abbreviations

AAV= adenovirus
ALE= alternative last exon
ALS= amyotrophic lateral sclerosis
AOB= accessory olfactory bulb
AON= accessory olfactory nucleus
APE1= apurinic/apyrimidinic endonuclease 1
AS= Alternative Splicing
ASDs=autism spectrum disorders
AS5= alternative splice site 5
ATSS= alternative transcription start site
Ca²⁺= calcium
CamK2= Ca²⁺ /calmodulin-dependent protein kinase 2
CELF= CUG-BP and ETR-3-like factor
CGE= Caudal Ganglionic Eminence
CITS= crosslink-induced truncation sites
CircRNA= circular RNA
CLIP= Cross-linking immunoprecipitation
CMV= cytomegalovirus
COIN= conditional by inversion allele
CRISPR-CAS9= Clustered Regularly Interspaced Short Palindromic Repeats
CRISPR associated protein 9
cKO= conditional knock-out
CX= neocortex
DCM= dilated cardiomyopathy
DE= differentially expressed
DGE= differential gene expression
DNA= deoxyribonucleic acid
DR= differentially regulated
DSCAM= Down syndrome cell adhesion molecule
EPL= external plexiform layer
ESE= exonic splicing enhancer
ESS= exonic splicing silencer
Exc= excitatory glutamatergic
FC= fold change
FingR= Fibronectin intrabodies generated with mRNA display

FISH= Fluorescence *in situ* hybridization
FPKM= Fragments Per Kilobase of transcript per Million
FUS= Fused in Sarcoma
GABA= γ -aminobutyric acid
GABA-R= γ -aminobutyric acid receptor
GE= gene expression
GFP= green fluorescent protein
GCL= granule cell layer
GL= glomeruli layer
GO= Gene Ontology
HA= Human influenza hemagglutinin
HC= hippocampus
HEK293T= Human Embryonic Kidney 293T
hnRNP= heterogeneous nuclear ribonucleoprotein
hSyn= human synapsin promoter
HVA= high voltage activity
IGF1= insulin growth factor 1
INs= interneurons
IP= immuno-precipitation
IPL= internal plexiform layer
iPSC-CMs= induced pluripotent stem cell derived cardiomyocytes
kDa= Kilo-Dalton
KH= heterogeneous nuclear K-homology
KO= knock-out
L5= layer 5
lncRNA= long non-coding RNA
LV= lentivirus
LTP= long-term potentiation
LVA= low voltage activity
MATR3= matrin3
MBNL= Muscleblind Like Splicing Regulator 1
MC= mitral cell
MCL=mitral cell layer
MC-T= Mitral and tufted cells
Mg²⁺= Magnesium
MGE= Medial Ganglionic Eminence

MOB= main olfactory bulb
MORF= MOnonucleotide Repeat Frameshift
mRNA= messenger RNA
Myom1=myomesin1
ncRNA= non-coding RNA
NMD= non sense mediated decay
NR1= NMDA receptor 1
NRXN3= neurexin 3
NSCs= neural stem cells
N2A= Neuroblastoma 2
OB= olfactory bulb
OR= olfactory receptor
OSN= olfactory sensory neurons
OT= olfactory tubercle
OXT= oxytocin
PABP= poly-A binding protein
PCA= principal component analysis
PCR= Polymerase chain reaction
PCX= piriform cortex
pPCX= posterior piriform cortex
PN= projection neuron
pre-mRNA= precursor mRNA
PV= Parvalbumin
p-val= p-value
PVN= paraventricular nucleus
PEVK= Proline, Glutamate, Valine and Lysine-rich region
Pyr= pyramidal
qPCR= quantitative PCR
RBD= RNA-binding domains
RBM20= RNA-binding motif,20
RBP= RNA-binding protein
RiboTRAP= tagged-ribosomal affinity purification
RMS= rostral migratory stream
RNA= ribonucleic acid
RNA-seq=RNA-sequencing
ROI= region of interest

RRM= RNA-recognition motif
RSRSP= arginine-serine-arginine- serine-proline
RT-PCR= Reverse transcription PCR
Scnn1a= Sodium Channel Epithelial 1 Subunit Alpha
SERCA2a= sarco/endoplasmic reticulum Ca²⁺-ATPase
SEZ= sub-ependymal zone
shRNA= short-hairpin RNA
SI= splicing index
SMI= size matched input
SMRT= single molecule, real-time
snRNA= small nuclear RNA
snRNP= small nuclear rna protein
ssDNA= single strand DNA
SST= Somatostatin
STFP= social transmitted food preference
SVZ= Sub-Ventricular Zone
TC= tufted cells
TDP-43= TAR DNA-binding protein 43
TF= transcription factor
TMT= Tandem Mass Tag
TPM= tropomyosin
TTN=titin
UTR= untranslated region
UV= ultraviolet
VGCC= voltage gated calcium channel
VGSC= voltage gated sodium channel
VIP= vasoactive intestinal peptide
VNO= vomeronasal organ
VST= Variance Stabilizing Transformation
VZ= Ventricular Zone
WB= western blot
WT= wild-type
YY1= Yin Yang 1
Znf= zinc finger motif

References

- Allen, S. E., Toro, C. P., Andrade, A., Lopez-Soto, E. J., Denome, S., & Lipscombe, D. (2017). Cell-Specific RNA Binding Protein Rbfox2 Regulates Ca(V)2.2 mRNA Exon Composition and Ca(V)2.2 Current Size. *eNeuro*, 4(5). <https://doi.org/10.1523/ENEURO.0332-16.2017>
- Apicella, A. J., & Marchionni, I. (2022). VIP-Expressing GABAergic Neurons: Disinhibitory vs. Inhibitory Motif and Its Role in Communication Across Neocortical Areas. *Front Cell Neurosci*, 16, 811484. <https://doi.org/10.3389/fncel.2022.811484>
- Bae, B., & Miura, P. (2020). Emerging Roles for 3' UTRs in Neurons. *Int J Mol Sci*, 21(10). <https://doi.org/10.3390/ijms21103413>
- Bailey, T. L., Boden, M., Buske, F. A., Frith, M., Grant, C. E., Clementi, L., Ren, J., Li, W. W., & Noble, W. S. (2009). MEME SUITE: tools for motif discovery and searching. *Nucleic Acids Res*, 37(Web Server issue), W202-208. <https://doi.org/10.1093/nar/gkp335>
- Bailey, T. L., Johnson, J., Grant, C. E., & Noble, W. S. (2015). The MEME Suite. *Nucleic Acids Res*, 43(W1), W39-49. <https://doi.org/10.1093/nar/gkv416>
- Barash, Y., Calarco, J. A., Gao, W., Pan, Q., Wang, X., Shai, O., Blencowe, B. J., & Frey, B. J. (2010). Deciphering the splicing code. *Nature*, 465(7294), 53-59. <https://doi.org/10.1038/nature09000>
- Barbosa-Morais, N. L., Irimia, M., Pan, Q., Xiong, H. Y., Gueroussov, S., Lee, L. J., Slobodeniuc, V., Kutter, C., Watt, S., Colak, R., Kim, T., Misquitta-Ali, C. M., Wilson, M. D., Kim, P. M., Odom, D. T., Frey, B. J., & Blencowe, B. J. (2012). The evolutionary landscape of alternative splicing in vertebrate species. *Science*, 338(6114), 1587-1593. <https://doi.org/10.1126/science.1230612>
- Bauer, E. P., Schafe, G. E., & LeDoux, J. E. (2002). NMDA receptors and L-type voltage-gated calcium channels contribute to long-term potentiation and different components of fear memory formation in the lateral amygdala. *J Neurosci*, 22(12), 5239-5249. <https://doi.org/10.1523/JNEUROSCI.22-12-05239.2002>
- Baughn, M. W., Melamed, Z., Lopez-Erauskin, J., Beccari, M. S., Ling, K., Zuberi, A., Presa, M., Gonzalo-Gil, E., Maimon, R., Vazquez-Sanchez, S., Chaturvedi, S., Bravo-Hernandez, M., Taupin, V., Moore, S., Artates, J. W., Acks, E., Ndayambaje, I. S., Agra de Almeida Quadros, A. R., Jafar-Nejad, P., . . . Cleveland, D. W. (2023). Mechanism of STMN2 cryptic splice-polyadenylation and its correction for TDP-43 proteinopathies. *Science*, 379(6637), 1140-1149. <https://doi.org/10.1126/science.abq5622>
- Berget, S. M., Moore, C., & Sharp, P. A. (1977). Spliced segments at the 5' terminus of adenovirus 2 late mRNA. *Proc Natl Acad Sci U S A*, 74(8), 3171-3175. <https://doi.org/10.1073/pnas.74.8.3171>
- Berghard, A., & Buck, L. B. (1996). Sensory transduction in vomeronasal neurons: evidence for G α o, G α i2, and adenylyl cyclase II as major components of a pheromone signaling cascade. *J Neurosci*, 16(3), 909-918. <https://doi.org/10.1523/JNEUROSCI.16-03-00909.1996>
- Bertero, A., Fields, P. A., Ramani, V., Bonora, G., Yardimci, G. G., Reinecke, H., Pabon, L., Noble, W. S., Shendure, J., & Murry, C. E. (2019). Dynamics of genome reorganization during human cardiogenesis reveal an RBM20-dependent splicing factory. *Nat Commun*, 10(1), 1538. <https://doi.org/10.1038/s41467-019-09483-5>
- Bhat, S., Dao, D. T., Terrillion, C. E., Arad, M., Smith, R. J., Soldatov, N. M., & Gould, T. D. (2012). CACNA1C (Cav1.2) in the pathophysiology of psychiatric disease. *Prog Neurobiol*, 99(1), 1-14. <https://doi.org/10.1016/j.pneurobio.2012.06.001>
- Black, D. L. (2003). Mechanisms of alternative pre-messenger RNA splicing. *Annu Rev Biochem*, 72, 291-336. <https://doi.org/10.1146/annurev.biochem.72.121801.161720>

- Black, D. L., & Grabowski, P. J. (2003). Alternative pre-mRNA splicing and neuronal function. *Prog Mol Subcell Biol*, 31, 187-216. https://doi.org/10.1007/978-3-662-09728-1_7
- Blencowe, B. J. (2006). Alternative splicing: new insights from global analyses. *Cell*, 126(1), 37-47. <https://doi.org/10.1016/j.cell.2006.06.023>
- Boussif, O., Lezoualc'h, F., Zanta, M. A., Mergny, M. D., Scherman, D., Demeneix, B., & Behr, J. P. (1995). A versatile vector for gene and oligonucleotide transfer into cells in culture and in vivo: polyethylenimine. *Proc Natl Acad Sci U S A*, 92(16), 7297-7301. <https://doi.org/10.1073/pnas.92.16.7297>
- Braunschweig, U., Barbosa-Morais, N. L., Pan, Q., Nachman, E. N., Alipanahi, B., Gonatopoulos-Pournatzis, T., Frey, B., Irimia, M., & Blencowe, B. J. (2014). Widespread intron retention in mammals functionally tunes transcriptomes. *Genome Res*, 24(11), 1774-1786. <https://doi.org/10.1101/gr.177790.114>
- Briganti, F., Sun, H., Wei, W., Wu, J., Zhu, C., Liss, M., Karakikes, I., Rego, S., Cipriano, A., Snyder, M., Meder, B., Xu, Z., Millat, G., Gotthardt, M., Mercola, M., & Steinmetz, L. M. (2020). iPSC Modeling of RBM20-Deficient DCM Identifies Upregulation of RBM20 as a Therapeutic Strategy. *Cell Rep*, 32(10), 108117. <https://doi.org/10.1016/j.celrep.2020.108117>
- Brill, M. S., Ninkovic, J., Winpenny, E., Hodge, R. D., Ozen, I., Yang, R., Lepier, A., Gascon, S., Erdelyi, F., Szabo, G., Parras, C., Guillemot, F., Frotscher, M., Berninger, B., Hevner, R. F., Raineteau, O., & Gotz, M. (2009). Adult generation of glutamatergic olfactory bulb interneurons. *Nat Neurosci*, 12(12), 1524-1533. <https://doi.org/10.1038/nn.2416>
- Brinegar, A. E., & Cooper, T. A. (2016). Roles for RNA-binding proteins in development and disease. *Brain Res*, 1647, 1-8. <https://doi.org/10.1016/j.brainres.2016.02.050>
- Burd, C. G., & Dreyfuss, G. (1994). RNA binding specificity of hnRNP A1: significance of hnRNP A1 high-affinity binding sites in pre-mRNA splicing. *EMBO J*, 13(5), 1197-1204. <https://doi.org/10.1002/j.1460-2075.1994.tb06369.x>
- Caceres, J. F., Stamm, S., Helfman, D. M., & Krainer, A. R. (1994). Regulation of alternative splicing in vivo by overexpression of antagonistic splicing factors. *Science*, 265(5179), 1706-1709. <https://doi.org/10.1126/science.8085156>
- Chaker, Z., Codega, P., & Doetsch, F. (2016). A mosaic world: puzzles revealed by adult neural stem cell heterogeneity. *Wiley Interdiscip Rev Dev Biol*, 5(6), 640-658. <https://doi.org/10.1002/wdev.248>
- Chen, G., Ning, B., & Shi, T. (2019). Single-Cell RNA-Seq Technologies and Related Computational Data Analysis. *Front Genet*, 10, 317. <https://doi.org/10.3389/fgene.2019.00317>
- Chen, K. H., Boettiger, A. N., Moffitt, J. R., Wang, S., & Zhuang, X. (2015). RNA imaging. Spatially resolved, highly multiplexed RNA profiling in single cells. *Science*, 348(6233), aaa6090. <https://doi.org/10.1126/science.aaa6090>
- Chen, M., & Manley, J. L. (2009). Mechanisms of alternative splicing regulation: insights from molecular and genomics approaches. *Nat Rev Mol Cell Biol*, 10(11), 741-754. <https://doi.org/10.1038/nrm2777>
- Cho, Y., Zhao, C. L., & Lu, H. (2017). Trends in high-throughput and functional neuroimaging in *Caenorhabditis elegans*. *Wiley Interdiscip Rev Syst Biol Med*, 9(3). <https://doi.org/10.1002/wsbm.1376>
- Chow, L. T., Gelinis, R. E., Broker, T. R., & Roberts, R. J. (1977). An amazing sequence arrangement at the 5' ends of adenovirus 2 messenger RNA. *Cell*, 12(1), 1-8. [https://doi.org/10.1016/0092-8674\(77\)90180-5](https://doi.org/10.1016/0092-8674(77)90180-5)
- Cid-Samper, F., Gelabert-Baldrich, M., Lang, B., Lorenzo-Gotor, N., Ponti, R. D., Severijnen, L., Bolognesi, B., Gelpi, E., Hukema, R. K., Botta-Orfila, T., & Tartaglia, G. G. (2018). An Integrative Study of Protein-RNA Condensates Identifies Scaffolding RNAs and Reveals Players in Fragile X-Associated Tremor/Ataxia Syndrome. *Cell Rep*, 25(12), 3422-3434 e3427. <https://doi.org/10.1016/j.celrep.2018.11.076>

- Coelho, M. B., Attig, J., Ule, J., & Smith, C. W. (2016). MatrIn3: connecting gene expression with the nuclear matrix. *Wiley Interdiscip Rev RNA*, 7(3), 303-315. <https://doi.org/10.1002/wrna.1336>
- Cookson, M. R. (2017). RNA-binding proteins implicated in neurodegenerative diseases. *Wiley Interdiscip Rev RNA*, 8(1). <https://doi.org/10.1002/wrna.1397>
- Crouch, E. E., & Doetsch, F. (2018). FACS isolation of endothelial cells and pericytes from mouse brain microregions. *Nat Protoc*, 13(4), 738-751. <https://doi.org/10.1038/nprot.2017.158>
- David, C. J., & Manley, J. L. (2010). Alternative pre-mRNA splicing regulation in cancer: pathways and programs unhinged. *Genes Dev*, 24(21), 2343-2364. <https://doi.org/10.1101/gad.1973010>
- Davila, N. G., Blakemore, L. J., & Trombley, P. Q. (2003). Dopamine modulates synaptic transmission between rat olfactory bulb neurons in culture. *J Neurophysiol*, 90(1), 395-404. <https://doi.org/10.1152/jn.01058.2002>
- de Groot, N. S., Armaos, A., Grana-Montes, R., Alriquet, M., Calloni, G., Vabulas, R. M., & Tartaglia, G. G. (2019). RNA structure drives interaction with proteins. *Nature Communications*, 10. <https://doi.org/ARTN> 3246
- 10.1038/s41467-019-10923-5
- Di Bartolomei, G., & Scheiffele, P. (2022). An Optimized Protocol for the Mapping of Cell Type-Specific Ribosome-Associated Transcript Isoforms from Small Mouse Brain Regions. *Methods Mol Biol*, 2537, 37-49. https://doi.org/10.1007/978-1-0716-2521-7_3
- Dobin, A., Davis, C. A., Schlesinger, F., Drenkow, J., Zaleski, C., Jha, S., Batut, P., Chaisson, M., & Gingeras, T. R. (2013). STAR: ultrafast universal RNA-seq aligner. *Bioinformatics*, 29(1), 15-21. <https://doi.org/10.1093/bioinformatics/bts635>
- Dominguez, D., Freese, P., Alexis, M. S., Su, A., Hochman, M., Palden, T., Bazile, C., Lambert, N. J., Van Nostrand, E. L., Pratt, G. A., Yeo, G. W., Graveley, B. R., & Burge, C. B. (2018). Sequence, Structure, and Context Preferences of Human RNA Binding Proteins. *Mol Cell*, 70(5), 854-867 e859. <https://doi.org/10.1016/j.molcel.2018.05.001>
- Dominissini, D., Moshitch-Moshkovitz, S., Schwartz, S., Salmon-Divon, M., Ungar, L., Osenberg, S., Cesarkas, K., Jacob-Hirsch, J., Amariglio, N., Kupiec, M., Sorek, R., & Rechavi, G. (2012). Topology of the human and mouse m6A RNA methylomes revealed by m6A-seq. *Nature*, 485(7397), 201-206. <https://doi.org/10.1038/nature11112>
- Doucette, W., & Restrepo, D. (2008). Profound context-dependent plasticity of mitral cell responses in olfactory bulb. *PLoS Biol*, 6(10), e258. <https://doi.org/10.1371/journal.pbio.0060258>
- Duan, W., Guo, M., Yi, L., Liu, Y., Li, Z., Ma, Y., Zhang, G., Liu, Y., Bu, H., Song, X., & Li, C. (2020). The deletion of mutant SOD1 via CRISPR/Cas9/sgRNA prolongs survival in an amyotrophic lateral sclerosis mouse model. *Gene Ther*, 27(3-4), 157-169. <https://doi.org/10.1038/s41434-019-0116-1>
- Dulac, C., & Axel, R. (1995). A novel family of genes encoding putative pheromone receptors in mammals. *Cell*, 83(2), 195-206. [https://doi.org/10.1016/0092-8674\(95\)90161-2](https://doi.org/10.1016/0092-8674(95)90161-2)
- Dulac, C., & Kimchi, T. (2007). Neural mechanisms underlying sex-specific behaviors in vertebrates. *Curr Opin Neurobiol*, 17(6), 675-683. <https://doi.org/10.1016/j.conb.2008.01.009>
- Dulac, C., & Wagner, S. (2006). Genetic analysis of brain circuits underlying pheromone signaling. *Annu Rev Genet*, 40, 449-467. <https://doi.org/10.1146/annurev.genet.39.073003.093937>
- Economides, A. N., Friendewey, D., Yang, P., Dominguez, M. G., Dore, A. T., Lobov, I. B., Persaud, T., Rojas, J., McClain, J., Lengyel, P., Droguett, G., Chernomorsky, R., Stevens, S., Auerbach, W., DeChiara, T. M., Pouyemirou, W., Cruz, J. M., Jr., Feeley,

- K., Mellis, I. A., . . . Yancopoulos, G. D. (2013). Conditionals by inversion provide a universal method for the generation of conditional alleles. *Proc Natl Acad Sci U S A*, 110(34), E3179-3188. <https://doi.org/10.1073/pnas.1217812110>
- Egger, V., Svoboda, K., & Mainen, Z. F. (2003). Mechanisms of lateral inhibition in the olfactory bulb: efficiency and modulation of spike-evoked calcium influx into granule cells. *J Neurosci*, 23(20), 7551-7558. <https://doi.org/10.1523/JNEUROSCI.23-20-07551.2003>
- Egger, V., Svoboda, K., & Mainen, Z. F. (2005). Dendrodendritic synaptic signals in olfactory bulb granule cells: local spine boost and global low-threshold spike. *J Neurosci*, 25(14), 3521-3530. <https://doi.org/10.1523/JNEUROSCI.4746-04.2005>
- Ehlers, M. D., Tingley, W. G., & Huganir, R. L. (1995). Regulated subcellular distribution of the NR1 subunit of the NMDA receptor. *Science*, 269(5231), 1734-1737. <https://doi.org/10.1126/science.7569904>
- Eid, J., Fehr, A., Gray, J., Luong, K., Lyle, J., Otto, G., Peluso, P., Rank, D., Baybayan, P., Bettman, B., Bibillo, A., Bjornson, K., Chaudhuri, B., Christians, F., Cicero, R., Clark, S., Dalal, R., Dewinter, A., Dixon, J., . . . Turner, S. (2009). Real-time DNA sequencing from single polymerase molecules. *Science*, 323(5910), 133-138. <https://doi.org/10.1126/science.1162986>
- El Marabti, E., & Younis, I. (2018). The Cancer Spliceome: Reprogramming of Alternative Splicing in Cancer. *Front Mol Biosci*, 5, 80. <https://doi.org/10.3389/fmolb.2018.00080>
- Fang, T., Je, G., Pacut, P., Keyhanian, K., Gao, J., & Ghasemi, M. (2022). Gene Therapy in Amyotrophic Lateral Sclerosis. *Cells*, 11(13). <https://doi.org/10.3390/cells11132066>
- Fantuzzo, J. A., Robles, D. A., Mirabella, V. R., Hart, R. P., Pang, Z. P., & Zahn, J. D. (2020). Development of a high-throughput arrayed neural circuitry platform using human induced neurons for drug screening applications. *Lab Chip*, 20(6), 1140-1152. <https://doi.org/10.1039/c9lc01179j>
- Faustino, N. A., & Cooper, T. A. (2003). Pre-mRNA splicing and human disease. *Genes Dev*, 17(4), 419-437. <https://doi.org/10.1101/gad.1048803>
- Feng, H., Bao, S., Rahman, M. A., Weyn-Vanhentenryck, S. M., Khan, A., Wong, J., Shah, A., Flynn, E. D., Krainer, A. R., & Zhang, C. (2019). Modeling RNA-Binding Protein Specificity In Vivo by Precisely Registering Protein-RNA Crosslink Sites. *Mol Cell*, 74(6), 1189-1204 e1186. <https://doi.org/10.1016/j.molcel.2019.02.002>
- Feng, H., Moakley, D. F., Chen, S., McKenzie, M. G., Menon, V., & Zhang, C. (2021). Complexity and graded regulation of neuronal cell-type-specific alternative splicing revealed by single-cell RNA sequencing. *Proc Natl Acad Sci U S A*, 118(10). <https://doi.org/10.1073/pnas.2013056118>
- Fenix, A. M., Miyaoka, Y., Bertero, A., Blue, S. M., Spindler, M. J., Tan, K. K. B., Perez-Bermejo, J. A., Chan, A. H., Mayerl, S. J., Nguyen, T. D., Russell, C. R., Lizarraga, P. P., Truong, A., So, P. L., Kulkarni, A., Chetal, K., Sathe, S., Sniadecki, N. J., Yeo, G. W., . . . Salomonis, N. (2021). Gain-of-function cardiomyopathic mutations in RBM20 rewire splicing regulation and re-distribute ribonucleoprotein granules within processing bodies. *Nat Commun*, 12(1), 6324. <https://doi.org/10.1038/s41467-021-26623-y>
- Ferguson, B. R., & Gao, W. J. (2018). PV Interneurons: Critical Regulators of E/I Balance for Prefrontal Cortex-Dependent Behavior and Psychiatric Disorders. *Front Neural Circuits*, 12, 37. <https://doi.org/10.3389/fncir.2018.00037>
- Filippello, A., Lorenzi, P., Bergamo, E., & Romanelli, M. G. (2013). Identification of nuclear retention domains in the RBM20 protein. *FEBS Lett*, 587(18), 2989-2995. <https://doi.org/10.1016/j.febslet.2013.07.018>
- Fishell, G., & Kepecs, A. (2020). Interneuron Types as Attractors and Controllers. *Annu Rev Neurosci*, 43, 1-30. <https://doi.org/10.1146/annurev-neuro-070918-050421>
- Foster, M., Sherrington, C. S. S., & University College, L. L. S. (1897). *A textbook of physiology. With C.S. Sherrington. Part 3. The central nervous system* (7th ed.). Macmillan. <https://historicaltexts.jisc.ac.uk/ukmhl-b21271458>

- https://suprimo.lib.strath.ac.uk/openurl/SU/SUVU01?u.ignore_date_coverage=true&rft.mms_id=9913122392302996
- Fuentealba, L. C., Rompani, S. B., Parraguez, J. I., Obernier, K., Romero, R., Cepko, C. L., & Alvarez-Buylla, A. (2015). Embryonic Origin of Postnatal Neural Stem Cells. *Cell*, 161(7), 1644-1655. <https://doi.org/10.1016/j.cell.2015.05.041>
- Furlanis, E., & Scheiffele, P. (2018). Regulation of neuronal differentiation, function, and plasticity by alternative splicing. *Annual Review of Cell and Developmental Biology* 34, 451-469.
- Furlanis, E., Traunmuller, L., Fucile, G., & Scheiffele, P. (2019). Landscape of ribosome-engaged transcript isoforms reveals extensive neuronal-cell-class-specific alternative splicing programs. *Nat Neurosci*, 22(10), 1709-1717. <https://doi.org/10.1038/s41593-019-0465-5>
- Gaj, T., Ojala, D. S., Ekman, F. K., Byrne, L. C., Limsirichai, P., & Schaffer, D. V. (2017). In vivo genome editing improves motor function and extends survival in a mouse model of ALS. *Sci Adv*, 3(12), eaar3952. <https://doi.org/10.1126/sciadv.aar3952>
- Gallego-Paez, L. M., Bordone, M. C., Leote, A. C., Saraiva-Agostinho, N., Ascensao-Ferreira, M., & Barbosa-Morais, N. L. (2017). Alternative splicing: the pledge, the turn, and the prestige : The key role of alternative splicing in human biological systems. *Hum Genet*, 136(9), 1015-1042. <https://doi.org/10.1007/s00439-017-1790-y>
- Gascon, S., Paez-Gomez, J. A., Diaz-Guerra, M., Scheiffele, P., & Scholl, F. G. (2008). Dual-promoter lentiviral vectors for constitutive and regulated gene expression in neurons. *J Neurosci Methods*, 168(1), 104-112. <https://doi.org/10.1016/j.jneumeth.2007.09.023>
- Gerstberger, S., Hafner, M., & Tuschl, T. (2014). A census of human RNA-binding proteins. *Nat Rev Genet*, 15(12), 829-845. <https://doi.org/10.1038/nrg3813>
- Geuens, T., Bouhy, D., & Timmerman, V. (2016). The hnRNP family: insights into their role in health and disease. *Hum Genet*, 135(8), 851-867. <https://doi.org/10.1007/s00439-016-1683-5>
- Gilbert, S. F. (2004). Mechanisms for the environmental regulation of gene expression. *Birth Defects Res C Embryo Today*, 72(4), 291-299. <https://doi.org/10.1002/bdrc.20026>
- Glasgow, S. D., McPhedrain, R., Madranges, J. F., Kennedy, T. E., & Ruthazer, E. S. (2019). Approaches and Limitations in the Investigation of Synaptic Transmission and Plasticity. *Front Synaptic Neurosci*, 11, 20. <https://doi.org/10.3389/fnsyn.2019.00020>
- Glisovic, T., Bachorik, J. L., Yong, J., & Dreyfuss, G. (2008). RNA-binding proteins and post-transcriptional gene regulation. *FEBS Lett*, 582(14), 1977-1986. <https://doi.org/10.1016/j.febslet.2008.03.004>
- Gomez, A. M., Traunmuller, L., & Scheiffele, P. (2021). Neurexins: molecular codes for shaping neuronal synapses. *Nat Rev Neurosci*, 22(3), 137-151. <https://doi.org/10.1038/s41583-020-00415-7>
- Gonatopoulos-Pournatzis, T., Niibori, R., Salter, E. W., Weatheritt, R. J., Tsang, B., Farhangmehr, S., Liang, X., Braunschweig, U., Roth, J., Zhang, S., Henderson, T., Sharma, E., Quesnel-Vallieres, M., Permanyer, J., Maier, S., Georgiou, J., Irimia, M., Sonenberg, N., Forman-Kay, J. D., . . . Blencowe, B. J. (2020). Autism-Misregulated eIF4G Microexons Control Synaptic Translation and Higher Order Cognitive Functions. *Mol Cell*, 77(6), 1176-1192 e1116. <https://doi.org/10.1016/j.molcel.2020.01.006>
- Gonzalez, C., Sims, J. S., Hornstein, N., Mela, A., Garcia, F., Lei, L., Gass, D. A., Amendolara, B., Bruce, J. N., Canoll, P., & Sims, P. A. (2014). Ribosome profiling reveals a cell-type-specific translational landscape in brain tumors. *J Neurosci*, 34(33), 10924-10936. <https://doi.org/10.1523/JNEUROSCI.0084-14.2014>
- Grabowski, P. J., & Black, D. L. (2001). Alternative RNA splicing in the nervous system. *Prog Neurobiol*, 65(3), 289-308. [https://doi.org/10.1016/s0301-0082\(01\)00007-7](https://doi.org/10.1016/s0301-0082(01)00007-7)
- Gregory, J. A., Hoelzli, E., Abdelaal, R., Braine, C., Cuevas, M., Halpern, M., Barretto, N., Schrode, N., Akbalik, G., Kang, K., Cheng, E., Bowles, K., Lotz, S., Goderie, S., Karch, C. M., Temple, S., Goate, A., Brennand, K. J., & Phatnani, H. (2020). Cell

- Type-Specific In Vitro Gene Expression Profiling of Stem Cell-Derived Neural Models. *Cells*, 9(6). <https://doi.org/10.3390/cells9061406>
- Gross, G. G., Junge, J. A., Mora, R. J., Kwon, H. B., Olson, C. A., Takahashi, T. T., Liman, E. R., Ellis-Davies, G. C., McGee, A. W., Sabatini, B. L., Roberts, R. W., & Arnold, D. B. (2013). Recombinant probes for visualizing endogenous synaptic proteins in living neurons. *Neuron*, 78(6), 971-985. <https://doi.org/10.1016/j.neuron.2013.04.017>
- Guo, J., Jia, J., & Jia, R. (2015). PTBP1 and PTBP2 impaired autoregulation of SRSF3 in cancer cells. *Sci Rep*, 5, 14548. <https://doi.org/10.1038/srep14548>
- Guo, W., Schafer, S., Greaser, M. L., Radke, M. H., Liss, M., Govindarajan, T., Maatz, H., Schulz, H., Li, S., Parrish, A. M., Dauksaite, V., Vakeel, P., Klaassen, S., Gerull, B., Thierfelder, L., Regitz-Zagrosek, V., Hacker, T. A., Saupe, K. W., Dec, G. W., . . . Gotthardt, M. (2012). RBM20, a gene for hereditary cardiomyopathy, regulates titin splicing. *Nat Med*, 18(5), 766-773. <https://doi.org/10.1038/nm.2693>
- Guo, W., Zhu, C., Yin, Z., Wang, Q., Sun, M., Cao, H., & Greaser, M. L. (2018). Splicing Factor RBM20 Regulates Transcriptional Network of Titin Associated and Calcium Handling Genes in The Heart. *Int J Biol Sci*, 14(4), 369-380. <https://doi.org/10.7150/ijbs.24117>
- Haddad, R., Lanjuin, A., Madisen, L., Zeng, H., Murthy, V. N., & Uchida, N. (2013). Olfactory cortical neurons read out a relative time code in the olfactory bulb. *Nat Neurosci*, 16(7), 949-957. <https://doi.org/10.1038/nn.3407>
- Hafner, M., Katsantoni, M., Koster, T., Marks, J., Mukherjee, J., Staiger, D., Ule, J., & Zavolan, M. (2021). CLIP and complementary methods. *Nature Reviews Methods Primers*, 1(1). <https://doi.org/ARTN 20>
- 10.1038/s43586-021-00018-1
- Halpern, M. (1987). The organization and function of the vomeronasal system. *Annu Rev Neurosci*, 10, 325-362. <https://doi.org/10.1146/annurev.ne.10.030187.001545>
- Halpern, M., & Martinez-Marcos, A. (2003). Structure and function of the vomeronasal system: an update. *Prog Neurobiol*, 70(3), 245-318. [https://doi.org/10.1016/s0301-0082\(03\)00103-5](https://doi.org/10.1016/s0301-0082(03)00103-5)
- Han, K., Yeo, G., An, P., Burge, C. B., & Grabowski, P. J. (2005). A combinatorial code for splicing silencing: UAGG and GGGG motifs. *PLoS Biol*, 3(5), e158. <https://doi.org/10.1371/journal.pbio.0030158>
- Hattori, D., Demir, E., Kim, H. W., Viragh, E., Zipursky, S. L., & Dickson, B. J. (2007). Dscam diversity is essential for neuronal wiring and self-recognition. *Nature*, 449(7159), 223-227. <https://doi.org/10.1038/nature06099>
- Hauser, D., Behr, K., Konno, K., Schreiner, D., Schmidt, A., Watanabe, M., Bischofberger, J., & Scheiffele, P. (2022). Targeted proteoform mapping uncovers specific Neurexin-3 variants required for dendritic inhibition. *Neuron*, 110(13), 2094-2109 e2010. <https://doi.org/10.1016/j.neuron.2022.04.017>
- Hayar, A., Karnup, S., Ennis, M., & Shipley, M. T. (2004). External tufted cells: a major excitatory element that coordinates glomerular activity. *J Neurosci*, 24(30), 6676-6685. <https://doi.org/10.1523/JNEUROSCI.1367-04.2004>
- Heiman, M., Schaefer, A., Gong, S., Peterson, J. D., Day, M., Ramsey, K. E., Suarez-Farinas, M., Schwarz, C., Stephan, D. A., Surmeier, D. J., Greengard, P., & Heintz, N. (2008). A translational profiling approach for the molecular characterization of CNS cell types. *Cell*, 135(4), 738-748. <https://doi.org/10.1016/j.cell.2008.10.028>
- Heyl, F., & Backofen, R. (2021). StoatyDive: Evaluation and classification of peak profiles for sequencing data. *Gigascience*, 10(6). <https://doi.org/10.1093/gigascience/giab045>
- Hippenmeyer, S., Vrieseling, E., Sigrist, M., Portmann, T., Laengle, C., Ladle, D. R., & Arber, S. (2005). A developmental switch in the response of DRG neurons to ETS transcription factor signaling. *PLoS Biol*, 3(5), e159. <https://doi.org/10.1371/journal.pbio.0030159>

- Hobert, O. (2016). Terminal Selectors of Neuronal Identity. *Curr Top Dev Biol*, 116, 455-475. <https://doi.org/10.1016/bs.ctdb.2015.12.007>
- Hobert, O., & Kratsios, P. (2019). Neuronal identity control by terminal selectors in worms, flies, and chordates. *Curr Opin Neurobiol*, 56, 97-105. <https://doi.org/10.1016/j.conb.2018.12.006>
- Hu, J., Qian, H., Xue, Y., & Fu, X. D. (2018). PTB/nPTB: master regulators of neuronal fate in mammals. *Biophys Rep*, 4(4), 204-214. <https://doi.org/10.1007/s41048-018-0066-y>
- Humphrey, J., Emmett, W., Fratta, P., Isaacs, A. M., & Plagnol, V. (2017). Quantitative analysis of cryptic splicing associated with TDP-43 depletion. *BMC Med Genomics*, 10(1), 38. <https://doi.org/10.1186/s12920-017-0274-1>
- Hwang, H. W., Park, C. Y., Goodarzi, H., Fak, J. J., Mele, A., Moore, M. J., Saito, Y., & Darnell, R. B. (2016). PAPERCLIP Identifies MicroRNA Targets and a Role of CstF64/64tau in Promoting Non-canonical poly(A) Site Usage. *Cell Rep*, 15(2), 423-435. <https://doi.org/10.1016/j.celrep.2016.03.023>
- Hwang, H. W., Saito, Y., Park, C. Y., Blachere, N. E., Tajima, Y., Fak, J. J., Zucker-Scharff, I., & Darnell, R. B. (2017). cTag-PAPERCLIP Reveals Alternative Polyadenylation Promotes Cell-Type Specific Protein Diversity and Shifts Araf Isoforms with Microglia Activation. *Neuron*, 95(6), 1334-1349 e1335. <https://doi.org/10.1016/j.neuron.2017.08.024>
- Ibrahim, E. C., Schaal, T. D., Hertel, K. J., Reed, R., & Maniatis, T. (2005). Serine/arginine-rich protein-dependent suppression of exon skipping by exonic splicing enhancers. *Proc Natl Acad Sci U S A*, 102(14), 5002-5007. <https://doi.org/10.1073/pnas.0500543102>
- Imai, T. (2014). Construction of functional neuronal circuitry in the olfactory bulb. *Semin Cell Dev Biol*, 35, 180-188. <https://doi.org/10.1016/j.semcdb.2014.07.012>
- Irimia, M., Weatheritt, R. J., Ellis, J. D., Parikshak, N. N., Gonatopoulos-Pournatzis, T., Babor, M., Quesnel-Vallieres, M., Tapial, J., Raj, B., O'Hanlon, D., Barrios-Rodiles, M., Sternberg, M. J., Cordes, S. P., Roth, F. P., Wrana, J. L., Geschwind, D. H., & Blencowe, B. J. (2014). A highly conserved program of neuronal microexons is misregulated in autistic brains. *Cell*, 159(7), 1511-1523. <https://doi.org/10.1016/j.cell.2014.11.035>
- Isaacson, J. S., & Scanziani, M. (2011). How Inhibition Shapes Cortical Activity. *Neuron*, 72(2), 231-243. <https://doi.org/10.1016/j.neuron.2011.09.027>
- Ito, J., Iijima, M., Yoshimoto, N., Niimi, T., Kuroda, S., & Maturana, A. D. (2016). RBM20 and RBM24 cooperatively promote the expression of short enh splice variants. *FEBS Lett*, 590(14), 2262-2274. <https://doi.org/10.1002/1873-3468.12251>
- Jaitin, D. A., Kenigsberg, E., Keren-Shaul, H., Elefant, N., Paul, F., Zaretsky, I., Mildner, A., Cohen, N., Jung, S., Tanay, A., & Amit, I. (2014). Massively parallel single-cell RNA-seq for marker-free decomposition of tissues into cell types. *Science*, 343(6172), 776-779. <https://doi.org/10.1126/science.1247651>
- Jones, S., Zylberberg, J., & Schoppa, N. (2020). Cellular and Synaptic Mechanisms That Differentiate Mitral Cells and Superficial Tufted Cells Into Parallel Output Channels in the Olfactory Bulb. *Front Cell Neurosci*, 14, 614377. <https://doi.org/10.3389/fncel.2020.614377>
- Kaessmann, H. (2010). Origins, evolution, and phenotypic impact of new genes. *Genome Res*, 20(10), 1313-1326. <https://doi.org/10.1101/gr.101386.109>
- Kaida, D., Schneider-Poetsch, T., & Yoshida, M. (2012). Splicing in oncogenesis and tumor suppression. *Cancer Sci*, 103(9), 1611-1616. <https://doi.org/10.1111/j.1349-7006.2012.02356.x>
- Kalsotra, A., Xiao, X., Ward, A. J., Castle, J. C., Johnson, J. M., Burge, C. B., & Cooper, T. A. (2008). A postnatal switch of CELF and MBNL proteins reprograms alternative splicing in the developing heart. *Proc Natl Acad Sci U S A*, 105(51), 20333-20338. <https://doi.org/10.1073/pnas.0809045105>

- Kanadia, R. N., Shin, J., Yuan, Y., Beattie, S. G., Wheeler, T. M., Thornton, C. A., & Swanson, M. S. (2006). Reversal of RNA missplicing and myotonia after muscleblind overexpression in a mouse poly(CUG) model for myotonic dystrophy. *Proc Natl Acad Sci U S A*, *103*(31), 11748-11753. <https://doi.org/10.1073/pnas.0604970103>
- Kato, H. K., Chu, M. W., Isaacson, J. S., & Komiyama, T. (2012). Dynamic sensory representations in the olfactory bulb: modulation by wakefulness and experience. *Neuron*, *76*(5), 962-975. <https://doi.org/10.1016/j.neuron.2012.09.037>
- Kepecs, A., & Fishell, G. (2014). Interneuron cell types are fit to function. *Nature*, *505*(7483), 318-326. <https://doi.org/10.1038/nature12983>
- Kersen, D. E. C., Tavoni, G., & Balasubramanian, V. (2022). Connectivity and dynamics in the olfactory bulb. *PLoS Comput Biol*, *18*(2), e1009856. <https://doi.org/10.1371/journal.pcbi.1009856>
- Khan, M. A., Reckman, Y. J., Aufiero, S., van den Hoogenhof, M. M., van der Made, I., Beqqali, A., Koolbergen, D. R., Rasmussen, T. B., van der Velden, J., Creemers, E. E., & Pinto, Y. M. (2016). RBM20 Regulates Circular RNA Production From the Titin Gene. *Circ Res*, *119*(9), 996-1003. <https://doi.org/10.1161/CIRCRESAHA.116.309568>
- Kikuta, S., Fletcher, M. L., Homma, R., Yamasoba, T., & Nagayama, S. (2013). Odorant response properties of individual neurons in an olfactory glomerular module. *Neuron*, *77*(6), 1122-1135. <https://doi.org/10.1016/j.neuron.2013.01.022>
- Kimoto, H., Haga, S., Sato, K., & Touhara, K. (2005). Sex-specific peptides from exocrine glands stimulate mouse vomeronasal sensory neurons. *Nature*, *437*(7060), 898-901. <https://doi.org/10.1038/nature04033>
- Kishore, S., Lubner, S., & Zavolan, M. (2010). Deciphering the role of RNA-binding proteins in the post-transcriptional control of gene expression. *Brief Funct Genomics*, *9*(5-6), 391-404. <https://doi.org/10.1093/bfpg/eq028>
- Kitamura, K., & Nimura, K. (2021). Regulation of RNA Splicing: Aberrant Splicing Regulation and Therapeutic Targets in Cancer. *Cells*, *10*(4). <https://doi.org/10.3390/cells10040923>
- Koopmans, F., van Nierop, P., Andres-Alonso, M., Byrnes, A., Cijssouw, T., Coba, M. P., Cornelisse, L. N., Farrell, R. J., Goldschmidt, H. L., Howrigan, D. P., Hussain, N. K., Imig, C., de Jong, A. P. H., Jung, H., Kohansalnodehi, M., Kramarz, B., Lipstein, N., Lovering, R. C., MacGillavry, H., . . . Verhage, M. (2019). SynGO: An Evidence-Based, Expert-Curated Knowledge Base for the Synapse. *Neuron*, *103*(2), 217-234 e214. <https://doi.org/10.1016/j.neuron.2019.05.002>
- Korlach, J., Bjornson, K. P., Chaudhuri, B. P., Cicero, R. L., Flusberg, B. A., Gray, J. J., Holden, D., Saxena, R., Wegener, J., & Turner, S. W. (2010). Real-time DNA sequencing from single polymerase molecules. *Methods Enzymol*, *472*, 431-455. [https://doi.org/10.1016/S0076-6879\(10\)72001-2](https://doi.org/10.1016/S0076-6879(10)72001-2)
- Korobeynikov, V. A., Lyashchenko, A. K., Blanco-Redondo, B., Jafar-Nejad, P., & Shneider, N. A. (2022). Antisense oligonucleotide silencing of FUS expression as a therapeutic approach in amyotrophic lateral sclerosis. *Nat Med*, *28*(1), 104-116. <https://doi.org/10.1038/s41591-021-01615-z>
- Kubo, N., Ishii, H., Xiong, X., Bianco, S., Meitinger, F., Hu, R., Hocker, J. D., Conte, M., Gorkin, D., Yu, M., Li, B., Dixon, J. R., Hu, M., Nicodemi, M., Zhao, H., & Ren, B. (2021). Promoter-proximal CTCF binding promotes distal enhancer-dependent gene activation. *Nat Struct Mol Biol*, *28*(2), 152-161. <https://doi.org/10.1038/s41594-020-00539-5>
- Kumar, S. S., & Buckmaster, P. S. (2007). Neuron-specific nuclear antigen NeuN is not detectable in gerbil substantia nigra pars reticulata. *Brain Res*, *1142*, 54-60. <https://doi.org/10.1016/j.brainres.2007.01.027>
- Kuninger, D. T., Izumi, T., Papaconstantinou, J., & Mitra, S. (2002). Human AP-endonuclease 1 and hnRNP-L interact with a nCaRE-like repressor element in the

- AP-endonuclease 1 promoter. *Nucleic Acids Res*, 30(3), 823-829.
<https://doi.org/10.1093/nar/30.3.823>
- Langwieser, N., Christel, C. J., Kleppisch, T., Hofmann, F., Wotjak, C. T., & Moosmang, S. (2010). Homeostatic switch in hebbian plasticity and fear learning after sustained loss of Cav1.2 calcium channels. *J Neurosci*, 30(25), 8367-8375.
<https://doi.org/10.1523/JNEUROSCI.4164-08.2010>
- Lee, H., Fenster, R. J., Pineda, S. S., Gibbs, W. S., Mohammadi, S., Davila-Velderrain, J., Garcia, F. J., Therrien, M., Novis, H. S., Gao, F., Wilkinson, H., Vogt, T., Kellis, M., LaVoie, M. J., & Heiman, M. (2020). Cell Type-Specific Transcriptomics Reveals that Mutant Huntingtin Leads to Mitochondrial RNA Release and Neuronal Innate Immune Activation. *Neuron*, 107(5), 891-908 e898.
<https://doi.org/10.1016/j.neuron.2020.06.021>
- Li, D., McIntosh, C. S., Mastaglia, F. L., Wilton, S. D., & Aung-Htut, M. T. (2021). Correction to: Neurodegenerative diseases: a hotbed for splicing defects and the potential therapies. *Transl Neurodegener*, 10(1), 41. <https://doi.org/10.1186/s40035-021-00267-w>
- Liang, X. H., Sun, H., Nichols, J. G., & Crooke, S. T. (2017). RNase H1-Dependent Antisense Oligonucleotides Are Robustly Active in Directing RNA Cleavage in Both the Cytoplasm and the Nucleus. *Mol Ther*, 25(9), 2075-2092.
<https://doi.org/10.1016/j.ymthe.2017.06.002>
- Liao, Y., Smyth, G. K., & Shi, W. (2014). featureCounts: an efficient general purpose program for assigning sequence reads to genomic features. *Bioinformatics*, 30(7), 923-930. <https://doi.org/10.1093/bioinformatics/btt656>
- Licatalosi, D. D., & Darnell, R. B. (2006). Splicing regulation in neurologic disease. *Neuron*, 52(1), 93-101. <https://doi.org/10.1016/j.neuron.2006.09.017>
- Lim, C. K. W., Gapinske, M., Brooks, A. K., Woods, W. S., Powell, J. E., Zeballos, C. M., Winter, J., Perez-Pinera, P., & Gaj, T. (2020). Treatment of a Mouse Model of ALS by In Vivo Base Editing. *Mol Ther*, 28(4), 1177-1189.
<https://doi.org/10.1016/j.ymthe.2020.01.005>
- Ling, J. P., Pletnikova, O., Troncoso, J. C., & Wong, P. C. (2015). TDP-43 repression of nonconserved cryptic exons is compromised in ALS-FTD. *Science*, 349(6248), 650-655. <https://doi.org/10.1126/science.aab0983>
- Ling, S. C., Polymenidou, M., & Cleveland, D. W. (2013). Converging mechanisms in ALS and FTD: disrupted RNA and protein homeostasis. *Neuron*, 79(3), 416-438.
<https://doi.org/10.1016/j.neuron.2013.07.033>
- Linke, W. A., & Bucker, S. (2012). King of hearts: a splicing factor rules cardiac proteins. *Nat Med*, 18(5), 660-661. <https://doi.org/10.1038/nm.2762>
- Linke, W. A., & Granzier, H. (1998). A spring tale: new facts on titin elasticity. *Biophys J*, 75(6), 2613-2614. [https://doi.org/10.1016/S0006-3495\(98\)77706-9](https://doi.org/10.1016/S0006-3495(98)77706-9)
- Linke, W. A., Ivemeyer, M., Mundel, P., Stockmeier, M. R., & Kolmerer, B. (1998). Nature of PEVK-titin elasticity in skeletal muscle. *Proc Natl Acad Sci U S A*, 95(14), 8052-8057.
<https://doi.org/10.1073/pnas.95.14.8052>
- Liu, N., Dai, Q., Zheng, G., He, C., Parisien, M., & Pan, T. (2015). N(6)-methyladenosine-dependent RNA structural switches regulate RNA-protein interactions. *Nature*, 518(7540), 560-564. <https://doi.org/10.1038/nature14234>
- Liu, X. X., Guo, Q. H., Xu, W. B., Liu, P., & Yan, K. (2022). Rapid Regulation of Alternative Splicing in Response to Environmental Stresses. *Front Plant Sci*, 13, 832177.
<https://doi.org/10.3389/fpls.2022.832177>
- Liu, Y., Beyer, A., & Aebersold, R. (2016). On the Dependency of Cellular Protein Levels on mRNA Abundance. *Cell*, 165(3), 535-550. <https://doi.org/10.1016/j.cell.2016.03.014>
- Liu, Z., Chen, Z., Shang, C., Yan, F., Shi, Y., Zhang, J., Qu, B., Han, H., Wang, Y., Li, D., Sudhof, T. C., & Cao, P. (2017). IGF1-Dependent Synaptic Plasticity of Mitral Cells in Olfactory Memory during Social Learning. *Neuron*, 95(1), 106-122 e105.
<https://doi.org/10.1016/j.neuron.2017.06.015>

- Lorenzi, P., Sangalli, A., Fochi, S., Dal Molin, A., Malerba, G., Zipeto, D., & Romanelli, M. G. (2019). RNA-binding proteins RBM20 and PTBP1 regulate the alternative splicing of FHOD3. *Int J Biochem Cell Biol*, *106*, 74-83. <https://doi.org/10.1016/j.biocel.2018.11.009>
- Loureiro, M., Achargui, R., Flakowski, J., Van Zessen, R., Stefanelli, T., Pascoli, V., & Luscher, C. (2019). Social transmission of food safety depends on synaptic plasticity in the prefrontal cortex. *Science*, *364*(6444), 991-995. <https://doi.org/10.1126/science.aaw5842>
- Love, M. I., Huber, W., & Anders, S. (2014). Moderated estimation of fold change and dispersion for RNA-seq data with DESeq2. *Genome Biol*, *15*(12), 550. <https://doi.org/10.1186/s13059-014-0550-8>
- Luo, L., Ambrozkiwicz, M. C., Benseler, F., Chen, C., Dumontier, E., Falkner, S., Furlanis, E., Gomez, A. M., Hoshina, N., Huang, W. H., Hutchison, M. A., Itoh-Maruoaka, Y., Lavery, L. A., Li, W., Maruo, T., Motohashi, J., Pai, E. L., Pelkey, K. A., Pereira, A., . . . Craig, A. M. (2020). Optimizing Nervous System-Specific Gene Targeting with Cre Driver Lines: Prevalence of Germline Recombination and Influencing Factors. *Neuron*, *106*(1), 37-65 e35. <https://doi.org/10.1016/j.neuron.2020.01.008>
- Ma, X. R., Prudencio, M., Koike, Y., Vatsavayai, S. C., Kim, G., Harbinski, F., Briner, A., Rodriguez, C. M., Guo, C., Akiyama, T., Schmidt, H. B., Cummings, B. B., Wyatt, D. W., Kurylo, K., Miller, G., Mekhoubad, S., Sallee, N., Mekonnen, G., Ganser, L., . . . Gitler, A. D. (2022). TDP-43 represses cryptic exon inclusion in the FTD-ALS gene UNC13A. *Nature*, *603*(7899), 124-130. <https://doi.org/10.1038/s41586-022-04424-7>
- Maatz, H., Jens, M., Liss, M., Schafer, S., Heinig, M., Kirchner, M., Adami, E., Rintisch, C., Dauksaite, V., Radke, M. H., Selbach, M., Barton, P. J., Cook, S. A., Rajewsky, N., Gotthardt, M., Landthaler, M., & Hubner, N. (2014). RNA-binding protein RBM20 represses splicing to orchestrate cardiac pre-mRNA processing. *J Clin Invest*, *124*(8), 3419-3430. <https://doi.org/10.1172/JCI74523>
- Macrides, F., Schoenfeld, T. A., Marchand, J. E., & Clancy, A. N. (1985). Evidence for Morphologically, Neurochemically and Functionally Heterogeneous Classes of Mitral and Tufted Cells in the Olfactory-Bulb. *Chemical Senses*, *10*(2), 175-202. <https://doi.org/DOI 10.1093/chemse/10.2.175>
- Madisen, L., Zwingman, T. A., Sunkin, S. M., Oh, S. W., Zariwala, H. A., Gu, H., Ng, L. L., Palmiter, R. D., Hawrylycz, M. J., Jones, A. R., Lein, E. S., & Zeng, H. (2010). A robust and high-throughput Cre reporting and characterization system for the whole mouse brain. *Nat Neurosci*, *13*(1), 133-140. <https://doi.org/10.1038/nn.2467>
- Mahadevan, V., Peltekian, A., & McBain, C. J. (2020). Translatome Analyses Using Conditional Ribosomal Tagging in GABAergic Interneurons and Other Sparse Cell Types. *Curr Protoc Neurosci*, *92*(1), e93. <https://doi.org/10.1002/cpns.93>
- Maimaiti, R., Zhu, C., Zhang, Y., Ding, Q., & Guo, W. (2021). RBM20-Mediated Pre-mRNA Splicing Has Muscle-Specificity and Differential Hormonal Responses between Muscles and in Muscle Cell Cultures. *Int J Mol Sci*, *22*(6). <https://doi.org/10.3390/ijms22062928>
- Malnic, B. (2007). Searching for the ligands of odorant receptors. *Mol Neurobiol*, *35*(2), 175-181. <https://doi.org/10.1007/s12035-007-0013-2>
- Malnic, B., Hirono, J., Sato, T., & Buck, L. B. (1999). Combinatorial receptor codes for odors. *Cell*, *96*(5), 713-723. [https://doi.org/10.1016/s0092-8674\(00\)80581-4](https://doi.org/10.1016/s0092-8674(00)80581-4)
- Mardinly, A. R., Spiegel, I., Patrizi, A., Centofante, E., Bazinet, J. E., Tzeng, C. P., Mandel-Brehm, C., Harmin, D. A., Adesnik, H., Fagiolini, M., & Greenberg, M. E. (2016). Sensory experience regulates cortical inhibition by inducing IGF1 in VIP neurons. *Nature*, *531*(7594), 371-375. <https://doi.org/10.1038/nature17187>
- Marin, O., & Muller, U. (2014). Lineage origins of GABAergic versus glutamatergic neurons in the neocortex. *Curr Opin Neurobiol*, *26*, 132-141. <https://doi.org/10.1016/j.conb.2014.01.015>

- Maticzka, D., Ilik, I. A., Aktas, T., Backofen, R., & Akhtar, A. (2018). uvCLAP is a fast and non-radioactive method to identify in vivo targets of RNA-binding proteins. *Nat Commun*, 9(1), 1142. <https://doi.org/10.1038/s41467-018-03575-4>
- Mauger, O., Lemoine, F., & Scheiffele, P. (2016). Targeted Intron Retention and Excision for Rapid Gene Regulation in Response to Neuronal Activity. *Neuron*, 92(6), 1266-1278. <https://doi.org/10.1016/j.neuron.2016.11.032>
- Mayeda, A., Munroe, S. H., Xu, R. M., & Krainer, A. R. (1998). Distinct functions of the closely related tandem RNA-recognition motifs of hnRNP A1. *RNA*, 4(9), 1111-1123. <https://doi.org/10.1017/s135583829898089x>
- Mayr, C. (2019). What Are 3' UTRs Doing? *Cold Spring Harb Perspect Biol*, 11(10). <https://doi.org/10.1101/cshperspect.a034728>
- Mayr, C., & Bartel, D. P. (2009). Widespread shortening of 3'UTRs by alternative cleavage and polyadenylation activates oncogenes in cancer cells. *Cell*, 138(4), 673-684. <https://doi.org/10.1016/j.cell.2009.06.016>
- Mazille, M., Buczak, K., Scheiffele, P., & Mauger, O. (2022). Stimulus-specific remodeling of the neuronal transcriptome through nuclear intron-retaining transcripts. *EMBO J*, 41(21), e110192. <https://doi.org/10.15252/embj.2021110192>
- Mazin, P. V., Khaitovich, P., Cardoso-Moreira, M., & Kaessmann, H. (2021). Alternative splicing during mammalian organ development. *Nat Genet*, 53(6), 925-934. <https://doi.org/10.1038/s41588-021-00851-w>
- McAllister, K., Mechanic, L. E., Amos, C., Aschard, H., Blair, I. A., Chatterjee, N., Conti, D., Gauderman, W. J., Hsu, L., Hutter, C. M., Jankowska, M. M., Kerr, J., Kraft, P., Montgomery, S. B., Mukherjee, B., Papanicolaou, G. J., Patel, C. J., Ritchie, M. D., Ritz, B. R., . . . Witte, J. S. (2017). Current Challenges and New Opportunities for Gene-Environment Interaction Studies of Complex Diseases. *Am J Epidemiol*, 186(7), 753-761. <https://doi.org/10.1093/aje/kwx227>
- McGinnis, W., & Krumlauf, R. (1992). Homeobox genes and axial patterning. *Cell*, 68(2), 283-302. [https://doi.org/10.1016/0092-8674\(92\)90471-n](https://doi.org/10.1016/0092-8674(92)90471-n)
- McVean, G. (2000). Evolutionary genetics: what is driving male mutation? *Curr Biol*, 10(22), R834-835. [https://doi.org/10.1016/s0960-9822\(00\)00787-9](https://doi.org/10.1016/s0960-9822(00)00787-9)
- McVean, G. A., & Hurst, G. D. (2000). Evolutionary lability of context-dependent codon bias in bacteria. *J Mol Evol*, 50(3), 264-275. <https://doi.org/10.1007/s002399910031>
- Meers, M. P., Bryson, T. D., Henikoff, J. G., & Henikoff, S. (2019). Improved CUT&RUN chromatin profiling tools. *Elife*, 8. <https://doi.org/10.7554/eLife.46314>
- Merkin, J., Russell, C., Chen, P., & Burge, C. B. (2012). Evolutionary dynamics of gene and isoform regulation in Mammalian tissues. *Science*, 338(6114), 1593-1599. <https://doi.org/10.1126/science.1228186>
- Merkle, F. T., Fuentealba, L. C., Sanders, T. A., Magno, L., Kessar, N., & Alvarez-Buylla, A. (2014). Adult neural stem cells in distinct microdomains generate previously unknown interneuron types. *Nat Neurosci*, 17(2), 207-214. <https://doi.org/10.1038/nn.3610>
- Merz, K., & Lie, D. C. (2013). Evidence that Doublecortin is dispensable for the development of adult born neurons in mice. *PLoS One*, 8(5), e62693. <https://doi.org/10.1371/journal.pone.0062693>
- Miller, T., Cudkowicz, M., Shaw, P. J., Andersen, P. M., Atassi, N., Bucelli, R. C., Genge, A., Glass, J., Ladha, S., Ludolph, A. L., Maragakis, N. J., McDermott, C. J., Pestronk, A., Ravits, J., Salachas, F., Trudell, R., Van Damme, P., Zinman, L., Bennett, C. F., . . . Ferguson, T. A. (2020). Phase 1-2 Trial of Antisense Oligonucleotide Tofersen for SOD1 ALS. *N Engl J Med*, 383(2), 109-119. <https://doi.org/10.1056/NEJMoa2003715>
- Mitani, S. (2017). Comprehensive functional genomics using *Caenorhabditis elegans* as a model organism. *Proceedings of the Japan Academy Series B-Physical and Biological Sciences*, 93(8), 561-577. <https://doi.org/10.2183/pjab.93.036>
- Miura, M., & Chen, H. (2020). CUT&RUN detects distinct DNA footprints of RNA polymerase II near the transcription start sites. *Chromosome Res*, 28(3-4), 381-393. <https://doi.org/10.1007/s10577-020-09643-0>

- Mori, K., Kishi, K., & Ojima, H. (1983). Distribution of dendrites of mitral, displaced mitral, tufted, and granule cells in the rabbit olfactory bulb. *J Comp Neurol*, 219(3), 339-355. <https://doi.org/10.1002/cne.902190308>
- Morinaga, A., Ito, J., Niimi, T., & Maturana, A. D. (2019). RBM20 Regulates CaV1.2 Surface Expression by Promoting Exon 9* Inclusion of CACNA1C in Neonatal Rat Cardiomyocytes. *Int J Mol Sci*, 20(22). <https://doi.org/10.3390/ijms20225591>
- Morse, S. V., Pouliopoulos, A. N., Chan, T. G., Copping, M. J., Lin, J., Long, N. J., & Choi, J. J. (2019). Rapid Short-pulse Ultrasound Delivers Drugs Uniformly across the Murine Blood-Brain Barrier with Negligible Disruption. *Radiology*, 291(2), 459-466. <https://doi.org/10.1148/radiol.2019181625>
- Murata, K., Kanno, M., Ieki, N., Mori, K., & Yamaguchi, M. (2015). Mapping of Learned Odor-Induced Motivated Behaviors in the Mouse Olfactory Tubercle. *J Neurosci*, 35(29), 10581-10599. <https://doi.org/10.1523/JNEUROSCI.0073-15.2015>
- Murayama, R., Kimura-Asami, M., Togo-Ohno, M., Yamasaki-Kato, Y., Naruse, T. K., Yamamoto, T., Hayashi, T., Ai, T., Spoonamore, K. G., Kovacs, R. J., Vatta, M., Iizuka, M., Saito, M., Wani, S., Hiraoka, Y., Kimura, A., & Kuroyanagi, H. (2018). Phosphorylation of the RSRSP stretch is critical for splicing regulation by RNA-Binding Motif Protein 20 (RBM20) through nuclear localization. *Sci Rep*, 8(1), 8970. <https://doi.org/10.1038/s41598-018-26624-w>
- Murphy, A. J., Li, A. H., Li, P., & Sun, H. (2022). Therapeutic Targeting of Alternative Splicing: A New Frontier in Cancer Treatment. *Front Oncol*, 12, 868664. <https://doi.org/10.3389/fonc.2022.868664>
- Nagayama, S., Enerva, A., Fletcher, M. L., Masurkar, A. V., Igarashi, K. M., Mori, K., & Chen, W. R. (2010). Differential axonal projection of mitral and tufted cells in the mouse main olfactory system. *Front Neural Circuits*, 4. <https://doi.org/10.3389/fncir.2010.00120>
- Nagayama, S., Homma, R., & Imamura, F. (2014). Neuronal organization of olfactory bulb circuits. *Front Neural Circuits*, 8, 98. <https://doi.org/10.3389/fncir.2014.00098>
- Nakka, K., Ghigna, C., Gabellini, D., & Dilworth, F. J. (2018). Diversification of the muscle proteome through alternative splicing. *Skeletal Muscle*, 8. <https://doi.org/ARTN10.1186/s13395-018-0152-3>
- Naritsuka, H., Sakai, K., Hashikawa, T., Mori, K., & Yamaguchi, M. (2009). Perisomatic-targeting granule cells in the mouse olfactory bulb. *J Comp Neurol*, 515(4), 409-426. <https://doi.org/10.1002/cne.22063>
- Nguyen, T. M., Schreiner, D., Xiao, L., Traunmuller, L., Bornmann, C., & Scheiffele, P. (2016). An alternative splicing switch shapes neurexin repertoires in principal neurons versus interneurons in the mouse hippocampus. *Elife*, 5. <https://doi.org/10.7554/eLife.22757>
- Nguyen, U. P., & Imamura, F. (2019). Regional differences in mitral cell development in mouse olfactory bulb. *J Comp Neurol*, 527(14), 2233-2244. <https://doi.org/10.1002/cne.24683>
- Noli, L., Capalbo, A., Ogilvie, C., Khalaf, Y., & Ilic, D. (2015). Discordant Growth of Monozygotic Twins Starts at the Blastocyst Stage: A Case Study. *Stem Cell Reports*, 5(6), 946-953. <https://doi.org/10.1016/j.stemcr.2015.10.006>
- Norris, A. D., Gao, S., Norris, M. L., Ray, D., Ramani, A. K., Fraser, A. G., Morris, Q., Hughes, T. R., Zhen, M., & Calarco, J. A. (2014). A pair of RNA-binding proteins controls networks of splicing events contributing to specialization of neural cell types. *Mol Cell*, 54(6), 946-959. <https://doi.org/10.1016/j.molcel.2014.05.004>
- Nystrom, S. L., & McKay, D. J. (2021). Memes: A motif analysis environment in R using tools from the MEME Suite. *PLoS Comput Biol*, 17(9), e1008991. <https://doi.org/10.1371/journal.pcbi.1008991>
- Oettl, L. L., Ravi, N., Schneider, M., Scheller, M. F., Schneider, P., Mitre, M., da Silva Gouveia, M., Froemke, R. C., Chao, M. V., Young, W. S., Meyer-Lindenberg, A.,

- Grinevich, V., Shusterman, R., & Kelsch, W. (2016). Oxytocin Enhances Social Recognition by Modulating Cortical Control of Early Olfactory Processing. *Neuron*, 90(3), 609-621. <https://doi.org/10.1016/j.neuron.2016.03.033>
- Ohno, S. (1970). *Evolution by gene duplication*. Allen & Unwin; Springer-Verlag.
- Orona, E., Rainer, E. C., & Scott, J. W. (1984). Dendritic and axonal organization of mitral and tufted cells in the rat olfactory bulb. *J Comp Neurol*, 226(3), 346-356. <https://doi.org/10.1002/cne.902260305>
- Pagani, F., & Baralle, F. E. (2004). Genomic variants in exons and introns: identifying the splicing spoilers. *Nat Rev Genet*, 5(5), 389-396. <https://doi.org/10.1038/nrg1327>
- Parikh, V. N., Caleshu, C., Reuter, C., Lazzeroni, L. C., Ingles, J., Garcia, J., McCaleb, K., Adesiyun, T., Sedaghat-Hamedani, F., Kumar, S., Graw, S., Gigli, M., Stolfo, D., Dal Ferro, M., Ing, A. Y., Nussbaum, R., Funke, B., Wheeler, M. T., Hershberger, R. E., . . . Ashley, E. (2019). Regional Variation in RBM20 Causes a Highly Penetrant Arrhythmogenic Cardiomyopathy. *Circ Heart Fail*, 12(3), e005371. <https://doi.org/10.1161/CIRCHEARTFAILURE.118.005371>
- Parikshak, N. N., Swarup, V., Belgard, T. G., Irimia, M., Ramaswami, G., Gandal, M. J., Hartl, C., Leppa, V., Ubieta, L. T., Huang, J., Lowe, J. K., Blencowe, B. J., Horvath, S., & Geschwind, D. H. (2016). Genome-wide changes in lncRNA, splicing, and regional gene expression patterns in autism. *Nature*, 540(7633), 423-427. <https://doi.org/10.1038/nature20612>
- Park, E., Pan, Z., Zhang, Z., Lin, L., & Xing, Y. (2018). The Expanding Landscape of Alternative Splicing Variation in Human Populations. *Am J Hum Genet*, 102(1), 11-26. <https://doi.org/10.1016/j.ajhg.2017.11.002>
- Paul, A., Crow, M., Raudales, R., He, M., Gillis, J., & Huang, Z. J. (2017). Transcriptional Architecture of Synaptic Communication Delineates GABAergic Neuron Identity. *Cell*, 171(3), 522-539 e520. <https://doi.org/10.1016/j.cell.2017.08.032>
- Paul, F. E., Hosp, F., & Selbach, M. (2011). Analyzing protein-protein interactions by quantitative mass spectrometry. *Methods*, 54(4), 387-395. <https://doi.org/10.1016/j.ymeth.2011.03.001>
- Pearson, J. C., Lemons, D., & McGinnis, W. (2005). Modulating Hox gene functions during animal body patterning. *Nat Rev Genet*, 6(12), 893-904. <https://doi.org/10.1038/nrg1726>
- Peterson, A. C., Russell, J. D., Bailey, D. J., Westphall, M. S., & Coon, J. J. (2012). Parallel reaction monitoring for high resolution and high mass accuracy quantitative, targeted proteomics. *Mol Cell Proteomics*, 11(11), 1475-1488. <https://doi.org/10.1074/mcp.O112.020131>
- Peterson, M. E., Chen, F., Saven, J. G., Roos, D. S., Babbitt, P. C., & Sali, A. (2009). Evolutionary constraints on structural similarity in orthologs and paralogs. *Protein Sci*, 18(6), 1306-1315. <https://doi.org/10.1002/pro.143>
- Pi, H. J., Hangya, B., Kvitsiani, D., Sanders, J. I., Huang, Z. J., & Kepecs, A. (2013). Cortical interneurons that specialize in disinhibitory control. *Nature*, 503(7477), 521-524. <https://doi.org/10.1038/nature12676>
- Pilaz, L. J., & Silver, D. L. (2015). Post-transcriptional regulation in corticogenesis: how RNA-binding proteins help build the brain. *Wiley Interdiscip Rev RNA*, 6(5), 501-515. <https://doi.org/10.1002/wrna.1289>
- Pittaras, E., Callebert, J., Chennaoui, M., Rabat, A., & Granon, S. (2016). Individual behavioral and neurochemical markers of unadapted decision-making processes in healthy inbred mice. *Brain Struct Funct*, 221(9), 4615-4629. <https://doi.org/10.1007/s00429-016-1192-2>
- Pittaras, E., Hamelin, H., & Granon, S. (2022). Inter-Individual Differences in Cognitive Tasks: Focusing on the Shaping of Decision-Making Strategies. *Front Behav Neurosci*, 16, 818746. <https://doi.org/10.3389/fnbeh.2022.818746>

- Quesnel-Vallieres, M., Dargaei, Z., Irimia, M., Gonatopoulos-Pournatzis, T., Ip, J. Y., Wu, M., Sterne-Weiler, T., Nakagawa, S., Woodin, M. A., Blencowe, B. J., & Cordes, S. P. (2016). Misregulation of an Activity-Dependent Splicing Network as a Common Mechanism Underlying Autism Spectrum Disorders. *Mol Cell*, *64*(6), 1023-1034. <https://doi.org/10.1016/j.molcel.2016.11.033>
- Raj, B., & Blencowe, B. J. (2015). Alternative Splicing in the Mammalian Nervous System: Recent Insights into Mechanisms and Functional Roles. *Neuron*, *87*(1), 14-27. <https://doi.org/10.1016/j.neuron.2015.05.004>
- Riedemann, T. (2019). Diversity and Function of Somatostatin-Expressing Interneurons in the Cerebral Cortex. *Int J Mol Sci*, *20*(12). <https://doi.org/10.3390/ijms20122952>
- Rimbault, C., Maruthi, K., Breillat, C., Genuer, C., Crespillo, S., Puente-Munoz, V., Chamma, I., Gauthereau, I., Antoine, S., Thibaut, C., Tai, F. W. J., Dartigues, B., Grillo-Bosch, D., Claverol, S., Poujol, C., Choquet, D., Mackereth, C. D., & Sainlos, M. (2019). Engineering selective competitors for the discrimination of highly conserved protein-protein interaction modules. *Nat Commun*, *10*(1), 4521. <https://doi.org/10.1038/s41467-019-12528-4>
- Roybon, L., Mastracci, T. L., Li, J., Stott, S. R., Leiter, A. B., Sussel, L., Brundin, P., & Li, J. Y. (2015). The Origin, Development and Molecular Diversity of Rodent Olfactory Bulb Glutamatergic Neurons Distinguished by Expression of Transcription Factor NeuroD1. *PLoS One*, *10*(6), e0128035. <https://doi.org/10.1371/journal.pone.0128035>
- Saito, Y., Yuan, Y., Zucker-Scharff, I., Fak, J. J., Jereb, S., Tajima, Y., Licatalosi, D. D., & Darnell, R. B. (2019). Differential NOVA2-Mediated Splicing in Excitatory and Inhibitory Neurons Regulates Cortical Development and Cerebellar Function. *Neuron*, *101*(4), 707-720 e705. <https://doi.org/10.1016/j.neuron.2018.12.019>
- Sakano, H. (2010). Neural map formation in the mouse olfactory system. *Neuron*, *67*(4), 530-542. <https://doi.org/10.1016/j.neuron.2010.07.003>
- Sanz, E., Bean, J. C., Carey, D. P., Quintana, A., & McKnight, G. S. (2019). RiboTag: Ribosomal Tagging Strategy to Analyze Cell-Type-Specific mRNA Expression In Vivo. *Curr Protoc Neurosci*, *88*(1), e77. <https://doi.org/10.1002/cpns.77>
- Sanz, E., Yang, L., Su, T., Morris, D. R., McKnight, G. S., & Amieux, P. S. (2009). Cell-type-specific isolation of ribosome-associated mRNA from complex tissues. *Proc Natl Acad Sci U S A*, *106*(33), 13939-13944. <https://doi.org/10.1073/pnas.0907143106>
- Scheiba, R. M., de Opakua, A. I., Diaz-Quintana, A., Cruz-Gallardo, I., Martinez-Cruz, L. A., Martinez-Chantar, M. L., Blanco, F. J., & Diaz-Moreno, I. (2014). The C-terminal RNA binding motif of HuR is a multi-functional domain leading to HuR oligomerization and binding to U-rich RNA targets. *RNA Biol*, *11*(10), 1250-1261. <https://doi.org/10.1080/15476286.2014.996069>
- Schindelin, J., Arganda-Carreras, I., Frise, E., Kaynig, V., Longair, M., Pietzsch, T., Preibisch, S., Rueden, C., Saalfeld, S., Schmid, B., Tinevez, J. Y., White, D. J., Hartenstein, V., Eliceiri, K., Tomancak, P., & Cardona, A. (2012). Fiji: an open-source platform for biological-image analysis. *Nat Methods*, *9*(7), 676-682. <https://doi.org/10.1038/nmeth.2019>
- Schmucker, D., Clemens, J. C., Shu, H., Worby, C. A., Xiao, J., Muda, M., Dixon, J. E., & Zipursky, S. L. (2000). Drosophila Dscam is an axon guidance receptor exhibiting extraordinary molecular diversity. *Cell*, *101*(6), 671-684. [https://doi.org/10.1016/s0092-8674\(00\)80878-8](https://doi.org/10.1016/s0092-8674(00)80878-8)
- Schneider, J. W., Oommen, S., Qureshi, M. Y., Goetsch, S. C., Pease, D. R., Sundsbak, R. S., Guo, W., Sun, M., Sun, H., Kuroyanagi, H., Webster, D. A., Coutts, A. W., Holst, K. A., Edwards, B. S., Newville, N., Hathcock, M. A., Melkamu, T., Briganti, F., Wei, W., . . . Wanek Program Preclinical, P. (2020). Dysregulated ribonucleoprotein granules promote cardiomyopathy in RBM20 gene-edited pigs. *Nat Med*, *26*(11), 1788-1800. <https://doi.org/10.1038/s41591-020-1087-x>

- Schoenfeld, T. A., Marchand, J. E., & Macrides, F. (1985). Topographic organization of tufted cell axonal projections in the hamster main olfactory bulb: an intrabulbar associational system. *J Comp Neurol*, 235(4), 503-518. <https://doi.org/10.1002/cne.902350408>
- Seiler, M., Peng, S., Agrawal, A. A., Palacino, J., Teng, T., Zhu, P., Smith, P. G., Cancer Genome Atlas Research, N., Buonamici, S., & Yu, L. (2018). Somatic Mutational Landscape of Splicing Factor Genes and Their Functional Consequences across 33 Cancer Types. *Cell Rep*, 23(1), 282-296 e284. <https://doi.org/10.1016/j.celrep.2018.01.088>
- Shah, A., Qian, Y., Weyn-Vanhenhenryck, S. M., & Zhang, C. (2017). CLIP Tool Kit (CTK): a flexible and robust pipeline to analyze CLIP sequencing data. *Bioinformatics*, 33(4), 566-567. <https://doi.org/10.1093/bioinformatics/btw653>
- Shalgi, R., Hurt, J. A., Lindquist, S., & Burge, C. B. (2014). Widespread inhibition of posttranscriptional splicing shapes the cellular transcriptome following heat shock. *Cell Rep*, 7(5), 1362-1370. <https://doi.org/10.1016/j.celrep.2014.04.044>
- Shendure, J., & Ji, H. (2008). Next-generation DNA sequencing. *Nat Biotechnol*, 26(10), 1135-1145. <https://doi.org/10.1038/nbt1486>
- Shepherd, G. M., & Erulkar, S. D. (1997). Centenary of the synapse: from Sherrington to the molecular biology of the synapse and beyond. *Trends Neurosci*, 20(9), 385-392. [https://doi.org/10.1016/s0166-2236\(97\)01059-x](https://doi.org/10.1016/s0166-2236(97)01059-x)
- Sikkel, M. B., Hayward, C., MacLeod, K. T., Harding, S. E., & Lyon, A. R. (2014). SERCA2a gene therapy in heart failure: an anti-arrhythmic positive inotrope. *Br J Pharmacol*, 171(1), 38-54. <https://doi.org/10.1111/bph.12472>
- Simms, B. A., & Zamponi, G. W. (2014). Neuronal voltage-gated calcium channels: structure, function, and dysfunction. *Neuron*, 82(1), 24-45. <https://doi.org/10.1016/j.neuron.2014.03.016>
- Skene, P. J., Henikoff, J. G., & Henikoff, S. (2018). Targeted in situ genome-wide profiling with high efficiency for low cell numbers. *Nat Protoc*, 13(5), 1006-1019. <https://doi.org/10.1038/nprot.2018.015>
- Skene, P. J., & Henikoff, S. (2017). An efficient targeted nuclease strategy for high-resolution mapping of DNA binding sites. *Elife*, 6. <https://doi.org/ARTN10.7554/eLife.21856>
- Smith, R. A., Miller, T. M., Yamanaka, K., Monia, B. P., Condon, T. P., Hung, G., Lobsiger, C. S., Ward, C. M., McAlonis-Downes, M., Wei, H., Wancewicz, E. V., Bennett, C. F., & Cleveland, D. W. (2006). Antisense oligonucleotide therapy for neurodegenerative disease. *J Clin Invest*, 116(8), 2290-2296. <https://doi.org/10.1172/JCI25424>
- Stanley, R. F., & Abdel-Wahab, O. (2022). Dysregulation and therapeutic targeting of RNA splicing in cancer. *Nat Cancer*, 3(5), 536-546. <https://doi.org/10.1038/s43018-022-00384-z>
- Sterne-Weiler, T., Weatheritt, R. J., Best, A. J., Ha, K. C. H., & Blencowe, B. J. (2018). Efficient and Accurate Quantitative Profiling of Alternative Splicing Patterns of Any Complexity on a Laptop. *Mol Cell*, 72(1), 187-200 e186. <https://doi.org/10.1016/j.molcel.2018.08.018>
- Sun, X., Liu, X., Starr, E. R., & Liu, S. (2020). CCKergic Tufted Cells Differentially Drive Two Anatomically Segregated Inhibitory Circuits in the Mouse Olfactory Bulb. *J Neurosci*, 40(32), 6189-6206. <https://doi.org/10.1523/JNEUROSCI.0769-20.2020>
- Surget, S., Khoury, M. P., & Bourdon, J. C. (2013). Uncovering the role of p53 splice variants in human malignancy: a clinical perspective. *Onco Targets Ther*, 7, 57-68. <https://doi.org/10.2147/OTT.S53876>
- Swedlow, J. R., Goldberg, I., Brauner, E., & Sorger, P. K. (2003). Informatics and quantitative analysis in biological imaging. *Science*, 300(5616), 100-102. <https://doi.org/10.1126/science.1082602>
- Tainaka, K., Murakami, T. C., Susaki, E. A., Shimizu, C., Saito, R., Takahashi, K., Hayashi-Takagi, A., Sekiya, H., Arima, Y., Nojima, S., Ikemura, M., Ushiku, T., Shimizu, Y.,

- Murakami, M., Tanaka, K. F., Iino, M., Kasai, H., Sasaoka, T., Kobayashi, K., . . . Ueda, H. R. (2018). Chemical Landscape for Tissue Clearing Based on Hydrophilic Reagents. *Cell Rep*, 24(8), 2196-2210 e2199. <https://doi.org/10.1016/j.celrep.2018.07.056>
- Takeuchi, H., & Sakano, H. (2014). Neural map formation in the mouse olfactory system. *Cell Mol Life Sci*, 71(16), 3049-3057. <https://doi.org/10.1007/s00018-014-1597-0>
- Tan, Q., Yalamanchili, H. K., Park, J., De Maio, A., Lu, H. C., Wan, Y. W., White, J. J., Bondar, V. V., Sayegh, L. S., Liu, X., Gao, Y., Sillitoe, R. V., Orr, H. T., Liu, Z., & Zoghbi, H. Y. (2016). Extensive cryptic splicing upon loss of RBM17 and TDP43 in neurodegeneration models. *Hum Mol Genet*, 25(23), 5083-5093. <https://doi.org/10.1093/hmg/ddw337>
- Tanaka, O., Sakagami, H., & Kondo, H. (1995). Localization of mRNAs of voltage-dependent Ca(2+)-channels: four subtypes of alpha 1- and beta-subunits in developing and mature rat brain. *Brain Res Mol Brain Res*, 30(1), 1-16. [https://doi.org/10.1016/0169-328x\(94\)00265-g](https://doi.org/10.1016/0169-328x(94)00265-g)
- Tapial, J., Ha, K. C. H., Sterne-Weiler, T., Gohr, A., Braunschweig, U., Hermoso-Pulido, A., Quesnel-Vallieres, M., Permanyer, J., Sodaei, R., Marquez, Y., Cozzuto, L., Wang, X., Gomez-Velazquez, M., Rayon, T., Manzanares, M., Ponomarenko, J., Blencowe, B. J., & Irimia, M. (2017). An atlas of alternative splicing profiles and functional associations reveals new regulatory programs and genes that simultaneously express multiple major isoforms. *Genome Res*, 27(10), 1759-1768. <https://doi.org/10.1101/gr.220962.117>
- Tasic, B., Menon, V., Nguyen, T. N., Kim, T. K., Jarsky, T., Yao, Z., Levi, B., Gray, L. T., Sorensen, S. A., Dolbeare, T., Bertagnoli, D., Goldy, J., Shapovalova, N., Parry, S., Lee, C., Smith, K., Bernard, A., Madisen, L., Sunkin, S. M., . . . Zeng, H. (2016). Adult mouse cortical cell taxonomy revealed by single cell transcriptomics. *Nat Neurosci*, 19(2), 335-346. <https://doi.org/10.1038/nn.4216>
- Tepe, B., Hill, M. C., Pekarek, B. T., Hunt, P. J., Martin, T. J., Martin, J. F., & Arenkiel, B. R. (2018). Single-Cell RNA-Seq of Mouse Olfactory Bulb Reveals Cellular Heterogeneity and Activity-Dependent Molecular Census of Adult-Born Neurons. *Cell Rep*, 25(10), 2689-2703 e2683. <https://doi.org/10.1016/j.celrep.2018.11.034>
- Thomas, A., Lee, P. J., Dalton, J. E., Nornie, K. J., Stoica, L., Costa-Mattioli, M., Chang, P., Nuzhdin, S., Arbeitman, M. N., & Dierick, H. A. (2012). A versatile method for cell-specific profiling of translated mRNAs in *Drosophila*. *PLoS One*, 7(7), e40276. <https://doi.org/10.1371/journal.pone.0040276>
- Thomson, S. R., Seo, S. S., Barnes, S. A., Louros, S. R., Muscas, M., Dando, O., Kirby, C., Wyllie, D. J. A., Hardingham, G. E., Kind, P. C., & Osterweil, E. K. (2017). Cell-Type-Specific Translation Profiling Reveals a Novel Strategy for Treating Fragile X Syndrome. *Neuron*, 95(3), 550-563 e555. <https://doi.org/10.1016/j.neuron.2017.07.013>
- Tischfield, D. J., & Anderson, S. A. (2017). Differentiation of Mouse Embryonic Stem Cells into Cortical Interneuron Precursors. *J Vis Exp*(130). <https://doi.org/10.3791/56358>
- Trapnell, C., & Salzberg, S. L. (2009). How to map billions of short reads onto genomes. *Nature Biotechnology*, 27(5), 455-457. <https://doi.org/10.1038/nbt0509-455>
- Traunmüller, L., Gomez, A. M., Nguyen, T.-M., & Scheiffele, P. (2016). Control of neuronal synapse specification by highly dedicated alternative splicing program. *Science*, 352, 982-986.
- Traunmüller, L., Gomez, A. M., Nguyen, T. M., & Scheiffele, P. (2016). Control of neuronal synapse specification by a highly dedicated alternative splicing program. *Science*, 352(6288), 982-986. <https://doi.org/10.1126/science.aaf2397>
- Traunmüller, L., Schulz, J., Ortiz, R., Feng, H., Furlanis, E., Gomez, A. M., Schreiner, D., Bischofberger, J., Zhang, C., & Scheiffele, P. (2023). A cell-type-specific alternative splicing regulator shapes synapse properties in a trans-synaptic manner. *Cell Rep*, 42(3), 112173. <https://doi.org/10.1016/j.celrep.2023.112173>

- Tufo, C., Poopalasundaram, S., Dorrego-Rivas, A., Ford, M. C., Graham, A., & Grubb, M. S. (2022). Development of the mammalian main olfactory bulb. *Development*, *149*(3). <https://doi.org/10.1242/dev.200210>
- Ule, J., Stefani, G., Mele, A., Ruggiu, M., Wang, X., Taneri, B., Gaasterland, T., Blencowe, B. J., & Darnell, R. B. (2006). An RNA map predicting Nova-dependent splicing regulation. *Nature*, *444*(7119), 580-586. <https://doi.org/10.1038/nature05304>
- Upadhyay, S. K., & Mackereth, C. D. (2020). Structural basis of UCUU RNA motif recognition by splicing factor RBM20. *Nucleic Acids Res*, *48*(8), 4538-4550. <https://doi.org/10.1093/nar/gkaa168>
- van den Brink, S. C., Sage, F., Vertesy, A., Spanjaard, B., Peterson-Maduro, J., Baron, C. S., Robin, C., & van Oudenaarden, A. (2017). Single-cell sequencing reveals dissociation-induced gene expression in tissue subpopulations. *Nat Methods*, *14*(10), 935-936. <https://doi.org/10.1038/nmeth.4437>
- van den Hoogenhof, M. M. G., Beqqali, A., Amin, A. S., van der Made, I., Aufiero, S., Khan, M. A. F., Schumacher, C. A., Jansweijer, J. A., van Spaendonck-Zwarts, K. Y., Remme, C. A., Backs, J., Verkerk, A. O., Baartscheer, A., Pinto, Y. M., & Creemers, E. E. (2018). RBM20 Mutations Induce an Arrhythmogenic Dilated Cardiomyopathy Related to Disturbed Calcium Handling. *Circulation*, *138*(13), 1330-1342. <https://doi.org/10.1161/CIRCULATIONAHA.117.031947>
- Van Nostrand, E. L., Freese, P., Pratt, G. A., Wang, X., Wei, X., Xiao, R., Blue, S. M., Chen, J. Y., Cody, N. A. L., Dominguez, D., Olson, S., Sundararaman, B., Zhan, L., Bazile, C., Bouvrette, L. P. B., Bergalet, J., Duff, M. O., Garcia, K. E., Gelboin-Burkhart, C., . . . Yeo, G. W. (2020). A large-scale binding and functional map of human RNA-binding proteins. *Nature*, *583*(7818), 711-719. <https://doi.org/10.1038/s41586-020-2077-3>
- Van Nostrand, E. L., Pratt, G. A., Shishkin, A. A., Gelboin-Burkhart, C., Fang, M. Y., Sundararaman, B., Blue, S. M., Nguyen, T. B., Surka, C., Elkins, K., Stanton, R., Rigo, F., Guttman, M., & Yeo, G. W. (2016). Robust transcriptome-wide discovery of RNA-binding protein binding sites with enhanced CLIP (eCLIP). *Nat Methods*, *13*(6), 508-514. <https://doi.org/10.1038/nmeth.3810>
- Van Nostrand, E. L., Pratt, G. A., Yee, B. A., Wheeler, E. C., Blue, S. M., Mueller, J., Park, S. S., Garcia, K. E., Gelboin-Burkhart, C., Nguyen, T. B., Rabano, I., Stanton, R., Sundararaman, B., Wang, R., Fu, X. D., Graveley, B. R., & Yeo, G. W. (2020). Principles of RNA processing from analysis of enhanced CLIP maps for 150 RNA binding proteins. *Genome Biol*, *21*(1), 90. <https://doi.org/10.1186/s13059-020-01982-9>
- Veldman, M. B., Park, C. S., Eyermann, C. M., Zhang, J. Y., Zuniga-Sanchez, E., Hirano, A. A., Daigle, T. L., Foster, N. N., Zhu, M., Langfelder, P., Lopez, I. A., Brecha, N. C., Zipursky, S. L., Zeng, H., Dong, H. W., & Yang, X. W. (2020). Brainwide Genetic Sparse Cell Labeling to Illuminate the Morphology of Neurons and Glia with Cre-Dependent MORF Mice. *Neuron*, *108*(1), 111-127 e116. <https://doi.org/10.1016/j.neuron.2020.07.019>
- Vinograd, A., Fuchs-Shlomai, Y., Stern, M., Mukherjee, D., Gao, Y., Citri, A., Davison, I., & Mizrahi, A. (2017). Functional Plasticity of Odor Representations during Motherhood. *Cell Rep*, *21*(2), 351-365. <https://doi.org/10.1016/j.celrep.2017.09.038>
- Vogel, C., & Marcotte, E. M. (2012). Insights into the regulation of protein abundance from proteomic and transcriptomic analyses. *Nat Rev Genet*, *13*(4), 227-232. <https://doi.org/10.1038/nrg3185>
- Vong, L., Ye, C., Yang, Z., Choi, B., Chua, S., Jr., & Lowell, B. B. (2011). Leptin action on GABAergic neurons prevents obesity and reduces inhibitory tone to POMC neurons. *Neuron*, *71*(1), 142-154. <https://doi.org/10.1016/j.neuron.2011.05.028>
- Vuong, C. K., Wei, W., Lee, J. A., Lin, C. H., Damianov, A., de la Torre-Ubieta, L., Halabi, R., Otis, K. O., Martin, K. C., O'Dell, T. J., & Black, D. L. (2018). Rbfox1 Regulates

- Synaptic Transmission through the Inhibitory Neuron-Specific vSNARE Vamp1. *Neuron*, 98(1), 127-141 e127. <https://doi.org/10.1016/j.neuron.2018.03.008>
- Wachowiak, M., Economo, M. N., Diaz-Quesada, M., Brunert, D., Wesson, D. W., White, J. A., & Rothermel, M. (2013). Optical dissection of odor information processing in vivo using GCaMPs expressed in specified cell types of the olfactory bulb. *J Neurosci*, 33(12), 5285-5300. <https://doi.org/10.1523/JNEUROSCI.4824-12.2013>
- Wamsley, B., Jaglin, X. H., Favuzzi, E., Quattrocchio, G., Nigro, M. J., Yusuf, N., Khodadadi-Jamayran, A., Rudy, B., & Fishell, G. (2018a). Rbfox1 Mediates Cell-type-Specific Splicing in Cortical Interneurons. *Neuron*, 100(4), 846-859 e847. <https://doi.org/10.1016/j.neuron.2018.09.026>
- Wamsley, B., Jaglin, X. H., Favuzzi, E., Quattrocchio, G., Nigro, M. J., Yusuf, N., Khodadadi-Jamayran, A., Rudy, B., & Fishell, G. (2018b). Rbfox1 Mediates Cell-type-Specific Splicing in Cortical Interneurons. *Neuron*. <https://doi.org/10.1016/j.neuron.2018.09.026>
- Wang, E. T., Sandberg, R., Luo, S., Khrebtkova, I., Zhang, L., Mayr, C., Kingsmore, S. F., Schroth, G. P., & Burge, C. B. (2008). Alternative isoform regulation in human tissue transcriptomes. *Nature*, 456(7221), 470-476. <https://doi.org/10.1038/nature07509>
- Watanabe, T., Kimura, A., & Kuroyanagi, H. (2018). Alternative Splicing Regulator RBM20 and Cardiomyopathy. *Front Mol Biosci*, 5, 105. <https://doi.org/10.3389/fmolb.2018.00105>
- Weatheritt, R. J., Sterne-Weiler, T., & Blencowe, B. J. (2016). The ribosome-engaged landscape of alternative splicing. *Nat Struct Mol Biol*, 23(12), 1117-1123. <https://doi.org/10.1038/nsmb.3317>
- Wilson, D. A., Best, A. R., & Sullivan, R. M. (2004). Plasticity in the olfactory system: lessons for the neurobiology of memory. *Neuroscientist*, 10(6), 513-524. <https://doi.org/10.1177/1073858404267048>
- Wu, N., Nishioka, W. K., Derecki, N. C., & Maher, M. P. (2019). High-throughput-compatible assays using a genetically-encoded calcium indicator. *Sci Rep*, 9(1), 12692. <https://doi.org/10.1038/s41598-019-49070-8>
- Wu, T., Hu, E., Xu, S., Chen, M., Guo, P., Dai, Z., Feng, T., Zhou, L., Tang, W., Zhan, L., Fu, X., Liu, S., Bo, X., & Yu, G. (2021). clusterProfiler 4.0: A universal enrichment tool for interpreting omics data. *Innovation (Camb)*, 2(3), 100141. <https://doi.org/10.1016/j.xinn.2021.100141>
- Xiao, R., Chen, J. Y., Liang, Z., Luo, D., Chen, G., Lu, Z. J., Chen, Y., Zhou, B., Li, H., Du, X., Yang, Y., San, M., Wei, X., Liu, W., Lecuyer, E., Graveley, B. R., Yeo, G. W., Burge, C. B., Zhang, M. Q., . . . Fu, X. D. (2019). Pervasive Chromatin-RNA Binding Protein Interactions Enable RNA-Based Regulation of Transcription. *Cell*, 178(1), 107-121 e118. <https://doi.org/10.1016/j.cell.2019.06.001>
- Yang, J., Hung, L. H., Licht, T., Kostin, S., Looso, M., Khrameeva, E., Bindereif, A., Schneider, A., & Braun, T. (2014). RBM24 is a major regulator of muscle-specific alternative splicing. *Dev Cell*, 31(1), 87-99. <https://doi.org/10.1016/j.devcel.2014.08.025>
- Ye, D., & Chen, H. (2022). Focused Ultrasound-Mediated Intranasal Brain Drug Delivery Technique (FUSIN). *Methods Mol Biol*, 2394, 501-513. https://doi.org/10.1007/978-1-0716-1811-0_26
- Yearim, A., Gelfman, S., Shayevitch, R., Melcer, S., Glaich, O., Mallm, J. P., Nissim-Rafinia, M., Cohen, A. H., Rippe, K., Meshorer, E., & Ast, G. (2015). HP1 is involved in regulating the global impact of DNA methylation on alternative splicing. *Cell Rep*, 10(7), 1122-1134. <https://doi.org/10.1016/j.celrep.2015.01.038>
- Yoon, S. O., Shin, S., Lee, H. J., Chun, H. K., & Chung, A. S. (2006). Isoginkgetin inhibits tumor cell invasion by regulating phosphatidylinositol 3-kinase/Akt-dependent matrix metalloproteinase-9 expression. *Mol Cancer Ther*, 5(11), 2666-2675. <https://doi.org/10.1158/1535-7163.MCT-06-0321>

- Yu, G., Wang, L. G., Han, Y., & He, Q. Y. (2012). clusterProfiler: an R package for comparing biological themes among gene clusters. *OMICS*, *16*(5), 284-287. <https://doi.org/10.1089/omi.2011.0118>
- Yuan, Q., Mutoh, H., Debarbieux, F., & Knopfel, T. (2004). Calcium signaling in mitral cell dendrites of olfactory bulbs of neonatal rats and mice during olfactory nerve Stimulation and beta-adrenoceptor activation. *Learn Mem*, *11*(4), 406-411. <https://doi.org/10.1101/lm.75204>
- Yuan, Y., Sun, J., You, T., Shen, W., Xu, W., Dong, Q., & Cui, M. (2022). Extracellular Vesicle-Based Therapeutics in Neurological Disorders. *Pharmaceutics*, *14*(12). <https://doi.org/10.3390/pharmaceutics14122652>
- Zeisel, A., Hochgerner, H., Lonnerberg, P., Johnsson, A., Memic, F., van der Zwan, J., Haring, M., Braun, E., Borm, L. E., La Manno, G., Codeluppi, S., Furlan, A., Lee, K., Skene, N., Harris, K. D., Hjerling-Leffler, J., Arenas, E., Ernfors, P., Marklund, U., & Linnarsson, S. (2018). Molecular Architecture of the Mouse Nervous System. *Cell*, *174*(4), 999-1014 e1022. <https://doi.org/10.1016/j.cell.2018.06.021>
- Zeisel, A., Munoz-Manchado, A. B., Codeluppi, S., Lonnerberg, P., La Manno, G., Jureus, A., Marques, S., Munguba, H., He, L., Betsholtz, C., Rolny, C., Castelo-Branco, G., Hjerling-Leffler, J., & Linnarsson, S. (2015). Brain structure. Cell types in the mouse cortex and hippocampus revealed by single-cell RNA-seq. *Science*, *347*(6226), 1138-1142. <https://doi.org/10.1126/science.aaa1934>
- Zeng, H., & Sanes, J. R. (2017). Neuronal cell-type classification: challenges, opportunities and the path forward. *Nat Rev Neurosci*, *18*(9), 530-546. <https://doi.org/10.1038/nrn.2017.85>
- Zhang, X., Chen, M. H., Wu, X., Kodani, A., Fan, J., Doan, R., Ozawa, M., Ma, J., Yoshida, N., Reiter, J. F., Black, D. L., Kharchenko, P. V., Sharp, P. A., & Walsh, C. A. (2016). Cell-Type-Specific Alternative Splicing Governs Cell Fate in the Developing Cerebral Cortex. *Cell*, *166*(5), 1147-1162 e1115. <https://doi.org/10.1016/j.cell.2016.07.025>
- Zhang, Y., Wang, C., Sun, M., Jin, Y., Braz, C. U., Khatib, H., Hacker, T. A., Liss, M., Gotthardt, M., Granzier, H., Ge, Y., & Guo, W. (2022). RBM20 phosphorylation and its role in nucleocytoplasmic transport and cardiac pathogenesis. *FASEB J*, *36*(5), e22302. <https://doi.org/10.1096/fj.202101811RR>
- Zhang, Z., Liu, Q., Wen, P., Zhang, J., Rao, X., Zhou, Z., Zhang, H., He, X., Li, J., Zhou, Z., Xu, X., Zhang, X., Luo, R., Lv, G., Li, H., Cao, P., Wang, L., & Xu, F. (2017). Activation of the dopaminergic pathway from VTA to the medial olfactory tubercle generates odor-preference and reward. *Elife*, *6*. <https://doi.org/10.7554/eLife.25423>
- Zheng, Z., Lauritzen, J. S., Perlman, E., Robinson, C. G., Nichols, M., Milkie, D., Torrens, O., Price, J., Fisher, C. B., Sharifi, N., Calle-Schuler, S. A., Kmecova, L., Ali, I. J., Karsh, B., Trautman, E. T., Bogovic, J. A., Hanslovsky, P., Jefferis, G., Kazhdan, M., . . . Bock, D. D. (2018). A Complete Electron Microscopy Volume of the Brain of Adult *Drosophila melanogaster*. *Cell*, *174*(3), 730-743 e722. <https://doi.org/10.1016/j.cell.2018.06.019>
- Zhu, Q., Liu, N., Orkin, S. H., & Yuan, G. C. (2019). CUT&RUNTools: a flexible pipeline for CUT&RUN processing and footprint analysis. *Genome Biol*, *20*(1), 192. <https://doi.org/10.1186/s13059-019-1802-4>

Acknowledgments

This work would not have been possible without the help and support of many people.

I am extremely grateful to my advisor Peter Scheiffle for giving me the opportunity to do my PhD in his laboratory. and for being an incredible mentor who helped me to be more structured, to think critically about my project and to gain knowledge on a wide variety of techniques. He inspired and encouraged me to be a better scientist throughout this whole journey. As for the many life lessons he taught me, I still have some issues accepting that “Life is not fair”, but I did learn that “It’s always a balance” , “It’s a learning curve” and “Shit happens!” and the only thing we can control is how we react to it.

I also would like to thank Alex Schier, Tania Barkat, Esther Creemers and Fiona Doetsch for the valuable inputs I received on my project and this thesis over the years.

I want to particularly thank R. Ortiz and D. Schreiner for setting up the eCLIP protocol and the pipeline of analysis and S. Falkner for the help with 2-photon imaging acquisition, but also L. Traunmüller, E. Furlanis for setting up the initial protocol for RiboTRAP purifications and for constant help and inputs on my project. Many thanks to O. Maunger for giving me the possibility to write a chapter of the Springer book series, for great feedback on the project and for personal support and Z. Chaker for constructive comments on the thesis and experiments with odor behavior in mice. I want to thank all the present and past members of the Scheiffle Lab for constant discussions and feedback, for creating a nice and stimulating environment but also for being good friends who always supported me. Especially, Zeynep, Charlotte, David and Maxime, but also Elisabetta and Lisa: I was truly happy to start this journey with you and you have been fundamental throughout these years.

Thanks are also due to P. de la Grange and A. Jolly at Genosplice for help with RNA seq and splicing analysis analysis, to sciCORE (<http://scicore.unibas.ch/>) scientific computing center at the University of Basel, for the analysis of RNA-sequencing datasets with support by the SIB - Swiss Institute of Bioinformatics. Sequencing and library preparations were performed with support from the Life Science Training Facility and the Quantitative Genomics Facility Basel and in particular Philippe Demaugin. I am thankful to all the Imaging Core Facility, but especially to Laurent Guerard for help in image analysis, Kai Schleicher and Alexia Loynton-Ferrand for technical help and Image acquisition. I would like to thank Frederic Schmitt, David Ueberschlag and Jorg Müller of the Animal Core Facility for taking care of my little friends – the mice, without whom this work could have never been possible, and for satisfying the many requests I had during these years. Thanks are also due to the Proteomic Core Facility, and in particular to Thomas Bock and Alexander Schmidt for help in data analysis and targeted proteomic. Finally, I would like to thank all the PhD Reps for working with me to

make the Biozentrum a great place to be, not only for the amazing science, but also for the community.

Last but not least, I would like to thank the many friends I made (and also the ones I lost) throughout these years, without whom this journey would not have been the same. In particular Riccardo, Federica, Elisa, Marta for always making me feel loved, Cinzia and Martina, for giving me back the energy I needed when I thought I lost it, Francesco, for standing by my side for a long time, Aurel for supporting me through this last year in an amazing way, inside and outside of work.

Infine il Grazie piu' grande va alla mia splendida enorme e chiassosa famiglia per esserci sempre stata nonostante la lontananza, in ogni momento, gioia o difficoltà: Mamma, Papà Vale e Arturo (il mio fratello con la coda), siete e sarete sempre le mie rocce, il mio porto sicuro dove tornare. Gigia Fede e le Giulie, siete la mia famiglia acquisita, ieri oggi e domani, vi voglio un bene immenso. Finally, I would like to thank myself, the Giulia of 6 years ago, for never giving up and for being resilient and stand up every time a challenge tried to stop her. Without all of you I would not be the person I am today, there is no place like HOME and I feel extremely lucky.

Curriculum Vitae

Contact details

Name: Giulia Di Bartolomei,
M.Sc. Date and place of birth: 16.07.1992;
Rome (Italy) Nationality: Italian
Contact information: giulia.dibartolomei@unibas.ch ; giulia.dibartolomei@mail.com
Mobile phone: +41779994059
Twitter: @giulidibba

Personal profile

I am highly passionate and curious about science with strong communication and interpersonal skills. I have more than six years of experience in molecular biology and neurobiology, working in cross-functional teams and multi-disciplinary environments. My goal is to unravel the complex mechanism underlying the regulation of neuronal gene expression in order to develop novel therapeutic avenues for the treatment of brain tumors and neurodegenerative diseases. I am able to prioritize and have excellent project and time management skills, which I use to work efficiently and to meet deadlines.

Personal skills

Fieldwork expertise:

- Extensive experience in fundamental and cutting edge molecular biology techniques
- Good knowledge in RNA-sequencing analysis
- Broad skillset of behavioral phenotyping and stereotactic injections in mice
- Expert in cell culture and neuronal primary cell culture
- Experienced with an array of microscopy techniques including fluorescent microscopy, confocal light microscopy, lightsheet microscopy, transmission electron microscopy, electron tomography and FIB-SEM dataset analysis.

Computational skills:

- Basic knowledge of R and Linux
- Intermediate knowledge of RNA-seq analysis pipelines (reads alignment, DE analysis, gene

- expression counts etc.)
- Good knowledge in statistics applied to simple and complex data sets
 - Image processing software: ImageJ/ Fiji, Neurolucida, Imaris, Blender, Huygens
 - MS Office (Word, Excel, Power Point, Point, Illustrator, Photo-shop)

Language skills:

- Italian (Native)
- English (Full professional working proficiency)
- French (Limited working proficiency)
- German (Elementary proficiency A2.3 level)

Teaching experience

09/2020 – Present Organization and teaching of “BioInformando” workshops in Italian high Schools (~40h per year).

BioInformando is a project that aims at teaching high school students analysis of RNA-sequencing datasets using R programming language.

05/2017 – Present Supervision of Bachelor students in experimental courses and critical scientific reading during the “1228E-01 – Blockkurs: Cell Biology and Neurobiology” (~ 30h per year)

Leadership and community activities:

07/2023 – 08/2023 Volunteer English Teaching. Support conservation and economic development in Madagascar by volunteering to support English teaching (GVI program)

11/2022 – Present Scientific writer for “La fondazione Ugo La Malfa” monthly magazine, Italy

09/2020 – Present Founder of “BioInformando” cultural society for bioinformatics project in Italian high-schools

06/2018 – 11/2021 PhD Representative at Biozentrum since 2018 for organization of career events and PhD retreats

09/2008 – 03/2017 Member of a choir and a musical company (Totti-Vocal Studio)

10/2015 – 10/2016 Student body president at La Sapienza university of Rome

07/ 2015 – 09/2015	<u>Participation in “Intercultura project”</u> - English summer program
02/2011	<u>Participation in “GeMun Project”</u> : United Nation simulation model workshop

Institutional Responsibilities

01/2019	Member of the Scientific Advisory Board (SAB) at Biozentrum, Basel University
10/2014-10/2016	Board member of student association at La Sapienza University, Rome

Education

03/2017 – Present	PhD in Neurobiology, University of Basel
10/2014 – 09/2016:	MSc in Genetic and Molecular Biology in basic and applied research, La Sapienza University of Rome
10/2011 – 10/2014:	BSc Biotechnology, La Sapienza University of Rome
07/2011	Scientific Diploma Liceo Scientifico Louis Pasteur, Rome (IT), 100/100

Work experience

03/2017 – Present	<u>PhD student</u> in the laboratory of Peter Scheiffele, Ph.D, Biozentrum, University of Basel (CH) Subject of studies: “Exploration of the role of RBM20 in cell type-specific alternative splicing programs in neurons” Expected date of PhD defense: February 2023
10/2016 – 03/2017	<u>Research intern</u> at EMBL Monterotondo, Roma (IT) Subject of studies: “Characterization of microglia-synapse interactions during development”
06/2016 – 09/2016 Trainee at	<u>Summer student</u> in the laboratory of Bernardo Sabatini, Summer

Harvard Medical School, Boston (MA), USA,

Subject of studies: "Study of Relaxin-3 neuropeptide release in Nucleus

Incertus"

10/2014 – 10/2016

Master Student in the laboratory of Cornelius Gross Ph.D, EMBL

Monterotondo (IT) and EMBL Heidelberg,(DE)

Subject of studies: "Characterization of microglia-synapse interactions during

development: seeing is believing!"

10/2011 – 10/2014
studi

Bachelor student in the laboratory of Stefano Biagioni, Università degli

di Roma La Sapienza, Rome (IT)

Subject of studies: "Study of the role of the transcription factor Egr-1 in the proliferation and differentiation of neural precursors from adult mice sub- ventricular zone of the brain"

Publications

Publications during the PhD:

Di Bartolomei G, Ortiz R, Schreiner D, Falkner S, Creemers E, Scheiffele P.

"Role of RBM20 alternative splicing factor in neurons" (in preparation)

Di Bartolomei G, Scheiffele P.

"An Optimized Protocol for the Mapping of Cell Type-Specific Ribosome-Associated Transcript Isoforms from

Small Mouse Brain Regions". *Methods Mol Biol.* 2022;2537:37-49. doi: 10.1007/978-1-0716-2521-7_3. PMID: 35895257.

Publications from prior the PhD:

Weinhard L, **Di Bartolomei G**, Bolasco G, Machado P, Schieber NL, Neniskyte U, Exiga M, Vadisiute A, Raggioli A, Schertel A, Schwab Y, Gross CT.; Nat Commun. 2018 Mar, 26;9(1):1228. "Microglia remodel synapses by presynaptic trogocytosis and spine head filopodia induction." doi: 10.1038/s41467-018-03566-5, <https://www.nature.com/articles/s41467-018-03566-5>

Weinhard L, Neniskyte U, Vadisiute A, **Di Bartolomei G**, Aygün N, Riviere L, Zonfrillo F, Dymecki S, Gross C.; Dev Neurobiol. 2018 Jun;78(6):618-626. doi: 10.1002/dneu.22568. Epub 2018 Jan 4. "Sexual dimorphism of microglia and synapses during mouse postnatal development." DOI: 10.1002/dneu.22568, <https://pubmed.ncbi.nlm.nih.gov/29239126/>

Honor and Awards

- | | |
|---------|---|
| 06/2018 | Second best Poster Prize at PhD retreat, Biozentrum (CHF 150) |
| 03/2016 | Giovanni Armenise-Harvard Summer Fellowship (EUR 2,700) |

Courses and Conferences

Invited speaker

- 11/2021 Panel Moderator and poster presentation of the Neuroscience panel at "Academia meets industry Innovation Symposium", Basel

Presentations at meetings

- 07/2022 FENS forum, Paris, France, (Poster presentation)
- 06/2022 Biozentrum Retreat, Sursee, Switzerland, (Poster presentation)
- 09/2021 Biozentrum Phd Retreat, Basel, (Poster presentation)
- 01/2021 Biozentrum Institute Annual Symposium, Basel, (Poster presentation)
- 01/2021 Biozentrum Institute Annual Symposium, Basel, (Poster presentation)
- 07/2019 "Inhibition in the CNS", GRC and GRS conferences, Maine (USA), (Poster presentation)
- 03/2019 Brain awareness week university of Basel, (Poster presentation)

- 06/2018 Biozentrum PhD Retreat, Basel, ([Poster presentation](#))
- 03/2016 EMBL workshop/conference "From 3D Light to 3D electron microscopy",
Heidelberg, ([Poster presentation](#))

Courses:

- 09/2020 [SIB training course](#) "Introduction to RNA-Seq: From quality control to pathway analysis"
- 08/2017 [SIB Course «Introduction to RNA-Seq»](#), Basel
- 05/2017 [IB & NCCR course](#) "First steps in computational biology for RNA Research", Lausanne
- 04/2017 [LTK Module 1](#): Introductory Course in Laboratory Animal Science, FELASA Category B Course (Zurich, Switzerland)
- 04/2016 [Workshop "From 3D Light to 3D electron microscopy"](#), Heidelberg

References

[Peter Scheiffele](#), Ph.D

(Graduate mentor), Biozentrum,

University of Basel Spitalerstrasse 40, 4056 Basel, Switzerland

Email: peter.scheiffele@unibas.ch

[Cornelius Gross](#), Ph.D

(Undergraduate mentor), EMBL,

Monterotondo, Italy

Email: Cornelius.Gross@embl.it

[Yannick Schwab](#), Ph.D

(Undergraduate mentor), EMBL,

Heidelberg, Germany

Email: yannick.schwab@embl.de

Major scientific achievements

During my master thesis at EMBL Heidelberg, I learned how to perform electron microscopy image acquisition and analyses including the reconstruction of neuronal dendritic arborization and analysis/quantification of microglia contacts. Upon acquiring these technical skills, I conducted independent experiments, the results of which contributed to the publication of Weinhard et al.;2018 , “Microglia remodel synapses by presynaptic trogocytosis and spine head filopodia induction”.

For a second project carried out in the group of professor Cornelius Gross, I performed imaging and quantification of synaptic spine size and density as well as microglia motility analyses. These results were published in the paper “Sexual dimorphism of microglia and synapses during mouse postnatal development” by Weinhard et al.; 2018. Together, these publications provide evidence for a direct role of microglia cells in neuronal pruning during development, a function of these cells that has been debated so far. Our study provides the first direct evidence for the elimination of presynaptic structures by microglia cells and highlights the phagocytic mechanisms underlying it.

My PhD was focusing on understanding the role of the cell type-specific splicing factor RBM20 in neuronal identity and synaptic specification in the murine olfactory bulb. Besides the consolidation and further development of my previous microscopy expertise, I acquired additional and more complex molecular and neurobiology skills. Among those, the most profound knowledge I have developed in mass spectrometry, RNA isolation and sequencing and omics data analyses. To become more independent in RNA-sequencing data analysis, I learned how to code in R and Linux languages. After I had taken several training courses, I have set up a pipeline for differential gene expression analysis, a tool that is now standard use in the laboratory. In parallel, I performed neuronal morphological analyses on two-photon acquired images from cleared olfactory bulb tissue and set up behavioral studies to uncover RBM20's role in brain function. Specifically, I measured the ability of mice to form and recall odor memory through a social transmitted food preference paradigm.

My comprehensive characterization of RBM20 function in neurons provides evidence that this protein does not only act as a splicing factor but also regulates gene expression in brain tissue. RBM20 knock-out mice show broad transcriptomic rearrangements both at the level of alternative splicing and the regulation of genes mainly involved in synaptic specification and cell metabolism. Moreover, compared to previous observations in the heart, neuronal RBM20 mRNA targets as well as its sub-nuclear localization are largely different. These observations point towards possible novel and yet to be explored roles of RMB20 in neurons. Altogether, my research contributes to the understanding of how splicing factors act in a broad and cell type-specific manner in order to coordinate gene expression and define neuronal intrinsic properties and synaptic specification. For the first time, we also provide a detailed description of how the expression and function of a single alternative splicing factor influences the morphological and functional specification of two different organs.

Based on the extensive experimental knowledge I have gained with RNA pulldown and RiboTag experiments, I was invited to contribute the chapter “An optimized protocol for the mapping of cell type-specific ribosome-associated transcript isoforms from small mouse brain regions” to the Springer book series. This detailed technical guide will now aid researchers across fields in setting up RNA pulldown and RiboTag experiments in their laboratories.

Finally, while working full time as a PhD student abroad, I realized the fundamental influence of the scientific education I had in my home country on my current research. Following the Coronavirus Outbreak In 2020, I therefore started to think about ways to do something in return. I created “BioInformando”, a program designed to foster bioinformatics education in Italian high-schools. My goals are to give students the opportunity to acquire the basics of programming languages by working on published RNA sequencing datasets and to provide insights into the everyday life of a scientist. Today, “BioInformando” is an association of four people and it is expanding to an increasing number of different schools across Italy year by year.

To further contribute to the scientific outreach, in 2022 I took on the responsibility to write the scientific section of the monthly magazine “Fondazione Ugo La Malfa”, which is a non-profit cultural activity aimed at deepening economic and political topics at both the national and international level.